Book of Abstracts

AMERICAN ELECTROMAGNETICS CONFERENCE (AMEREM 2010)

Held jointly with

ANTENNA TECHNOLOGY AND APPLIED ELECTROMAGNETICS

14th INTERNATIONAL SYMPOSIUM (ANTEM 2010)

5-8 July 2010, Ottawa
Ontario, Canada

ANTEM/AMEREM

July 5 – 9, 2010
Ottawa, ON, Canada
http://antem.ee.umanitoba.ca/antem_amerem2010/

Call for Papers

Conference Chairs:
ANTEM
Zhizhang (David) Chen, Chair
Dalhousie University
Z.Chen@dal.ca

Michel M. Ney, Co-chair
TELECOM Bretagne
michel.ney@telecome-bretagne.eu

AMEREM
Lot Shafai, Chair
University of Manitoba
shafai@ee.umanitoba.ca

ANTEM/AMEREM Steering Committee:
David Giri
Pro-Tech
Giri@DVGiri.com

Carl E. Baum
University of New Mexico
cebaum@ece.unm.edu

Lot Shafai
University of Manitoba
shafai@ee.umanitoba.ca

ANTEM Technical Program Committee Chair:
Aldo Petosa
CRC
aldo.petosa@crc.ca

AMEREM Technical Program Committee Chairs:
HPEM
Walid Chamma
Defence R&D Canada
Walid.Chamma@drdc-rddc.gc.ca

Satish Kashyap
Defence R&D Canada
Satish.Kashyap@drdc-rddc.gc.ca

Behzad Kordi
University of Manitoba
bkordi@ee.umanitoba.ca

UWB
Joe LoVetri, UWB
University of Manitoba
lovetri@ee.umanitoba.ca

Eric Mokole
Naval Research Laboratory
mokole@radar.nrl.navy.mil

Jan Rhebergen
DMO
JB.Rhebergen@mindef.nl

UXO
Yogadhish Das
Defence R&D Canada
Yoga.Das@drdc-rddc.gc.ca

Russell Harmon
US Army Research Laboratory
Russell.Harmon@us.army.mil

Motoyuki Sato
Tohoku University
sato@cneas.tohoku.ac.jp

The 14th International Symposium on Antenna Technology and Applied Electromagnetics [ANTEM] will be held jointly with the American Electromagnetics Conference [AMEREM] July 5 – 9, 2010.

ANTEM addresses emerging topics on Antennas, Electromagnetics and RF Systems.

AMEREM brings together the:
- High-Power Electromagnetics Conference (HPEM)
- Ultra-Wideband, Short-Pulse Electromagnetics Conference (UWB)
- Unexploded Ordnance Detection and Range Remediation Conference (UXO)

We invite you to join us for the ANTEM/AMEREM 2010 Symposium. The technical sessions will be coordinated amongst the joint symposia to provide a comprehensive and well-balanced program and is intended to provide an international forum for the exchange of information on state-of-the-art research in antennas, propagation, and electromagnetic engineering. Authors are invited to submit contributions for review and possible presentation at the symposia on topics of interest to ANTEM, and AMEREM. In addition to regularly scheduled oral presentations, there will be distinguished lecturers and special sessions. We look forward to seeing you in the beautiful city of Ottawa.

Conference Location

The conference will be held in Canada's capital city Ottawa. Ottawa is a picturesque city with beautiful waterways, historic architecture, and an abundance of parklands and open space. The conference site will be at the Fairmont Château Laurier, which reflects the confidence, dignity and style of Ottawa, and stands as a testament to this dynamic, thriving city. It is located in the heart of Canada's capital next door to the Parliament Buildings, this landmark hotel is a magnificent limestone edifice with turrets and masonry reminiscent of a French château.


Ottawa, Canada

General Information

The language of the conference is English. A valid passport is required for entry to Canada. Please contact the Canadian embassy nearest you for specific details and visa requirements.

There will be a Student Paper Competition as well as a Technical Exhibition during the conference. A conference room rate will be offered at the Fairmont Château Laurier, other hotels nearby offer their own rates which may or may not be the same as the conference rate. More information will be posted on the website as it becomes available.

ANTEM authors are invited to submit a 4-page paper and AMEREM authors are invited to submit a 1-page abstract via online submission. The format of all submissions is PDF and must be created according to IEEE specifications. Submissions will be reviewed by the Technical Program Committees and notice of acceptance or rejection will be emailed to the corresponding author. Accepted submissions will be published in the conference proceedings and on IEEE Xplore. Publication will be subject to the presenting author (or one author, in the case of multiple authors) being pre-registered by the early registration deadline. To make a submission or for additional information please visit the website at http://antem.ee.umanitoba.ca/antem_amerem2010/

IMPORTANT DATES
January 5, 2010 - Deadline for Submissions
March 5, 2010 - Notification of Acceptance
May 5, 2010 - Early Registration Deadline

IEEE · University of Manitoba · Electron Devices Society · Ottawa AP/MTT Joint Chapter · URSI

2010 14th International Symposium on Antenna Technology and Applied Electromagnetics [ANTEM] and the American Electromagnetics Conference [AMEREM]

Some Thoughts Concerning Extending the Performance of Switched Oscillators

Carl E. Baum
Department of Electrical and Computer Engineering
University of New Mexico
Albuquerque New Mexico 87131

The switched oscillator is an appropriate source for mesoband high-power electromagnetic (HPE) sources. The oscillator is a quarter-wavelength ($\lambda/4$) transmission line driving a high-impedance load (antenna) at one end with a closing switch at the other end. As one increases frequency the oscillator length is decreased. The cross-section dimensions are also decreased due to the $\lambda/4$ requirement. The smaller dimensions lead to smaller stored energy for a given characteristic impedance Z_c of a coaxial transmission line. One is limited by the spacing between inner and outer conductor required for a given charge voltage. Roughly speaking, for a given spacing the capacitance (and hence energy) is proportional to the characteristic dimension ℓ, as ℓ^2. Thus the energy does as f^{-2} where f is the oscillator resonant frequency.

To get the energy back up one can look at decreasing Z_c, while maintaining the electrode spacing. Going away from a simple coaxial geometry to one that can be called "folded" increases the electrode surface area (and hence capacitance) while maintaining the short transit times to the terminals as required.

Our design considerations are based on a tradeoff between charge voltage and capacitance limited by the transit time (based on oscillator frequency). The techniques discussed in this paper allow for larger oscillator capacitance within the constraints.

An important consideration is the dielectric medium. High-pressure hydrogen gas has been used, but other media are possible. One possibility at lower voltages (and lower pressures) might involve a trombone configuration, for example with an oil dielectric. This would allow a variable oscillator frequency. This also depends on the ease of implementing the various techniques discussed in this paper.

978-1-4244-5050-3/10/$26.00 ©2010 IEEE

Use of Crosspol to Suppress Early-Time Scattered Signal

Carl E. Baum
University of New Mexico
Department of Electrical and Computer Engineering
Albuquerque New Mexico 87131

Recent papers have explored some techniques for suppressing early-time scattering from scatterers in the presence of targets of interest which one wishes to detect and identify. An example of such a scatterer is the human body in the presence of some weapon of interest.

The basic approach involves discriminating between angle-independent backscattering (backscattered field parallel/antiparallel to the incident field), and scattering characterized by target orientation, i.e., scattering natural modes linearly polarized based on target orientation instead of incident field. The foregoing papers accomplish this by differencing the returns from two orthogonal incident polarizations to approximately remove any aspect-independent scattering. This involves using delay lines and an inverter to obtain two returns, time-shifted from each other for subsequent analog differencing of the two returns. When one of the channel polarizations is aligned parallel to the target-natural-mode linear scattering, a maximum target return is obtained. The analog differencing is important so that the digital recording of the late-time target signal has more dynamic range (not diminished by the large early-time signal).

This paper discusses an alternate technique. This involves transmitting in a single linear polarization and receiving orthogonal to this polarization, i.e., looking at crosspol. This alternate approach is simpler but perhaps less sensitive. In both cases, we need to consider the rotation of the radar polarization(s) about the propagation axis, so as to maximize the signal scattered from the target. One can envision mechanical (rotation) techniques as well as electronic techniques involving electronic combinations of h and v channels. A simpler technique involves two radars with the h channel polarization differing by 45 degrees between the two radars, each radar operating independently so as to interrogate the target at different times. A similar technique also applies to the two-channel systems.

978-1-4244-5050-3/10/$26.00 ©2010 IEEE

2010 14th International Symposium on Antenna Technology and Applied Electromagnetics [ANTEM] and the American Electromagnetics Conference [AMEREM]

Transmission/Reflection at a Dielectric Slab

Carl E. Baum
University of New Mexico
Department of Electrical and Computer Engineering
Albuquerque New Mexico 87131

In the design of high-power electromagnetic radiators and the associated pulsed power, one often encounters the problem of transitioning electromagnetic waves between different media (e.g., air, vacuum, SF_6, oil). For fast pulses (or hypoband CW high frequencies) one is concerned about reflections at the interface between the two media. Often a solid dielectric is used to separate the two media. If there is a pressure differential across this barrier, one must use appropriately strong materials to withstand the force. At the same time one is sometimes concerned with the mass (and volume) associated with the dielectric interface.

Consistent with the above, one must also be concerned with the electromagnetic properties of the interface to avoid unwanted reflections and transmit the electromagnetic wave in an optimally useful form for its intended use farther along the wave-propagating system. This leads one to consider various types of interface designs for their relative advantages in the intended application.

So we now have several possible techniques for transitioning electromagnetic waves at single frequencies through a dielectric interface with only small reflection (i.e., near unity transmission). These include the Brewster angle phenomenon, half-wavelength thickness, and thin reinforced diaphragm. Within each of these categories there are various optional shapes for the interface at a pyramidal-horn exit.

978-1-4244-5050-3/10/$26.00 ©2010 IEEE

Some Planar Geometries for Small Antennas With Switched Oscillators for THz Mesoband Radiators

Carl E. Baum
University of New Mexico
Department of Electrical and Computer Engineering
Albuquerque New Mexico 87131

In making very small antennas for extremely high frequencies (say THz regime), construction is a big problem. For this reason, planar geometries of conducting films on dielectrics are often used. This constrains our antenna geometries to some degree.

For mesoband radiators (typically damped sinusoids) the switched oscillator has proven to be a useful source. In this case a quarter-wave transmission-line switched oscillator of low characteristic impedance is used to drive an antenna of somewhat higher impedance. This increases the voltage transient above that of the charging voltage V_0 of the oscillator. We would like to construct such switched oscillators also in a compatible planar geometry.

There are some possible geometries for planar switched oscillators and antennas. We can start with a single-ended planar switched oscillator. Being in the form of a bow-tie antenna, one of the isosceles-triangular parts is made to contain the switched oscillator. Note that this antenna and oscillator are mounted on a dielectric substrate, with perhaps another layer of dielectric on the other side of the metal. This will lower the resonant frequency, for which one must allow.

We can also have differential version. In this case we have two antenna sections connected to opposite ends of a differential switched oscillator. The outer conductor for the switched oscillator is now in two separate parts which can be electrically connected by vias, (or viae) if desired. Using symmetry these conductors are initially at zero potential with connection to zero potential on the symmetry plane transverse to the antenna (orthogonal to the electric field). Noting that the two antennas are electrically connected by a pair of common triangular conductors, which give a different impedance condition than at the outer ends (open), one will need to adjust the antenna design to bring it into a common resonance condition with the switched oscillator.

Optimizing THz antennas presents some significant challenges. For damped sinusoidal waveforms switched-oscillator sources are appropriate. The miniature construction details can pose difficulties. While conducting sheets on a single dielectric substrate are possible, they have disadvantages. Multiple conducting sheets with possible multiple dielectrics allow for increased performance. Combining these with lens and reflectors can lead to even greater performance.

978-1-4244-5050-3/10/$26.00 ©2010 IEEE

SEM-Based Approach for Accurate Modeling of Transient EM Radiation Processes in Ultra-WideBand Antennas

Diego Caratelli and **Alexander Yarovoy**
Delft University of Technology, IRCTR, 2628 CD Delft, the Netherlands
E-mail: d.caratelli@tudelf.nl

The answer to the growing demand for high-performance ultra-wideband (UWB) systems for wireless communications and radar applications is one of the present challenges for the industrial and scientific community. In this context, accurate electromagnetic field prediction models, useful to analyze the time-domain radiation properties of complex antennas [1], are highly desirable. Unfortunately, except for a few classes of radiators such as aperture and impulse radiating antennas, analytical models for the representation of the transient electromagnetic field distribution in Fraunhofer region are not available in the scientific literature. Therefore, in most cases intensive numerical tools are to be used to compute the far-field parameters of interest. However, such an approach does not provide an integral physical insight into the mechanisms which are responsible for the electromagnetic behavior of the structure, and requires large computational times and storage of a large amount of data. To overcome this limitation, a suitable semi-analytical formulation based on the singularity expansion method (SEM) is described in this paper. Using the proposed procedure, the radiated field is presented directly in the time domain as the superposition of outgoing propagating non-uniform spherical waves related to the complex resonant processes occurring in the structure under analysis. To this end, any time-domain integral-equation or finite-difference technique can be adopted to carry out the full-wave analysis within a volume surrounding the antenna, and to determine on-the-fly in step with the numerical simulation a spherical harmonic expansion of the equivalent electric and magnetic currents excited on a suitable Huygens surface enclosing the radiating structure. Then, a pole/residue representation of the currents is derived by a dedicated time-domain vector fitting procedure [2]. In this way, closed-form expressions of the time-domain effective height and antenna gain [3] can be obtained in terms of a new class of incomplete spherical Bessel functions. Furthermore, the suggested approach allows for a significant reduction of the computational resources.

The accuracy of the developed technique is assessed by application to an ultra-wideband resistively-loaded bow-tie antenna for ground-penetrating radar (GPR) applications, whose geometry is shown in Fig. 1. The transient response of the structure evaluated using the proposed model has been found to be in good agreement with the reference solution obtained by means of a full-wave locally conformal finite-difference time-domain ($FDTD$) technique.

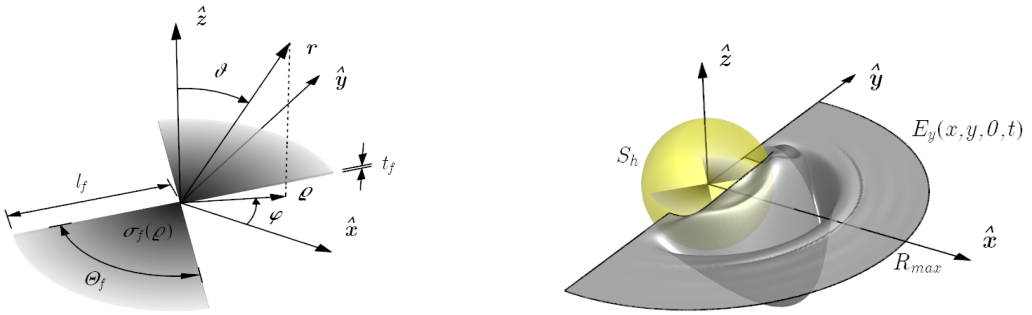

Figure 1: Three-dimensional view of an ultra-wideband resistively loaded bow-tie antenna (a) and spatial distribution of the $y-$component of the electric field excited along the $E-$plane at the spherical-wave delayed time $\tau = 5\,ns$ (b). Antenna characteristics: $l_f = 40\,cm$, $\Theta_f = 75°$, $t_f = 1\,mm$. Maximum observation distance: $R_{max} = 1.5\,m$.

Acknowledgements – This research has been partly carried out in the framework of the *STARS* project funded by the Dutch government.

References

1. A. Shlivinski, E. Heyman, and R. Kastner, "Antenna characterization in the time domain," IEEE Trans. Antennas Propagat., vol. 45, no. 7, pp. 1140-1149, July 1997.
2. D. Caratelli, A. Yarovoy, and L. P. Ligthart, "Unified time- and frequency-domain approach for accurate modelling of electromagnetic radiation processes in ultra-wideband antennas," European Microwave Conference 2009, Rome, Italy, pp. 946-949, Oct. 2009.
3. E. G. Farr and C. E. Baum, "Extending the definitions of antenna gain and radiation pattern into the time domain," Sensor and Simulation Note 350, Nov. 1992.

978-1-4244-5050-3/10/$26.00 ©2010 IEEE

Detection and Classification of Low Metal Antipersonnel Landmines Using Ground Penetrating Radar

L. Anitori[1], **D. Deiana**[1], and **J. S. F. Kerkkamp**[2]

[1] *TNO Defence, Security and Safety, The Hague, The Netherlands*
[2] *TU Delft, Delft, The Netherlands*
E-mail: laura.anitori@tno.nl

In this paper we present some results on detection and classification of low metal content anti personnel (AP) landmines performed using a modified version of the Auto Regressive (AR) modeling algorithm presented in [1]. This algorithm is used for generating an AR model (i.e. AR coefficients) for each A-scan of a B-scan obtained from a Ground Penetrating Radar (GPR). A statistical distance is computed between the AR coefficients of the measured GPR time signal and the AR coefficients of a reference database (containing the AR models of the mines of interest) and a detection is declared if this distance is below a given threshold.
Since this algorithm is based on computing a similarity measure between the AR coefficients of a reference database and the measured GPR trace, it is important to understand the AR model sensitivity, i.e. how different the AR model coefficients will be if we measure the same mine in a different scenario, for eample in a different soil or in the same soil but with a different moisture, or if the mine is buried at a different depth or the mine is tilted. For this purpose we simulated a number of mines, with both very low metal content (SIM6, SIM12, SIM20) and with a metal case (SIM20AL) using the GPRmax software tool [2] and we varied the burial depths and the mine orientations. An example of a simulated SIM6 mine together with the statistical distances to the reference AR models is shown in figure 1. For each simulated mine we created a reference AR model of the same mine with no tilt and at fixed burial depth. For example, figure 1a (SIM 6 at 2 cm depth and no tilt) was used as our reference from the database for SIM6. In figures 1a and 1b, the top plot shows the simulated scenario (mine type, depth and orientation), the middle plot shows shows the B-scan obtained from simulation with GPRmax, while the bottom plot shows the statistical distance between the AR model of the simulated B-scan (middle plot) and the database AR models of all simulated mines.

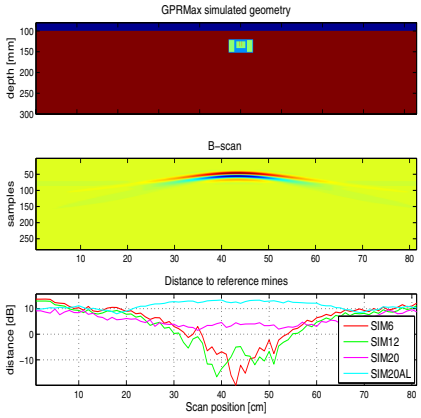

(a) SIM6 at 2cm depth and 0^o tilt.

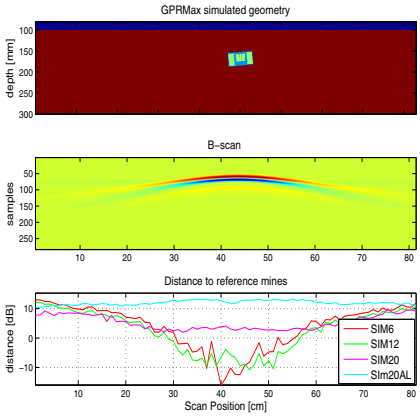

(b) SIM6 at 5cm depth and 5^o tilt.

Figure 1: **Simulations of a SIM6 AP landmine at different burial depths and with different tilt angles.**

From these simulations we conclude that the AR based detection algorithm seems to be robust to different burial depths of the same mine and to rotations only up to a few degrees. In fact, increasing the rotation angle leads often to wrong classification. On the other hand, we should account for similarities amongst the simulated mines. For example, if we look at SIM6 and SIM12 mines, they have exactly the same structure, the only difference between the two being the diameter and the thickness.

References

1. J. B. Rhebergen, H. A. Lensen, R. van Wijk, J. M. H. Hendrickx, L. van Dam, and B. Borchers, "Prediction of soil effects on GPR signatures," Defence and Security Symposium, SPIE, Ed., Orlando, FL, pp. 705715. 2004.

2. http://www.gprmax.org/

978-1-4244-5050-3/10/$26.00 ©2010 IEEE

Detection Technology Tests by the NATO RTO SCI-193 Task Group "Detection and Neutralisation of Route Threat"

Arnold Schoolderman
TNO Defence, Security and Safety, The Hague, The Netherlands
e-mail: arnold.schoolderman@tno.nl

One of the main threats in the current out-of-area operations of NATO forces is that posed by the route threat. This threat includes various deployments of explosive devices such as landmines and various forms of Improvised Explosive Devices (IEDs) being encountered today in Iraq and Afghanistan. The activities of SCI-193 Task Group concentrate on applicable countermeasures for these various explosive threat deployments by investigating the physical and operational capabilities and limitations of techniques for stand-off detection and neutralisation of route threats. The investigation activities are supported by demonstrations, tests and trials of existing and emerging detection and neutralisation techniques considered to be suitable for countering the existing and future threat deployments mentioned.

The Task Group executed a first test, the so-called Pilot Test, in October 2008 at a military test site in the U.S.A. In this test, the suitability for the detection of the route threat was assessed for five readily available systems: a command-wire detector, two non-linear junction detectors, a polarized light camera and a hyper-spectral imager. The test site was prepared in the week before the actual test by members of the Task Group with help of the local test site staff. Four test teams designed test procedures for the four detection technologies considered and executed the four tests concurrently. The Pilot Test was not controlled sufficiently to make quantitative or final conclusions regarding the physical and operational capabilities and limitations of the systems under test for detection of route threat. However, familiarity with the technologies was acquired and basic performance data was collected, analyzed and reported on. In the presentation an overview of the Pilot Test will be given.

A second SCI-193 test is planned to be executed in June 2010 in France. Apart from further tests of wire detectors, detection technologies different from those addressed in the Pilot Test will be tested. Four test teams are put together that will draft test plans for the wire detectors, for detection systems that will be mounted on a vehicle, for hand-held dual-sensor detectors and for two explosives detection systems. The vehicle-mounted detection technologies under test include visual stereo change detection, laser-radar change detection, a vehicle-wide ground penetrating radar (GPR) array and a thermal infra-red camera for the detection of anomalies on-route. In hand-held dual-sensor detectors a metal detector is combined with a GPR in order to reduce the number of false alarms as compared to a stand-alone metal detector. Both an explosives detection system based on Raman spectroscopy and the use of remotely guided explosives detection dogs will be trialed. In the presentation a first impression of the execution of these tests will be given and, as far as availability and the classification level permits, preliminary test results will be presented.

978-1-4244-5050-3/10/$26.00 ©2010 IEEE

Impulse-regime analysis of metamaterial-based leaky-wave antennas and applications

J. S. Gomez-Diaz[1], **A. Alvarez-Melcon**[1], and **C. Caloz**[2]
[1] *Technical University of Cartagena, Cartagena, E-30202, Spain.*
[2] *Ecole Polytechnique, Montreal, QC, H3T 1J4, Canada.*
E-mail: jsebastian_gomez@ono.com

Recently, ultra wideband (UWB) systems have grown in popularity due to their high data rate capability and their strong immunity to multipath interference. Metamaterial-based leaky-wave antennas [1] may provide novel and unique solutions for UWB systems, owing to their intrinsically dispersive behavior and subsequent compressive impulse properties. However, such antennas have been characterized almost exclusively in the harmonic regime to date.

This work presents an analytical and numerical study of composite-right/left-handed leaky-wave (CRLH) antennas (LWAs) operated in the impulse regime. An extended transmission line (TL) approach is used for this purpose. Consider a matched TL excited by a modulated pulse. Even without any wave reflected from the load, two distinct sets of currents exist, one along each conductor of the TL. In order to compute the total radiation from the TL, the currents along each TL conductor are analyzed individually. For the sake of completeness, three different TL are considered. In the case of a **TL with right-handed conductors**, the currents on the two conductors will have the same magnitude but opposite phases, which results in far-field cancelation and radiation suppression. In the case of the **classical dipole antenna**, the two sets of currents have the same magnitude and the same phase, and therefore produce far-field radiation. In the case of a **TL structure with CRLH conductors**, when the line is operated in the fast-wave (radiative) region, one set of currents exhibits a specific phase variation with respect to the other one. This phase variation is analytically related to the complex propagation constant of the LWA. The analysis of the current contribution of the two TL conductors leads to an accurate prediction of the LWA far-field radiation. When the CRLH TL is operated outside the fast-wave region (i.e. in the guided-wave region), both sets of currents have the same magnitude and opposite phases, leading to far-field radiation cancelation.

It will be shown how the proposed TL approach allows an *efficient* description of interesting phenomena and the characterization of complex UWB systems, and excellent agreement with measurement will be presented. Specifically, a *real-time spectrogram analyzer* (RTSA) [2] and a *frequency resolved electrical gating* (FREG) systems [3] will be considered. These systems characterize, both in time and frequency, an unknown UWB test signal, employing for this purpose the *spectro-spatial decomposition* property of CRLH LWAs [2]. While the full-wave analysis of such systems requires several hours (for RTSA) or even days (for FREG), the proposed approach reduces the computational cost to only a few seconds (for RTSA) and minutes (for FREG), while ensuring very good accuracy with respect to full-wave and measured data. Finally, the *spatio-temporal Talbot phenomenon* [4] is considered. This phenomenon reproduces at microwaves, with novel features, the spatial Talbot effect well-known in optics, based on the dispersive response of a CRLH LWA array. The proposed approach is able to completely characterize this phenomena in just seconds, while full-wave analysis requires hours of computation. Here again, excellent agreement with measurement will be shown.

Acknowledgements – This work was supported in part by the Spanish Ministry of Education and Science under Grant FPU-AP2006015 and project TEC2007-67630-C03-02.

References

1. C. Caloz and T. Itoh, "Electromagnetic Metamaterials: Transmission Line Theory and Microwave Applications", Hoboken, Wiley and IEEE Press, 2006.
2. S. Gupta, S. Abielmona, C. Caloz, "Microwave Analog Real-Time Spectrum Analyzer (RTSA) based on the Spatial-Spectral Decomposition Property of Leaky-Wave Structures", *IEEE Trans. Microwave Theory Tech.*, vol. 57,no. 12, pp. 2989-2999, Dec. 2009.
3. S. Gupta, J. S. Gomez-Diaz and C. Caloz, "Frequency Resolved Electrical Gating Principle for UWB signal Characterization using Leaky-Wave structures", in Proc. *European Microwave Conf.*, Rome, Italy, Oct. 2009.
4. J. S. Gomez-Diaz, S. Gupta, A. Alvarez-Melcon and C. Caloz, "Tunable Talbot Imaging Distance using an Array of Beam-Steered Metamaterial Leaky-Wave Antennas", *J. App. Phys.*, vol. 106, pp. 084908:1-8, Oct. 2009.

978-1-4244-5050-3/10/$26.00 ©2010 IEEE

Protection Circuits for IT Equipment under HPEM Conditions

F. Brauer, J. L. ter Haseborg, S. Potthast
Hamburg University of Technology, Institute of Measurement Technology and EMC, Hamburg, Germany
E-mail: f.brauer@tu-harburg.de

The ability to communicate depends on a reliable data transfer for almost every technical system for civilian or military applications. With the growing number of electromagnetic interferences (EMI), especially high power electromagnetics (HPEM), such as UWB-(ultra wideband), DS-(damped sinusoids) or HPM-(high power microwave) sources, communication systems are more and more vulnerable. In supposable scenarios it is already possible, that these sources could be used by terrorists to disturb electronic systems on purpose. This threat is known as intentional electromagnetic interferences (IEMI) [1]. IT networks represent most of the communication systems. COTS IT components are widely spread out on the market and are already used in huge areas of current applications. An error or a momentary breakdown of the data transfer can be extremely critical for some applications (e.g. civil aviation). The investigation of protection elements to harden these systems is therefore inevitable.

In this contribution different protection circuits (originally for the ESD protection of IT data transmission lines) are investigated under HPEM conditions as defined in [2]. For an exemplary COTS IT test network on the one hand passive elements are connected additionally in the transmission lines without influencing the system configuration. On the other hand active protection circuits are used with a stand-alone Ethernet test network. Therefore special circuits compliant to the Ethernet standard have been developed (a detailed description of the protection circuits will be shown in the presentation). In the passive state of the test system the protection elements are exposed with typical, coupled HPEM disturbance signals. The response is measured and simulated in SPICE and is evaluated in the time and frequency domain. In addition, the system is regarded in the active state (during a data transfer) under influence of HPEM interferences with or without protective elements. With the help of Ethernet analysis software the number of errors (i.e. retransmissions) can be plotted during disturbing the system. Figure 1 shows an exemplary result with passive and one active protection circuit during disturbance of the IT network system with UWB pulses with a rising pulse repetition rate.

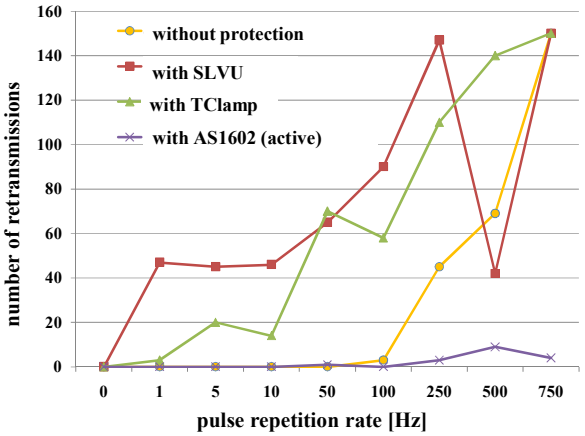

Fig. 1 –Ethernet data transmission errors during disturbance with UWB pulses with a rising pulse repetition rate for different additional protection elements

The results provide the basis for the development of new, customized protection concepts and for integrating COTS protection circuits into existing IT systems.

Acknowledgments - The authors would like to thank the BWB (Germany) and the WIS (Scientific Research Institute for Protection Technologies, Munster, Germany) for financial funding and support of this work.

References

1. W.A. Radasky, C.E. Baum, and M.W. Wik, "Introduction to the Special Issue on High-Power Electromagnetics (HPEM) and Intentional Electromagnetic Interference (IEMI)", IEEE TRANSACTIONS ON ELECTROMAGNETIC COMPATIBILITY, vol. 46, no. 3, pp. 314–321.
2. F. Brauer, F. Sabath, J. L. ter Haseborg, “Susceptibility of IT network systems to interferences by HPEM”, IEEE EMC Symposium, August 17-21 2009, Austin, Texas, USA
3. F. Brauer, J. L. ter Haseborg, “Untersuchung von Schutzelementen für IT-Systeme gegen HPEM-Bedrohungen”, Kleinheubacher Tagung, September 28 – October 01 2009, Miltenberg, Germany

978-1-4244-5050-3/10/$26.00 ©2010 IEEE

HPM Susceptibility of COTS Equipment Suitable for UAV Applications

T. Nilsson, M. Bäckström
Combitech AB, SE-581 88 Linköping, Sweden
E-mail: tony.nilsson@saabgroup.se

The increased use of COTS (Commercial-off-the-shelf) equipment, even for use in mission critical applications, motivates investigations of its vulnerability to Intentional EMI, such as the threat from HPM (High Power Microwaves). This paper presents an experimental investigation of 5 COTS systems that could be possible candidates for use in Saab's UAV (Unmanned Aerial Vehicle) Skeldar. The 5 systems are:

- GPS, operating frequency ~ 1575 MHz
- C2-Link (Command & Control), operating frequency ~ 400 MHz
- RALT (Radar Altimeter) operating frequency ~ 4 GHz
- Video-Link, operating frequency ~ 1,2 GHz
- FCU (Flight Control Unit)

The tactical UAV Skeldar is a fully autonomous, mobile system with VTOL and hovering capacity. It has a length 4 m, a height of 1.2 m and a total weight of 200 kg, including payload. It has a radius of action of about 100 km, flight time of 4-5 hours and a maximum speed of 150 km/h.

In the first part of this paper we assume that Skeldar is certified to comply with the HIRF (High Intensity Radiated Fields) requirements according to ED-14/RTCA DO160, which are normally used in certification of civil aircraft. For the frequency interval considered here the requirements, in terms of electric field strength (peak), is 700 V/m between 0,4 and 1 GHz; 2 kV/m between 1 and 2 GHz and 3 kV/m between 2 and 6 GHz. Note that these requirements are not applicable for in-band front-door coupling. Assuming this immunity level we first calculate the tactical limitations for Skeldar, in terms of the distance it has to keep from a hypothetical HPM weapon in order to operate free from interference. The HPM weapon is assumed to have the following parameters:

- Output pulse power: 2,5 GW
- Frequency: tunable between 0,4 to 6 GHz
- Antenna gain: 18 to 42 dB_i (corresponding to an effective antenna area of 3,1 m^2)

The result is that the distance from the assumed HPM weapon has to be, depending on the frequency, several kilometres in order to operate safely.

After these initial considerations the results from the immunity testing of the 5 chosen COTS candidate systems are presented. In the analyses of the susceptibilities we do not take into account the protection that would be provided if the systems were integrated into Skeldar. The susceptibility tests were made at 1,3; 2,85; 3,0 and 5,71 GHz (not all frequencies were used for all EUT's), and also at the in-band frequency of each EUT (except for the FCU which has no in-band front-door coupling path). The tests were carried out in our reverberation chamber and for the GPS and the C2-link also at high field levels at the Swedish Microwave Test Facility (MTF). The results of the susceptibility testing of the 5 systems were:

- GPS: Out-of band interference at field levels down to 25 V/m. Permanent damage occurred at 8 kV/m.
- C2-link: Out-of band interference at field levels down to 200 V/m. No permanent damage was demonstrated at levels up to 27 kV/m.
- RALT: No out-of band interference at field levels up to 1,6 kV/m.
- Video-link: No out-of band interference at field levels up to 1,6 kV/m.
- FCU: No interference at field levels up to 1,6 kV/m.

The conclusions of the study are:

- The testing of interference levels showed that neither the possible COTS GPS nor the C2-Link is compatible with the HIRF requirements assumed to be valid for Skeldar. For the GPS the deviation is significant. This indicates that the security distance that would have to kept to the assumed HPM weapon would be extremely large.
- There are no results for the RALT, FCU and Video-link, which shows that the HIRF-requirements are not met. For the RALT the levels for in-band interference were larger than expected

None of the tested possible COTS candidate systems, except from an updated version of the FCU, is used in Skeldar.

Acknowledgments – We thank colleagues at Saab Aerosystems and at the Swedish Defence Material Administration (FMV) for valuable comments and discussions.

978-1-4244-5050-3/10/$26.00 ©2010 IEEE

The Method Uncertainty – Is the Compromise Acceptable?

Dr Anthony Wraight[1], Paul Watkins[1], Dr Mats Bäckström[2]
[1]QinetiQ, Cody Technology Park, Ively Road, Farnborough, Hampshire, GU14 0LX, England
[2] Combitech AB, SE-581 88 Linköping, Sweden. Also at the Royal Institute of Technology (KTH), Stockholm.

Abstract

Simulators exist for a variety of High Power Electromagnetic (HPEM) Environments that allow assessment of the response of a system or equipment. These assessments give an understanding of required safety margins to minimise risk. The measurement methods have evolved such that the understanding of the response is balanced against the time and cost of performing such an assessment. However, there is inherent uncertainty with this approach and it is useful to understand the uncertainties associated with the method (for example simulator characteristics, equipment set-up etc) in addition to those associated with the measurement instrumentation.

This paper discusses the contributions to a method uncertainty drawing upon limitations in HPEM test methods. Definitions will be given along with examples of uncertainties that could be applied to the various categories.

978-1-4244-5050-3/10/$26.00 ©2010 IEEE

Low Level Swept Current – An Example Method Uncertainty

Dr Anthony Wraight[1], Paul Watkins[1], Dr Richard Hoad[1], Andrew Lambourne[1]
[1]QinetiQ, Cody Technology Park, Ively Road, Farnborough, Hampshire, GU14 0LX

Abstract

Low Level Coupling (LLC) methods are used internationally to support clearances of both civil and military aircraft. The test methods are designed such that they cover electromagnetic interaction mechanisms from kHz to GHz giving useful information about how external electromagnetic environments couple to a system of interest. The data collected supports the derivation of an appropriate safety margin.

This paper explores limitations in the Low Level Swept Current (LLSC) method. This method provides a measure of internally induced current as a result of an external electromagnetic field between 1MHz and 400MHz. Statistical analysis will be applied to the limitations of LLSC in order to derive a method uncertainty. Examples will be given for both frequency domain and time domain environments.

978-1-4244-5050-3/10/$26.00 ©2010 IEEE

Magnetic Field Distortion while Underground Detonation of Small Power Chemical Blasting Charge

M.M. Filatov, V.I. Butin, O.A. Ksenofontova, V.F. Molochkov, O.A. Gerasimchuk
VNIIA, Moscow, Russian Federation, 127055
E-mail: filatov@niiit.ru , vniia@vniia.ru

When performing work under the ISTC Project No. 835 *Investigation of Electromagnetic Signals Accompanying Underground Chemical Blasts* there were carried out model underground blasts of chemical explosive charges in order to study characteristics of electromagnetic distortion generated by detonation of explosives. This paper represents routine of experiments, typical experimental results and qualitative model for interpreting magnetic field disturbance.
Induction type sensors were used for measuring of the magnetic field disturbance. Signals from the sensors were recorded using SONY two-channel analog audio recorders MZ-R50. Explosive charge detonation was initiated using igniting fuse. After the experiments the recorded analog data was converted into digital form using TDS-540D oscilloscope.
Figure 1 shows typical transient processes obtained for one of the underground explosions; Table 1 includes the parameters of the blast; orientation of the sensors relative to the blast epicenter is given in Figure 1, on the right.

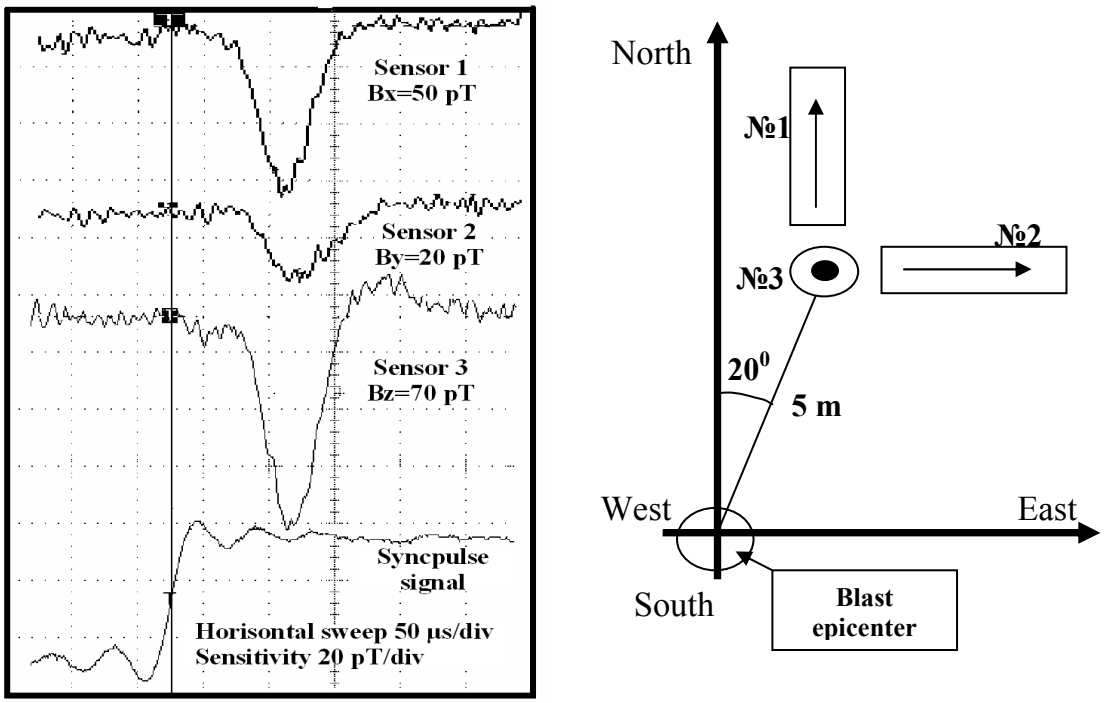

Figure 1: **Magnetic field pulses and orientation of sensors**

Table 1: **Parameters of the blast**

Date, No. and type of blast	02.07.99, No. 21, camouflet at 2.3 m depth
Charge	Cylinder of TH 50/50, D 60 x 420 mm^2, weight 2.0 kg
Charge orientation	Horizontal (East - West)
Detonation direction	East - West

The well-known seismoelectrical and magnetic induction effects are taken as a basis of the qualitative model interpreting experimental results obtained. While developing the model the following assumptions and hypotheses were taken: explosive charge detonation causes radial movement of ambient soil under the action of propagating shock wave increasing its conductivity due to the appearance of seismoelectrical effect; in the process of conducting region expansion the current caused by magnetic induction effect is induced inside it. This current causes short-term disturbance of the magnetic field. The direction and value of the induced current are determined by the conducting region expansion velocity, its conductivity, as well as direction and module of the Earth magnetic field vector.

Acknowledgments - The work fulfilment was financially supported by the ISTC under Project No. 835.

978-1-4244-5050-3/10/$26.00 ©2010 IEEE

Operation of a Reverberation Chamber with Pulsed Microwave Signals

Chr. Adami, Chr. Braun, P. Clemens, H.-U. Schmidt, M. Suhrke, H.-J. Taenzer
Fraunhofer INT, Appelsgarten 2, 53879 Euskirchen, Germany
E-mail: Michael.Suhrke@int.fraunhofer.de

For immunity and emission measurements the reverberation chamber (RC) is an increasingly attractive alternative to traditional EMC tests with TEM fields in anechoic chambers or GTEM cells. We operate a small aluminium RC with a working volume of 0.7 m × 1.0 m × 1.2 m at outer dimensions of 1.2 m × 1.9 m × 2.5 m. According to the calibration, field strengths for an input power of 1W between 100 and 180 V/m are obtained in the frequency range from 520 MHz to 18 GHz. Besides basic investigations on the applicability for time dependent measurements with microwave pulses our RC is intended for susceptibility measurements on smaller test objects with high field strengths. In order to couple high power above 10 kW into the chamber in a wide frequency range we use a self-developed discone antenna. Investigations at low input power with this transmitting antenna yield almost no differences to commercial horn antennas. The same applies to the use of an E-field probe as receiving antenna in comparison to those horn antennas. We obtain field strengths within the working volume of more than 20 kV/m. With a typical test object, e. g. an IT network device, they decrease almost by a factor of two. Alternatively to the pulse generator we use power amplifiers (200 W) for CW measurements in the frequency range from 0.8 to 7.5 GHz.

In the frequency range between 500 MHz and 3.5 GHZ we determine the quality factor of the chamber from the decay time of the received signal after excitation with a pulse long enough to be in the stationary regime. For the quality factor of the empty chamber we obtain results between 3000 and 30000 and values between 1000 and 10000 for the chamber loaded with a typical test object. From the results for the quality factor we derive field strengths normalized to an input power of 1 W between 110 and 160 V/m which coincides well with the results from the calibration. From the time dependent behaviour of the reflected signals in the transmitting antenna after pulsed excitation we are able to extract the portion of power reflected directly in the antenna and the portion reflected only after having traversed the chamber (Fig. 1, left). From this observation we propose to define the net input power as the difference between injected power and power reflected directly in the antenna (see e. g. discussion in [1,2]). Finally, the contribution discusses statistical properties of the received signals and the reflected signals in the transmitting antenna after pulsed excitation both in the stationary and the transient regimes. The standard deviation shows an overshooting of the signals in the transient regime during switch-on and switch-off of the pulse which is also seen in the strong time dependent fluctuations of the signals for different stirrer positions in these regimes (Fig. 1, right).

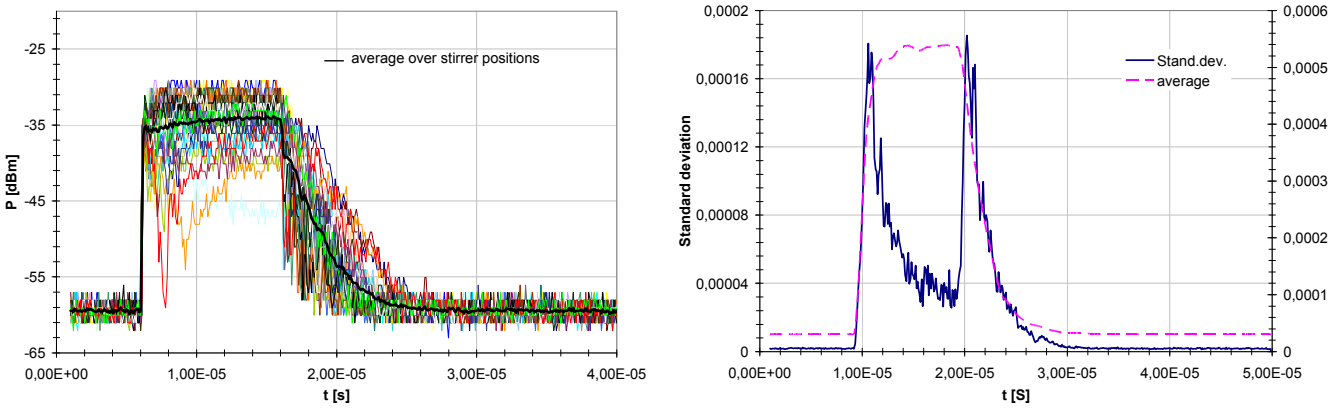

Figure 1: **Left: Reflected power at transmitting antenna for different stirrer positions and f = 1 GHz, average with respect to stirrer positions - thick black line. Right: Standard deviation of power at receiving antenna for f = 1 GHz (left scale), average power is shown for orientation (right scale).**

References

1. IEC 61000-4-21: "Electromagnetic Compatibility (EMC) – Part 4-21: Testing and measurement techniques – Reverberation chamber test methods", August 2003.

2. Wei, X. C. and Li, Er-Ping: "Transmitting Antenna's Reflected Power and its Influence on Reverberation Chamber Calibration", IEEE Transactions on Electromagnetic Compatibility 49 (2007), pp. 366-370

978-1-4244-5050-3/10/$26.00 ©2010 IEEE

Jamming Jammers Jamming GSM Phones

Daniel Månsson[1,2]
[1]*High Voltage Valley, Ludvika, Sweden, SE-771 28*
[2]*Royal Institute of Technology (KTH), Electromagnetic Engineering, Stockholm, Sweden, SE-100 44*
E-mail: daniel.mansson@highvoltagevalley.org

Scientific research and investigations [1] have shown that our society is highly vulnerable to intentionally created electromagnetic interference (IEMI) that can be used to sabotage the normal operations of systems associated with critical infrastructure components. There are many system design factors contributing to this vulnerability, but the availability of commercial, inexpensive and easy-to-use electromagnetic sources that can be used as disturbance weapons is an aspect that cannot directly be controlled by engineers. This is important as in the process of creating electromagnetic compatibility between (and within) systems; limiting source emissions is one method of improving the compatibility (besides limiting the coupling paths between systems and hardening these).
In this paper, we have investigated three samples of a low-cost (≈160 USD) handheld GSM jammer, commercially available on the internet. These are isotropic frequency band specific noise emitters. The output spectra were examined by the use of a reverberation chamber and the interference ability was tested (successfully) against commercial GSM phones. However, note that, due to the frequency bands used, the normal operation of a 3G enabled phone was not affected by the jammers. The two possible output spectra, depending on power emission setting of the jammer, are shown in Fig. 1 below.
Also, the immunity of the jammers themselves against electromagnetic disturbances was tested also by the use of a reverberation chamber. It was found that the normal operation of the jammers could be interfered with both in-band as well as out-of-band of the operational frequencies. A range of different upset events (as defined in [2]) could be induced in the jammers (see Fig. 2, permanent damage level not shown).

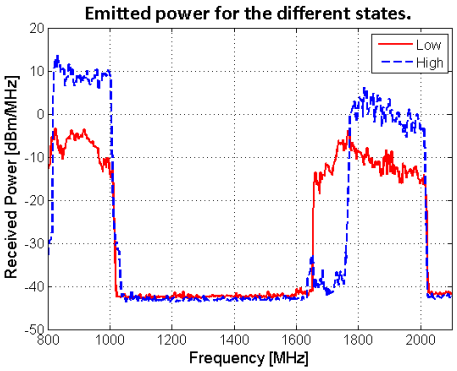

Figure 1: **Output spectra of the jammers.**

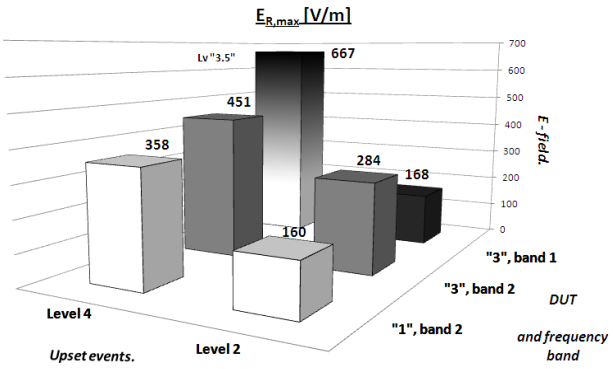

Figure 2: **Susceptibility data of the jammers (maximum of a rectangular component of the electric field).**

Similarly to the "Active Denial System" presented by, e.g., Raytheon, the knowledge of the electric field threshold levels can for upset events be used to disrupt the function of these isotropic jammers. An IEMI scenario that is often given is the use of balloons to lift a large number of jammers over a crowd in a city, making it very difficult for law enforcement to easily counteract the interference source. However, a high directivity (narrow main antenna lobe) HPEM source could disrupt the normal operation of the jammers by inducing a system crash or permanent damage to the jammers, without causing interference to surrounding systems. Thus, limiting source emissions and restoring electromagnetic compatibility.

It is clear that inexpensive jammers that can interfere with GSM systems can be acquired from easily available homepages on the internet and, according to statements there, jammers are frequently being used by people. However, these GSM jammers are themselves vulnerable to disturbances that can be used to counteract them.

Acknowledgments – Olof Lundén at the Swedish Defence Research Agency (FOI) is greatly acknowledged for the help with the experiments and Mats Bäckström at Combitech AB is deeply acknowledged for the good discussions.

References

1. W. A. Radasky, C. E. Baum, M.W. Wik, "Introduction to the special issue on high-power electromagnetics (HPEM) and intentional electromagnetic interference (IEMI)", IEEE Transactions on Electromagnetic Compatibility, vol. 46, 2004.
2. D. Månsson, R. Thottappillil, M. Bäckström, O. Lundén, "Vulnerability of European Rail Traffic Management System to Radiated Intentional EMI", IEEE Transactions on Electromagnetic Compatibility, vol. 50, 2008.

978-1-4244-5050-3/10/$26.00 ©2010 IEEE

Electrical Parameters of Compact Intracloud Lightning Discharges

Amitabh Nag and **Vladimir A. Rakov**
Department of Electrical and Computer Engineering, University of Florida, Gainesville, Florida, USA
E-mail: amitabh@ufl.edu

There is a distinct class of lightning discharges that produce both (1) intense HF-VHF radiation bursts (much larger than those from any other cloud-to-ground or "normal" cloud discharge process) and (2) single bipolar electric field pulses (so-called Narrow Bipolar Pulses or NBPs) having typical full widths of 10 to 30 μs. They are referred to as Compact Intracloud Discharges (CIDs). Figure 1 shows wideband electric and magnetic fields, electric field derivative, and narrowband VHF (36 MHz) radiation burst produced by a typical CID.

Based on experimental evidence of multiple reflections and modeling, we infer that the CID is essentially a bouncing-wave phenomenon. The shortest radiating-channel length appears to be about 100 m. The reflections are responsible for fine structure of both electric field and dE/dt signatures of CIDs, as well as, by inference, for "noisiness" of dE/dt waveforms and for accompanying HF-VHF bursts. From modeling CID as a wave traveling on an elevated vertical transmission line and comparing model-predicted electric fields with measurements we estimated that the effective current reflection coefficients at channel ends should be in the range of 0 to -0.5, the wave propagation speed ranges from 0.3 to 3 x 10^8 m/s, and the upper bound on channel length is about 1000 m. In these calculations, we assumed that the current wave had a risetime of 6 μs and a total duration of 30 μs. Influence of current risetime on field waveforms was also examined, and it was found to be typically in the range from about 2 to 8.5 μs.

We used the vertical Hertzian dipole approximation to estimate electrical parameters of the 48 located CIDs from their measured electric fields. For nine events, we could estimate CID channel lengths from observed reflection signatures in dE/dt waveforms and assumed propagation speeds which cover the entire range of allowed values. The channel lengths for these nine events, for v = 2.5 x 10^8 m/s, ranged from 108 to 142 m. The minimum, maximum, and geometric mean values of peak current (I_p), current risetime (RT), charge transfer (ΔQ) for the first 5 μs, peak radiated power (P_{rad}), and energy (ΔW) radiated for the first 5 μs, are summarized in Table 1. For the remaining 39 events, which did not exhibit reflection signatures, the electrical parameters were estimated for different assumed values of channel length. For example, the geometric mean values of I_p for the assumed channel lengths of 170, 350, and 500 m were 132, 64, and 45 kA, respectively.

Table 1: **Electrical parameters of nine CIDs whose channel lengths were estimated from reflection signatures (v = 2.5 x 10^8 m/s).**

Parameter	I_p, kA	RT, μs	ΔQ, mC	P_{rad}, GW	ΔW, kJ
Minimum	87	3.0	79	12	7.5
Maximum	259	9.5	496	70	52
GM	143	5.4	303	29	24

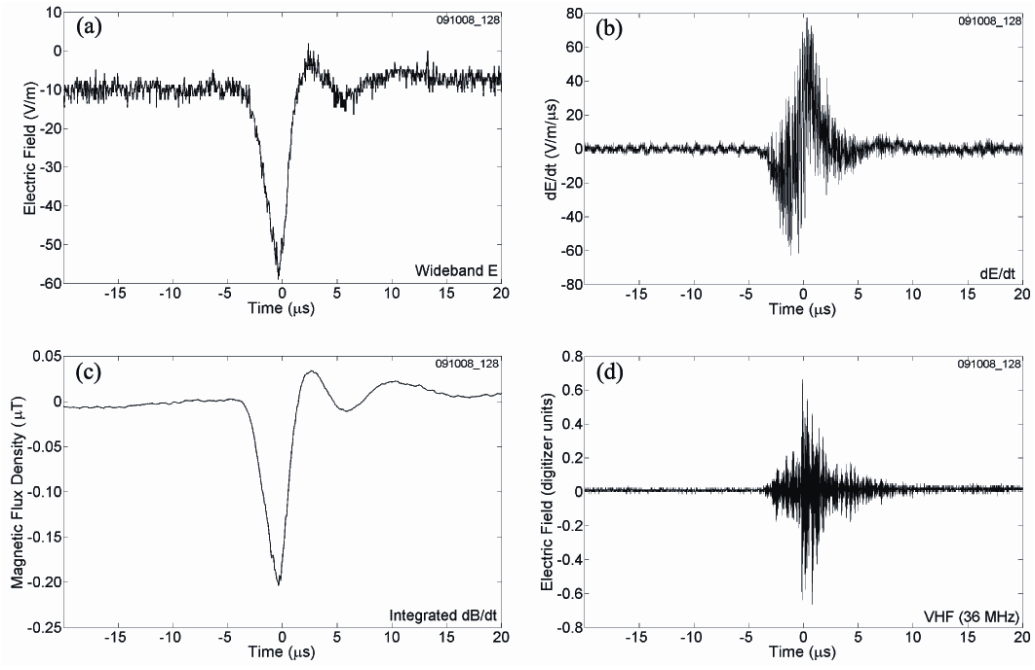

Figure 1: **(a) Wideband electric field, (b) electric field derivative (dE/dt), (c) magntic field (integrated magnetic field derivative), and (d) narrowband VHF (36 MHz) radiation burst produced by a CID that occurred at a distance of 17 km from the measuring station in Gainesville, Florida.**

978-1-4244-5050-3/10/$26.00 ©2010 IEEE

RELATION BETWEEN LIGHTNING CHARACTERISTICS IN WINTER AND ASPECT OF OUTAGES DUE TO IT

Shigeru Yokoyama[1], Takatoshi Shindo[1], and **Akira Asakawa[1]**
[1]*Central Research Institute of Electric Power Industryhe, Yokosuka, Japan, 240-0196*
E-mail:yokoyama@criepi.denken.or.jp

Thunderstorms frequently occur along the coast of the Sea of Japan from October through February. For a long time the same protection methods have been used against both lightning in winter(winter ligthning) and lightning in summer . Observation results have clarified that characteristics of winter lightning are quite different from those of lightning in summer. Recent statistics of lightning outages have revealed that the aspect of outages due to winter lightning is quite different from that due to lightning in summer. This paper shows the relation between the characteristics of winter lightning and the aspect of lightning outages in winter.

1.Characteristics of lightning in winter

-Occurrence of lightning

Since lightning in winter is produced under the environmental conditions of the cold Siberian airmass and the comparatively warm sea current flowing in the Sea of Japan, it can occur not only in the afternoon but at any time .

-Concentration of flashes to a high structure

Although the average frequency of lightning flashes in winter is less than that in summer, winter lightning are likely to concentrate to a high structure. A 200-meter–high stack of a thermal plant facing the Sea of Japan was hit by lightning 174 times for 7 years in winter ,on the other hand it was hit by lightning only once in summer for the same 7 years. Figure 1 shows winter lightning hitting a broadcasting tower. Usually a leader progresses from a high structure upward .

-Lightning current with long duration

Lightning currents with long duration are often observed in winter. Figure 2 shows the example of long duration. lightning current with over 900 coulombs. Positive currents with over 300 coulombs are not unusual in winter.

-High ratio of positive lightning

Representative value of the rate of positive currents out of total currents is about 10% in summer. On the other hand , the rate of positive currents is 30-50 % for lightning in winter along the coast of the Sea of Japan.

-Superposition of pulse currents on a long current waveform

Pulse currents superimposed on a long current waveform are frequently observed for winter lightning.

2. Aspects of lightning outages on various infrastructures and electronic facilities

-Power transmission lines

Outage ratio (outage numbers per lightning strokes) is larger in winter than in summer. Especially double circuit outages (DCOs) occupy over 50% of total outages in winter . DCOs due to lightning in summer occupy only 10%.

-Overhead power distribution lines

Outage ratio is larger in winter than in summer like transmission lines. Some statistics shows that the ratio for lightning in winter is 13 times as large as that in summer. The outage ratio of facilities is different between for summer seasons and for winter seasons. The ratio of damaged surge arresters out of total damages including transformers, insulators and etc. is 25% in winter, while that is 8 % in summer.

-Payment of fire insurance based on the cause of thunder

In Japan the amount of payment is comparatively large in the area where winter lightning is frequent.

-Wind turbine blades

In Japan Outages in wind turbine blades are remarkable in the area where winter lightning is frequent.

3. Relation between lightning characteristics in winter and outage statistics

We have got many data of lightning in winter by the observation for these 30 years in the coastal area on the Sea of Japan. We have got important information from the observational results so far, but we need more data to comprehend the lightning in winter sufficiently so as to design the lightning protection for various infrastructures and electronic facilities against winter lightning. Several characteristics of lightning and environmental conditions play important role for the unusual aspect of outages or damages due to lightning in winter. It is very important to suppose the lightning characteristics at a target area by the aspects of lightning outages and to assess the lightning hazards using the observation results.

Figure 1: Winter ligthtning (upward leader)

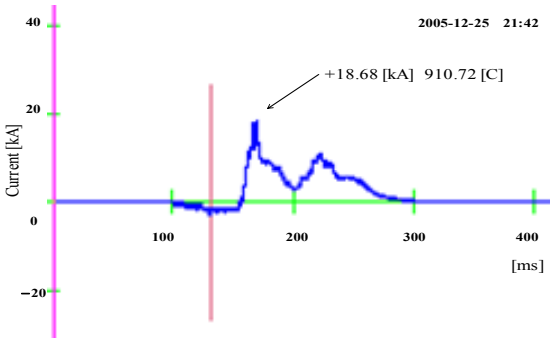

Figure 2 :Positive lightning current with long duration

978-1-4244-5050-3/10/$26.00 ©2010 IEEE

Instrumentation of the Säntis Telecommunication Tower in Switzerland for Lightning Current Measurement

Carlos Romero[1], Abraham Rubinstein[2], Mario Paolone[3], Farhad Rachidi[1], Marcos Rubinstein[2], Pierre Zweiacker[1], and **Bertrand Daout[4]**

[1]*Swiss Federal Institute of Technology (EPFL), Lausanne, Switzerland*
[2]*University of Applied Sciences of Western Switzerland, Yverdon, Switzerland*
[3]*University of Bologna, Bologna, Italy*
[4]*Montena EMC, Rossens, Switzerland*

E-mail: Farhad.Rachidi@epfl.ch

This contribution reports on the progress in a new project to instrument the Säntis telecommunication tower on the Saint Gallen region of Switzerland. The 125-m tower sits on top of the 2505-m mount Säntis (See Fig. 1.a). An analysis of lightning location system data over the past 10 years has revealed that this tower is struck by lightning more often than any other tower in Switzerland [1]. The lightning current will be measured at two different heights, 20 m and 67 m, using, at each height, two sensors, a Rogowski coil, whose output will be processed by an analog integrator to obtain a replica of the current waveform, and a B-dot sensor for the measurement of the current time derivative (Fig. 1b).

An over-the-Internet remote maintenance, monitoring and control system has been designed and built using National Instruments Compact-RIO modules linked via 100Base-FX fiber optics Ethernet to a control room that is connected to the Internet over a standard ADSL link on the Säntis.

Sensitive equipment will be located near each measurement point on the tower inside a specially designed metallic box. The boxes were designed to withstand the harsh conditions of the tower in terms of humidity, temperature, electromagnetic compatibility and space constraints.

The sensors' output is coupled to the high-speed digitizer (NI PCI-5122) via a fiber optic analog-to-digital / digital-to-analog link. The selected links, excluding the fibers, are manufactured by Terahertz and they exceed the output bandwidth of the Rogowski coils by a factor greater than 5 (*25MHz -3dB* cutoff and DC response with a sampling rate of *100MS/s*) and have a 12-bit resolution at *±5V*, giving a SNR_{max}=*74dB*. An industrial *850nm* monomode fiber is used to carry the optical signals.

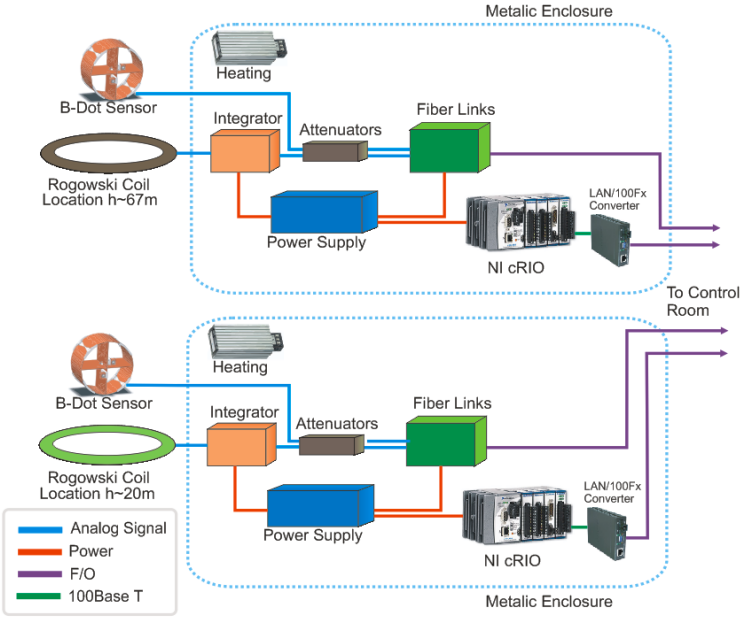

Figure 1: **(a) Säntis Telecommunication Tower near St. Gallen in northeastern Switzerland, (b) schematic of the current measurement system on the Säntis Telecommunication Tower.**

Acknowledgments – This work has been carried out within the framework of the European COST Action P18. Financial support from the Swiss Office for Education and Research SER (Project No. C07.0037) and the Swiss National Science Foundation (Project No. 200021-122457) are acknowledged.

References

1. A. Rubinstein, C. Romero, M. Paolone, F. Rachidi, M. Rubinstein, P. Zweiacker, B. Daout, "Lightning measurement station on Mount Säntis in Switzerland", 10th International Symposium on Lightning Protection, Curitiba, Brazil, November 9-13, 2009.

978-1-4244-5050-3/10/$26.00 ©2010 IEEE

Dependence of Ultra-Wideband Peak Power Measurements on Makes of Microwave Spectrum Analyzers

Akio Yokokawa [1], Atsushi Tomiki [2], and Takehiko Kobayashi [1]
[1] *Wireless Systems Laboratory, Tokyo Denki University*
[2] *Institute of Space and Astronautical Science, Japan Aerospace Exploration Agency*

E-mail: yokokawa@grace.c.dendai.ac.jp

Microwave Spectrum analyzers (SAs) are widely used to measure average and peak power spectra of ultra wideband (UWB) signals. Whereas the average power is measured in a 1-MHz resolution bandwidth (RBW), the UWB peak power is usually defined in a 50-MHz RBW in accordance with an ITU-R recommendation [1]. Most of the SAs, however, are not equipped with the 50-MHz RBW, and hence the power spectrum measured in a narrower RBW must be converted into the 50-MHz-RBW peak power spectrum. The conversion formula, however, has not been well established. The RBW is defined by CISPR [2] with an impulse bandwidth (IBW) for peak power measurement, but most SAs do not strictly follow the CISPR definition. In the present paper, the IBWs of seven different SAs (A to G) were measured by using an impulse signal (duration = 10 ns), as shown in Fig. 1. Next, three different UWB signals (MB-OFDM, DS-UWB, and DS-SS) were measured in a 1-MHz RBW with seven SAs, and then the power spectra were converted into 50-MHz peak power spectra by applying the conventional (using RBW) and new (using IBW) formulas [3]. These UWB signals were also measured with a digital storage oscilloscope (DSO) and then fast-Fourier-transformed into 50-MHz-RBW spectra. The converted spectra of the DS-UWB signal are depicted in Fig. 2. The spectra converted by RBW scattered more than 4 dB in comparison with the DSO measurement, but those by IBW fell within approximately 1 dB. For the three signals, the new formula using IBW instead of RBW yielded the consistent peak power spectra, which were found to be independent of the makes of SAs and to agree with the DSO measurement. The use of IBW-based formula is recommended for the UWB peak power measurement.

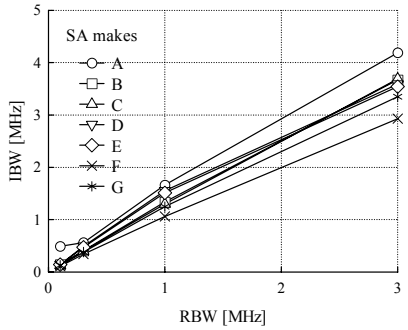

Fig. 1. The measured impulse bandwidth versus the resolution bandwidth for seven different SAs.

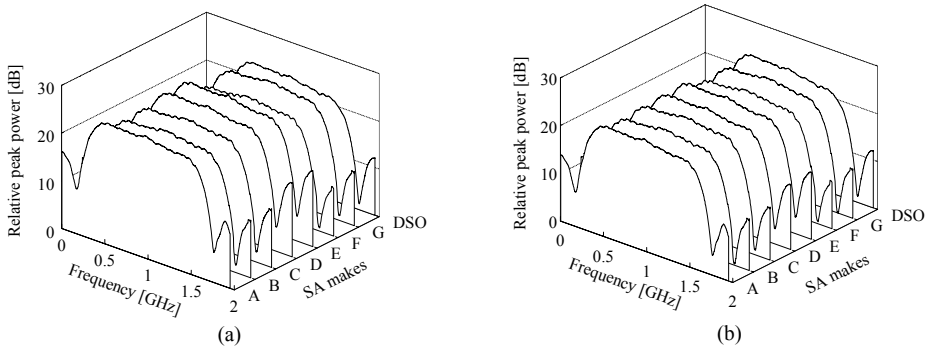

Fig. 2. Power spectra of DS-UWB signal converted from measurements with SAs A to G (RBW = 1 MHz) by using: (a) RBW and (b) measured IBW, and measured with DSO and fast –Fourier-transformed.

Acknowledgments - The authors would like to thank Anritsu Inc. and Rohde & Schwarz Japan K.K. for their help in lending spectrum analyzers. The authors also thank N. Onodera of Tektronix Japan Ltd. for his help.

References

1. Rec. ITU-R, SM. 1754, 2006.
2. CISPR Publication 16-1-1, 2004.
3. J. Takada *et al*., IEICE Trans. Fundamentals, E88-A, 9, pp. 2252-2263, 2005.

978-1-4244-5050-3/10/$26.00 ©2010 IEEE

Scattering properties of a diplexer for S/X band gigawatt level high power microwaves

Guolin Li, Ting Shu, Chengwei Yuan, Jun Zhang, Zhenxing Jin, Qiang Zhang, Jie Yang and Dapeng Wu

College of Optoelectronic Science and Engineering, National University of Defense Technology, Changsha, 410073, P.R.China

As the HPM technologies gradually matured, technologies for enhancing the output capacities of high power microwaves are becoming more and more attractive. One solution for enhancing the output capacities of HPM sources is taking advantage of frequency selective surface (FSS) to form a diplexer for microwave beams with different frequencies. In this paper, the S band HPM is reflected by the FSS in the diplexer and the X band microwave transmits through the FSS to have the same propagation direction with each other. However, according to our previous work, when the peak power and pulse duration increase, the microwave breakdown problem become obvious. To increase the power handling capacity, a diplexer with a new metallic FSS consists of several cylindrical rods is fabricated. The further experiments reveal that, the radiation pattern of the applied antenna itself and the radiation patterns reflected or transmitted by the FSS are in good agreement. With the illumination of 1.8GW, 80ns S/X band high power microwaves, no pulse shortening or flashover phenomenon has occurred.

Index terms: Frequency selective surface, high power microwave, diplexer

978-1-4244-5050-3/10/$26.00 ©2010 IEEE

An all solid-state, rolled strip pulse forming line with low impedance and compact structure

Shi Yang, Hui-Huang Zhong, Bao-Liang Qian, Han-Wu Yang, Cheng-Wei Yuan, Zhi-Qiang Li

(College of Photoelectrical Science and Engineering, National University of Defense Technology,

Changsha, 410073, People's Republic of China)

***Abstract*:** An all solid-state and compact pulsed power device is constructed and investigated extensively. A new model of an all solid-state, rolled strip pulse forming line (PFL) with low impedance and compact structure is introduced and its characteristic parameters are analyzed theoretically. The electromagnetic field distribution and the formation process of the pulse are calculated by software. Based on the theoretical analysis and simulated results, a rolled strip PFL configuration with 20 kV output voltage, 230 ns pulse duration, and 0.5 Ω characteristic impedance was designed and manufactured. The strip line uses mylar (DMD film) as the dielectric and a copper tape as the conductor. When it is unrolled, the dimension of the strip line is 23000 mm×400 mm×1.6 mm. It turns into a cylinder of diameter 311 mm after the strip is rolled. The size and weight are ten times smaller than those of traditional dielectric (oil or pure water) PFL with the same required electrical parameters. Two experiments were performed using the strip line as a transmission line and a PFL, respectively. In the experiment of transmission line, there was a voltage signal delay of 115 ns, and the signal distortion was not initiated obviously. The PFL experiment showed that a 17.8 kV, 270 ns (FWHM) voltage pulse being quasi-square wave on the load was obtained.

***Index Terms*: Pulsed power, Rolled strip pulse forming line; Characteristic impedance; DMD film**

978-1-4244-5050-3/10/$26.00 ©2010 IEEE

Horizontal Fast Rise EMP Project

D. Belt, A. Mazuc and D. Brown,
Naval Air Systems Command
Patuxent River, MD 20670

During the past 25 years, the Horizontally Polarized Dipole (HPD) Simulator shown in Figure 1, has provided the High Altitude Electromagnetic Pulse (HEMP) early time (E1) T&E capability to various Naval programs such as the E-6A/B, the Executive Transport VH Helicopter, F/A-18 A/B/C/D/E/F/G, and other Office of Secretary of Defense (OSD) programs. These programs as well as new programs (e.g. the Navy's new P-8 Poseidon multi-mission maritime patrol aircraft and the Joint Strike Fighter (JSF) (three variants)) have EMP (E1) T&E requirements. The Defense Threat Reduction Agency (DTRA) with the help of the Naval Air Systems Command (NAVAIRSYSCOM) and Air Force Systems Command is developing a new military standard for HEMP protection of military aircraft, MIL-STD-3023 (Draft). The new mil-standard addresses test and hardening methods, test environments, and hardness margins for various aircraft mission types. The need to provide a quality high level test environment continues and is expected to grow dramatically. Increases in T&E workload require a reliable test capability within the DoD that satisfies the classified environment specified in MIL-STD-2169B; the environment for aircraft and weapon systems testing.

Figure 1: E-6A at the HPD
Naval Air Warfare Center, Aircraft Division, Patuxent River MD

The test capability for large aircraft and weapon systems located at Patuxent River is scheduled to be upgraded by the Horizontal Fast Rise Electromagnetic Pulse Project (HFREMP) in mid 2010. The HFREMP project will develop and field a new environmentally sealed, fast rise, EMP pulser to produce the environment specified in MIL-STD-2169B. It will provide a significant increase in test capacity (more test days and time per day) and correct deficiencies noted by DTRA in an assessment of the current capability. The new pulser will provide enhanced reliability through the use of

978-1-4244-5050-3/10/$26.00 ©2010 IEEE

new parts, support equipment, technology, and decrease downtime due to humidity and weather. The HFREMP project also improves the elliptical hybrid antenna and developed an alternative antenna, a horizontally polarized guided wave antenna. This paper presents the specifications, design approach, and status of the HFREMP pulser project with a primary focus on the design and development of the two horizontally polarized antennas. The HFREMP project is funded through the Central Test and Evaluation Investment Program (CTEIP). CTEIP was established by the DoD to provide joint initiatives, avoid unwarranted duplication of capability, and increase interoperability through capability improvement projects for the DoD Major Ranges and Test Facility Bases (MRTFB).

Coherent Amplification of High Power Microwave and Terahertz Radiation from Electron Beams-Plasma Systems

Balram Prasad [1], **Kenneth R. Grimm** [2]
[1] *Physical Scientist, Retired, Defense Threat Reduction Agency, Ft Belvoir, VA*
(Currently consultant to ITT Advance Science & Engineering)
[2] *Electromagnetic Research Engineer, BAE Systems, Inc., Technology Solutions and Services, Ft Belvoir, VA*

E-mail: balramprasad@gmail.com

Counter-streaming large-diameter electron beams, interacting with ionized gas plasma in a steady-state laboratory experiment, have been observed to generate coherent microwave radiation at twice the plasma frequency ($2\omega_p$) and radiating with a quadrupole radiation pattern. The microwave power density was non-linearly enhanced over the power density obtained from the single beam-plasma system. When the counter-streaming electron beams interacting with the plasma volume reach a steady state and had the same average beam energy, the radiated microwave power-density scaled exponentially with the average input electron-beam energy and increased with ion mass of the plasma. These exciting experimental results were published in 1984 [1], and are characteristic of a "MASER" like action in a colliding electron beams-plasma system. However, until now, a theoretical explanation of this effect has been unavailable. In this paper, we employ quantum formalism of the weak plasma turbulence theory for 'plasma emission' in solar atmospheres [2] and [3], and show that the experimental results observed in [1] are accurately explained, giving a proof-of-concept for a classical 'MASER' in a steady state colliding beams-plasma system. A quasi-quantum or semi-classical theory of three-wave interaction processes in a steady state plasma gas, pumped by a single electron-beam and/or two opposing electron beams, is developed for analyzing all the results of the laboratory experiment. The three–wave scattering involves electron beam excited longitudinal Langmuir, L and Ion-acoustic S waves to produce Raleigh scattering of longitudinal $L \pm S = L'$ waves in the plasma which will further scatter against the L waves to produce a third wave that is transverse, represented by $L + L' \rightarrow T_2 (2\omega_p)$ radiation. An analytical expression for the second harmonic radiation power, $P(2\omega_p)$, is derived for the total microwave radiation output in the steady state experimental plasma interaction volume that involves only plasma parameters and electron beam parameters. These parameters can be optimized to produce a new stable source of high power microwave radiation from electron beam-plasma systems. Besides the 3-wave scattering of Langmuir L and Raleigh scattered longitudinal L' waves, the so-called Raman scattering processes also do occur as denoted by $L + T_2 \rightarrow T_3 (3\omega_p)$, $L + T_3 \rightarrow T_4 (4\omega_p)$, and generalized to $L + T_n \rightarrow T_{n+1} \{(n+1)\omega_p\}$, where $n \geq 2$, each n of which depends on the calculation of the value of T_2 wave described above. Hence the third and higher harmonic spectral emissions in the same beam plasma system have been calculated separately as in [3]. The theoretical expressions of the radiation power of the second harmonic and that of the third and higher harmonic spectra have been developed in [4]. The analytical expressions of the $P(2\omega_p)$ and $P\{(n+1)\omega_p\}$ in this work, allow numerical prediction of the Terahertz (THz) spectral region radiation power at hyper-band frequencies having potentially enormous power levels. By operating the triple plasma machine used in [1] at optimized beam and plasma parameters, 30 to 50 kilo watts of radiated wave power in the 0.1 to 3 THz spectrum can be produced and used as a source of hyper-band (very wideband) THz radiation. The hyper-band source of high power THz radiation has many applications for national defense.

References

[1] T. Intrator, N. Hershkowitz, and C. Chan, "Experimental observations of nonlinearly enhanced $2\omega_{UH}$ electromagnetic radiation excited by steady-state colliding electron beams, "Phys. Fluids 27(2), Feb. 1984.
[2] Iver H. Cairns, Second harmonic plasma emission involving ion sound waves, J. Plasma Physics, (1987) , vol. 38, part 2, pp 179-198.
[3] Iver H. Cairns, Third and higher harmonic plasma emission due to Raman Scattering, J. Plasma Physics, (1987) vol. 38, part 2, pp 199- 208.
[4] B. Prasad, Multiple Harmonic Emission from Electron Beams Excited Gaseous Plasmas, Abstract published in the proceedings of AMEREM Symposium 2002, Naval PG School, Annapolis, MD.

978-1-4244-5050-3/10/$26.00 ©2010 IEEE

FDTD Modeling of Polarization of a Conductor in a Quasi-Uniform Electric Field

Yoshihiro Baba[1] (ybaba@mail.doshisha.ac.jp)
Vladimir A. Rakov[2] (rakov@ece.ufl.edu)
[1]Department of Electrical Engineering, Doshisha University, Kyotanabe, Kyoto 610-0321, Japan
[2]Department of Electrical and Computer Engineering, University of Florida, Gainesville, FL 32611, United States

Using the finite-difference time-domain (FDTD) method for solving Maxwell's equations, we have examined the polarization process of a vertical conductor in a quasi-uniform (but not static) external electric field. The objective of this study is to model some basic processes possibly related to lightning initiation in thunderclouds. Lightning initiation may involve the creation of an elongated conducting region in the cloud ("lightning seed") by a high-energy cosmic-ray particle via the runaway breakdown mechanism that requires an order of magnitude lower electric fields than the conventional breakdown. This "lightning seed" would be polarized in the cloud electric field and serve to enhance the electric field near its extremities possibly to the values required for the conventional breakdown (Rakov 2004 [1]). Solomon *et al.* (2001 [2]) estimated the conductivity of the "lightning seed" to be of the order of 10^{-4} S/m. According to Gurevich *et al.* (2003 [3]), the formation of a "lightning seed" in the cloud by a cosmic-ray particle with energy of 10^{16} eV via the runaway breakdown mechanism is associated with a current pulse having an amplitude of 100-200 A. Further, Gurevich and Zybin (2005 [4]) hypothesized that the compact intracloud discharges (CIDs) giving rise to narrow bipolar pulses (NBPs) also involved the runaway breakdown and were similar to the lightning initiation process, the difference between the two being related to generally higher altitudes (>10 km) at which CIDs occurred. CID peak currents are expected to be of the order of tens of kiloamperes.

In this study, the quasi-uniform electric field was excited between two large circular parallel plates, whose radius and spacing were each 500 m, by a uniform vertical electric-field source placed at the periphery of the cylindrical computational domain. The magnitude of excitation electric-field was set to 100 kV/m. The length of conductor, located along the axis of the domain and equidistant from the plates, was set to 100 m, and its radius was set to 1 m. The following results were obtained.

The peak of the polarization current is significantly influenced by the external electric-field risetime (RT) when the conductivity is relatively high ($\sigma = 10^4$ S/m): 1.8, 0.67, and 0.35 kA for RT = 2, 5, and 10 μs, respectively. On the other hand, it is not much influenced by the risetime when the conductivity is relatively low ($\sigma = 10^{-4}$ S/m): 100, 76, and 75 A for RT = 2, 5, and 10 μs, respectively. Although the electric field at the conductor extremity is not much influenced by the external-field risetime or the conductivity, it increases more slowly with time as the conductivity decreases. The electric field enhancement factor at the conductor extremities is about 15.

The peak of the polarization current increases with increasing the conductor radius. As expected, the electric field at the conductor extremity is reduced as the radius increases.

When the conductivity increases from 0 to 10^{-4} S/m linearly within 5 μs, the risetime and magnitude of the polarization current are almost the same as those for the case of the constant conductivity of 10^{-4} S/m (76 A). When the conductivity of the 100-m-long conductor increases from 0 to 10^4 S/m linearly within 5 μs, the magnitude (20 kA) of the polarization current is much larger than that for the case of the constant conductivity of 10^4 S/m (0.67 kA).

When a conductor of constant conductivity $\sigma = 10^{-4}$ or 10^4 S/m extends from 0 to 100 m at a rate of 300 m/μs (the speed of light), the polarization current and the electric field at the conductor extremities are similar to those for a 100-m-long conductor whose conductivity linearly increases from 0 to 10^{-4} or 10^4 S/m within 5 μs.

References

[1] V. A. Rakov. "Initiation of lightning in thunderclouds," *Recent Res. Devel. Geophysics*, vol. 6, pp. 1-35, Research Signpost, India, 2004.

[2] R. Solomon, V. Schroeder, and M. B. Baker, "Lightning initiation -- conventional and runaway-breakdown hypotheses," *Q.J.R. Meteorol. Soc*., vol. 127, pp. 2683-2704, 2001.

[3] A. V. Gurevich, L. M. Duncan, A. N. Karashtin, and K. P. Zybin, "Radio emission of lightning initiation," *Phys. Lett. A*, vol. 312, pp. 228-237, 2003.

[4] A. V. Gurevich, and K. P. Zybin, "Runaway breakdown and the mysteries of lightning," *Physics Today*, pp. 37-43, May 2005.

978-1-4244-5050-3/10/$26.00 ©2010 IEEE

Electromagnetic Model of Lightning Channel of Ground-to-Cloud Stroke Specific to Winter Lightning

Masaru Ishii, and **Mikihisa Saito**
The University of Tokyo, Tokyo, Japan, 153-8505
E-mail: ishii@iis.u-tokyo.ac.jp

Electromagnetic models of lightning return strokes have been proposed [1] to reproduce the electric and magnetic field waveforms, which are highly dependent on the distance from the lighting channel [2]. An electromagnetic model represents the lightning channel by a lossy antenna, and the associated electromagnetic fields are calculated numerically. It has lower degree of freedom compared with engineering models of a lightning channel [2], and such restriction may be favorable to study the influence of the lightning channel geometry on the waveforms of associated lightning electromagnetic pulses (LEMP) in the time range from zero to few hundreds of microseconds.

High-current upward lightning discharges were discovered only recently, which are the causes of high number of double circuit transmission-line faults in winter in Japan [3]. An example of the electric field waveform associated with a negative ground-to-cloud (−GC) stroke is shown in Fig. 1, characterized by a narrow positive large pulse followed by a narrow pulse of similar amplitude in the opposite polarity. The full width at half maximum (FWHM) of the narrow first pulse is mostly less than 20 μs, which is much narrower than typical pulse widths, several tens of μs, of LEMP from normal return strokes. The peak current indicated in Fig. 1 is estimated from the normalized peak electric field by using the same relationship only applicable to subsequent negative return strokes, though this estimation may contain considerable error.

A proposed electromagnetic model of a –GC stroke consists of a vertical channel attached to ground, which represents an upward leader, and a short horizontal channel on the top of the vertical channel. Both channels are connected with a switch and a voltage source in series, and switching occurs in the altitude. NEC-4 is employed for the calculation. Fig. 2 shows a calculated electric field waveform at 60 km. R, L and r indicated in the figure are loaded resistance, inductance and radius of the model channel, respectively. The calculated waveform reproduces the overall shape of the initial bipolar pulse from natural –GC strokes reasonably. By increasing loaded resistance, the amplitudes of the second and the third peaks of the calculated waveform decrease.

Similarly, positive ground-to-cloud strokes in winter which produce characteristic bipolar LEMP can also be reproduced by an electromagnetic model having a longer horizontal branch. The channel geometries of the proposed electromagnetic models are constructed based on observation of VHF radiation [4] from lightning discharges. The calculated result may indicate adequacy of the inferred structure of the lightning channels, as well as the usefulness of the electromagnetic model in studying lightning phenomena.

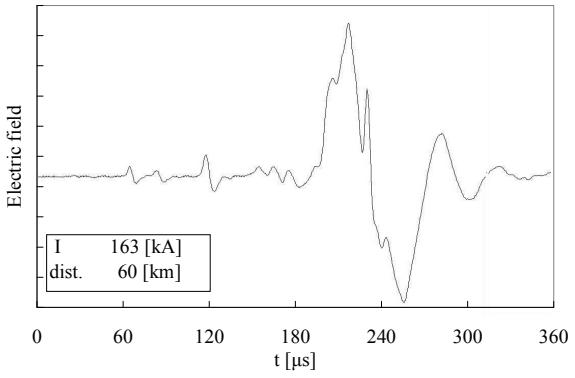

Figure 1: **Electric field waveform associated with negative upward lightning stroke (−GC) simultaneously recorded with a transmission-line fault in winter in Japan.**

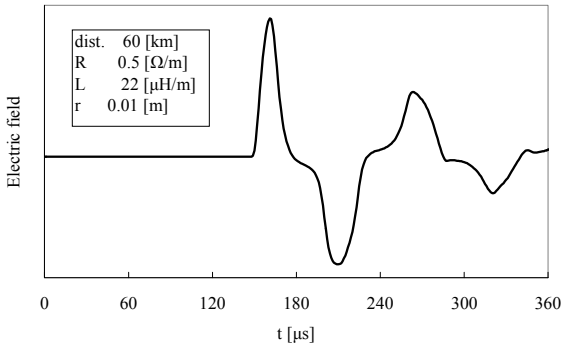

Figure.2: **Electric field waveform at 60 km from model lightning channel of −GC stroke calculated by electromagnetic model.**

References

1. Y. Baba, and M. Ishii, "Characteristics of Electromagnetic Return-Stroke Models," IEEE Transactions on Electromagnetic Compatibility, vol. 45, No. 1, pp.129-135, 2003.
2. V. A. Rakov, and M. A. Uman, Lightning - Physics and Effects, Cambridge, U. K.: Cambridge University Press, 2003.
3. M. Ishii, and M. Saito, "Lightning Electric Field Characteristics Associated with Transmission-Line Faults in Winter," IEEE Transactions on Electromagnetic Compatibility, vol. 51, No. 3, pp.459-465, 2009.
4. M. Ishii, M. Saito, and N. Itamoto, "High Current Upward Lightning Flashes in Winter," Proc. 13th Int. Conf. on Atmospheric Electricity, Beijing, pp.321-324, 2007.

978-1-4244-5050-3/10/$26.00 ©2010 IEEE

Microwave Pulse Compression Experiments at Low and High Power

Everett G. Farr[1], Leland H. Bowen[1], Carl E. Baum[2] and William D. Prather[3]
[1]*Farr Research, Inc., Albuquerque, NM, USA, 87123*
[2]*University of New Mexico, Albuquerque, NM, 87131*
[3]*Air Force Research Laboratory, Directed Energy Directorate,Kirtland AFB, NM, 87117*
E-mail: efarr@farr-research.com

We describe here experiments to develop the technique of Microwave Pulse Compression (MPC). This is a method of concentrating and amplifying the power of a microwave pulse by reducing its duration. It is thought that this technique may be of use as a source for vulnerability testing . MPC involves exciting a resonant cavity with a microwave source, and then firing a shorting switch that destroys the resonance condition, as shown in Figure 1. The compressed pulse is then delivered to the output port at a higher peak power and smaller pulse width than the original microwave pulse. Power is pumped into a resonant rectangular waveguide, whose length is an integral number of half guide wavelengths. The cavity is bounded at the input by an inductive iris, and at the output with an H-plane tee with sliding short. After power has built up, a switch is fired that destroys the cavity resonance, and the power exits at the output. To demonstrate the technique, we built two MPC devices operating at 1.3 GHz, one operating at low power, and the other at high power. In our low-power MPC device, we amplified 1 kW up to 33 kW, at a repetition rate of 10-50 Hz. In our high-power MPC device, we amplified 2.8 MW up to 50 MW, at a repetition rate of 5-160 Hz. All of our switches were triggered gas switches with trigatrons, filled with either low-pressure air (~10-13 mTorr) at low power, or ~20 psig SF_6 at high power. Future work could involve three areas. First one could increase the power with a smoother cavity and by sealing leaks, so one could operate at higher pressure. Second one could design a more compact microwave source, to make the entire system more portable. Third, one could design a frequency-tunable cavity, to allow more flexibility in vulnerability testing.

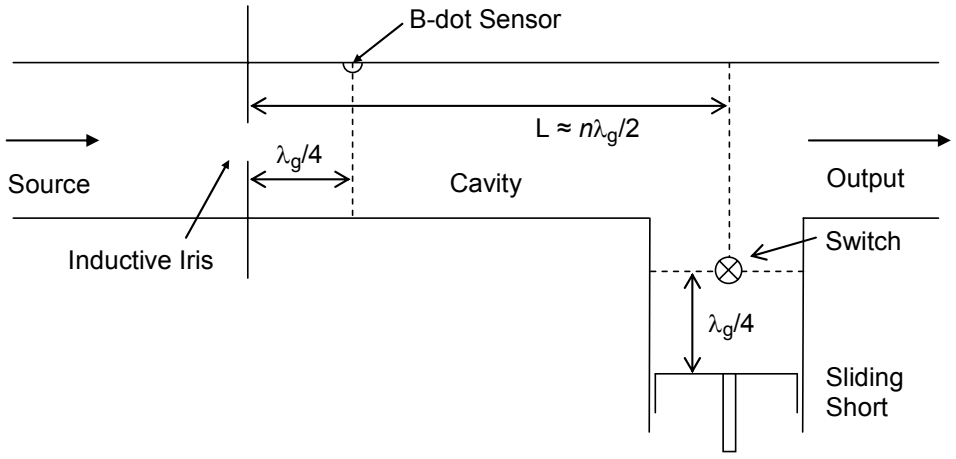

Figure 1: **A sketch of Microwave Pulse Compressor, looking at the broad side of the waveguide.**

978-1-4244-5050-3/10/$26.00 ©2010 IEEE

Microwave compressors with operating H_{11} mode doubling the maximum output power

Yury G.Yushkov, Sergey N.Artemenko, Vladimir A.Avgustinovich and **Sergey A.Novikov**
Tomsk Polytechnic University, Tomsk, Russia, 634028
E-mail: nsa@npi.tpu.ru

A compressor with a volume cavity usually has one switch and one output element. That considerably limits the output power depending on electrical strength of these elements. One option to overcome the limit is using one switch for two storage volumes or several outputs in a single cavity.

The compressors used in experiments were circular ones where the H_{11} mode was switched to set the extraction mode of operation [1]. It was shown that the interference switch on the basis of circular waveguide H-tee is capable to operate up to the critical diameter of H_{21} mode. That was exhibited by the transition losses - frequency relationship which showed the losses falling down at approximately the critical frequency of H_{21} mode. Conditions of effective switching of a travelling H_{11} wave in a waveguide were determined at low power and high power measurements. At high power experiments the switching conditions were realized by forming a plasma area of high pressure gaseous discharge. The level of switched power was determined by the parameters of available primary microwave source and was within 400 MW. The waveguide diameter was as large as the critical diameter of H_{01} and E_{11} modes. The studied switches were used in new designs of compressors with increased output maximum power. The paper presents the external view and construction of S-band compressors which supply doubling of maximum output power and beyond. The single switch was used to provide simultanuous operation of two cavities which doubled the output power and also it was uused in the single cavity with four parallel outputs. Estimations showed that these type of compressors could provide several megawatts of output power of the 3...10 ns output pulses at 17...22 dB amplification factor.

References

1. V. A. Avgustinovich, S. N. Artemenko and V. L. Kaminsky, Studying of microwave compressor switch in a circular waveguide. Instruments and Experimental Techniques, vol. 52, 2009.

978-1-4244-5050-3/10/$26.00 ©2010 IEEE

Method Development for compensation of coaxial cable loss in measuring

Seung-Moon Han[1], Sun-Mook Hang[1], Joo-Il Hong[1], Uk-Youl Huh[1], Chang-Soo Huh[1], and **Jin-Soo Choi[2]**
[1]*Inha University, Inchon, South Korea*
[2]*Agency for Defence Development, Daejeon, South Korea*
E-mail: holyjoyhan@hotmail.com

HPEM (High Power Electromagnetics) phenomena analysis on any equipments or facilities is very important & critical schemes on nowadays [1]. Especially Measuring Wide or Hyper wide band HPEM signals with any antennas, coaxial cables which are attached to the sensors or antennas is very critical on signal distortion of the coaxial cable due to signal dispersion and loss. Especially very fast rise time Wide Band HPEM signals are more sensitive according to cable characteristics. In this research, the new compensation method for measuring EMP signal is studied and pulse measurement library of the coaxial cable used in the experiment. The S21-parameter of the coaxial cable is measured and it is mathematically modeled for equation generating. For time domain EMP signal, Complex Laplace transform and Cauchy's contour integral theorem with two singularities are used. To consider the pulse dispersion and loss, the change of pulse rise time, FWHM, peak values are mathematically calculated. The results show that the time parameters of pulse have little change and change of pulse peak value is very critical with 20% error. The coaxial compensation library for pulse distortion is developed with time constants of double exponential pulse and pulse time parameters.

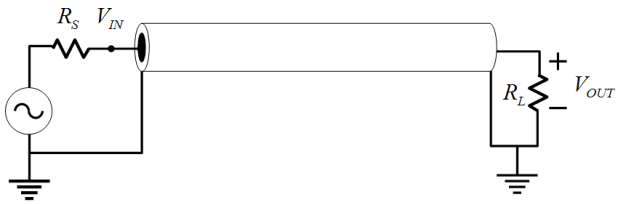

Figure 1: **use of long coaxial cable**

Acknowledgments – This work has been supported by ADD (Agency for Defense Development) and DAPA (Defense Acquisition Program Administration)

References

1. William A. Radasky, Carl E. Baum, Manuem W. Wik, "Introduction to the Special Issue on High-Power Electromagnetics (HPEM) and Intentional Electromagnetic Interference (IEMI)", *IEEE Trans. Electmagn. Compat.*, vol. 46, no. 3, Aug 2004

978-1-4244-5050-3/10/$26.00 ©2010 IEEE

Power Gain and Energy Patterns of Impulse Radiating Antennas (IRAs)

D. V. Giri
Pro-Tech, 11-C Orchard Court, Alamo, CA 94507-1541
Dept. of Electrical & Computer Engineering, University of New Mexico, Albuquerque, NM 87131

and

F. M. Tesche
EM Consultant, 1519 Miller Mountain Road, Saluda, NC 28773
Holcombe Dept. of Electrical and Computer Engineering
Clemson University, Box 340915, Clemson, SC 29634-0915

Abstract

Gain and beam width of antennas vary with frequency and are well defined in the frequency domain. Standardized definitions of these performance parameters do not yet exist in the time domain for pulsed antennas. In this presentation, we define a peak power gain of a reflector type of an IRA along its optical axis. In doing so, well established expressions of the radiated far fields have been used. This peak power gain is valid at one instant of time, when the electric field on axis reaches its peak value in the far field.

Furthermore, one question that often comes up is "how is the energy from the pulser radiated in space?" A power pattern is a cumbersome descriptor for a hyperband antenna such as an IRA because of the multitude of frequencies involved. In this note we explore the energy pattern of the IRA which holds good both in time and frequency domains. An energy pattern is useful in visualizing where the energy provided to the IRA is going. It is further noted that the energy and power patterns are identical for a CW antenna, where as they can be vastly different for pulsed antennas.

978-1-4244-5050-3/10/$26.00 ©2010 IEEE

INDUCED TRANSIENTS ON AN UNDERGROUND CABLE BY HYPERBAND SIGNALS

K. Sunitha[1], M. Joy Thomas[1] and D. V. Giri[2]

[1]Pulsed Power and EMC Laboratory, Dept. of Electrical Engineering
Indian Institute of Science, Bengaluru- 560012, INDIA

[2]Pro-Tech, 11-C Orchard Court, Alamo, CA 95407-1541 USA
Dept. of Electrical and Computer Engineering, Univ. of New Mexico, Albuquerque, NM

Abstract

Impulse radiating antennae have wide variety of applications such as the detection of buried objects, ionospheric research and target discrimination in a cluttered environment. The hyperband electromagnetic fields coming out of the IRAs can interfere with the objects in the path where it travels. This can be an object laid underground or any object on or above the ground.

Underground cables are used to a greater extent now-a-days for communication purposes in urban cities and towns. Some of the frequencies of the electromagnetic fields from an IRA can easily penetrate through the soil and can reach the buried cable. This will illuminate the cable with the UWB fields and induce currents and voltages in it. Since the communication cables or even the buried data cables are connected to sensitive equipment, even a slight rise in the voltage or the current at the terminals of the equipments can become a serious problem for the smooth operation of the system. In this aspect it is worthwhile to determine the effect of an IRA's electromagnetic field on the cables laid underground. Treating this as an electromagnetic compatibility problem, the victim circuit becomes the cable, the source of interference being the electric field from the IRA and the air and soil forms the path of propagation of the interference signal to the victim circuit. As a first step to this computation, we need to know the exact nature of the electromagnetic field from an IRA at different distances from the antenna. Using the concept of the reflection and transmission of the field at the earth's surface, the amount of the field coupling to the cable can be found. This in turn can be used for the determination of the induced current and voltage on the cable which give an exact measure of the interference on the cable. This work deals with the coupling effect of IRA fields on buried telephone cables.

978-1-4244-5050-3/10/$26.00 ©2010 IEEE

Wideband TLM Modeling of Planar Antennas on Saturated Ferrite Substrate

Arij Farhat, Sandrick Le Maguer, Patrick Queffelec and Michel Ney

Lab-STICC - UMR 3192, Telecom Bretagne, Technopôle Brest-Iroise, CS 83818 - 29238 BREST Cedex 3, France

***Abstract* — A generalized TLM modeling method has been developed and applied for the design of patch antennas which substrate is a saturated ferrite. The model is rigorously constructed by using Maxwell's equations that make it a unified general TLM formulation. The permeability tensor of the saturated ferrite is derived from the Polder formulations. Results, compared with a commercial simulator, give good agreement for the studied structures. Our aim is to insert a new permeability tensor model for non-saturated ferrite materials in the TLM algorithm to allow the simulation of microwave structures integrating ferrites whatever their magnetization state.**

***Index Terms* — TLM, dispersive and anisotropic media, ferrite, microstrip, patch antenna, permeability tensor.**

I. INTRODUCTION

The anisotropic properties of ferrite materials are widely used to insure the non-reciprocal character of several microwave devices such as circulators and isolators. Their field-dependent permeability enables the operating of tunable circuits (filters, phase shifters, etc.). More recently, their high refractive index has found interest in the size reduction of patch antennas. It has been demonstrated that antennas with a magneto-dielectric substrate exhibiting a permeability greater than its permittivity shows better performances that those deposited on purely dielectric substrates [1].

In order to assist the design of ferrite-based microwave devices, one needs to have a proper design tool enabling the prediction of the microwave behavior of ferrite samples whatever their magnetization state. For instance, it is considered to use hexaferrite materials that operate at the remanent state to work out self-biased circulators. It would be also very interesting to be able to predict the variation of the performances of patch antennas deposited on a ferrite substrate as a function of its magnetization state.

Magnetized ferrites are anisotropic media. Their electromagnetic properties must be represented by a tensor quantity, named the permeability tensor. Therefore, usual permeability model based on the Polder formulations [2] is only valid for a saturated sample. The objective of the research is manifolds: First, to develop a rigorous model for field computation in such complex media and second to insert an innovative model of non-saturated ferrites [3] into the algorithm.

Indeed, presently there is no commercial simulator capable to account for the presence of non-saturated magnetic materials that imply complex physical phenomena such as:

- Non-homogenous internal polarization field implying non-homogeneous permeability,
- Non-saturated zones in plate ferrite samples due to demagnetizing fields even for substrates biased with a strong DC field,
- Dynamic interactions between magnetic domains and grains in non-saturated regions of the ferrite substrate,
- Magnetostatic modes.

The above phenomena must be accounted for in the model as they strongly affect the performances of the device in terms of bandwidth, insertion losses, etc. Also, for circulators they can preclude their miniaturization [4].

Finally, the time-domain character of the TLM not only allows a wide band characterization but also accounts for the presence of potential non linearities.

In order to predict the dynamic behaviour of polycrystalline ferrites for arbitrary magnetization state, it is proposed a theoretical approach which gives access to all components of the tensor as a function of the DC bias field strength and direction, of the sample geometry and static magnetic characteristics such as saturation magnetization, anisotropic magnetocrystalline field. Finally, sample structural properties (magnetic domains and grains shape) are accounted for by the model. Details of the theoretical approach proposed can be found in [3].

In the present paper, the first step of the research is described, i.e., to extend the TLM to dispersive and anisotropic media. Some pioneer work, based on the circuit analogy, to implement dispersive non isotropic media has been done in TLM [5]. This paper focuses on a formulation based directly on field Maxwell's equations [6]. It gives a clear and systematic derivation that constitutes a general approach which can be applied to any type of media.

II. TLM THEORETICAL MODEL

Let us consider a general anisotropic and dispersive medium in which electromagnetic quantities are governed by the general Maxwell curl equations in time-domain:

978-1-4244-5050-3/10/$26.00 ©2010 IEEE

$$\begin{bmatrix} \nabla\times\vec{H} \\ -\nabla\times\vec{E} \end{bmatrix} - \begin{bmatrix} \vec{J}_{ef} \\ \vec{J}_{mf} \end{bmatrix} = \frac{\partial}{\partial t}\begin{bmatrix} \varepsilon_0\vec{E} \\ \mu_0\vec{H} \end{bmatrix} + \begin{bmatrix} \underline{\underline{\sigma}}_e * \vec{E} \\ \underline{\underline{\sigma}}_m * \vec{H} \end{bmatrix} + \frac{\partial}{\partial t}\begin{bmatrix} \varepsilon_0\underline{\underline{\chi}}_e & 0 \\ 0 & \mu_0\underline{\underline{\chi}}_m \end{bmatrix} * \begin{bmatrix} \vec{E} \\ \vec{H} \end{bmatrix} \quad (1)$$

where χ_e and χ_m stand for the electric and the magnetic susceptibilities respectively, subscript *e* and *m* for electric and magnetic, * denotes the convolution operation, c_0 the vacuum light velocity and double underlined quantities are tensors [5]. For the SCN (Symmetrical Condensed Node) TLM, the presence of materials affects the field values at the node center.

These values are computed from the incident voltages travelling in the node arms by the following convolution process:

$$\begin{bmatrix} E_x \\ E_y \\ E_z \\ H_x \\ H_y \\ H_z \end{bmatrix}_c = [t]^{-1} \otimes \begin{bmatrix} E_x \\ E_y \\ E_z \\ H_x \\ H_y \\ H_z \end{bmatrix}_r \quad (2)$$

where the tensor $[t]^{-1}$ describes the anisotropic and dispersive electromagnetic properties of the material in the frequency domain.

Subsequently, a digital filtering is performed to carry out the above convolution in time domain and is based on the following approach: We start first with a set of points known analytically in the frequency domain which is in our case each element of the tensor $[t]^{-1}$. Then, by applying Prony's decomposition, an approximation of each term of the tensor is performed. Finally, we proceed to a digital filtering by performing a bilinear *z* transformation to obtain (2) in time-domain.

The application of the general procedure described by Peña and Ney in [6] for general media is new and not straightforward. However, it has the advantage to allow the development for all TLM nodes such as hybrid (HSCN) or super condensed (SSCN) nodes, by following the same general procedure. Consequently, it needs lots of complex manipulations and the detailed procedure will be described later. The present paper focuses on preliminary results.

III. Preliminary Validation Test

A. Microstrip line on ferrite substrate

A 14mm long, 0.6mm wide, 50 microstrip on a 1 mm thick ferrite substrate with the following characteristics: $4\pi Ms = 350\ G$, DC bias field $H_0 = 2940\ Oe$, $\Delta H = 33\ Oe$, $\varepsilon_r = 13.69$ was simulated under HFSS © [7], a commercial simulator based on the frequency domain Finite Element Method. For the saturated ferrite that is biased with magnetic DC field along the z-axis, the relative permeability tensor at a frequency ω, namely the Polder's tensor, is given by:

$$\mu = \begin{pmatrix} 1+\chi(\omega) & j\kappa(\omega) & 0 \\ -j\kappa(\omega) & 1+\chi(\omega) & 0 \\ 0 & 0 & 1 \end{pmatrix} \quad (3)$$

where $\chi(\omega)$ and $\kappa(\omega)$ are defined in [2].

The time domain results are transformed to the frequency domain using the FFT. The insertion loss S_{21} parameter given by both TLM and HFSS simulations are compared in Fig 1. Simulated results are in good agreement.

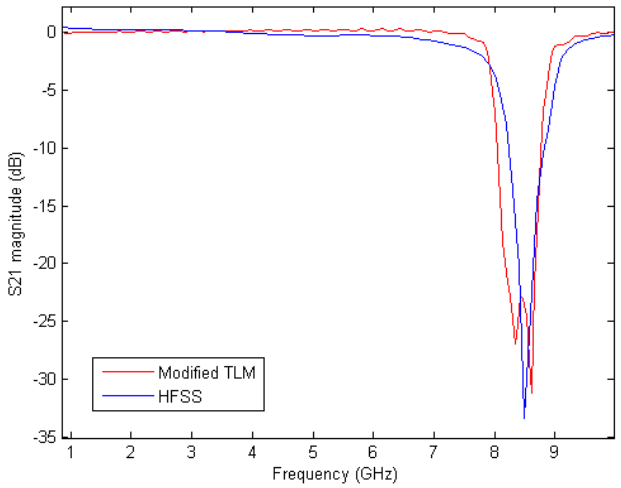

Fig. 1. The insertion loss S_{21} of the microstrip on magnetized ferrite substrate.

B. Microstrip patch antenna on ferrite substrate

A microstrip patch antenna on ferrite substrate with a fundamental resonance frequency of $f_0 = 8.0$ GHz as shown in Fig. 2 was also simulated. The patch is copper sputtered on ferrite.

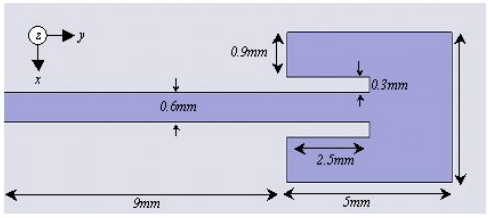

Fig. 2. Dimensions of the microstrip patch antenna, $f_0 = 8.0$ GHz.

The S_{11} parameter given by both TLM and HFSS simulations for the demagnetized and saturated ferrite substrates are compared respectively in Fig. 3 and Fig 4.

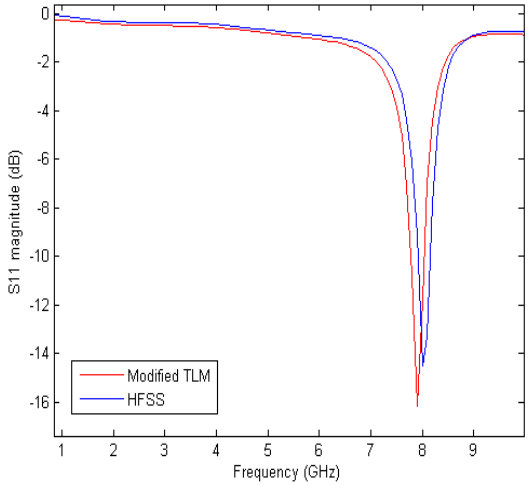

Fig. 3. S11 parameter of the microstrip patch antenna on demagnetized ferrite substrate, f_0= 8.0 GHz.

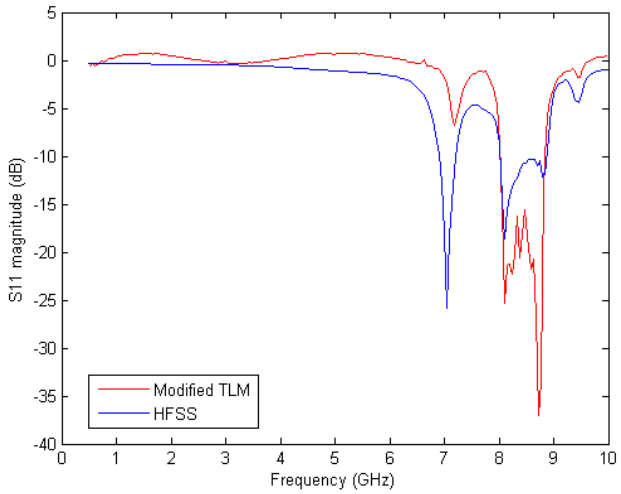

Fig. 4. S11 parameter of the microstrip patch antenna on saturated ferrite substrate.

Without the applied magnetic filed, the patch antenna has a fundamental resonance frequency of 8.0 GHz. The applied magnetic field shifts the fundamental resonance frequency and also generates new resonance frequencies.

The new resonance frequency is at 7.1, 8.1, 8.8 and 9.45 GHz. These frequencies, generated by the magnetized ferrite, are predicted by the new modified TLM algorithm and are in close agreement with the HFSS results.

As one can observe in Tab. 1, comparison between two different approaches yields some good matching.

TABLE I
PATCH f_0=8.0 GHZ
COMPARISON BETWEEN TLM AND HFSS

Patch antenna resonance frequency [GHz] (HFSS)	Patch antenna resonance frequency [GHz] (TLM)	Relative difference [%]
7.10	**7.193**	**1.3**
8.10	**8.098**	**0.02**
8.80	**8.718**	**0.9**
9.45	**9.480**	**0.3**

Note that assumptions used in the formulation of the Polder's tensor cause errors in simulation. A completely saturated magnetization state and a uniform applied DC magnetic field are assumed. All the above assumptions are only approximations of the real magnetic properties of ferrite and experimental conditions. The Polder's tensor formulation of the ferrite permeability does not include hysteresis phenomenon or the dynamic coupling between grains in polycrystalline ferrites which cause a broadening of the gyromagnetic absorption region.

Also the space and time discretization used in the TLM method cause numerical dispersion and that result in errors in simulated resonance frequencies. In addition, copper losses are not included in this TLM simulation. All the above factors may explain for the above differences observed between the simulated results.

VII. CONCLUSION AND FUTURE WORK

The TLM algorithm was established for the case of general anisotropic and dispersive media. The theoretical derivation was revisited, starting with Maxwell's equations, without invoking circuit analogy. The procedure is general and can be applied to derive the algorithm for extended TLM nodes. Preliminary results computed in the case of a dispersive and anisotropic medium show that the model is accurate when compared with a frequency domain approach.

Examples for non-saturated ferrites media in waveguides for which experimental measurements are available will be presented during the conference.

The ultimate objective is to insert a new pseudo analytic model for unsaturated hexaferrite that are used for planar non reciprocal components implemented in LTCC technology.

REFERENCES

[1] H. Mosallaei and K. Sarabandi, "Magneto-dielectrics in electromagnetics: concept and applications", IEEE Transactions on Antennas and Propagation, vol. 52, no. 6, pp. 1558–1567, June 2004.

[2] D. Polder, "On the theory of ferromagnetic resonance," Philosophical magazine, vol. 40, pp. 99-115, January 1949.

[3] P. Gelin, and P. Quéffélec, "Generalized Permeability Tensor Model: Application to Barium Hexaferrite in a Remanent State for Self-biased Circulators," IEEE Transactions on Magnetics, vol. 44, n°1, pp. 24-31, Jan. 2008.

[4] A. Guennou, B. Della, P. Quéffélec, P. Gelin, and J.L. Mattei, "Influence of the magnetic field nonuniformity on an X-band microstrip Y-junction circulator bandwidth: theory/experiment comparison," IEEE Transactions on Magnetics, vol. 43, n°6, pp.2642-2644, June 2007.

[5] J. Paul, C. Christopoulos, "Generalized material models in TLM\ Part 2: Materials with frequency-dependent properties," IEEE Trans. Antennas Propagation, vol. 47, no. 10, pp. 1535-1542, Oct. 1999.

[6] N. Peña and M. M. Ney, "A General Formulation of a Three - dimensional TLM Condensed Node with the Modeling of Electric and Magnetic Losses and Current Sources," 12th Annual Review of Progress in Applied Comp. Electromagnetics, Monterey, CA, pp. 262-269, March 18-22, 1996.

[7] 3D EM Field Simulation, HFSS, www.ansoft.com, 2009.

Principles of Ultrawideband Noise Radar with Applications towards Detection of Obscured Targets

Ram M. Narayanan[1] and Thayananthan Thayaparan[2]
[1]*Department of Electrical Engineering, Pennsylvania State University, University Park, PA 16802, USA*
[2]*Defence R&D Canada – Ottawa, 3701 Carling Avenue, Ottawa, ON K1A 0Z4, Canada*
E-mail: ram@engr.psu.edu

Recent years have seen the need to covertly detect targets concealed behind optically opaque barriers, such as humans behind walls and weapons under clothing. Random noise radar is an attractive and viable option for use in these applications. Random noise radar refers to techniques and applications that use incoherent noise as the probing transmit waveform. Research work in this area has been conducted since the late 1950s [1]. However, only in the last few years have commercial chips reached to GHz frequencies and made such systems practical. In such a system, the transmit signal is pure thermally generated noise. A major advantage of using noise as the transmit signal is its inherent immunity from radio frequency and electromagnetic interferences and improved spectrum efficiency. The reflected signal from the target is cross-correlated with a time-delayed replica of the transmit waveform. When the internal delay exactly equals the round-trip time to the target, a peak is obtained in the correlation signal; otherwise, the correlator output is zero. The range resolution is inversely proportional to the transmit bandwidth, and a 1-GHz bandwidth yields a range resolution of 15 cm. In 2004, a Task Group (TG) on Noise Radar Technology was established by NATO to further develop this technology for military applications with active DRDC participation.

A conventional noise signal is not phase-coherent since the transmit waveform is incoherent. Thus, the correlation process captures only the amplitude but not the phase of the return signal. However, a technique called *heterodyne correlation*, overcomes this problem in a unique and novel manner [2]. In this method, the return signal from the target is cross-correlated with a time-delayed and frequency-offset replica of the transmit signal. The frequency-offset waveform is achieved by beating the noise signal with a phase-locked oscillator at the offset frequency. When this is done, the correlator output at the correct time-delay is always exactly at the offset frequency, superimposed with the Doppler frequency shift caused by target motion. In addition, the correlator output is zero at time delays that do not match the round trip time to the target. Since the correlator output is at the offset frequency, its relative phase can be obtained by comparing its waveform with the phase-locked offset frequency oscillator in a phase detector. Thus, the phase of the reflected signal can be extracted despite the fact that the illuminating waveform is totally incoherent. By measuring phase, even low micro-Doppler frequency modulations can be analyzed and small target movements estimated, as shown in many applications.

Advantages of noise radar include [3,4]: (1) *Clutter rejection*: Since the noise waveform is spread over a wide frequency range, it has the necessary diversity to reduce clutter and multipath effects; (2) *Electromagnetic compatibility*: Many noise radars can occupy the same spectral band, with negligible cross-interference as the signal from one will not correlate with the others' transmit replica; (3) *Spectrum efficiency*: Due to the uncorrelated and non-interference nature of the waveform, these systems possess enhanced spectral occupancy; (4) *Ease of signal processing*: Thermal noise is easy to generate, and modulators with good linearity or antennas with good impulse response are not needed; (5) *Frequency shaping*: The noise spectrum can be shaped to enhance detection of specific target types, prevent signal leakage into adjacent bands, or prevent in-band spectral fratricide with friendly systems; (6) *Thumbtack range-Doppler ambiguity function*: Both range and Doppler can be simultaneously estimated and independently controlled by varying bandwidth and integration time; (7) *Immunity from interference and jamming*: External signals caused by jammers or other interfering transmitters will not correlate with the time-delayed transmit replica and hence will yield zero output; (8) *Immunity from detection*: Since the waveform is not repeatable, it does not appear as an intentional signal on the adversary's receiver.

The paper will summarize the theory of random noise radar and provide examples of applications involving detection of obscured objects.

References

1. B.M. Horton, "Noise-modulated distance measuring systems," *Proceedings of the IRE*, vol. 47, pp. 821–828, May 1959.
2. R.M. Narayanan, Y. Xu, P.D. Hoffmeyer, and J.O. Curtis, "Design, performance, and applications of a coherent ultrawideband random noise radar," *Optical Engineering*, vol. 37, pp. 1855–1869, June 1998.
3. T. Thayaparan and C. Wernik, *Noise Radar Technology Basics*, DRDC TM 2006-266, Ottawa, December 2006, 46 p.
4. R.M. Narayanan, "Through-wall radar imaging using UWB noise waveforms," *Journal of the Franklin Institute*, vol. 345, pp. 659–678, September 2008.

978-1-4244-5050-3/10/$26.00 ©2010 IEEE

Through-Wall Sensing of Personnel at Standoff Distances using Passive Bistatic WiFi Radar

Kevin Chetty[1], Karl Woodbridge[2], Graeme E. Smith[3], Hui Guo[2], Waddah Al-Ashwal[2] and **Matthew Ash[2]**
[1]*UCL Centre for Security and Crime Science, University College London, London, UK, WC1E 7HN*
[2]*Department of Electronic and Electrical Engineering, University College London, London, UK, WC1E 7JE*
[3]*Centre for Advanced Commuications, Villanova University, Villanova, PA 19085*
E-mail: k.chetty@ucl.ac.uk

Non-cooperative detection and tracking of personnel targets that are obscured by walls has attracted a growing interest from the security & surveillance industries. Furthermore the rapid rollout of wireless networks has provided a ubiquitous source of signal transmissions that may be exploited to uncooperatively detect personnel targets using passive bistatic radar systems. In our previous work we have performed an ambiguity function analysis to investigate the detection characteristics of passive WiFi radar, and demonstrated experimentally the first detections of personnel in high clutter indoor environments [1]. In this study we examine the ability of passive WiFi radar to uncooperatively and covertly detect targets moving behind walls at standoff distances. The bistatic topology of our experimental setup is shown in Figure 1.

As well as demonstrating the through-wall detection capability of passive WiFi radar, analysis of the data showed that our new interference suppression technique based on the CLEAN algorithm used in radio-astronomy can improve the signal to interference ratio (SIR) by ~9 dB. Furthermore, it is able to recover target responses masked by the sidelobes associated with the direct signal interference (DSI) in situations where a decrease in the radial velocities along the bistatic bisectors caused near-zero Doppler shifts. Target detections were achieved using antennas having gains of 24 and 15 dBi. The results showed that the 24 dBi high gain, narrow beamwidth antenna gave superior SIR's and lower clutter responses at zero Doppler. It was also established that the wall, which is made up of 22 cm of brick and 9 cm of breeze block, attenuated the reflected target signals by approximately 30 dB.

The experiments were conducted so that one surveillance antenna (Node 2) could detect the response of a person moving behind a wall, while for comparison another surveillance antenna (Node 1) formed a 'mirror image' bistatic triangle to monitor the target response directly (without obstruction due to a wall). A WiFi access point (AP) was positioned inside the building and stimulated to illuminate a person target 4.0 m away. A reference channel (not shown in Figure 1) was located next to AP and used to monitor the signals output from it. A number of experimental variables were examined and the recorded data was processed using the cross-ambiguity function [1]. Figure 2 shows a range-Doppler surface plot of the measured through-wall target response from Node 2 for a person running towards the WiFi AP. The measured bistatic range (24 m) and Doppler shift (47 Hz) respectively correspond to that expected, and predicted by theory. The measured SNR and SIR were found to be 52 dB and 16 dB respectively. In Figure 2 the direct signal interference (DSI) component at zero Doppler has been suppressed using our CLEAN algorithm. In summary, the findings from this study suggest that there is good potential to use passive WiFi radar as a low cost through-wall detection sensor with widespread applicability.

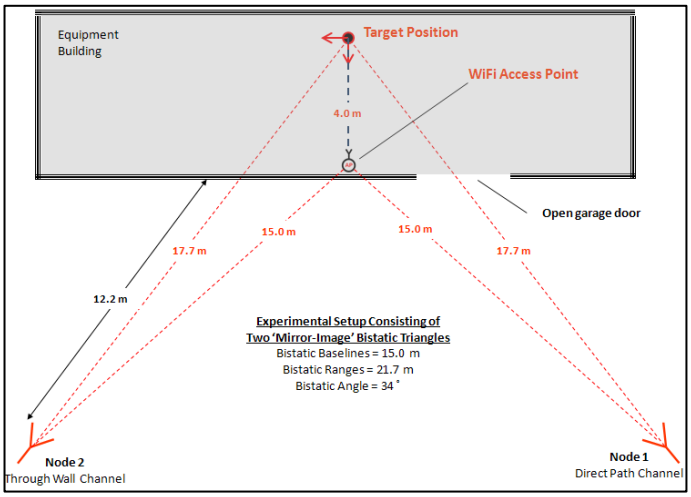

Figure 1: **Experimental geometry. Node 2 records target responses through a wall while Node 1 directly measures the response.**

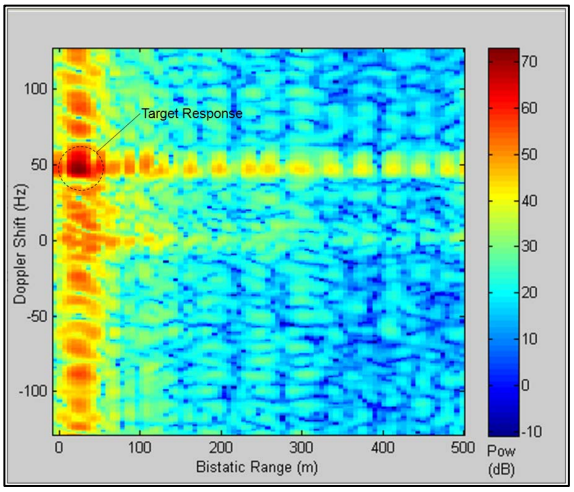

Figure 2: **Range-Doppler surface plot showing the response of a personnel target moving behind a wall.**

References

1. K. Chetty, G. E. Smith, H. Guo, and K. Woodbridge "Target detection in high clutter using passive bistatic WiFi radar," IEEE Radar Conference, Pasadena, USA. 2009.
2. N. J. Willis, Bistatic Radar. First Edition, SciTech Publishing Inc, 1997.

978-1-4244-5050-3/10/$26.00 ©2010 IEEE

The Sensitivity of Coupling of IEMI Waveforms to Cables

W. Radasky, K. Smith
Metatech Corporation, Goleta, California USA
E-mail: wradasky@aol.com

Intentional electromagnetic interference (IEMI) is known as a security threat to commercial electronic equipment and systems. Over the past ten years there have been significant efforts to test equipment to radiated fields to determine their susceptibility. One of the problems in such testing has been to determine the susceptibility contribution of the attached power and communications cables attached to the equipment under test. Due to the fact that the frequency content of many IEMI threat waveforms is often above 1 GHz, there is a strong sensitivity of the angle of incidence and polarization of the incident field and the relative orientation of the cables included in the tests.

This paper will examine the sensitivity of the cable coupling for the parameters of interest and will establish a probabilistic database for coupling. This information should be useful to those performing tests and analyses in the future to determine the susceptibility of commercial electronics and their attached cables to IEMI threats.

978-1-4244-5050-3/10/$26.00 ©2010 IEEE

Performances of a Prototype Impulse Radiation System in Japan

Hidenori Sekiguchi[1], Shinji Seto[1], and **Tetsuya Tominaga[2]**
[1]*National Institute of Information and Communications Technology, Tokyo, Japan, 184-8795*
[2]*NTT Corporation, Tokyo, Japan, 180-8585*
E-mail: hide@nict.go.jp, setos@nict.go.jp, tominaga.tetsuya@lab.ntt.co.jp

The security of electronic equipments and systems is feared by intentional electromagnetic interference (IEMI), because they might generate an error in high power electromagnetic environments [1]. In the present study, we have investigated an impulse radiation system, for the purpose of evaluating the immunity of the electronic equipments by high-power and wide-band electromagnetic disturbances. In this paper, we report on our prototype impulse radiation system, which is composed on a pulse generator and a half-reflector impulse radiating antenna (HIRA).
Figure 1 shows the configuration diagram of our impulse radiation system. Table 1 and Figure 2 show the performances and the output signal waveform of the pulse generator, respectively. Figure 3 shows the photograph of the HIRA. The diameter is 0.9 m, the focus length is 0.34 m. Figure 4 and 5 show the gain and the transmission coefficient of the HIRA, respectively. In Figure 4, the points and the dashed line show the measurement points and the approximated curve by a common logarithm, respectively. The radiated signal waveform from the HIRA can be calculated and predicted from Figure 2, 4 (the approximated curve), and 5, by means of a discrete Fourier transform (DFT) and an inverse DFT (IDFT). Figure 6 shows the predicted radiated signal waveform at a distance of 3 m from the HIRA. As shown to the numerical calculation result predicted in Figure 6, it is found that our prototype impulse radiation system produces an impulse-like electromagnetic field waveform with a peak amplitude of about 9 kV/m at a distance of 3 m from the HIRA. Table 2 shows the performances of our prototype impulse radiation system as shown in Table B.3 of the reference [2].
The corresponding measurement results are currently under experimentation and the comparison results will be presented at the symposium. In the future work, the prototype impulse radiation system will be upgraded.

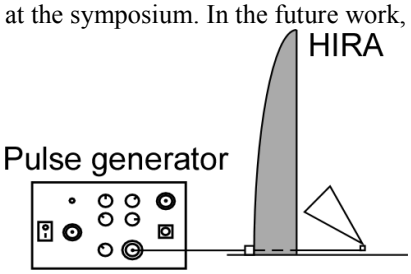

Figure 1: **Impulse radiation system**

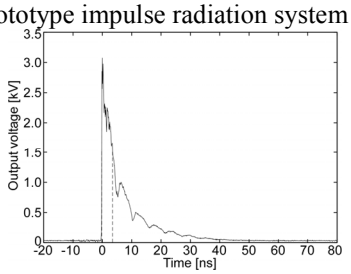

Figure 2: **Output signal waveform of the pulse generator**


Figure 3: **Photograph of the HIRA**

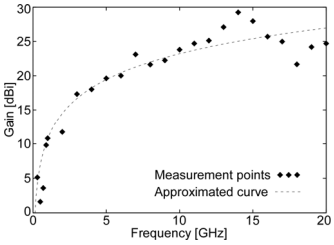

Figure 4: **Gain of the HIRA**

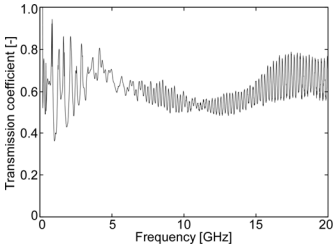

Figure 5: **Transmission coefficient of the HIRA**

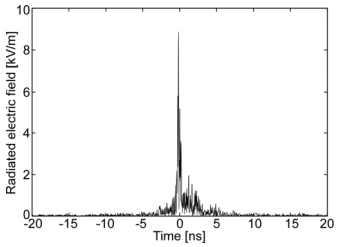

Figure 6: **Radiated signal waveform**

Table 1: **Performances of the pulse generator**

Output impedance	50 ohms
Peak voltage	> 3 kV
Rising time / FWHM	~ 100 ps / ~ 4 ns
PRF	800 Hz

Table 2 : **Performances of the impulse radiation system**

Near field	Far field	rE	Band-ratio	Band
9 kV/m at 3 m	Not available	27 kV	1	Mesoband

Acknowledgments – This research was partially supported by a Strategic Information and Communications R&D Promotion Programme (SCOPE) (073103006, 2007) from the Ministry of Internal Affairs and Communications, Japan and a Grant-in-Aid for Young Scientists (B) (21760302, 2009) from the Ministry of Education, Culture, Sports, Science and Technology, Japan.

References

1. W. A. Radasky, C. E. Baum, and M. W. Wik, "Introduction to the Special Issue on High-Power Electromagnetics (HPEM) and Intentional Electromagnetic Interference (IEMI)," IEEE Transactions on Electromagnetic Compatibility, vol. 46, 2004.
2. INTERNATIONAL ELECTROTECHNICAL COMMISSION (IEC), "IEC 61000-2-13: Electromagnetic compatibility (EMC) - Part 2-13: High-power electromagnetic (HPEM) environments - radiated and conducted", 2005.

978-1-4244-5050-3/10/$26.00 ©2010 IEEE

Electromagnetic Effect of Lightning Stroke to Multi-Buildings System

Jinliang He, Shunchao Wang, Bo Zhang, Rong Zeng
State Lab of Power Systems, Dept. of Electrical Engineering, Tsinghua University
Beijing, 100084, China
hejl@tsinghua.edu.cn

In large cities, because of the high price of the land, many tall buildings are always built in a small area with a lot of communal facility around them. Thus, multi-line structures with multi-grounding system are set up. When lightning strikes one building, high currents will flow through the structure steels and dissipate into the soil through the grounding system of buildings. The ground potential difference by such high currents may cause damage to electronic equipment not only in this building but also in other buildings nearby it. The electronic equipment near the building struck by lightning will be effected not only by the interferences due to the potential differences among the grounding systems, but also by the interferences from lightning induced voltages. So, how to accurately model and predict the transient electromagnetic fields near the multi-line structures with multi-grounding system is very important.

Many papers have investigated the transient electromagnetic fields around the multi-line structures. But almost all of them considered the ground as the perfect conductor, which means that the potentials at the multi-line structures' grounding points are all zero. In fact, because the soil resistivity is not small, potential differences always exist among the grounding points, especially when the lightning occurs near the multi-line structures. Not only the induced current but also the current produced by the potential differences among the grounding points will flow through the structures. Thus, when the transient electromagnetic fields near the multi-line structures are investigated, more accurate approaches should take account of the effect of the soil resistivity.

In this paper, an approach based on the moment method and the circuit theory is developed to analyze the transient electromagnetic fields around the multi-line structures by near-field lightning strokes. The approach can take account of the induced current and the potential differences among the grounding points at the same time. The current distribution at the near structure of the lightning striking point is analyzed. The influence of the lightning strike on the nearby grounding systems is investigated. Because the impedance of the grounding electrode is very large and the most effective part of a grounding system at transient is the part near the current injected point, connecting the grounding systems has little effect on the ground potential rise of each grounding systems. On the other hand, the electromagnetic interference on the cables connecting different buildings are presented when a lightning strikes one building of the multi-buildings system.

978-1-4244-5050-3/10/$26.00 ©2010 IEEE

Development of ALIS Hand-held Dual sensor for Humanitarian Demining

Motoyuki Sato[1]
[1]*Tohoku University, Sendai, Japan, 980 8576*
E-mail: sato@cneas.tohoku.ac.jp

ALIS is a hand-held dual sensor developed by Tohoku University, Japan since 2002[1-5]. Dual sensor is a general name of sensor for humanitarian demining, which are equipped with metal detector and GPR. ALIS is the only one hand-held dual sensor which can record the sensor position with sensor signals. Therefore, the data can be processed after data acquisition, and can increase the imaging capability. ALIS has been tested in some mine affected countries including Afghanistan (2004), Egypt(2005), Croatia(2006-) and Cambodia(2007-). Mine fields in each country has different conditions and soil types. Therefore tests at the real mine fields are very important.

At the same time, International organizations such as ITEP(International Test and Evaluation Program for Humanitarian Demining : http://www.itep.ws/) are conducting evaluation tests of sensors for humanitarian demining under controlled conditions, and provide technical information of sensors to the end users.

Operational tests at real mine fields have been conducted in Cambodia in collaboration with CMAC (Cambodian Mine Action Center) since April 2009. Two sets of ALIS were operated by ALIS-team of CMAC for two months, and more than 30 mines were detected. For example during one month in July 2009, ALIS cleared 4,192 m^2 area, and detected 9 mines, which are all PMN-2 type. Metal detector detected 1,193 objects, and deminers judged 484 of them as possible mines, and 709 as metal fragments. This means, 709 points out of 1193 points (app. 60%), did not have to be prodded, and it can reduce the time of demining operation drastically. This is the most important capability of ALIS.

Figure 1: **ALIS in operation in Cambodia**

Acknowledgments –This work was supported by JSPS Grant-in-Aid for Scientific Research (S) 18106008.

References

1. X. Feng, J. Fujiwara , Z. Zhou., T. Kobayashi and M. Sato, “Imaging algorithm of a Hand-held GPR MD sensor (ALIS),” Proc. Detection and remediation technologies for mines and minelike targets X, Proc. of SPIE Vol. 5794, 1192-1199, 2005.
2. M. Sato, "Dual Sensor ALIS Evaluation Test in Afghanistan, “ IEEE Geoscience and Remote Sensing Society Newsletter, 22-27, 2005.
3. M. Sato M., and K.Takahashi, “The Evaluation Test of Hand Held Sensor ALIS in Croatia and Cambodia, “Proc. Detection and remediation technologies for mines and minelike targets X II, Proc. SPIE, 6553, 65531D-1-65531D-9. 2007.
4. http://www.alis.jp/
5. http://www.jst.go.jp/kisoken/jirai/EN/index-e.html

978-1-4244-5050-3/10/$26.00 ©2010 IEEE

Imaging Algorithm of ALIS Hand-held Dual sensor

Motoyuki Sato[1]
[1]*Tohoku University, Sendai, Japan, 980 8576*
E-mail: sato@cneas.tohoku.ac.jp

Detection of buried anti-personnel mines by GPR is unfortunately very difficult by interpretation of raw GPR profiles mainly due to strong clutter. ALIS[1-5] a hand-held dual sensor developed by Tohoku University is equipped with a sensor tracking system, and can acquire the sensor position information with metal detector and GPR data sets. The GPR data acquired with the sensor position information is processed after scanning the ALIS sensor over area of about 1m by 1m. In ALIS, we reconstruct a 3-D GPR image by Kirchhoff migration algorithm[1]. The Kirchhoff migration gives the output wave field $P_{out}(x_{out}, y_{out}, z, t)$ at a subsurface scatter point (x_{out}, y_{out}, z) from the input wave field $P_{in}(x_{in}, y_{in}, z = 0, t)$, which is measured at the surface (z=0). The integral solution used in migration is given by:

$$P_{out}(x_{out}, y_{out}, z, t) = \frac{1}{2\pi}\iint\left[\frac{\cos\theta}{r^2}P_{in}\left(x_{in}, y_{in}, z=0, t+\frac{r}{v}\right) + \frac{\cos\theta}{vr}\frac{\partial}{\partial t}P_{in}\left(x_{in}, y_{in}, z=0, t+\frac{r}{v}\right)\right]dxdy \quad (1)$$

where v is the RMS velocity at the scatter point (x_{out}, y_{out}, z) and $r = 2\sqrt{(x_{in}-x_{out})^2 + (y_{in}-y_{out})^2 + z^2}$, which is the distance between the input point $(x_{in}, y_{in}, z=0)$ and scatter point (x_{out}, y_{out}, z). $\cos\theta$ is obliquity factor or directivity factor, which describes the angle dependence of amplitudes and is given by the cosine of the angle between the direction of propagation and the vertical axis z. $1/vr$ is the spherical spreading factor. The time derivative of the measured wave field yields the 90-degree phase shift and adjustment of the amplitude spectrum.

A migrated GPR data gives 3-D reconstructed subsurface image. However, we found that the horizontal slice image (C-scan) is very useful for data interpretation in real situations. It should be noticed that ALIS does not use signal processing to reduce the reflection from the ground surface. The ground surface in real mine fields is quite rough, and the signal processing normally used for GPR acquired on a even ground surface, such as mean average subtraction does not work in our case. However, we found the migration drastically improves the quality of the reconstructed image, and the image of mines can clearly be shown. Fig.1(a) is one example of GPR horizontal profile (C-scan) after migration processing was applied to the raw data shown in Fig.1(b). PMN-2 (produced in former USSR) anti-personnel landmine is the target in these GPR profiles.

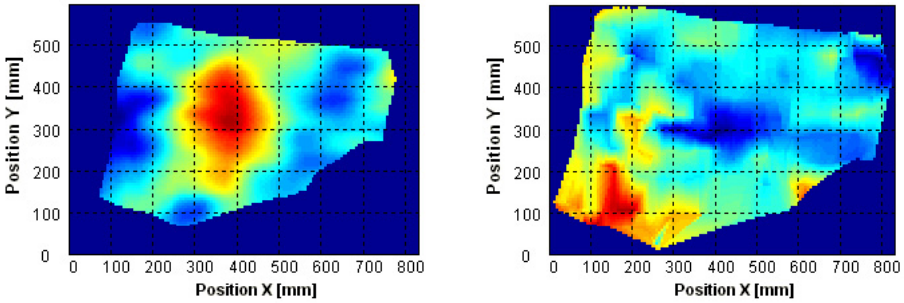

(a) Processed Image by Migration (b) Raw GPR profile

Figure 1: **Visualized image of a buried PMN-2 by ALIS**
(02 July 2009 by PG-2 data No.28, Cambodia)

Acknowledgments –This work was supported by JSPS Grant-in-Aid for Scientific Research (S) 18106008.

References

1. X. Feng, J. Fujiwara , Z. Zhou., T. Kobayashi and M. Sato, “Imaging algorithm of a Hand-held GPR MD sensor (ALIS),” Proc. Detection and remediation technologies for mines and minelike targets X, Proc. of SPIE Vol. 5794, 1192-1199, 2005.
2. M. Sato, "Dual Sensor ALIS Evaluation Test in Afghanistan, “ IEEE Geoscience and Remote Sensing Society Newsletter, 22-27, 2005.
3. M. Sato M., and K.Takahashi, “The Evaluation Test of Hand Held Sensor ALIS in Croatia and Cambodia, “Proc. Detection and remediation technologies for mines and minelike targets X II, Proc. SPIE, 6553, 65531D-1-65531D-9. 2007.

978-1-4244-5050-3/10/$26.00 ©2010 IEEE

Useful Signal Detection in Harmonic Radar System and Noisy Environment Using Complex Cosine Wavelet Transform

Radomir Pavlik, Vladimir Polacek
VOP-026 Sternberk, s.p., VTUO Brno Division, Brno, Czech Republic, 63700
E-mail: pavlik@vtuo.cz

The harmonic radar based on non-linear junction detection (NLJD) principle shows considerable capability to remote detection of non-explosive components used in construction of improvised explosive devices (IEDs) and mines. It can be considered as a supporting but important sensor platform as a part of reconnaissance system in the frame of personnel and vehicle protection support system [1].
As the secondary radiated signal in the harmonic radar system is usually very weak (in the order of levels of −80 dBm or less) and the detection distance range is in units to tens of meters, the analysis of an effective signal detection at the receiver part is very important also with regard to possibility of increasing sensitivity and hence the radar detection range. Using time-frequency and time-scale methods increases opportunities for analysis and obtaining features significant for useful signal detection. It is well known that mainly wavelet transform has good localization properties primarily in the detection of discontinuities and noise suppression in the analyzed signal.
The possibility of choosing a suitable mother wavelet (base function) for signal transformation enables to analyze the given signal pattern by a matched base function which is one of the main advantages of wavelets over Fourier-based methods. The received signal in the harmonic radar system under consideration, which has a narrowband character with a strong spectral component at a higher harmonic of irradiating signal, can be considered as signal patterns with finite energy and shape derived from the cosine (or sine) function. On the basis of general characteristics of the analyzed signal, the custom Complex Cosine Wavelet was designed in accordance with the wavelet function used in [2] given by

$$\psi(t) = \sqrt{\frac{2f_b}{\pi}}\cos(f_b t)\, e^{2\pi j f_c t}, \tag{1}$$

where f_b is the bandwidth parameter and f_c is the central frequency of the wavelet.
This paper deals with the application of the family of complex wavelets with optimal properties for the signal detection in harmonic radar system (based on a functional sample of experimental multi-channel detection system) by discretized Continuous Wavelet Transform (CWT) and subsequent implementation in MATLAB. Application option is presented on signal decomposition through Complex Cosine Wavelet and detection of maxima in the transformed scale domain, see Fig 1, where the relation between maxima of the rescaled scalogram and instantaneous frequency can be seen.

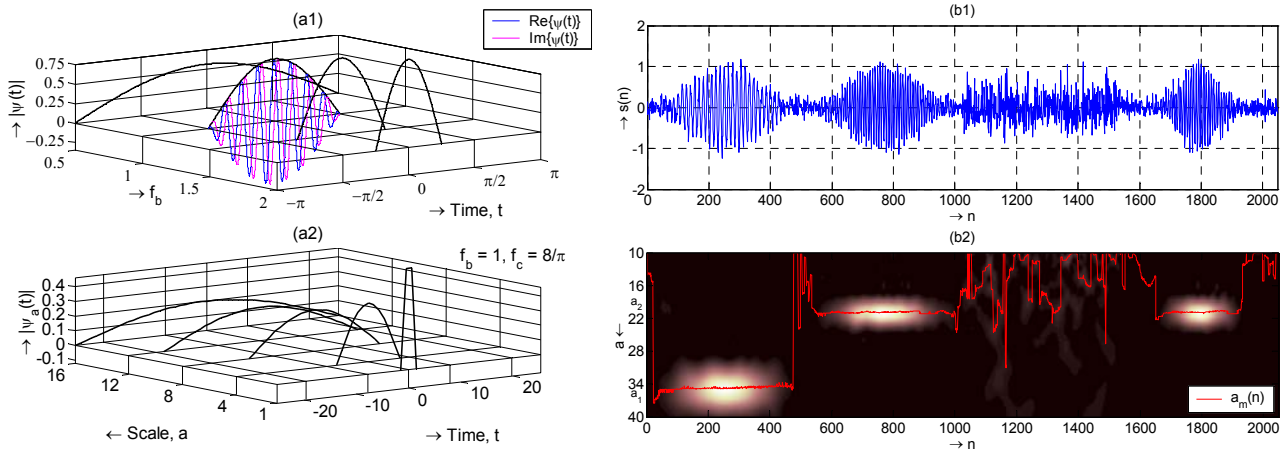

Figure 1: **(a1) Complex Cosine mother wavelets for $f_c = 8/\pi$, real and imaginary parts are plotted for $f_b = 1$, (a2) set of dilated wavelets with effective support of $[-\pi/2, \pi/2]$, $f_b = 1$; (b1) analyzed signal containing four waveform segments of the same finite length of $N/4 = 512$ samples with SNR = 10 dB (two sinusoidal pulses with envelope according to Hanning window with frequency f_1, resp. f_2, noise waveform, Gaussian RF pulse with center frequency f_2 and 5% bandwidth at a level of −6 dB with respect to the normalized signal peak), (b2) the CWT rescaled scalogram plot using a Complex Cosine Wavelet with the ridge $a_m(n)$ found from the maxima: $N = 2048$, f_1 corresponds to $a_1 = 34.768$ and f_2 to $a_2 = 20.861$.**

References

1. R. Pavlik, I. Hertl, V. Polacek, M. Strycek, "An Experimental Investigation into the Advanced Harmonic Radar Detection System", In proceedings from International Radar Symposium IRS 2009, Hamburg, 2009, pp. 109–113.
2. R. Pavlik, "Binary PSK/CPFSK and MSK Bandpass Modulation Identifier Based on the Complex Shannon Wavelet Transform", Journal of Electrical Engineering (JEEEC), Vol. 56, No. 3-4, 2005, pp. 71–77.

978-1-4244-5050-3/10/$26.00 ©2010 IEEE

Canadian Regulatory Requirements for Radio Frequency Exposure Compliance of Radiocommunication Apparatus

Josette Gallant[1] and Hughes Nappert[1]

[1]Industry Canada, Spectrum Information Technology and Telecommunications, Directorate of Regulatory Standards

Keyword

Wireless devices, regulations, SAR, RF exposure

Abstract

In the past decade, development and implementation of new wireless devices have increased substantially. The general public now uses these devices as part of their day to day life when communicating with others. Since these wireless communication apparatus emit radio frequency (RF) fields, the Government of Canada takes various steps to protect Canadians from RF exposure that exceeds established limits. Industry Canada's Radio Standard Specifications 102 (RSS-102) titled *Radio Frequency Exposure Compliance of Radiocommunication Apparatus (All Frequency Bands)*, sets out the requirements and measurement techniques used to evaluate RF exposure compliance of radiocommunication apparatus designed to be used within the vicinity of the human body. RSS-102 has adopted the specific absorption rate (SAR) and RF field strength limits set forth in Health Canada's RF exposure guideline, *Safety Code 6*. International measurement standards and other internationally recognized measurement procedures are also incorporated by reference in this Canadian regulatory document for SAR and RF exposure evaluation.

Industry Canada verifies that wireless equipment deployed in the Canadian marketplace complies with technical standards during its life cycle. This activity is done through the Department's market surveillance program.

978-1-4244-5050-3/10/$26.00 ©2010 IEEE

Critical Infrastructure Protection Priorities for EMP

G. H. Baker
James Madison University, Harrisonburg, Virginia, USA, 22801
E-mail: BakerGH@jmu.edu

The Commission to Assess the Threat to the United States from Electromagnetic Pulse Attack has provided a compelling case for protecting civilian infrastructure against the effects of EMP. As with protecting infrastructure against any hazard, it will be important to take a risk-based priority approach for EMP, recognizing that it is fiscally impracticable to protect everything. In this regard, EMP is particularly challenging in that it interferes with electrical and electronic data, control, transmission, and communication systems organic to nearly all infrastructures in a simultaneous and wide-scale manner. And, for nuclear burst altitudes of 100s of kilometers, the exposed geography approaches continental scale. EMP events thus represent a high-consequence disaster class that is unique in its coverage and ubiquitous system debilitation. Such disasters deserve particular attention with regard to preparedness and recovery since assistance from non-affected regions of the nation could be scarce or nonexistent. The problem of where to begin in developing a protection program, at first blush, seems overwhelming. Developing an affordable EMP protection approach based on system priorities is possible, though challenging. The presentation explains a rationale for priority attention to the electric power grid and emergency systems. National, regional, and local responsibilities are considered. System protection approaches are also addressed.

References

1. W. R. Graham et al, Report of the Commission to Assess the Threat to the United States from Electromagnetic Pulse (EMP) Attack: Critical National Infrastructures, April, 2008
2. G. H. Baker and C. J. Elliott, Homeland Security: Engaging the Frontlines, JMU Institute for Infrastructure and Information Assurance and NAS Federal Facilities Council Symposium Proceedings, May 2006.

978-1-4244-5050-3/10/$26.00 ©2010 IEEE

Multipath Analyses and Experiments for Moving Personnel Indoor

Pawan Setlur, Moeness Amin, and **Fauzia Ahmad**
Radar Imaging Lab, Center for Advanced Communications, Villanova University, Villanova, PA, 19085, USA
E-mail:fauzia.ahmad@villanova.edu

Through-the-wall radar systems address the desire to detect, localize, track, and classify targets behind walls or inside buildings. Doppler discrimination of movement from stationary background clutter can be used for motion detection and tracking in through-the-wall applications. Due to the rich multipath indoor environment, the target return is contaminated by several multipaths due to reflections off walls, floor, and/or ceiling, which could compromise detection and yield high false positives. Therefore, it is imperative to distinguish between the direct path and the multipaths. In this paper, a multipath model is considered which assumes a single diffused moving target in an enclosed urban structure or beside a close wall. For simplicity, we consider only adjacent walls, noting that the extension of the analyses provided for multipaths to other walls and floor is straightforward. The model is described in Fig. 1 in which near field measurements are assumed. The direct non-line of sight path is denoted as path-A, and the multipath components are the other paths denoted as path-B, path-C, and path-D, respectively. Detailed analyses including key equations which aid in computing the angles of incidence and refraction corresponding to various paths in Fig. 1 are provided in [1]. For urban sensing applications, frequencies from 0.5GHz to 3GHz are typically used to interrogate the scene. This frequency spectrum is shared by many other devices or services, and wideband radars are prone to unintentional interference. In other words, use of wideband radars such as range-Doppler radars may be prohibitive, and use of narrowband radars is advocated. We, therefore, analyze the multipath in the Doppler domain only. When the multipath is well separated in the Doppler domain, it can be excised using simple filters, provided the true Doppler peak has been identified in the Doppler domain. The Doppler peak identification is addressed next.

Consider the case when the target is moving along the radar line of sight. For this special case, we present experimental results wherein we can identify the Doppler peak corresponding to the true target using the proposed model when the Doppler spectrum is contaminated with several peaks arising from the multipath. The target is moving head on towards the radar and parallel to a concrete side wall (thickness 0.2m, and dielectric constant 7.66) which is 0.467m away. Note that the experimental data has no front wall through which the radar system is looking. However, the radar return also contains contributions from the floor. The multipath model is first used to identify the true Doppler peak, and is then used to generate the corresponding Doppler spectrum (blue curve) shown in Fig. 2. The measured Doppler spectrum (black curve) is also provided in Fig. 2 for comparison. It is readily seen that the modeled and the measured results are in agreement, i.e., the dominant spectral peaks of the modeled and measured Doppler spectra coincide with each other. In general, when the target is moving at an angle with respect to the line-of-sight, the direct path and multipaths can be identified from the proposed model using both Doppler and angle information obtained from a passive phased array used in conjunction with Doppler radar. We further note that the proposed model can be also applied to multipath exploitation radar [2], and can be used to track the target when the direct path is occluded and multipath alone is present.

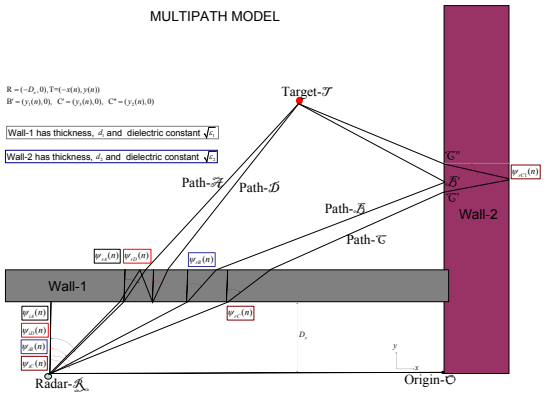

Fig. 1. Model with adjacent walls.

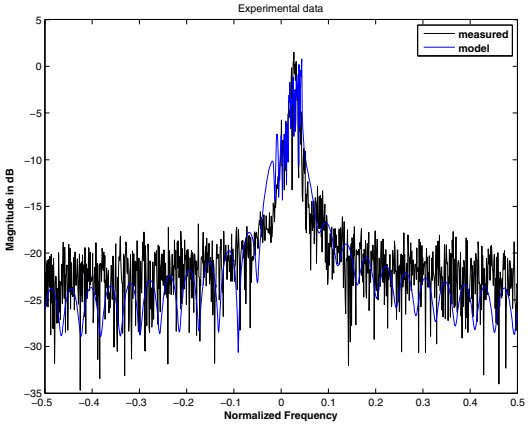

Fig. 2. Modeled and measured spectra-Experimental

References

1. P. Setlur, M. Amin, and F. Ahmad, "Multipath analyses of moving targets in enclosed structures using Doppler radars," in Proc. SPIE, Apr 5-9, Orlando, FL, April 2010.
2. R. Linnehan, and J. Schindler, "Multistatic scattering from moving targets in multipath environments," in Proc. IEEE Radar Conf., Pasedena, CA, May 2009.

978-1-4244-5050-3/10/$26.00 ©2010 IEEE

Optimal Detection Waveforms based on Signature Exploitation Techniques for Urban Sensing

Fauzia Ahmad and Moeness G. Amin
Radar Imaging Lab, Center for Advanced Communications, Villanova University,
800 Lancaster Ave, Villanova, PA 19085, USA
E-mail: fauzia.ahmad@villanova.edu

In typical through-the-wall radar operational environments, the possible targets considered in the scene of interest are known in advance, examples being humans and weapons. Sufficient *a priori* information about the properties and characteristics of these targets, such as shape, size, and composition, is available. The goal of the radar system is to detect the presence of the target of interest and to determine its location. Waveform design techniques based on target signature exploitation make use of the *a priori* information for improved target detection. In this paper, we specifically focus on the matched illumination signature exploitation concept in which the transmit pulse shape is designed such that it maximizes the signal-to-clutter-and-noise-ratio (SCNR) at the output of the receiver matched filter [1]. We consider an AK-47 assault rifle as the target of interest and assume monostatic radar operation. Target impulse responses over the 1-8 GHz frequency range are obtained as a function of the aspect angle using EM modeling software for a vertical rifle. The matched illumination concept was applied to the impulse responses covering full 360° aspect and the corresponding optimal waveforms were obtained for the case of white noise and zero clutter. Magnitude spectra of the AK-47 and the corresponding optimal transmission waveforms for each aspect angle between 0° and 359° are depicted in Fig. 1, which shows that for each aspect angle, the energy in the optimal waveform is concentrated in a narrow frequency band, corresponding to the frequency of the highest target response. The output SNR corresponding to the optimum waveform was compared to that of a chirp waveform of the same duration and energy. The SNR as a function of aspect angle using the optimum signal and the chirp waveform is provided in Fig. 2. On the average, the optimum waveform provides an improvement of 4.5 dB over the chirp signal. It is noted that the receiver filter is matched to the expected target echo rather than the transmitted waveform.

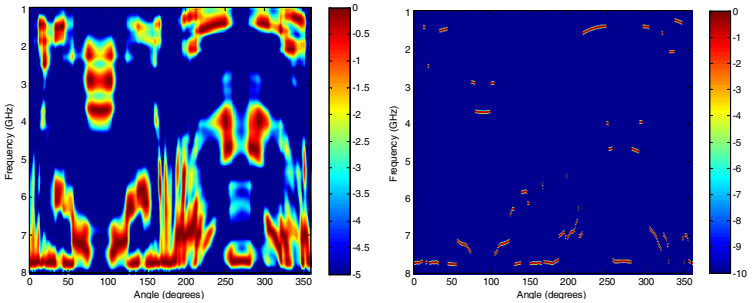

Figure 1: **Magnitude spectra of AK-47 (left) and optimal waveforms (right)**

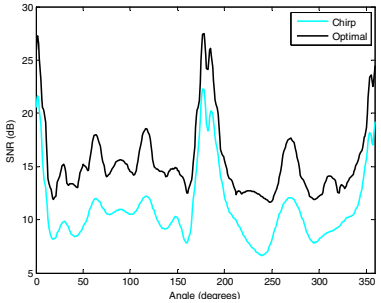

Figure 2 : **SNR improvement over a chirp**

The optimal waveforms in Fig. 1 were designed given perfect knowledge of the target impulse responses at various aspect angles. In practical situations, this information may not always be available especially when the target is behind walls. Therefore, it is desirable to have a single waveform designed for all possible target orientations, generally over 360° in azimuth. We consider stochastic-based matched illumination approach, wherein the target is modeled as a random process and the target impulse responses corresponding to various orientations are considered as sample realizations [2]. Waveform design is based on the target average RCS behavior, characterized by the target power spectrum, over angle. The orientation independent waveform designed using the stochastic approach for the Ak-47 is shown in Fig. 3, whereas Fig. 4 provides the SNR as a function of aspect using the stochastic and chirp waveforms. Note that the receive filter is matched to the transmitted signal for the chirp, and to the received signal corresponding to the average statistical impulse response characterization derived from the known power spectrum for the stochastic signal.

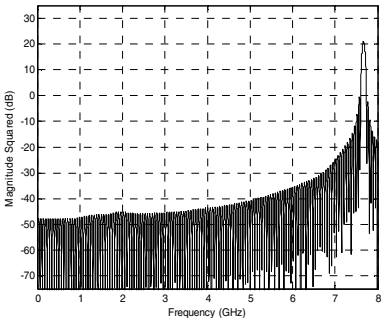

Figure 3: **Magnitude spectrum of stochastic waveform**

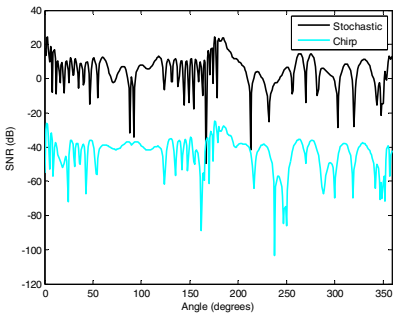

Figure 4 : **SNR improvement over a chirp**

References

1. H. Estephan, M. Amin, and K. Yemelyanov, “Waveform design for through-the-wall radar imaging applications,” in Proc. of the SPIE Defense and Security Symposium, vol. 6943, Orlando, FL, March 2008.
2. R. Romero, J. Bae, and N. Goodman, "Theory and application of SNR- and MI-based matched illumination waveforms," IEEE Trans. on Aerospace and Electronic Systems, to appear.

978-1-4244-5050-3/10/$26.00 ©2010 IEEE

Modeling of Buried Wire Detection using Radio-Frequency Transmitter-Receiver Pairs (Session UX13)

S. E. Irvine
Defence Research and Development Canada - Suffield, Medicine Hat, AB, T1A 8K6
Email: Scott.Irvine@drdc-rddc.gc.ca

Buried utility detection remains an important component of industry due to constantly evolving infrastructure, and the ability to locate these utilities quickly is crucial for reducing cost in time and resources. Similarly, civilian and military security also have the same requirements of timeliness and cost-effectiveness on wire detection, however, with the additional constraint that there is no potential foreknowledge of the location of the wire. Since typical wire detectors and locators rely on transmission and scattering of radio-frequency electromagnetic waves from the wire/utility in question, a firm understanding of the underlying physical principles is critical to develop and optimize technology used to find buried utilities.

Herein I describe a novel electromagnetic simulation for modeling wire detection using radio-frequency electromagnetic waves. The model is based on numerical solution of a formulation originally derived to determine the current distribution in a wire due to a local magnetic dipole [1]. This model determines a general response function of a wire detector system as it traverses a wire. It is assumed that the wire detector is composed of a single transmitter coil and a single receiver coil, and simulations proceed according to three steps: (1) using the transmitter dipole parameters, calculate the current distribution within the wire to be detected, (2) integrate over the current distribution to determine the magnetic field at the location of the dipole receiver, and (3) repeat steps (1) and (2) for various locations along the traversal path. While any number of distinct traversal paths is possible, I only consider the simplest case of a linear, straight line trajectory directly over the buried wire. This is not a limitation of the model, but a standard that is chosen to simplify analysis.

The theoretical basis and implementation of the model are first discussed. This is followed by a presentation of general results that underlie buried utility detection. Finally, the model is applied to cases where the transmitter and receiver dipoles are fixed together and move as a complete unit. Several key parameters are addressed in relation to device optimization, and include frequency of operation as well as transmitter-receiver dipole orientations.

References

1. D. A. Hill, “Magnetic Dipole Excitation of an Insulated Conductor of Finite Length,” IEEE Transactions on Geoscience and Remote Sensing, vol. 28, 1990.

978-1-4244-5050-3/10/$26.00 ©2010 IEEE

Flow of Geomagnetically Induced Currents in an Electric Power Transmission Network

Risto J. Pirjola
Finnish Meteorological Institute, P.O. Box 503, FI-00101 Helsinki, Finland
E-mail: risto.pirjola@fmi.fi

Space weather affecting in the near-Earth space and on the ground is a result of solar activity, e.g. [1]. At the Earth's surface space weather processes lead to geomagnetically induced currents (GIC) in technological networks, such as electric power transmission grids, oil and gas pipelines, telecommunication cables and railway equipment, e.g. [2]. GIC are a possible source of malfunction or damage in the particular system, and so studies of GIC are of great practical significance. Power networks are the most important systems regarding GIC today. Their problems result from saturation of transformers, which may in the worst cases lead to wide blackouts and permanent damage of equipment, e.g. [3]. The most famous GIC failure so far has been the power blackout in Québec, Canada, in March 1989, e.g. [4]. This paper is specifically focussed on GIC in power systems.

The evaluation of GIC risks in a power network and the design of possible countermeasures require estimation of expected GIC magnitudes in transformers. This can be achieved by model calculations supplemented by GIC recordings at some sites. Although in principle GIC can flow all over a large galvanically-connected power grid, which should thus be included as a whole in a GIC calculation, practical reasons dictate that the network should be restricted somehow.

By applying a power grid test model obtained based on an old configuration of the Finnish 400 kV network and introduced in [5], this paper provides, for the first time, a systematic numerical investigation about the flow of GIC induced in one part of a network to other parts. We show that GIC do not flow very long distances (= several hundreds or thousands of kilometers) in a power grid. This is practically a good result as it justifies the neglect of the parts of the network that lie far a way from the area considered. Thus, for example, if GIC in a country are of primary interest, possible connections to networks in other countries can usually be ignored in model computations. The conclusions about the flow of GIC obtained in this paper in a way generalise the earlier results discussed in [5], [6] and [7].

References

1. V. Bothmer, and I. A. Daglis (eds.), Space Weather – Physics and Effects. Springer, Praxis Publishing, Chichester, UK, 438 pp., 2007.
2. D. H. Boteler, R. J. Pirjola, and H. Nevanlinna, "The effects of geomagnetic disturbances on electrical systems at the earth's surface," Advances in Space Research, vol. 22, no. 1, 17-27, 1998.
3. J. G. Kappenman, "Geomagnetic Disturbances and Impacts upon Power System Operation," The Electric Power Engineering Handbook, 2nd Edition, edited by L. L. Grigsby, CRC Press/IEEE Press, Chapter 16, 16-1 - 16-22, 2007.
4. L. Bolduc, "GIC observations and studies in the Hydro-Québec power system," Journal of Atmospheric and Solar-Terrestrial Physics, vol. 64, no. 16, 1793-1802, 2002.
5. R. Pirjola, "Properties of matrices included in the calculation of geomagnetically induced currents (GICs) in power systems and introduction of a test model for GIC computation algorithms," Earth, Planets and Space, vol. 61, no. 2, 263-272, 2009.
6. R. J. Pirjola, and A. T. Viljanen, "Geomagnetic Induction in the Finnish 400 kV Power System, Environmental and Space Electromagnetics," edited by H. Kikuchi, Springer-Verlag, Tokyo, Printed in Hong Kong, Chapter 6.4, 276-287, 1991.
7. R. Pirjola, "Effects of space weather on high-latitude ground systems," Advances in Space Research, vol. 36, no. 12, doi: 10.1016/j.asr.2003.04.074, 2231-2240, 2005.

978-1-4244-5050-3/10/$26.00 ©2010 IEEE

On the Use of Probabilistic Risk Analysis for IEMI

E. Genender[1], **S. Fisahn**[1], **H. Garbe**[1], and **S. Potthast**[2]

[1] *Leibniz Universität Hannover, Institute of the Basics of Electrical Engineering and Measurement Science, D-30167 Hannover, Germany*

[2] *Bundeswehr Research Institute for Protective Technologies and NBC-Protection, D-29623 Munster, Germany*

E-mail: Genender@ieee.org

Due to the interconnection of modern electronic systems such as IT-Networks it becomes impossible to predict the reliability of the whole system solely deterministically. The system needs to be decomposed in smaller elements which are easier to analyze by itself. Despite the functional structure of the system also the electromagnetic topology needs to be taken into consideration. Critical system elements may be placed in shielded rooms where the deterministic calculation of electromagnetic fields is not reasonable because slight changes in this environment can drastically change the electromagnetic field structure in that enclosure. Furthermore, there is also a big variety of electromagnetic threats that the system can be exposed to. Due to these uncertainties a complex system must be analyzed statistically. Hence, there is a need for a systematical analysis method which takes the uncertainties from different sources into consideration and which combines this knowledge in order to predict the risk. Moreover, the analysis should enable to identify the main contributors to the risk. The objective of this contribution is first to define the expression risk and second to present some of the aspects of probabilistic risk assessment and to show how those can be applied to IEMI problems.

Often the expression *risk* is misleadingly used in EMC for describing the sources or the effects of the EMI. However, the most common definition of risk is the combination of the consequence of a threat and the probability of this consequence. Mathematically the risk R can be expressed:

$$R = \Sigma_{i=1}^{N} C_i \cdot p(C_i), \tag{1}$$

where C_i is the i-th consequence and $p(C_i)$ its probability. Possible applications of the risk as defined in equation (1) will be discussed for the case of IEMI. In order to calculate the risk of a certain electromagnetic environment the two quantities C_i and $p(C_i)$ have to be determined.

Sabath[1] presented several ways to characterize the consequences of IEMI. These included the classification by the physical effects, duration and functional effects. The probability of the i-th consequence $p(C_i)$ can be decomposed into the probability of the threat $p(T)$ and the conditional probability of this consequence given the occurrence of the threat T:

$$p(C_i) = p(C_i|T)p(T). \tag{2}$$

Since there are different types of threats and under the assumption that these threats never occur at the same time equation (2) can be extended to

$$p(C_i) = p(C_i|T_1)p(T_1) + \cdots + p(C_i|T_j)p(T_j) + \cdots + p(C_i|T_M)p(T_M). \tag{3}$$

The occurrence probability $p(T_j)$ of intentional threats depends on the mobility and technological challenge of the sources. The higher the mobility of a source and the lower its technological challenge the higher is the occurrence probability of this threat[2]. In order to determine the conditional probability $p(C_i|T_j)$ the system has to be investigated in more detail. In previous works Camp[3] examined the susceptibility of individual electronic components such as microcontrollers, boards or whole PCs. However, in order to predict the risk for an interconnected system the knowledge about the failure probability of individual elements has to be combined. For that, the functional structure as well as the electromagnetic topology have to be examined. Different methods known from risk assessment such as the fault tree analysis or importance analysis might be useful tools. Their application to IEMI problems will be discussed.

References

1. F. Sabath, "Classification of electromagnetic effects at system level", EMC Europe 2008, Hamburg, Germany
2. F. Sabath, H. Garbe, "Risk potential of radiated HPEM environments", IEEE EMC 2009, Austin, USA
3. M. Camp, H. Gerth, H. Garbe, H. Haase, "Predicting the Breakdown Behavior of Microcontrollers under EMP/UWB Impact Using a Statistical Analysis", IEEE Transactions on Electromagnetic Compatibility, vol. 46, No.3, 2004

978-1-4244-5050-3/10/$26.00 ©2010 IEEE

Parametric Studies of Weapon Signatures and the Influence of the Human Body in Concealed Weapon Detection Based on Late-time Responses

Natalia K. Nikolova[1] and Thayananthan Thayaparan[2]
[1]*Department of Electrical and Computer Engineering, McMaster University, Hamilton, ON L8S 4K1, Canada*
[2]*Defence R&D Canada – Ottawa, 3701 Carling Avenue, Ottawa, ON K1A 0Z4, Canada*
E-mail: nikolova@ieee.org

Every structure has intrinsic resonant frequencies, which depend on its size, shape, composition and constitutive parameters. At the resonant frequencies, the target radar cross-section is enhanced leading to distinct maxima in the amplitude spectrum of the radar return. The resonances in a time-dependent radar return determine its late-time portion. Thus, the techniques relying on resonance for weapon detection and identification are referred to as late-time response (LTR) techniques [1-7]. The advantage of the resonant target signature is that it is aspect independent, i.e., it does not depend on the direction of illumination. On the other hand, the direction of illumination must allow for sufficient incident power to reach the target and excite the resonant modes. This is important in concealed weapon detection where the human body may shield a weapon from direct illumination. In this respect, the polarization of the incident wave is also important in the ability to excite the dominant natural modes [6-7]. Likewise, the LTR radar return typically contains co-polarized and cross-polarized components both of which carry important, often complementary, information [4-6].

We carry out a parametric study of the resonant signatures of small weapons (knives, handguns) in terms of: (i) the weapon size, (ii) shape, (iii) orientation with respect to the direction of illumination and the polarization of the incident wave, as well as (iv) the weapon position on the human body. The signatures are extracted via time-domain simulations [8] assuming plane-wave excitation. The weapon signature is identified through the complex-valued far-zone scattered field in a monostatic scenario, i.e., the scattered field is recorded at the direction from which the incident wave arrives. The weapon is in open space or is suspended on the human body. When the weapon is in open space, the studied signature is denoted as S_w. When the weapon is suspended on the human body, two simulations are necessary to extract the signature – one with the human body alone and one with the body (in exactly the same position) and the weapon on it. In the first simulation, the far field scattered by the human is denoted as S_h. In the second simulation, the response S_{hw} is that of the human with the weapon. We can then obtain the weapon signature when suspended on the human body as

$$S_w^{(h)} = S_{hw} - S_h \,. \tag{1}$$

Some of the conclusions include: (1) The mean length of a Γ-shaped (e.g., handgun) or I-shaped (e.g., knife) weapon of a thin cross-section can be used to predict approximately the wavelength of the dominant resonant mode (multiplying by 2). The resonant peaks in the amplitude spectrum of the return are sharp implying high Q and modal purity. (2) For Γ- or I-shaped objects of relatively thick cross-sections, the amplitude-spectrum curves are similar to those of objects with thin cross-sections but are likely to broaden and shift toward lower frequencies. (3) When the aspect ratio of an object approaches unity (e.g., sphere, cube, grenade), the cross-sectional length of the object (e.g., the sphere diameter) when multiplied by a factor of π produces the approximate value of the wavelength at the lowest-frequency resonance. (4) The bandwidth from 300 MHz to 3 GHz is suitable for detecting small and large handguns, medium- to large-size knives, as well as hand grenades. (5) The presence of the human body alters the weapon signature significantly, i.e., S_{hw} is very different from S_w. The dominant-resonance frequency is slightly lower than that in open space. Direct illumination is not necessary for detection.

References

1. A. R. Hunt, R. D. Hogg, and W. Foreman, "Concealed weapons detection using electromagnetic resonances," *SPIE Conference on Enforcement and Security Technologies*, Boston, MA, Nov. 1998, pp. 62–67.
2. A. R. Hunt and R. D. Hogg, "A stepped-frequency CW radar for concealed weapon detection and through the wall surveillance," in *SPIE Proc. on Sensors and Command, Control, Communications and Intelligence (C3I) Technologies for Homeland Defense and Law Enforcement*, SPIE Proc. vol. 4708, 2002, pp. 99–105.
3. AKELA, "Demonstration of a concealed weapons detection system using electromagnetic resonances, final report", US Dept. of Justice, 2001, on line: http://www.ncjrs.gov/pdffiles1/nij/grants/190134.pdf.
4. J. Hausner and N. West, "Radar based concealed threat detector," *IEEE MTT-S Int. Microwave Symp*., June 2007, pp. 765–768.
5. J. Hausner and N. West, "Radar based concealed threat detector," *IEEE Int. Conference on Microwaves, Communications, Antennas and Electronic Systems*, 2008 (COMCAS 2008), pp. 1–8.
6. M. Gashinova, M. Cherniakov, and A. Vasalos, "UWB signature analysis for detection of body-worn weapons," *Int. Conference on Radar (CIE 2006)*, pp. 1–4.
7. N. Shuley and D. Longstaff, "Role of polarization in automatic target recognition using resonance descriptions," *Electronic Lett.*, vol. 40, no. 4, Feb. 2004, online no: 20040170.
8. CST Microwave Studio, CST Computer Simulation Technology AG, http://www.cst.com/.

978-1-4244-5050-3/10/$26.00 ©2010 IEEE

Target Detection and Identification using Model Based Parameter Estimation for Noise Radar

Raviraj S. Adve[1], Natalia Nikolova[2] and Thayananthan Thayaparan[3]
[1]*Department of Electrical & Computer Engineering, University of Toronto, Toronto, Ontario M5S 3G4, Canada*
[2]*Department of Electrical and Computer Engineering, McMaster University, Hamilton, ON L8S 4K1, Canada*
[3] *Defence Research & Development Canada – Ottawa, 3701 Carling Avenue, Ottawa, ON K1A 0Z4, Canada*
E-mail: rsadve@comm.utoronto.ca

This paper deals with target detection and identification for concealed weapons detection in a noise radar system. In the application considered, the weapons are concealed by a human body. The targets are identified by estimating their resonance frequencies [1] and relative amplitudes in the reflected signals. These resonances are compared to a database obtained using numerical simulations. The resonances are estimated using model based parameter estimation (MBPE), specifically the Cauchy and Matrix Pencil methods, for the detection and identification of strategic targets for noise radar.

The Cauchy method [2] models the frequency domain response of the target as a ratio of two complex polynomials. In this approach, the target is excited and the return signal transformed to the frequency domain. Such an approach is naturally suited to a CW radar. The return signal is then modeled as

$$X_c(f) = \frac{\sum_{q=0}^{Q} a_q f^q}{\sum_{p=0}^{P} b_p f^p}, \tag{1}$$

where $X_c(f)$ is the received signal in the frequency domain after clutter cancellation. The zeros and poles of the system are determined by the polynomial coefficients $\{a_p, p = 1,\ldots, P\}$ and $\{b_q, q = 1,\ldots, Q\}$. The Cauchy method provides an efficient approach to determining these system parameters.

The Matrix Pencil approach [3-5] models the time domain return signal, $z(t)$, as a sum of complex exponentials.

$$z(t) = \sum_{p=1}^{P} A_p e^{z_p t}; \qquad z_p = \alpha_p + j\beta_p, \tag{2}$$

Again, the information identifying the target is embedded in the number of poles P and the poles themselves, z_p. In addition, the amplitude coefficients, A_p, associated with the poles allow for target detection, providing a level of confidence to avoid false detections.

A fundamental limitation for broadband noise systems is clutter and multipath. The data used in this paper are generated using numerical electromagnetic software simulations of chosen targets with and without a human body in the vicinity. The template poles are obtained using the responses for the targets in free space.

References

1. A. R. Hunt, R. D. Hogg, and W. Foreman, "Concealed weapons detection using electromagnetic resonances," *SPIE Conference on Enforcement and Security Technologies*, Boston, MA, Nov. 1998, pp. 62–67.
2. R.S. Adve, T.K. Sarkar, S.M. Rao, E.K. Miller and D.R. Pflug, "Application of the Cauchy method for extrapolating/interpolating narrowband system responses", *IEEE Trans. on Microwave Theory and Techniques*, vol. 45, no. 5, pp. 837-845, May 1997.
3. R.S. Adve, T.K. Sarkar, O.M. Pereira-Filho and S.M. Rao, "Extrapolation of time-domain responses from three-dimensional conducting objects utilizing the matrix pencil technique", *IEEE Trans. on Antennas and Propagation*, vol. 45, no. 1, pp. 147-156, Jan. 1997.
4. Y. Hua and T. K. Sarkar, "Matrix pencil method for estimating parameters of exponentially damped/undamped sinusoids in noise," *IEEE Trans. Acoust., Speech, Signal Processing*, vol. 38, pp. 814–824, May 1990.
5. O. M. Pereira-Filho and T. K. Sarkar, "Using the matrix pencil method to estimate the parameters of a sum of complex exponentials," *IEEE Antennas Propagat. Mag*., vol. 37, pp. 48–55, 1995.

978-1-4244-5050-3/10/$26.00 ©2010 IEEE

A Review of IRAs and UWB Antenna Measurement Systems

Everett G. Farr[1]
[1]*Farr Research, Inc., Albuquerque, NM, USA, 87123*
E-mail: efarr@farr-research.com

We summarize here a number of UWB antennas and related components that have been developed by us over the past decade. Many of these are variations on Impulse Radiating Antennas, which consist of a parabolic reflector and an ultra-wideband feed. The most commonly requested version is 46 cm in diameter, and operates over nearly two decades of bandwidth, from 250 MHz to 20 GHz. It is shown in Figure 1, and it radiates a clean impulse, with full-width half-max of 32 ps. Such broad bandwidth has been useful in testing that currently requires the use of multiple antennas. Such devices come in several sizes, and in a collapsible version reminiscent of an umbrella. We also review the Folded Horn, which is a very compact mesoband antenna, and the lens IRA. Finally, we review our time domain antenna measurement system. We review the hardware used, and the software algorithms for processing raw data into standard parameters such as gain and S_{11}. Our version of the hardware operates over 900 MHz to 20 GHz, and it characterizes non-dispersive antennas as low as 200 MHz. The entire system is easily stored in a small shed and can be set up outdoors and aligned in an hour. This range is easily used outdoors because it is relatively insensitive to temperature stability. Time-gating is used to eliminate ground bounce from the data, so an anechoic chamber is not needed. We compare data taken on our system to that taken from more conventional frequency domain systems.

Figure 1: **A IRA with diameter of 46 cm.**

978-1-4244-5050-3/10/$26.00 ©2010 IEEE

Source Localization and Imaging Using Multiple Signal Classification Technique in EMI Sensing Array

Lin-Ping Song[1], **Leonard R. Pasion**[2], **Stephen D. Billings**[2], and **Douglas W. Oldenburg**[1]

[1] *Department of Earth and Ocean Sciences, University of British Columbia 6339 Stores Road, Vancouver, BC, Canada, V6T 1Z4*

[2] *Sky Research Inc, Suite 112A, 2386 East Mall, Vancouver, BC, Canada, V6T 1Z3*

E-mail: lpsong@eos.ubc.ca

The source localization problem arises when using an electromagnetic induction (EMI) sensor to detect objects and discriminate UXO from clutter. To extract polarization tensor parameters from the EMI response, we have to first find source locations for a single or multiple objects. The latter is a more challenging problem. Moreover under a number of practical cases, when only using the spatial response distribution, we have difficulties of deciding if an anomaly within the field view is due to a single object or two or more objects. In this paper, we present a new three-dimensional source imaging technique to localize buried sources in the subsurface without prior knowledge of the number of objects.

The theoretical foundation of our imaging technique is based upon the orthogonal property of a signal subspace and a noise subspace in a multi-static response matrix defined in a sensor array. With an array of transmitters and receivers, we formulate a Tx-array based imaging operator and an Rx-array based imaging operator. Both operators can be applied individually or jointly to the null space singular vectors decomposed from the measured data. This is a multiple signal classification process [1] which is equivalently a back-propagation of data from measurement space to image space. In ideal cases, the perfect orthogonality can be achieved at or near a target location and a spatial metric function based on the orthogonal correlation shows a peak at that location. Over a region of interest, three-dimensional source imaging can be quickly obtained by evaluating each potential location since the array imaging operators are computed just one time and stored for any subsequent use with different data sets. The technique is, in principle, applicable to arbitrary sensor array geometries but requires that the number of Tx and Rx should be larger than the number of dipolar polarizations that need to be resolved. The immediate application of the technique is to the TEMTADS sensor system designed by the Naval Research Laboratory, which consists of a 5 x 5 array of transmitters and receivers. We evaluate the new imaging technique using test-stand data and field data, collected at San Luis Obispo, CA. and compare it with other focusing algorithms like beamforming [2]. Beyond source imaging, the theory developed here might be useful as an experimental tool in the design of a sensor array to optimally resolve objects.

References

1. R. O. Schmidt, "Multiple emitter location and signal parameter estimation," IEEE Trans. Antennas Propagat., 34, pp. 276-280, 1986.
2. L.-P. Song, D. W. Oldenburg1, L. R. Pasion, and S. D. Billings, "Adaptive Focusing for Source Localization in EMI Sensing of Metallic Objects: A Preliminary Assessment," Journal of Environmental and Engineering Geophysics, 13 (3), pp. 131-145, 2008.

978-1-4244-5050-3/10/$26.00 ©2010 IEEE

An Examination of the Validity of Methods Used to Calculate Compton Currents in Early Time HEMP Environment Codes

James L. Gilbert[1], William A. Radasky[1], and **Kenneth S. Smith[1]**
[1]*Metatech, Goleta,USA, 93117*
E-mail:jim.gilbert@metatechcorp.com

Since the first computations of the high-altitude electromagnetic pulse (HEMP) were performed in the late 1960s, there have been few publications that have critically examined some of the numerical modeling assumptions made at the time. Because of recent interest in more advanced air chemistry modeling, based on experimental measurements, questions also arose concerning the accuracy of the computation of the Compton currents used in state-of-the-art HEMP codes.

The HEMP code features of interest that are evaluated here include: the numerical process of injecting Compton electrons, given a specific photon energy; the accuracy of the model of approximating thin-angle scattering for the Compton electrons (known as the obliquity treatment) in the Compton current and ionization rate; and the model (and its solution) of computing the Compton currents and ionization rates in retarded time, which necessarily complicates the equations to be solved. The most questionable of these features is the obliquity treatment

In the obliquity treatment, the movement of a guide particle is tracked, including its slowing down by collisions with atomic electrons and its acceleration by electric and magnetic fields, but not the change of its direction by angular scattering. Instead, each guide particle is taken to represent an ensemble of particles whose angular scattering causes them to form a "cloud" around the guide particle, and the cloud is described solely by the mean square of angle of motion of the individual electrons in the cloud with respect to the guide particle. The obliquity factor is defined as

$$\eta = \frac{1}{\cos\theta} \tag{1}$$

where θ is the angle with respect to the guide particle. The primary question relating to the use of the obliquity factor is whether using the average obliquity factor for the electron distribution in expressions sufficiently approximates using the motion of the individual electrons.

This can be compared with a Monte Carlo approach based on simulating directly the angular scattering of each Compton electron and is intrinsically noisier than using obliquity. Computational limitations of the early 1970s led to the use of the obliquity approach for the early time HEMP codes. Now that PCs have many times the computational power of the mainframe computers of that time, we can use larger numbers of particles to determine the accuracy of the obliquity approach. In this presentation, we describe the development of a real time macroparticle simulation code for Compton electrons and compare the results with the obliquity treatment and with retarded time simulations. The motivation of this effort is to verify the treatment of Compton electrons in HEMP environment codes by constructing the macroparticle simulation code from the original references and performing the calculations in real time to verify the use of retarded time for the particle equations of motion. We find that the errors introduced by the obliquity approximation are small for the transverse currents and the ionization during the later portion of the Compton electron track, but more substantial errors are made in the early portion of the track, particularly for Compton electrons produced by high energy gamma rays as these electrons lag less behind the gamma wavefronts.

978-1-4244-5050-3/10/$26.00 ©2010 IEEE

Enhanced Inversion of Multiple Objects as Applied to New-Generation EMI Sensor Arrays

Lin-Ping Song[1], **Leonard R. Pasion**[2], **Stephen D. Billings**[2], and **Douglas W. Oldenburg**[1]

[1] *Department of Earth and Ocean Sciences, University of British Columbia 6339 Stores Road, Vancouver, BC, Canada, V6T 1Z4*

[2] *Sky Research Inc, Suite 112A, 2386 East Mall, Vancouver, BC, Canada, V6T 1Z3*

E-mail: lpsong@eos.ubc.ca

To accurately recover polarization tensor parameters of buried objects for effective UXO discrimination, we recently developed an inversion technique to process overlapping signals contributed from two or more objects within the field of sensor view [1]. One of the key steps in our multiple-object inversion is to select suitable multi-start locations drawn from random sampling over a region of interest. From selected starting points, a sequential procedure is then applied to determine the nonlinear parameter of locations/orientation of objects and their dynamic polarizabilities over a sensor specific time window. In the application, it is desirable to use the smallest amount of random sampling in the multi-start strategy to achieve a balance between computational effort and accuracy. On the other hand, to ensure that the technique is always robust and accurate, simple oversampling might be used to reduce possibility of being trapped in local minima due to limited sampling. In this paper, we will report a modified version of the technique in which some mechanisms are used to guide a spatial sampling process, aiming to improve the technique's ability to resolve closely spaced sources (e.g., some difficulty scenarios like shallow and deep sources sensed together) and enhance its global convergence.

Starting from to our previous strategy where candidate solutions (population) are sought over a large area, we attempt improvements by further probing promising location areas over which a re-sampling can be conducted or an effective constraint adaptively imposed based on the measured data. Two strategies are adopted for this purpose. One is to employ an evolutionary strategy for detecting the optimal solution set through communication, cooperation, and competition among the individuals of the population. This evolutionary technique is designed for any sensor array. For a structured sensor array (e.g., TEMTADS designed by the Naval Research Laboratory), we explore a fast method of a three-dimensional source imaging by exploiting the orthogonality of a signal subspace and a noise subspace in the multi-static response matrices. As a result, the peak locations of orthogonal correlations and their vicinities in the image define the target interest of areas. Once promising location spaces are found, we apply a nonlinear optimization to refine and determine all solution parameters. This hybrid technique is demonstrated with test-stand data and field data, collected with TEM TADS and MetalMapper systems at San Luis Obispo, CA.

References

1 L.-P. Song, D. W. Oldenburg, L. R. Pasion and S. D. Billings, "Transient electromagnetic inversion for multiple targets," Proc. of SPIE, Vol. 7303, 73030R1-12, 2009.

978-1-4244-5050-3/10/$26.00 ©2010 IEEE

A Boltzmann Equation Technique for the Calculation of Air Conductivity Effects in Early Time HEMP Environment Codes

James L. Gilbert[1], Kenneth S. Smith[1], and **William A. Radasky[1]**
[1]*Metatech, Goleta,USA, 93117*
E-mail:jim.gilbert@metatechcorp.com

In this presentation, we describe a method for solving the Boltzmann equation for secondary electrons appropriate for use in high altitude EMP (HEMP) field generation codes. In US HEMP codes, the air conductivity is determined by either of two techniques:

1. In most EMP codes, the secondary electron distribution is assumed to be in instantaneous equilibrium with the magnitude of electric field divided by the air density. When this is the case, the conductivity due to secondary electrons is the electron density multiplied by the electron charge multiplied by a mobility that is a function of E/ρ_r. The electron density is determined by solving rate equations in which the electron-ion attachment and the avalanche rates are also dependent on E/ρ_r. There are two differential equations to be solved each time step, one each for the electron and negative ion densities.
2. For rapidly changing electric fields, particularly at higher altitudes, a swarm theory modification was made to account for the electron inertia and the delay required for electron distributions to come into equilibrium with E/ρ_r. Swarm theory is based on taking velocity moments of the Boltzmann equation for the secondary electrons and truncating the resulting series of equations with the $v_x^2+v_y^2+v_z^2$ moment, which yields the scalar characteristic energy for the swarm. This is appropriate when the momentum exchange collision frequency is much larger than the energy exchange collision frequency. This approach still assumes that the distribution in velocity is known as a function of characteristic energy, but allows this energy, as well as the average velocity of the electrons, to change more slowly than E/ρ_r. Because the inertia of the electrons appears in the swarm equations for the velocity, Langmuir oscillations can be seen in calculations with the swarm model. There are six differential equations to be solved each time step – one each for the secondary electron and negative ion densities, three for the secondary electron swarm velocity and one for the secondary electron swarm characteristic energy.

In this method presented here, we solve the Boltzmann equation by expansion of angular derivatives in spherical harmonics and finite difference the magnitude of the velocity. This gives a set of equations that must be solved implicitly using a sparse matrix solver – one based on the conjugate gradient technique is used here. For early time HEMP applications, the spatial derivatives in the Boltzmann equation may be neglected and the equation becomes

$$\frac{\partial f}{\partial t}+\frac{q\vec{E}}{m}\cdot\vec{\nabla}_v f=\left.\frac{df}{dt}\right|_{elastic}+\left.\frac{df}{dt}\right|_{inelastic}+S_f-D_f \tag{1}$$

where we have separated the collision term into elastic and inelastic scattering terms. S_f and D_f are the sources and sinks (drains) of secondary electrons, respectively. The distribution function is expanded in spherical harmonics

$$f(v_i,\theta,\phi)=\sum_{lm} f_{ilm}Y_{lm}(\theta,\phi) \tag{2}$$

and the Fokker-Planck approximation for multiple small angle elastic collisions is used, together with a downscattering matrix for the inelastic collision. This has the advantage that the Fokker-Planck scattering is diagonal in this basis

$$\int d\Omega\, Y_{lm}^*(\theta,\phi)\nabla_{\theta,\phi}^2 Y_{lm}(\theta,\phi)=-l(l+1) \tag{3}$$

This is really just a statement that the higher harmonics decay more rapidly for multiple small angle scattering. The term for the acceleration of the electrons in the electric field is, unfortunately, not so simple, and the expansion results in terms that are the Clebsch-Gordon coefficients of atomic quantum mechanics. In the presentation, we will show comparisons of the secondary electron currents calculated for the axisymmetric case with the instantaneous equilibrium model and swarm theory for various electric field time histories, and discuss limitations associated with determining the inelastic term downscatter matrix from electron swarm experiments.

978-1-4244-5050-3/10/$26.00 ©2010 IEEE

A Review of Low Tech Pulsed Threat Generators for Conducted IEMI

Lars Ole Fichte[1], Johannes Hagmann[1], Stefan Potthast[2], Martin Schaarschmidt[2], Stefan Dickmann[1]

[1] Helmut-Schmidt-University, University of the Federal Armed Forces Hamburg, Germany
[2] Bundeswehr Research Institute for Protective Technologies and NBC-Protection, Munster, Germany

E-mail: lars-ole.fichte@hsu-hh.de

The purpose of this paper is to investigate the possibility of destructive interference with computer components using high energy pulses, coupled into the casing of the computer via power or data lines. A number of pulse generators can be found for the generation of such pulses, be it for general EMC purposes or for the generation of high power ultra-wideband pulses for testing the immunity of electronic devices. For a realistic assessment of real world IEMI threats, one must take into account that most aggressors will not have access to this kind of “high-tech” hardware, due to lack of funding or export restrictions. More probable is one of the two following scenarios:

1. A potential aggressor with little or no technical background will revert to the use of commercially available devices which were developed for a different purpose, such as tazers, electric shock batons, electrical fence energizers etc. Consequently, we must discuss suitable devices and the possibility to misuse them. The aggressor might try to modify those “dual use” pulse generators slightly to maximize their potential to inflict damage, using well known devices such as pulse forming networks.
2. For the second scenario we assume that a technical expert, such as an engineering student or a physicist, makes use of their technical knowledge to pick a circuit for generating potentially harmful pulses from literature. They build and optimize it with a certain purpose in mind, for example a maximum voltage or maximum rise time of a pulse.

For the first scenario the following commercial high voltage sources were chosen for our experiments: A low-cost electric stun baton, a professional tazer and an electrical fence energizer. In the first investigations we measured the pulse emitted by the source without any modifications. As a result the stun gun generated a pulse rise of approximately 20 μs and a maximum voltage of 25 kV, even though the device was specified to provide ca. 250 kV in the worst case. These pulses are bipolar and shaped like a damped sinus. In a second step additional components were used to optimize the generated pulses. The sources were connected to a high voltage peeking capacitor and a spark gap, working as a pulse forming network. These pulses were coupled into a generic power supply network and were measured at different output ports, such as power plugs, fuses etc.

For the second scenario, a number of undergraduates used reverse engineering on an stun gun. As a first step, the power transformer was redesigned using high voltage MOSFETs and power diodes better suited to the tasks, shortening of the pulse rise time from 17 μs to 3 ns, while maintaining the maximum voltage of 10 kV. Additional efforts involved a optimization of the spark gap and led to a lessening of unwanted parasitic inductance in the pulse-forming part of the circuit. The result was a output voltage of 25 kV. Using the sources coming from these scenarios we were able to transfer pulses with 20 kV amplitude and 4 ns rise time over the power lines and through the input filter of a computer and to reliably affect diverse computer components.

978-1-4244-5050-3/10/$26.00 ©2010 IEEE

EMT-based Susceptibility Analysis of Extended Multiconductor Transmission Lines

Benedikt Schetelig[1], Lars Ole Fichte[1], Stefan Potthast[2], Stefan Dickmann[1]

[1] Helmut-Schmidt-University, University of the Federal Armed Forces Hamburg, Germany
[2] Bundeswehr Research Institute for Protective Technologies and NBC-Protection, Munster, Germany
E-Mail: benedikt.schetelig@hsu-hh.de

To assure the immunity of cable-wired communication systems to external electromagnetic influences, it is essential to know the disturbances coupled into the connecting cables to carry out an evaluation at the inputs of the connected devices based on its prescriptive limits. Especially in complex systems, we have to deal with large cable bundles. Numerical calculations of such cable structures require a lot of computation power, while an analytical approach is normally restricted to simple geometries.

In this paper, a simplified susceptibility analysis of a very long multiconductor transmission line is performed. It is assumed that the regarded transmission line is placed in a multi-cavity structure. In particular, it is supposed that some parts of the transmission line are mounted in areas of high electromagnetic exposure, for example because of the presence of large apertures (windows, doors). The remaining parts of the multiconductor transmission line are placed in metallic cable channels with low direct EM exposure. For simplification, in the first example to be analyzed, it is defined that there is only one area of high exposure at the beginning of the cable (left side of the transmission line) and that the remaining part including the termination, representing an attached device, is mounted in the cable channel (right side).

Because of the segmentation of the transmission line, one can apply the theory of electromagnetic topology (EMT) for step-by-step calculation of the total structure. It is possible to transfer the termination inside the cable channel to the beginning of it and use the resulting equivalent input impedance to perform a calculation of the field-to-cable coupling in the area of high EM exposure. The resulting current on the transmission line at the beginning of the cable channel can be used to determine the current at the far right end of the channel where the electronic device is placed. This transformation of impedances along a line is well-known for single transmission lines. When it is applie to analyze multiconductor transmission lines in setups close to real-world scenarios, the problem gets a little bit more complicated. Because of the coupling between the wires themselves as well as with the surrounding metallic enclosure, a simple impedance transformation is not longer possible. Furthermore, the single termination load of a single transmission line is replaced by up to $3n-1$ different loads on a n wire cable. For this reason, it is necessary to consider the boundary conditions valid for multiconductor cables.

In this contribution, several approaches are developed to perform a topological segmentation with the aim to reduce the demands of computation power when the total cable structure is analyzed. We present possibilities of a simplified calculation of field-to-multiconductor transmission line coupling in electrically large structures, where only parts of the regarded cable is directly exposed to EM fields. A hybrid approach combining transmission line theory and field theory is applied. In addition, a reduced consideration of the cable path allows a simplified, but still good estimation of the induced current at the electronic device, attached to the end of the line and shielded against the field. This way, it is possible to estimate quickly the induced currents to a multiconductor transmission lines, which is only partly visible to the incident electromagnetic field.

978-1-4244-5050-3/10/$26.00 ©2010 IEEE

Use of Domain Decomposition in Time-Domain for IEMI Estimation on Multi-room Structures

Jules Keghie[1], Lars Ole Fichte[1], Stefan Potthast[2], Stefan Dickmann[1]

[1] Helmut-Schmidt-University, University of the Federal Armed Forces Hamburg, Germany
[2] Bundeswehr Research Institute for Protective Technologies and NBC-Protection, Munster, Germany

Analyzing the susceptibility of electrical systems to Intentional Electromagnetic Interference (IEMI) becomes more and more important. This is in part due to the relatively easy access to potential components needed for building those interfering sources; but also to the high level of component integration in electronics. Investigations on IEMI interactions with complex systems have been conducted in several publications. The analysis of those interactions for electrical large systems is usually done by means of the topological approach introduced by Baum, Liu and Tesche.

In this paper we propose a procedure that facilitates IEMI susceptibility investigations for electrical large systems made up of many well connected cavities. The procedure we propose starts with a topological analysis of the system and takes the concept of good shielding approximation into account, which has been introduced by Baum. In a second step, we classify the degree of electromagnetic coupling between the different sub-volumes of the geometry of interest as strong or weak coupling, according to the result of the topological analysis. This allows us to decompose the original problem (that may contain several cavities) into a finite set of sub-problems consisting only of sub-volumes which interact through a strong coupling. Field computation using a 3D solver can then be achieved sequentially along the structure, asdescribed below.

The proposed procedure makes use of the sequential behavior when dealing with time domain phenomena and is therefore more effective in this domain. The use of this procedure in the frequency domain also leads to good results for the early times / high frequencies, but higher security margins for lower frequencies have to be considered in this case . This is due to the fact that the segmentation of an electrically very large system into many smaller sub-systems removes some late times/ low frequencies information during the computation of the overall system response against IEMI. It is useful for the estimation of the IEMI coupling on multi-rooms where the electrical dimension of the whole structure is so large that a numerical analysis of the whole system at higher frequencies using 3D simulation codes is not efficient.

We start with the computation of field quantities like currents flowing on a virtual monopole antenna inside the sub-volumes nearest to the interfering IEMI source. This calculation is done in the time domain. After that, we use the resulting currents as sources in the further computation of the fields in the sub-volumes farther from the IEMI source but adjacent to the previous ones. We apply this procedure sequentially along the structure until we reach the sub-volume where our equipment of interest is located. At this stage an estimation of the IEMI coupling at the input of the target electronics can be accomplished by computing a transfer function between the current on the last fictive monopole antenna and the coupling structures of the target. With this estimation it is possible to predict the behavior of EM fields in rooms which are not directly affected by IEMI using the transfer functions between the fictive monopole antenna along the path from the IEMI source to the target. The frequency domain response of the target can be obtained using Fourier transform.

978-1-4244-5050-3/10/$26.00 ©2010 IEEE

M-Sequence Based Single Chip UWB-Radar Sensor

M. Kmec[1], M. Helbig[1], R. Herrmann[1], P. Rauschenbach[2], J. Sachs[1], K. Schilling[1]
[1]*Ilmenau University of Technology, Ilmenau, Germany*
[2]*Meodat GmbH, Ilmenau, Germany*
E-mail: martin.kmec@tu-ilmenau.com

The steady growing areas of UWB application push the requests for new enhanced UWB radar systems. A very promising solution for novel UWB device realisations is based on the so called M-sequence approach - a concept with unique symbiosis of high frequency electronics and associated signal processing, first introduced in [1]. One of its most important benefits is in the relatively low signal levels which have to be handled by the radar circuitry. Hence the low cost SiGe BiCMOS process (break down voltage about 2V) can be used for monolithic integration of the whole M-sequence radar RF electronics.
In recent time, there have been great advancements in the investigation of various UWB M-sequence device architectures based on multi-chip structures with separate ultra-wideband ASICs [2]. For instance we have realised and successfully tested a set of ASIC based modules which covers operational frequency bands in the baseband region from DC to about 20 GHz, as well as we have performed the first experiments in the cm- and mm-wave ranges. The gained knowledge, cost reduction endeavour and the need for UWB-systems of increasing complexity (e.g. MIMO UWB sensor arrays) have motivated the first monolithic integration of the complete RF-part of the M-sequence UWB radar electronics into one SiGe die (also see Figure 1). This first realised M-sequence based radar system-on-chip (SOC) is equipped with one transmitter and two receiver channels. The packaged IC can handle signals in the frequency range from near DC up to 18 GHz. This corresponds to impulses with Full Width at Half Maximum (FWHM) of about 50 ps.

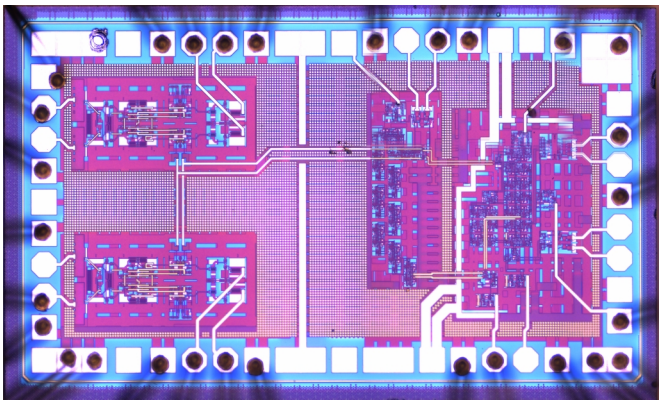

Figure 1: **Single chip radar die**

The final article will describe the unique radar SOC in more detail mainly from the point of view of circuit architecture and chip design. Additionally we will refer to advantages and disadvantages of a single chip UWB device realization and new principles to compensate unwanted effects resulting from full RF-integration. On the one hand the key benefits of system-on-chip integration are typically in the overall system performance and reliability improvements due to reduced interconnect and package parasitics, smaller package count and the higher integration level. Furthermore, power supply requirements are reduced because fewer high-frequency signals that require usually 50-Ω interfaces are routed off-chip. On the other hand, the single chip architecture comprises broadband high frequency high power output and sensitive input devices on the same substrate or package respectively. Thus, the undesired signal coupling or crosstalk can degrade the performance of the sensitive receive circuitry and thus of the whole system. An investigation of these effects will be presented trying to answer interesting questions regarding the on-chip handling of high-frequency ultra-broadband signals. Finally, a few measurement examples will be shown to demonstrate the operation of the discussed SOC-sensor in the baseband frequency region.

Acknowledgments – This work has been granted by the German Research Foundation (DFG).

References

1. J. Sachs, P. Peyerl, "A New Principle for Sensor-Array-Application," Proceedings of 16th IEEE Instrumentation and Measurement Technology Conference, IMTC/99, Venice, Italy, May 24-26, 1999, p. 1390-1395
2. M. Kmec, R. Herrmann, J. Sachs, P. Peyerl, P. Rauschenbach, "Extended Approaches for M-Sequence based UWB Systems", Ultra-Wideband Short-Pulse Electromagnetics 8, edited by Tyo, J. Scott; Baum, Carl E.; Stone, Alexander P.

978-1-4244-5050-3/10/$26.00 ©2010 IEEE

Measurement of the attenuation of buildings and structures and comparison with published data

R. Hoad, S. P. Watkins, A. Wraight, A. Lambourne, A. Leaver and **B. Petit**
QinetiQ,Cody Technology Park, Farnborough, Hampshire, UK, GU14 0LX
E-mail: rhoad@qinetiq.com

Intentional Electromagnetic Interference (IEMI) can pose a threat to existing and established facilities. Buildings, structures or barriers in the path of the Radio Frequency (RF) signal will reduce or attenuate the magnitude of the RF signal and therefore provide a degree of inherent protection. However, not all materials have the same attenuation and the level of attenuation can vary with frequency. The attenuation can be affected for example by factors such as the surface treatment of the material, e.g. metal coating on glass to provide thermal insulation, as well as the age and state of the construction material, e.g. if concrete is wet or dry.
Measurements of the attenuation of a three story office building have been conducted. Internal room structures which provide enhanced attenuation but are still manufactured from common low cost building materials have also been designed, produced and tested. This data has been analaysed and compared with published data [1-4] on complete buildings and building materials attenuation data. Rules of Thumb have been produced for the inherent attenuation provided by buildings for radiated IEMI threats.

References

1. W. C. Stone, 'NIST Construction Automation Program Report No. 3, Electromagnetic Signal Attenuation in Construction Materials', Building and Fire Research Laboratory Gaithersburg, Maryland 20899, NIST United States Department of Commerce Technology Administration National Institute of Standards and Technology, October 1997
2. P. Pauli and D. Moldan, 'Reduction and shielding of RF and Microwaves', Electromagnetic Environments and Health in Buildings Conference, May 2002, London, UK
3. C. Holloway, 'Propagation and Detection of Signals Before, During and After the Collapse of Large Structures', NIST, Boulder, United States, 1st August 2009
4. IEEE Std 473-1985, 'IEEE Recommended Practice for an Electromagnetic Site Survey (10 kHz to 10 GHz)', , Reaffirmed September 26, 1991

978-1-4244-5050-3/10/$26.00 ©2010 IEEE

Compact Ultrashort Rise Time Electromagnetic Bench Test

J. Raimbourg[1]
[1]*CEA/DAM – Ile de France, F91297, Arpajon, France*
E-mail: joel.raimbourg@cea.fr

Properties of electromagnetic pulse (EMP) generated in laser facilities depend on the pulse duration, energy, and intensity of the laser. For lasers with nanosecond to picosecond pulse duration, laser-plasma interactions can produce "hot electrons" in the 10 keV to MeV range. Only a small fraction of these hot electrons escape the target because of large electrostatic fields associated with these escaping electrons. However, the dominant source of electromagnetic pulse at these laser facilities is due to these escaping electrons. Taking into account the target chamber attenuation, the EMP level in the target bay could be up to 10 kV/m and the spectrum ranges from 100 MHz to 5 GHz.
Diagnostics developed for laser-produced plasmas should comply with this electromagnetic environment. One of the main difficulties is the single shot aspect of the process. All diagnostics must work under EMP level condition during the experiment. A temporary dysfunction is not permitted in our case.
In order to test diagnostic immunity, we built an ultra short rise time EMP bench test. The designed system is composed of three parts: a generator, an oscillator and an antenna.
The 10 kV, 100 ps rise time generator is connected to a double ridge guide antenna. It produces electric fields up to 10 kV/m with a rise time lower than 100 ps. A gas-tube lightning protector is inserted at the antenna input. The firing threshold occurs at 10 kV (with a 100 ps pulse) for a regular 1.5 kV/µs product. The antenna is discharged into the shorted spark gap. It induces an oscillating current which is converted into radiation by the antenna.
The susceptibilities of the different diagnostics tested with this bench are presented.

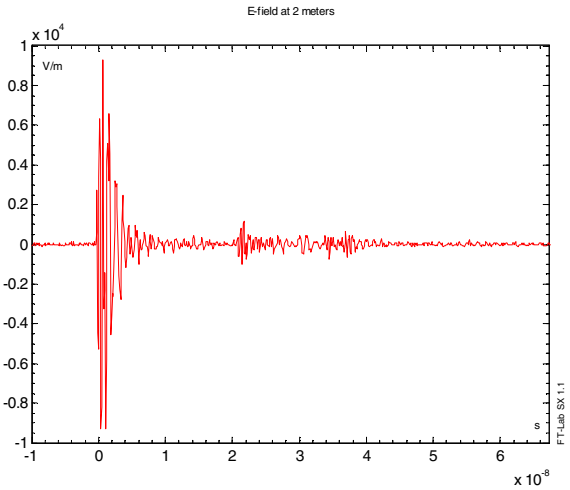

Figure 1: **E-field generated at 2 meters**

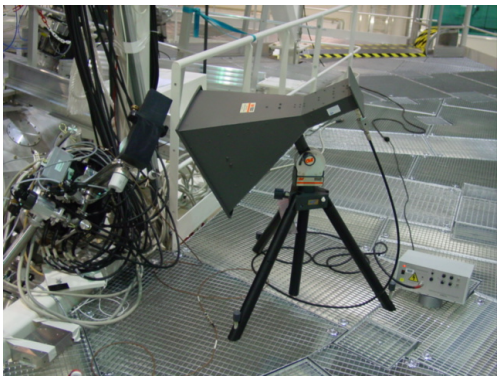

Figure 2: **Testing diagnostic susceptibility in-situ**

978-1-4244-5050-3/10/$26.00 ©2010 IEEE

Reverberation Chamber vs. Semianechoic Chamber

Lubos Suchy, Libor Palisek
VOP-026 Sternberk, s.p., Olomoucka 1841/175,
785 01, Sternberk, Czech Republic

E-mail: l.suchy@vtupv.cz

Immunity testing against electromagnetic field is one of the common requirements for electronics especially in case high reliability is required. This testing is normally carried out in semianechoic chamber where equipment under test is directly irradiated by antenna placed in specified position according to relevant standards (MIL-STD-461 method RS 103, EN 61 000-4-3, etc.). The alternative method for this regular method is testing in reverberation chamber (RC). Now there is a question how comparable the results achieved with these two methods are and which conditions has to be fulfilled.

The aim of these practically realized experiments is to verify the effects of electromagnetic field on electronic equipment behavior when these equipment are tested in semianechoic chamber as well as in reverberation chamber for defined conditions. Penetration of electromagnetic field through regular metal cover of chosen sample will be investigated by measurements of electromagnetic field components. Next electromagnetic field coupling in to wires placed in metal cover will be found. On the basis of gained results from testing the endeavor will be to give conclusions with conditions which are necessary to be fulfilled and with statement how much results from testing gained from regular method use (semianechoic chamber) correspond to results from immunity testing with alternative method (RC). It should give information for which conditions it is possible to compare the results from both methods.

978-1-4244-5050-3/10/$26.00 ©2010 IEEE

Modified Traveling Current Source Return Stroke Model

J.M.Cvetic[1], and **F.Heidler[2]**
[1]*Faculty of Electrical Engineering Belgrade, Belgrade, Serbia*
[2]*University of the Federal Armed Forces, EIT 7, Munich, Germany*
E-mail: cvetic_j@etf.rs

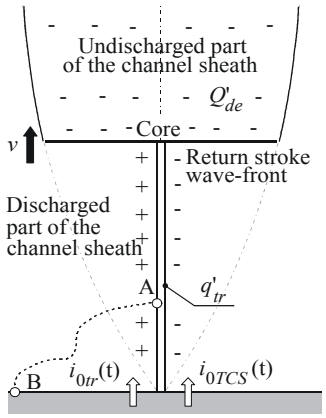

Fig. 1 Side view of the channel containing the core and the corona sheath during the return stroke stage

Abstract: The classical traveling current source (TCS) model [3] without current reflections from the striking point is extended to take into account the current component caused by the transferred line charge density along the channel core below the return stroke wave-front. In the modified TCS model (MTCS) the distribution of the channel current is uniform i.e. there is no line charge along the core below the return stroke wave-front. Assumptions adopted in this study for the MTCS model have yielded final results similar to those of the Bruce-Golde (BG) model [1]. Nevertheless, the physical picture of the discharge differs significantly from that of the BG model, and moreover the results could be quite different if one assumed a net positive line charge density along the channel core. Side view of the lightning channel containing channel core and the corona sheath during the return stroke stage is depicted in Fig.1. The rotational electric field component generated by the axial time-variable current is neglected compared to the electrostatic field component near the core. Due to the perfectly conducting channel core and the absence of the rotational electric field, the voltage drop between point A and point B at the ground surface is zero, Fig.1, It follows that the radial electrostatic field component near the core is zero i.e. the additional channel-base current component $i_{0tr}(t)$ is generated. This component carries positive charge neutralizing the negative line charge q'_{tr} adding to the existing channel-base current. Moreover, due to the vicinity of the negative charge in the corona sheath above the return stroke wave-front and the finite conductivity of the channel core, an excess of positive charges along the core should be expected. However, for the purpose of this paper their presence is neglected although there is clear experimental proof of their existence [2], [4]. Transferred line charge density component q'_{tr} for the TCS model is derived in [1]. The total negative transferred charge (seen from the channel base) is

$$q_{tr}\big|_{z=0} = -\int_0^{vt} i_{0TCS}(t+z/c)/c\,dz\,, \quad t \ge 0\,,\ z \le vt\,. \tag{1}$$

where i_{0TCS} is the channel-base current in the TCS model. According to the aforestated assumption, the transition channel-base current component i_{0tr} carrying positive charge is

$$i_{0tr} = \left|dq_{tr}/dt\right|_{z=0} = (1/c)\int_0^{vt} (di_{0TCS}(\xi)/dt)\,dz + (v/c)\,i_{0TCS}[t(1+v/c)]\,, \quad \xi = t+z/c\,,\ t \ge z/v\,. \tag{2}$$

Since $di_{0TCS}(\xi)/dt = (di_{0TCS}(\xi)/dz)\,c$, (2) reduces to

$$i_{0tr}(t) = \int_0^{vt} di_{0TCS}(t+z/c) + (v/c)\,i_{0TCS}(kt) = k\,i_{0TCS}(kt) - i_{0TCS}(t)\,, \quad k = 1+v/c\,. \tag{3}$$

The total channel-base current according to the MTCS model is

$$i_{0MTCS}(t) = i_{0tr} + i_{0TCS} = k\,i_{0TCS}(kt)\,. \tag{4}$$

If $v \ll c$, (4) reduces to the current expression in the TCS model [3]. If $v \le c$ the differences are more pronounced, the current is stronger and its peak appears earlier. The deposited line charge density component Q'_{de} as a function of the channel-base current in the TCS model is derived in [1]. Substituting it into (4) the line charge density component in the MTCS model can be expressed as

$$Q'_{de}(z) = i_{0MTCS}(z/v)/v\,. \tag{5}$$

The deposited line charge component (5) is the same as in the BG model [1]. It is easy to show that the current distribution is uniform below the return stroke wave-front i.e. $i_{MTCS}(z,t) = i_{0MTCS}(t)$, $z \le vt$. Therefore, in the MTCS model there is no transferred line charge density component along the channel core. The transition channel-base current component (3) diminishes if there are current reflections from the ground, for the ground reflection factor $0 \le R \le 1$, [3].

References

1. R.Thottappillil, V.A.Rakov and M.A.Uman,"Distribution of charge along the lightning channel: Relation to remote electric and magnetic fields and to return-stroke models," J. Geophys.Res., vol.102, D6, 1997.
2. J.Schoene, M.A.Uman, V.A.Rakov, K.J.Rambo, J.Jerauld and G.H.Schnetzer, "Test of the TL model and the TCS model with triggered lightning return strokes at very close range" J. Geophys. Res. vol. 108, D23, 2003.
3. F.Heidler, "Review and Extension of the TCS – Model to Consider the Current Reflections at Ground and at the Upper End of the Lightning Channel," Journal of Lightning Res., vol.1, 2007.
4. M. Miki, V.A. Rakov, K. J. Rambo, G.H. Schnetzer, and M.A. Uman, "Electric field near triggered lightning channels measured with Pockels sensors," J. Geophys. Res., vol.107, D16, 2002.

978-1-4244-5050-3/10/$26.00 ©2010 IEEE

HPEM Environment – Crucial Parameters

Libor Palisek, Lubos Suchy
VOP-026 Sternberk, s.p., Olomoucka 1841/175,
785 01, Sternberk, Czech Republic

E-mail: l.palisek@vtupv.cz

The part of High Power Electromagnetics (HPEM) environment is electromagnetic environment which can be caused by directed energy weapons (DEW) use. This electromagnetic threat depends on availability of suitable power technologies which can generate high power electromagnetic fields within the certain distance. Signals generated by such technologies are usually called HPM (High Power Microwaves) and UWB (Ultra Wide Bandwidth). These signals are in microwave region due to possibility to create directed energy with antenna of reasonable sizes. Other basic important parameters of used signals are pulse width and repetition rate. These parameters depend on state of the art technologies.

The aim of this study is to evaluate the influence of HPM and UWB parameters on effects on electronics. All basic parameters like frequency, pulse width and repetition rate will be taken in to account. Results from transfer function measurements as well as results from electromagnetic susceptibility measurements will be presented and evaluated. Both typical failures (temporary as well as permanent damage) of electronics will be considered. The results related to permanent damage of electronics will be compared with results from simulations with use of model based on electro-thermal analogy (PSpice model). At the end of this presentation recommendation for parameters of HPM and UWB for effective influence on electronics will be carried out.

978-1-4244-5050-3/10/$26.00 ©2010 IEEE

Analytic Methods for Coupling to Cables with Large Numbers of Component Wires - Excitation by External Fields

James L. Gilbert[1]
[1]*Metatech, Goleta,USA, 93117*
E-mail:jim.gilbert @metatechcorp.com

When nearest neighbor interactions in a cable containing a large number of component wires, it was shown in a previous presentation [1] that the capacitance matrix is proportional to the transverse Laplacian operator

$$C = -6b^2 C_{od} \nabla_\perp^2 \tag{1}$$

where C_{od} is the capacitance per unit length between neighbor wires in a hexagonal array and $2b$ is the spacing between neighbor wires. This was used to show that the equation for forward propagating modes in the transmission line was given by a diffusion equation

$$\frac{\partial F}{\partial z} = 3vb^2 RC_{od} \nabla_\perp^2 F \tag{2}$$

if the dielectric material between wires was uniform. In Equation (2), v is the propagation velocity in the uniform dielectric, R is the resistance per unit length in an individual wire and $F=I+vQ$, where I is the wire current and Q is the charge per unit length on the wire. This correspondence was used to derive the decay of modes on the cable bundle corresponding to injection into the bundle on a single wire, and was generalized to include the effects of non-nearest neighbor interactions in a hexagonal array. Since that presentation, we have noted that the technique is more general and holds for non-uniform dielectrics as well, as long as they possess the necessary degree of n-fold rotational symmetry.

This technique has been extended to the calculation of surface terms and the coupling of external fields to the wire arrays, permitting the calculation of the excitation by external electric and magnetic fields in an analytic manner. In this presentation we will present examples of the coupling to wire arrays and the use of the finite element technique to calculate the coefficients involved for non-uniform dielectrics.

References

1. J. L. Gilbert, "Analytic Methods for Coupling to Cables with Large Numbers of Component Wires," *EUROEM 2008*, Lausanne.

978-1-4244-5050-3/10/$26.00 ©2010 IEEE

Novel Magnetic Radiative Structures inspired by Metamaterial Concepts

Toshiro Kodera[1,2] and Christophe Caloz[1]

[1] École Polytechnique de Montréal, Poly-Grames Research Center,
Centre de Recherche en Électronique Radiofréquence (CREER),
Montréal, QC, H3T 1J4, Canada
[2] Yamaguchi University, Ube-shi, 755-8611, Japan

Over the past century, the gyrotropic properties of ferrite materials have been widely exploited in microwave applications. Although ferrites have been extensively used in microwave components and systems, there have been surprisingly few reports on ferrite-based radiative structures, such as antennas, reflectors and transceivers.

Recently, there has been tremendous interest in engineered artificial materials known as metamaterials. While these metamaterials have been mostly based on lumped-element resonator configurations so far, ferrites, which exhibit interesting dispersive responses from their molecular (spin) structure, can offer advantageous avenues to metamaterials.

In this context, this talk will present a number of radiative phenomena and devices, inspired by metamaterial concepts, which were developed in the group of the authors. Specifically, it will present the full-wave derivation, the design and implementation of full-space frequency and bias scanning leaky-wave antennas [1], combined antenna-diplexer/duplexers [2], low-profile monopoles [3], and self-biased integrated millimeter-wave ferromagnetic nanowire components with double ferromagnetic resonances [4].

References

[1] T. Kodera and C. Caloz, "Uniform ferrite-loaded open waveguide structure with CRLH response and its application to a novel backfire-to-endFire Leaky-Wave Antenna," *IEEE Trans. Microwave Theory Tech.*, vol. 57, no. 4, pp. 784–795, April 2009.

[2] T. Kodera and C. Caloz, "Leaky-wave antenna integrated duplexer using CRLH uniform ferrite-loaded open waveguide," in Proc. *IEEE MTT-S Int. Microwave Symp. Dig.*, Boston, MA, June 2009.

[3] T. Kodera and C. Caloz, "Low-profile leaky wave electric monopole loop antenna using the $\beta = 0$ regime of a ferrite-loaded open waveguide," *IEEE Trans. Antennas and Propagation*, submitted.

[4] V. Boucher, L.-P. Carignan, T. Kodera, C. Caloz, A. Yelon, and D. Mnard, "Effective permeability tensor and double resonance of interacting bistable ferromagnetic nanowires," *Phys. Rev. B*, vol. 80, pp. 224402:1-11, Dec. 2009.

978-1-4244-5050-3/10/$26.00 ©2010 IEEE

High fidelity physics-based EM models for application to through-wall microwave tomographic inverse problems

Peter B. Weichman
BAE Systems, Advanced Information Technologies
6 New England Executive Park, Burlington, MA 01803

A range of powerful numerical EM forward modeling algorithms will be reviewed, based on rigorous analytic solutions to the Maxwell equations, developed for application to 3D building tomographic inverse problems based on microwave remote sensing. Building layout estimation is a nonlinear inverse problem with a potentially huge number of degrees of freedom. Moreover, the microwave propagation physics involves multiple reflection, transmission, and diffraction events, presenting a major challenge to the creation of a high fidelity, numerically efficient forward model. Numerical efficiency is critical because many iterations of the forward model are required for solution of the inverse problem.

Efficiency requirements dictate a ray-based geometrical optics approach, which is accurate at high frequencies where scatterers appear smooth on the scale of the wavelength. On the other hand, absorption (mostly from water content) increases sharply with frequency, and microwave penetration into the deep interior attenuates. Balancing these competing requirements these, one infers that the most useful part of the electromagnetic (EM) spectrum is the 0.7–2 GHz band (15–50 cm wavelengths).

Reflection and transmission of rays from perfect, flat walls (including floors and ceilings), but with arbitrary layered structure, are the simplest to model, however more realistic walls have periodic transverse internal structure, such as studs, rebar, brick or concrete block. In this case, an incident ray splits into a finite, discrete set of outgoing rays satisfying a Bragg condition. The periodic structure also leads to a coupling of the incoming ray to the spectrum of trapped waveguide modes that exist within such a wall. In an insulating (nonabsorptive) wall the perfect transmission of such modes along it leads to complex, long-lived reverberating tails. The results will be illustrated using an exact solution for a model of a wall containing thin, cylindrical, metallic rebar. Also important in some cases are diffractive interactions with smaller elements, such as edges (e.g., door jambs and window frames). These lie outside of ray theory, but isolated diffraction events may be incorporated into an "enhanced" theory by importing precomputed microscopic scattering characteristics—the so-called uniform theory of diffraction (UTD).

Inverse problem complexity must be dealt with through a mutually informative combination of data acquisition, search algorithm design, model regularization and use of prior knowledge. In some cases available data is essentially limited, and the complexity unavoidable. However, the concept of operations for the building tomography problem often allow for collection of a very diverse data set, with multiple arrays of transmitters and receivers distributed over a wide range of positions. This may be used to greatly reduce the problem complexity. In particular, spatially diverse placement of transmitters and receivers allows one to reduce a global simultaneous search over all of the building parameters (a practical impossibility), to a sequence of more manageable local searches. Moreover, the ability to either directly measure, or to Fourier synthesize in postprocessing, localized time domain pulses allows one to organize the search according to the depth of the feature in the building. Such an hierarchical approach, in which nearer structures are sequentially inferred and their effects removed from the signal to resolve the next deepest structure, potentially allows a very efficient solution to the inverse problem.

However, that there are fundamental limitations to even this procedure due to several colluding effects. First, the number of structures contributing to the signal in a given time window increases rapidly with depth. At the same time, their individual contribution to the signal, due to multipathing, wavefront spreading, and absorption, decreases rapidly. Moreover, nearer structures cannot be characterized perfectly, and later time reverberation from them will be imperfectly subtracted. Such residual noise, together with that from the unmodeled diffracting structures (as well as unmodeled imperfections in large structures), can very quickly overwhelm the signals of interest. Careful sensitivity studies will be presented that illustrate the fundamental limitations of the inversions. Limited inversions of real data collected from a simple building will also be described. Noise and uncertainties in real data are found to far surpass those in numerical experiments.

Acknowledgments: This work was supported in part by the DARPA VisiBuilding program.

978-1-4244-5050-3/10/$26.00 ©2010 IEEE

DESIGN, CONSTRUCTION AND TEST OF A HALF IMPULSE RADIATING ANTENNA

Felix Vega[1,2], Nicolas Mora[1], Farhad Rachidi[1], Nestor Peña[3], Francisco Roman[2]

[1]*Swiss Institute of Technology of Lausanne (EPFL), Lausanne, Switzerland*
[2]*National University of Colombia, Bogota, Colombia*
[3]*Los Andes University, Bogota, Colombia*

E-mail: felix.vega@epfl.ch

The Impulse Radiating Antenna (IRA) was first presented by Baum in [1]. This device has been used to produce impulse electric fields in several applications, such as immunity testing. The Half-IRA (HIRA) is a "monopolar" version of the IRA. This configuration avoids the use of high voltage baluns, facilitating the connection of transmission line-based pulse generators.

The HIRA here presented consists of a 2-m diameter half parabolic reflector above a 2.5 m x 2.5 m ground plane. The focal to diameter (F/D) relationship is 0.42. The feeders were designed to obtain an antenna's input impedance Z_i=100Ω. Figure 1 presents a picture of the realized antenna.

The antenna is connected to a coaxial Pulse Forming Line (PFL) generator, isolated in SF6 at 7 bars of pressure, producing 600-ps risetime,16-kV peak signals.

Figure 2 shows the antenna's feeding voltage $V(t)$, reconstructed from the measurement of the magnetic field at the dish surface. As expected, the pulse amplitude is about 15 kV and the risetime is 600 ps.

The radiated electric field $E(t)$ on boresight depends on the antenna diameter D, the input impedance Z_i, the distance R, and the feeding voltage $V(t)$ [2]. Figure 3 shows, in black, the electric field measured with a B-Dot sensor at 3 m from the focal point. In the same figure, we have plotted in red the expected electric field using the analytical formula in [2] and starting from the feeding voltage shown in Figure 2. It can be seen that the predicted field is in very good agreement with the measured waveform.

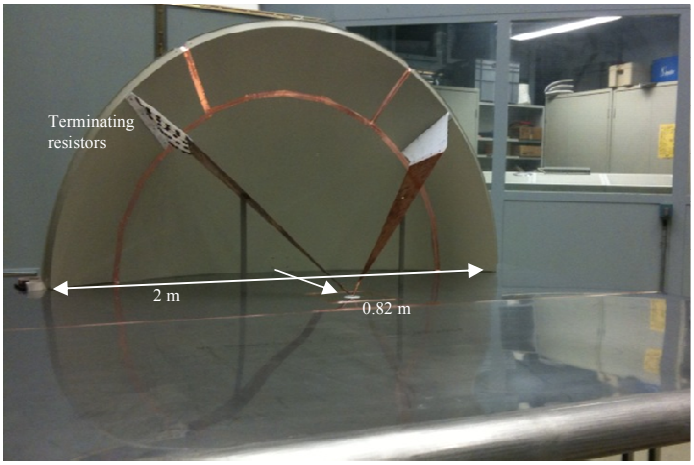

Figure 1. Half IRA

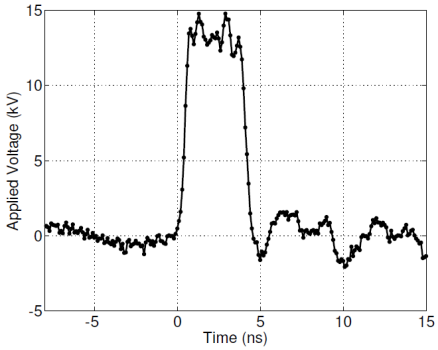

Figure 2. Antenna's driving voltage $V(t)$

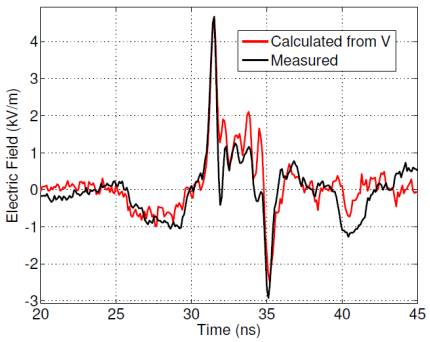

Figure 3. Radiated electric field

Acknowledgments - This work is financially supported by the EPFL-SDC (Swiss Agency for Development and Cooperation) Fund and the Cattleya project.

References

1. C. E. Baum, "Radiation of Impulse-Like waveforms," Sensor and Simulation Note 321, 25, November 1989.
2. O. V. Mikheev et al., "New Method for Calculating Pulse Radiation from an Antenna with a Reflector", IEEE Transactions on Electromagnetic Compatibility, Vol. 39, Nr. 1, pp. 48-54, 1997.

978-1-4244-5050-3/10/$26.00 ©2010 IEEE

A through-wall SAR system for mapping building interiors

Pascale Sévigny, **David DiFilippo**, **Tony Laneve**, and **Brigitte Chan**
Defence R&D Canada, Ottawa, Canada, K1A 0Z4
E-mail: pascale.sevigny@drdc-rddc.gc.ca

Mapping the interior of buildings is of great interest to military forces operating in an urban battlefield. DRDC Ottawa is currently investigating the potential of using synthetic aperture radar (SAR) techniques to perform high-resolution stand-off 3-D imaging of objects concealed behind walls or other materials. The operational concept involves a vehicle-mounted radar driven along a straight path in front of a building of interest. Potentially, this imaging radar would allow for the mapping of the interior room layout, including the location of walls, doors and furniture. In this paper we present the current status of the DRDC Ottawa through-wall SAR (TWSAR) testbed and show preliminary experimental results.

The TWSAR testbed is a radar prototype consisting of both custom and commercial-off-the-shelf (COTS) components, operating at L-band and using a 2-GHz bandwidth waveform for high range resolution. The technique of stretch processing, consisting of mixing the received signal with a replica of the transmitted signal, is used to provide a narrowband intermediate frequency (IF) signal that can be easily sampled with COTS digitizers. The IF signal is sampled at 100 Msamples/s and digital down-conversion and decimation are performed to produce the baseband in-phase and quadrature (I & Q) components of the signal. The transmit and receive antennas consist of two modified bowtie elements, designed and manufactured by the Communications Research Centre (CRC) Advanced Antenna Technology Section (RAATLab). The azimuth antenna pattern is quasi-omnidirectional and the elevation beamwidth is $\geq 60^\circ$. These antennas thus illuminate a large volume. Synthetic aperture radar techniques are used in the azimuth or along-track direction to improve resolution. An array in elevation is currently in development to provide resolution in the elevation direction for ground clutter and multipath rejection.

In Figure 1, a picture of the TWSAR testbed and its antennas mounted on a mobile lab is shown. In Figure 2, a preliminary SAR image is shown, processed without any wall compensation, of a wood frame building with vinyl siding and an underlying layer of asbestos-cement siding. In the image, the mobile lab was located at 0-m range. A map layout of the building's rooms and furniture is overlaid on the image to help identification.

Figure 1: **TWSAR testbed and mobile lab**

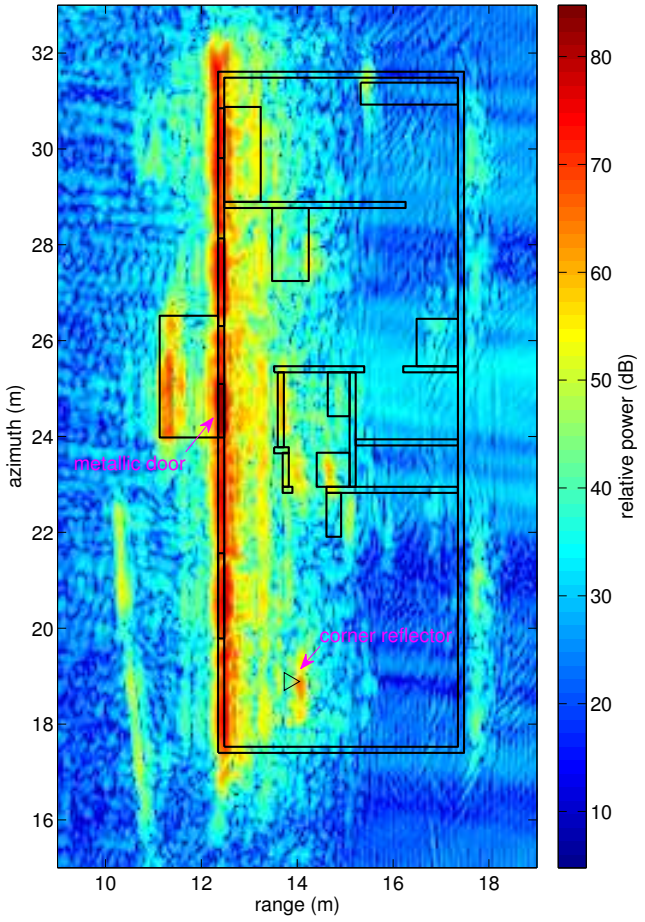

Figure 2: **SAR image of wood building with vinyl siding and an underlying layer of asbestos-cement siding**

978-1-4244-5050-3/10/$26.00 ©2010 Crown

Fast Forward Models for Through-Wall and Multipath EM Propagation

Edward H. Hill III
BAE Systems AIT
6 New England Executive Parkway
Burlington, MA 01803
Email: edward.h.hill@baesystems.com

I. Introduction

For more than three decades, ray-based (or "extended geometric optics") computer models have been used to perform forward-model predictions of various EM propagation scenarios. In recent years, advances in computer hardware and improved algorithms have enabled forward models which are sufficiently rapid to enable model-based reasoning. In simple terms, a large number of possible physical scenarios can be hypothesized, (approximately) evaluated, and compared with observed or previously simulated data sets. When used in conjunction with an appropriate optimization framework, the hypothesized models can, in reasonable time-frames, converge to reveal desired physical details from, for example, through-wall and other complicated multipath EM propagation experiments.

Here, two related computer models for EM propagation are presented and discussed. Both models employ fast ray-based methods derived from extended geometric optics approximations to the underlying physics. And, both programs were written primarily to support model-based inversions. Details of the model development and selected results are supplied.

A. ATrace : A Model for Through-Wall Propagation

Leveraging work performed for previous UXO investigations, BAE Systems AIT developed a classic "shooting-and-bouncing rays" (SBR) model for EM propagation called ATrace. Written in a mixture of C++ and Fortran, the primary goals of ATrace were to enable the simulation of EM propagation through and around typical building materials and geometries including:

- model EM transmission and reflection from layered homogeneous media (*e.g.*; walls composed of various layers such as thermal insulation and sheathing),
- simulate Bragg diffraction effects in walls with stark material contrasts and periodic patterns (*e.g.*; rebar within poured concrete), and
- account for propagation within rooms, hallways, and typical adjacent spaces.

In conjunction with observed EM reflection data sets, ATrace has been used to perform model-based inversions of multi-wall scenarios [1]. In addition, it has been used to investigate possible frequencies for hypothetical through-wall imaging systems and to investigate the strength and effects of various Bragg phenomena. Selected results will be presented.

B. BTrace : A Model for Multipath Specular Propagation

Building upon the work done for ATrace, a second model was written to tackle multipath propagation scenarios involving potentially deeper and more complicated reflection geometries. Called BTrace, it implements a beam-tracing approach originally introduced by Heckbert and Hanrahan [2] and later applied to sound reflections by Funkhouser *et al* [3] and to EM propagation Fortune *et al* [4].

Given a transmitter or receiver location and a scene composed of a potentially large number of flat-faced (representable as a mesh of triangular surfaces) objects, BTrace determines (to numerical precision and to a pre-specified maximum bounce depth) all possible line-of-of-sight and reflection pathways for specular EM propagation from/to a transmitter/receiver. The intermediate result of BTrace is called a "beam tree" and it efficiently encodes the three-dimensional hull of all possible visibility-with-reflection pathways using polygons which are treated as feasible regions in a linear programming sense. The intermediate representation is compact and readily traversed. It supports rapid evaluation of the containment of points or the fractional intersection of objects (surfaces) within the visibility hull. And, with all the reflection pathways determined, BTrace uses the same layered-media specular reflection model as ATrace to determine the per-frequency response along each path.

BTrace implementation details and selected results will be presented.

References

[1] "Theoretical and experimental study of through-wall microwave tomography inverse problems," *Journal of the Franklin Institute*, vol. 345, no. 6, pp. 592 – 617, 2008, advances in Indoor Radar Imaging.

[2] P. S. Heckbert and P. Hanrahan, "Beam tracing polygonal objects," *Computer Graphics*, vol. 18, no. 3, pp. 119–127, July 1984.

[3] T. Funkhouser, N. Tsingos, I. Carlbom, G. Elko, M. Sondhi, J. E. West, G. Pingali, P. Min, and A. Ngan, "A beam tracing method for interactive architectural acoustics," *J. Acoust. Soc. Am.*, vol. 115, no. 2, pp. 739–756, Feb 2004.

[4] S. Fortune, "Topological beam tracing," in *SCG '99: Proceedings of the fifteenth annual symposium on Computational geometry*. New York, NY, USA: ACM, 1999, pp. 59–68.

978-1-4244-5050-3/10/$26.00 ©2010 IEEE

Ultra-wide Bandwidth Antenna 101

Chi-Chih Chen
ElectroScience Laboratory, Dept. of Electrical and Computer Engineering, The Ohio State University, 1320 Kinnear Rd., Columbus, OH 43212 USA
chen.118@osu.edu

Introduction

There has been a continuous interest in UWB antennas that operates over a wide frequency range for multiple channels or systems. Recent FCC ruling for allowing operating UWB signals in various sensing, imaging and communication applications as well as technology advances in software-defined radios and software-defined radars once again revive the interest of UWB antenna development.

The term "UWB" has often been used loosely. The original FCC definition of "UWB" adopts 25% or more fractional bandwidth. Here, UWB is referred to a bandwidth more than 2:1 for frequency range where realized gain is above operation requirement. Although some literatures commonly use bandwidth based on the frequency range where return loss level is less than -10 dB, low return loss does not necessarily imply strong radiation, nor does it says anything about the radiation pattern. For instance, return loss means little for antennas with resistive loading, commonly used for increasing bandwidth. There are also plenty of literatures that discussed detailed design procedures and parameters about UWB antennas. Unfortunately, many of them fell short of providing insights about antenna operations and wave behaviors. Modern powerful computation capability seems to turn more antenna designers into antenna optimizers who seek to rely on massive computation power to come up with an "improved" or "optimized" antenna design. No doubt, this approach is indeed attractive to young antenna engineers who have many modeling tools and experiences but have not yet developed good physical understanding about antenna operations, especially for complex antennas. Therefore, this paper focuses on discussion fundamental principles and formations of UWB antennas.

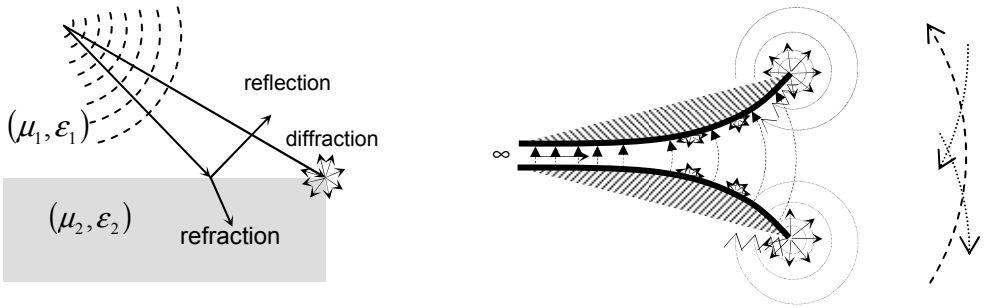

Fig. 1 Scattering of electromagnetic waves (a) material changes (b) geometry changes.

What Is An Antenna?

Some consider an antenna as an impedance transformer between a transmission line and the open space. Others define an antenna as coupler that couples electromagnetic energy into space. Readers who use most antennas made of good (or poor) conductors probably

978-1-4244-5050-3/10/$26.00 ©2010 IEEE

are used to think of an antenna as a current guiding structure that somehow converts the conduction currents into radiation. It is probably more appropriate to consider an antenna as scattering structures that are strategically arranged near an excitation source to produce strong net scattered fields in the far fields. This definition obviously means that an antenna needs not to be made of conductors. Instead, any materials that have the right properties for creating and controlling EM scattering can be used to design an antenna.

It is also important to recognize that the difference between a transmission line and an antenna lies only in the amount of net radiation generated in the far fields, not in the geometry itself! For instance, an open-end two-wire "transmission line" can become a good "antenna" if the spacing between the wires is not small compared to wavelengths such that the diffraction from both wires and wire ends do not mostly cancel each other. For the same reason, a "horn antenna" may become just an open-end "waveguide" if the aperture becomes small compared to the wavelength.

What Makes an UWB Antenna?

An UWB antenna is an antenna capable of producing a similar radiation patterns and gain over a very wide frequency range (more than 2:1 bandwidth) with realized gain level satisfying mission requirement. In general, UWB antennas can be classified in the following three types based on how wideband radiation is achieved. It is unusual for Type-I UWB antennas to have more than 3:1 bandwidth. Type-II UWB antenna offers superior pulse response but may have low efficiency (if absorptive loading applied) or frequency-dependent gain and patterns. Many Type-II antennas can achieve 9:1 bandwidth. Type-III UWB antennas offer frequency-independent gain and patterns but are often dispersive. The following sections will provide more analysis of these three types of UWB antennas.

Type-I	Perturb electromagnetic resonance to broaden the resonant peak.
Type-II	Allow only one dominant radiation region that is physically small compared to wavelengths.
Type-III	Maintain a "similar" effective radiation/scattering geometry (shape and dimension) in terms of wavelength.

Type-I UWB Antennas

This type of UWB antenna achieves bandwidth by introducing incoherent resonance and effectively lowering the quality factor of the electromagnetic resonance. Most Type-I UWB antennas are variations of dipoles or monopoles. A thin wire dipole radiates mainly from the superposition of diffractions from two ends as illustrated in Fig.2(a). The relative magnitude and phase relationship between these diffracted fields ultimately determine its bandwidth and pattern behavior. As a result, such antenna has strong frequency-dependent gain and patterns. It is well know that a bowtie dipole design has a much broader bandwidth compared to a thin-wire dipole. This is achieved by introducing more incoherent diffractions as illustrated in Fig.2(b) which involved four corner diffraction terms and two edge diffraction terms. Since not all diffractions have the same phase at a given frequency and pattern angle, the total radiated fields exhibit a wider bandwidth. A wider phase distribution of all contributing scattering terms as in the case of wide bowtie angle leads to wider bandwidth as long as it is less than 90 degrees. There are many other published two-dimensional or three-dimensional variations of dipoles [1]-[3] that showed bandwidths of up to 3:1. The upper frequency limit of this type of UWB

antenna is usually limited by the excitation of higher modes which cause pattern narrowing and multiple radiation lobes.

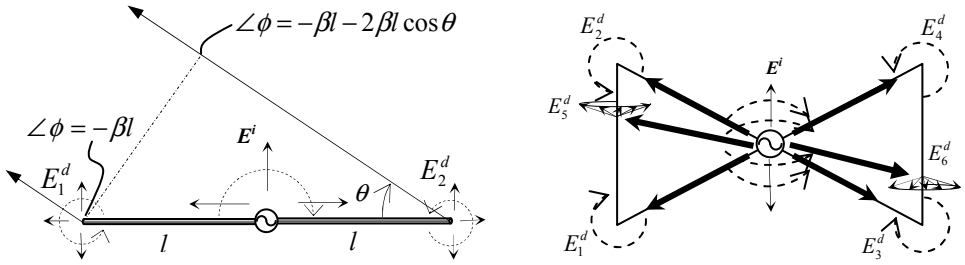

(a) thin-wire dipole (b) bowtie dipole

Fig. 2 Comparison of the radiation/scattering of a thin-wire dipole and a bowtie dipole.

Type-II UWB Antennas

Type-II UWB antennas achieve wide bandwidth by controlling diffractions on antenna structures via careful geometry design or proper utilization of absorptive loading. Type-II UWB antennas often produce some degree of frequency-dependent gain and patterns due to the fact that diffraction and absorption are functions of frequency [4].

Absorptive loading is an effective way to achieve this goal at the price of lower antenna efficiency. Therefore, the art of absorptive loading is to utilize the minimum amount of absorptive treatment to reduce diffractions down to acceptable levels. This would require some knowledge about the types and causes of dominant diffraction events. Both electric and magnetic absorptive materials have been used. Resistively loaded dipoles [5]-[7] and resistively loaded horns [8] are well known examples. Another way to reduce the diffraction effect is to properly shape antenna geometry to avoid strong localized diffractions which usually arise from abrupt discontinuities as illustrated in Fig.3. The low-frequency limit of this deign occurs when the arm length is less than half of the wavelength. With such a short length, the curvature becomes ineffective and significant diffractions arise at the ends of antenna arms.

The high-frequency limit is determined by the pattern distortions caused by the curvature smoothness and the starting curvature. However, such a design often exhibits frequency-dependent gain and pattern. Typically, the resultant boresight gain increases with frequency and beamwidth decreases with frequency. Common examples of Type-II UWB antennas include tapered-slot antennas [9]-[11], rolled-edge horns [12] and ridged horns [13]. Of course, both curved-arm and absorptive loading can also be applied simultaneously to further reduce antenna size and to achieve a better pattern stability at the expense of antenna efficiency [8].

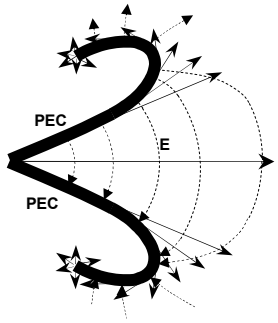

Fig.3 Smooth diffraction control using curved arms.

Type-III UWB Antennas

Type-III UWB antennas are probably the most widely used UWB antennas. This type of antennas adopts frequency-independent or frequency-scaled geometries such as the angle-defined geometry, complimentary geometry and log periodic geometry [14]-[16]. However, employing such geometries alone does not guarantee a UWB antenna. Proper

feeding scheme, structure coupling, and truncations must all be considered to achieve frequency-independent UWB antenna. At a given frequency, most radiation in this type of antenna occurs in a localized "active region" where all radiations add constructively. Log periodic dipole arrays and spiral antennas are good examples [21]. Several useful design guidelines for this type of antenna include

1) composed of frequency-scaled EM resonant structures connected in series
2) active region should be able to produce effective radiation with desired radiation properties such as pattern and polarity during resonance
3) feed from highest frequency region
4) frequency-scaled active region geometry as frequency sweeps

References

[1] Agrawall, N.P., Kumar, G., and Ray, K.P.: "Wide-band planar monopole antennas," IEEE Trans. Antennas Propag., 1998, 46, (2), pp.294–295.

[2] Z.N. Chen, M.Y.W. Chia and M.J. Ammann, "Optimization and comparison of broadband monopoles," IEE Proc. Microw. Ant. Propag., 2003, 150, pp.429–435.

[3] K.G. Thomas, N. Lenin and R. Sivaramakrishnan, "Ultrawideband Planar Disc Monopole," IEEE Trans. Ant. Propagat., vol.54, no.4, pp.1339-1341, Apr. 2006.

[4] R. G. Kouyoumjian and P. H. Pathak, "A uniform geometrical theory of diffraction for an edge in a perfectly conducting surface," Proc. IEEE, 62, pp.1448-1461, Nov. 1974.

[5] T.T. Wu and R.W.P. King, "The cylindrical antenna with nonreflectingr esistive loading," IEEE Trans. Antennas and Propagat., vol.13. pp.369-373. May 1965.

[6] L.C. Shen, R.W.P. King, "Corrections to "The cylindrical antenna with nonreflecting resistive loading," IEEE Trans. Ant. Propagat.,13, pp.998. Nov. 1965

[7] M. Kanda "A relatively short cylindrical broadband antenna with tapered resistive loading for picoseconds measurements," IEEE Trans. Antennas Propagat., vol.26. pp.439-447, May 1978.

[8] L.-C. Chang and W.D. Burnside, "An Ultrawide-Bandwidth Tapered Resistive TEM Horn Antenna," IEEE Trans. Ant. Propagat. 48, pp.1848–1857, Dec. 2000.

[9] "Antenna Engineering Handbook", 4th Edition, J.L. Volakis, Chapter 9, McGraw Hill, 2007.

[10] Janaswamy and D.HSchaubert, "Analysis of the tapered slot antenna," IEEE Trans. Antennas Propag., vol. AP-35, pp. 1058–1064, Sep. 1987.

[11] E. Gazit, "Improved design of the Vivaldi antenna," IEE Proc. Micro. Antennas Propag., 1988, 135, (2), pp. 89-92

[12] K. Y. A. Lai, A. L. Sinopoli, and W. D. Burnside, "A novel antenna for ultrawide-band applications," IEEE Trans. Ant. Propagat., vol.40, pp.755–760, July 1992.

[13] C. Bruns, P. Leuchtmann, and R. Vahldieck, "Analysis and Simulation of a 1-18-GHz broadband double-ridged horn antenna," IEEE Trans. on Electromagnetic Compatibility, vol. 45, pp. 55-60, Feb. 2003.Li et al 2003.

[14] J.D. Dyson, "The Equiangular Spiral Antenna," IRE Trans. Antennas. Propagat., vol. 7, pp. 181-187, April 1959.

[15] B. R.-S. Cheo, V.H. Rumsey and W.J. Welch, "A solution to the frequency-independent antenna problem," IRE Trans. Ant. Propagat., pp.527–534,Nov. 1961.

[16] D. Isbell, "Log periodic dipole arrays," IEEE Trans. Antennas Propagat.., vol.8, no.3, pp.260-267, May 1960.

[17] "Antenna Engineering Handbook", 4th Edition, J.L. Volakis, Chapter 13, McGraw Hill, 2007.

Computer-Aided Simulation of Human Exposure to HPEM Signals

M. Clemens[1], S. Dickmann[2], A. El Ouardi[1], V. Hansen[1], B. Römer[3], M. Schaarschmidt[3], J. Streckert[1]

[1]Bergische Universitaet Wuppertal, FB E, Chair of Electromagnetic Theory, Rainer-Gruenter-Straße 21, D-42119 Wuppertal;
[2]Helmut Schmidt University, University of the Federal Armed Forces Hamburg, Department of Electrical Engineering, Holstenhofweg 85, D-22043 Hamburg;
[3]Bundeswehr Research Institute for Protective Technologies and NBC Protection (WIS), Humboldtstr. 1, D-29633 Munster

Beside power supply and radio communication systems which have been extensively investigated during the last decades, pulsed high-power sources as applied by law enforcement and emergency services to disrupt or destroy electronic systems and equipment, are potential candidates for electromagnetically provoked biological effects in exposed human bodies. The resulting impact to the human body is quantified by physical basic parameters, such as electrical current densities, specific absorption rates and the like. For those the admissible values (so-called “basic restrictions”) for general public and for occupational exposure are quite consistently recommended by numerous national and international guidelines (e.g. [ICNIRP 1998]). The basic parameters vary with frequency, intensity and direction of incidence of the electromagnetic (EM) immission. They depend on size, shape, and individual posture of the exposed person and moreover on the electromagnetic properties of the immediate environment.

Since measurements of the EM field distributions and thereby of the basic parameters within the human body are not possible, numerical field solvers combined with highly resolved anatomically correct 3D computer models of humans, with realistic configurations of EM sources, and with environmental structures are used in order to predict those power thresholds of different HPEM signals which correspond to the basic restrictions. Arbitrary exposure scenarios with single or grouped human body models differing by size, weight and gender can be simulated and assessed with respect to the tolerable EM exposure by application of the finite integration technique (FIT) or of the finite difference method (FD), according to the requirements of the specific signal as a small-band (HPM, DS) or as a wide-band version (UWB).

A general result of our dosimetrical studies concerning HPEM signals instead of e.g. mobile telecommunication signals (with their low-power narrow-band characteristics) is the increasing importance of the local specific absorption (SA) within the head against the local specific absorption rate (SAR). This is due to the fact that the maximum SA, which was introduced by the regulatory boards as a measure for auditory effects (“microwave hearing”), must be regarded momentarily during a pulse while the SAR values are to be averaged over any 6-minutes period.

The presentation will show different examples of numerically computed and evaluated scenarios, but will mainly concentrate on the simulation technology and its limits and opportunities.

ICNIRP (International Commission on Non-Ionizing Radiation Protection): Guidelines for Limiting Exposure to Time-Varying Electric, Magnetic, and Electromagnetic Fields (up to 300 GHz). Health Phys., 74, 494-522, 1998.

978-1-4244-5050-3/10/$26.00 ©2010 IEEE

From Soil Measurements to Detector Performance − How to Predict Soil Influence on EMI and GPR Sensors

Jan Igel[1], Sven Altfelder[2], Volker Hennings[2], Holger Preetz[1], and Kazunori Takahashi[1]
[1]Leibniz Institute for Applied Geophysics, Hannover, Germany
[2]Federal Institute for Geosciences and Natural Resources, Hannover, Germany
E-mail: jan.igel@liag-hannover.de

Electromagnetic induction technique (EMI) has been used for landmine detection for a long time. Recently, ground-penetrating radar (GPR) is used more and more often as a stand-alone detector or in combination with EMI sensors. Both techniques are strongly influenced by electromagnetic soil properties, albeit in a different manner. There is a lack of information on electromagnetic soil properties of different soils under various conditions and on how these properties influence different detectors [1]. We present measuring techniques and results of lab and field measurements of physical soil properties and their spatial variability on different scales. The data are statistically analysed and we appraise the results with regard to the performance of EMI and GPR sensors.

The most important soil property influencing **EMI sensors** is magnetic susceptibility and its frequency dependence and to a minor degree electric conductivity [2]. In particular, soils from tropical regions are known to have often a negative effect on EMI sensors. Therefore, we investigated magnetic properties on a set of more than 500 tropical soil samples gathered over the whole tropical belt. More than one third of the samples are likely to have an either severe or very severe impact on the performance of metal detectors. As a result of our investigation we identified two factors that have an influence on soil magnetic properties: the parent rock of the soils and their degree of weathering [3]. With our dataset, we deduced a classification system to predict soil magnetic properties on the basis of geological and soil maps. We exemplarily applied our system to the country of Angola and present a map which displays the predicted performance of EMI sensors identifying regions with higher and lower impact on EMI sensors [4]. This map can be used as a help for planning demining activities, e.g. for choosing an adequate detector model or other detection techniques.

In contrast to EMI sensors, **GPR sensors** are affected by dielectric permittivity and electric conductivity. As GPR bases on the propagation and reflection of electromagnetic waves, it does not detect the physical property of the mine itself, but reacts on the contrast of electric properties of the mine versus the soil. Hence, it is also influenced by the small-scale variability of soil properties, particularly if they are in the same range of size as the target. Heterogeneity of soil causes noise in the data which, in extreme cases, can completely mask the signal of the mines. The effect of soil heterogeneity on GPR is first investigated by computer simulations. In order to get realistic synthetic data, we measured the spatial distribution of electric conductivity and dielectric permittivity on several soils. The spatial variability and correlation of the field data are described by a geostatistical analysis. Based on this analysis, synthetic random media can be generated which have the same properties as the soil in situ and which are further used for finite-differences (FD) calculations of electromagnetic wave propagation. We get realistic synthetic GPR data including the noise which is generated by soil variability. From our synthetic data we can conclude that for most soils the variability of dielectric permittivity has a much larger influence than the variability of electric conductivity [5]. In addition, we present real GPR field data collected on test lanes that support the conclusions drawn from synthetic data.

References

1. Y. Das, J. E. McFee, and G. Cross, "Soil properties database for humanitarian demining: A proposed initiative", p. 1–9, In World Congr. of Soil Sci., 17th, Bangkok, Thailand. Soil and Fertilizer Soc. of Thailand, Bangkok, 2002.
2. Y. Das, "Effects of soil electromagnetic properties on metal detectors", IEEE Transactions on Geoscience and Remote Sensing, 44,6: 1444–1453, 2006.
3. H. Preetz, S. Altfelder, and J. Igel, "Tropical Soils and Landmine Detection – An Approach for a Classification System", Soil Science Society of America Journal, 72, (1): 151 – 159, 2008.
4. H. Preetz, and V. Hennings, "Predicting metal detector performance for landmine clearance – Soil magnetic map of Angola", Environmental Earth Sciences, http://www.springerlink.com/openurl.asp?genre=article&id=doi:10.1007/s12665-009-0285-0, 2009.
5. J. Igel, " The Small-Scale Variability of Electrical Soil Properties − Influence on GPR Measurements", In: GPR 2008: 12th International Conference on Ground Penetrating Radar, June 16-19, Birmingham, UK, 2008.

978-1-4244-5050-3/10/$26.00 ©2010 IEEE

Development of a Through Wall UWB System for Three-Dimensional Imaging using Time Domain Tools

Yazhou Wang
Min Kao EECS Department
The University of Tennessee
Knoxville, TN 37996, USA
ywang34@utk.edu

Aly E. Fathy
Min Kao EECS Department
The University of Tennessee
Knoxville, TN 37996, USA
fathy@eecs.utk.edu

***Abstract*—In this paper, we have developed an UWB 3-D imaging radar using time domain tools. Compared to the previously designed 2-D radar, the newly developed system can improve the target discrimination/identification in through wall detections by localizing the targets and recovering their shapes simultaneously. This capability will greatly help in discriminating human beings from other objects. The developed 3-D UWB radar utilizes a 2-D planar array for transmitting and receiving. The full steering is implemented using mechanical movement of the wideband Tx/Rx antennas which cover the range from 2-10 GHz. The radar system transmits a 300ps pulse periodically as the detection signals and uses a low-cost solution to sample the received UWB signals. The 3-D microwave beamformer and the experimental 3-D imaging results will be discussed in details.**

Keywords-UWB; radar; through-wall imaging; three-dimensional; time domain

I. INTRODUCTION

UWB radar is superior to the conventional narrowband radar systems for through wall sensing due to its good penetration characteristics, robustness to multipath reflection and excellent performance in severe clutter environment. Relevant literatures have introduced the development of UWB radar in both frequency domain and time domain. The design of UWB system using frequency domain technique is limited by its complexity in signal source and signal processing and most of the systems are still based on the expensive, bulky vector network analyzer (VNA) [1]-[2]. Contrarily, the advance of UWB commercial hardware has made it relatively easy to generate and process UWB signals using time domain tools. A 2-D UWB radar was previously implemented in our group using time domain technique to detect and track the position of target behind the wall in real time [3].

In this paper, we extend our previous system into a 3-D imaging radar, which goes beyond targets localization to their shape recognition. The design strategy is discussed in details, including the radar transceiver architecture, hardware development (e.g. wideband Vivaldi antenna, Gaussian pulse generator), data sampling and collection technique, and 3-D microwave beamformer. The performance of the 3-D UWB radar is validated experimentally using an emulated human target. The paper is organized as follows. After a brief introduction in section I, the radar transceiver architecture, as well as the wideband signal sampling using a low-cost solution will be presented in section II. Section III introduces the design of a wideband Vivaldi antenna covering the whole UWB band while section IV introduces the design of a tunable Gaussian pulse generator with input buffer circuitry. In section V, the 3-D microwave beamforming algorithm is presented. Finally, our experiment to recover the 3-D images of an emulated human model is introduced.

II. UWB RADAR TRANSCEIVER DEVELOPMENT

A detailed block diagram of the UWB radar system is outlined in Fig. 1. A 10 MHz clock (PRF) from the FPGA is amplified by a buffer before driving a Gaussian pulse generator to generate a 300ps Gaussian pulse signal. The pulse is then modulated by an 8 GHz carrier signal. The modulated signal passes through two stages of amplification and is then transmitted via a wideband Vivaldi antenna. At the Rx link, the wideband Rx antenna is moved mechanically to acquire the signals at different positions, which are then amplified by a wideband low noise amplifier. Next, the signals are down-converted into I and Q channels by mixing the same 8 GHz carrier with the received signals. Then, the recovered I and Q data are low-pass filtered and amplified before being sent to the analog-to-digital converter for sampling using the equivalent-time sampling scheme [4]. Next, all the sampling data are sent to a Xilinx Vertex-4 FPGA circuitry for storage. Last, the collected data is transferred to the computer through RS232 serial port and a 3-D microwave beam-forming algorithm [5] is applied to recover the 3-D image.

The data acquisition module has been actualized by using an off-the-shelf Xilinx Virtex-4 FPGA board with a Texas Instrument CDC5801 low-jitter clock multiplier/divider, and two 8-bit MAX104 ADC evaluation boards with a 2.2 GHz analog input bandwidth, as shown in Fig. 2. According to Nyquist's sampling theorem, a minimum sampling rate of 4 Gsps is required to digitize the 300ps pulse signal, which occupies a bandwidth of approximately 2 GHz. However, the MAX104 ADC only supports a maximum conversation rate of 1 Gsps with an external 1 GHz clock; and the commercial high speed ADC is really expensive. Therefore, an equivalent-time sampling method [4] is applied and it is really a low-cost solution. The signal is digitized using the 100 MHz clock from FPGA board and 10 samples are collected at the 1st signal cycle. Then a 200ps time delay generated by CDC5801 is placed on the sampling trigger clock before sampling the next signal cycle. After 50 signal cycles, a complete pulse signal is sampled and acquired. This equivalent-time sampling scheme leads to a 5 Gsps equivalent conversion rate, which can digitize the 300ps signal without any distortions.

978-1-4244-5050-3/10/$26.00 ©2010 IEEE

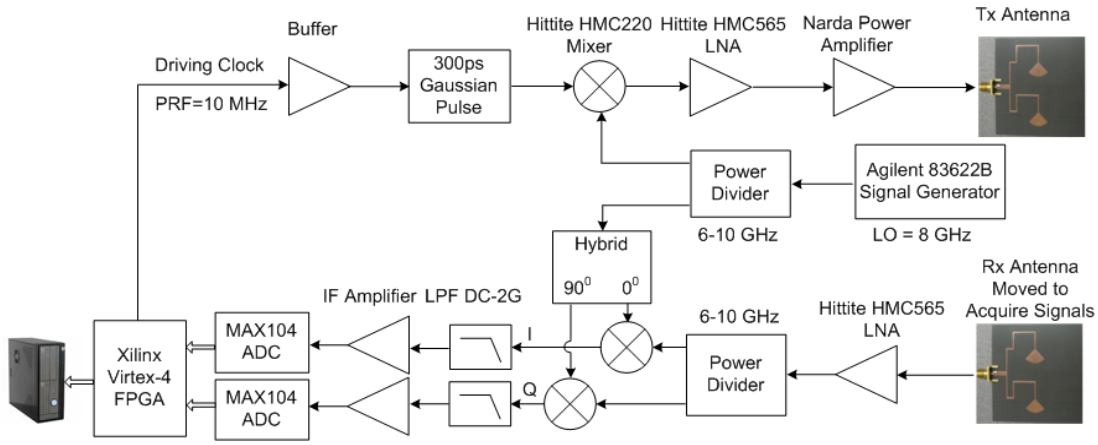

Fig. 1. Detailed block diagram of the UWB radar transceiver

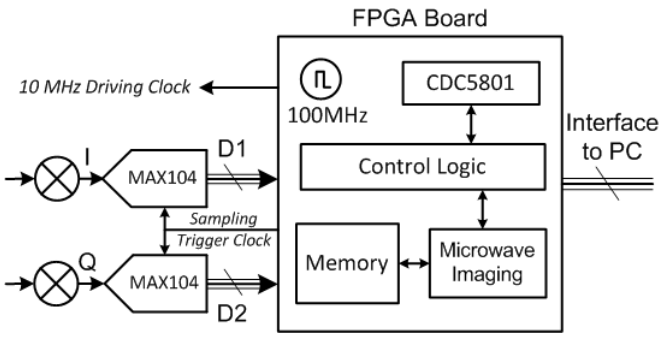

Fig. 2. Diagram of data acquisition and digital control

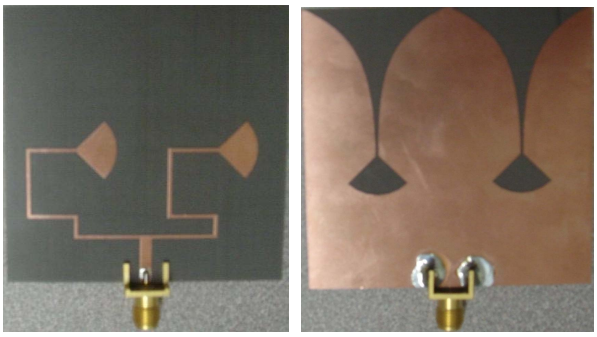

(a) top view (b) bottom view

Fig. 3. Photograph of the fabricated 2-10 GHz Vivaldi antenna

III. Wideband Vivaldi Antenna Design

A 2-10 GHz antenna has been developed for the reconfigurable UWB system using tapered slot Vivaldi structure [6]. The parameters of the tapered slot, including the opening rate, taper length and taper width, have been optimized to pursue a wideband match and a compact size simultaneously. A wideband transition from the microstrip line to the slotline has been successfully designed and is used to feed the radiating tapered slot [7]. The single exponential tapered slot is matched at 100Ω. Next, a smooth 100Ω to 50Ω transition is performed to achieve the 50Ω impedance at the feed port. The fabricated Vivaldi antenna has a size of 6cm × 6cm.

The developed antenna has been fabricated on a 31-mil thick Rogers RT5880 substrate, and its top and bottom views are shown in Fig. 3. The measured return loss of the wideband Vivaldi antenna matches the simulated results very well, as shown in Fig. 4. Both simulated and experimental results indicate a good match over the 2-10 GHz frequency range. Fig. 5 demonstrates satisfactory measured radiation patterns of the Vivaldi antenna over the operating frequency range. Good directional radiations are acquired at both the E and H planes. The measured patterns at 10 GHz show that the designed Vivaldi antenna has a 3dB beamwidth of 30^0 at E-plane and 60^0 at H-plane.

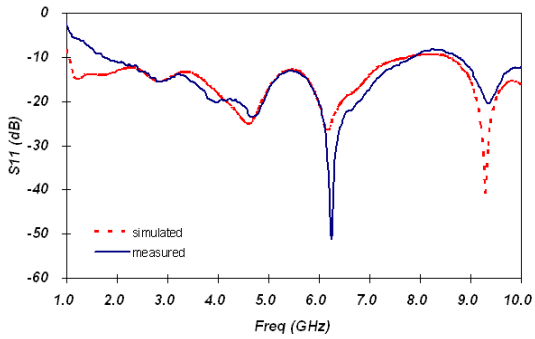

Fig. 4. Simulated and measured return loss

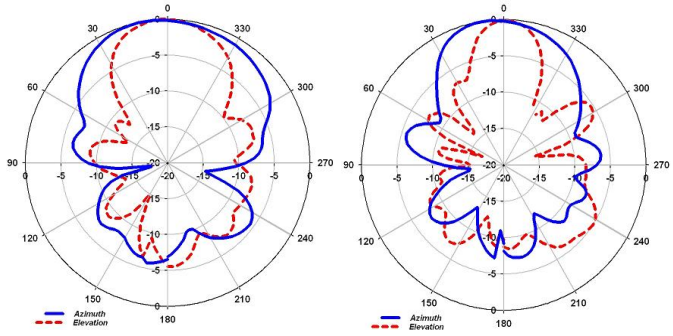

(a) 6 GHz (b) 10 GHz

Fig. 5. Measured radiation pattern versus frequency

IV. Tunable Gaussian Pulse Generator

A tunable Gaussian pulse generator [8] has been designed and tested using Aeroflex-Metelics MSD700 step recovery diode (SRD), as indicated in Fig. 6. The diode has a transition time (i.e. snap time) of 60ps and can generate pulses with sharp rise time and rich harmonics. A parallel microstrip short stub in the circuitry is used to tune the pulse width. Shorter the microstrip stub, narrower the pulse width. By manually changing the length of the microstrip stub, the developed Gaussian pulse generator has a wide tunable pulse duration covering a 300ps to 1ns range, as shown in Fig. 7.

The Gaussian pulse generator is driven by the 10 MHz clock from FPGA board in the radar system. However, the FPGA output is too low in current to drive the pulse generator. Hence, a buffer is added at the pulse generator input to amplify the current of the 10 MHz clock, as shown in Fig. 6. The wideband operational amplifier OPA2674 from Texas Instruments is used to design the buffer and it provides a 220MHz bandwidth and a maximum 500mA output current.

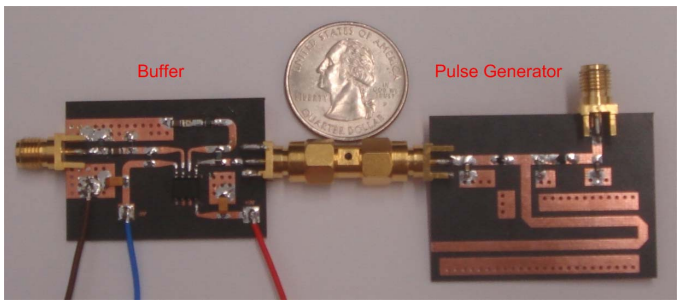

Fig. 6. Photograph of the fabricated tunable Gaussian pulse generator with input buffer circuitry

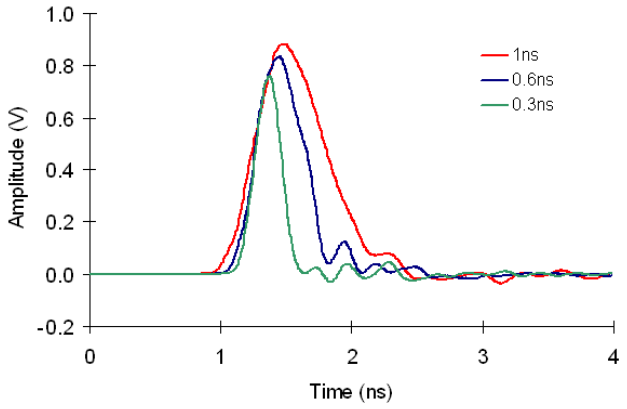

Fig. 7. Measured Gaussian pulse generator output (pulse width tunable from 300ps to 1ns)

V. 3-D Microwave Beamforming Algorithm

A 3-D wideband microwave beamformer is used to recover the target image in our radar system based on the delay and sum algorithm. To recover the 3-D images, the surveillance space is divided into numerous voxels using x, y and z and a planar array is used to transmit/receive the signals, as shown in Fig. 8. For any selected voxel (x, y, z), Equation (1) is used to calculate the imaging information, where $s_{m,n}(x,y,z)$ indicates the signal scattered by voxel (x,y,z) and received by Rx antenna (m,n); $w_{m,n}(x,y,z)$ introduces the magnitude compensation for different scattering loss, propagation loss and through wall attenuation; $\varphi_{m,n}(x,y,z)$ introduces the phase adjustment for different phase delays. However, it is very complicated and tedious to calculate the $w_{m,n}(x,y,z)$ and $\varphi_{m,n}(x,y,z)$ for a 3-D structure. Therefore, instead of solving this 3-D calculation directly, we will simplify this model first by employing a coordinate translator, as indicated in [5]. The yz plane will rotate an angle β along the x axis to achieve a new coordinate system using x', y' and z'. The selected antenna and the selected voxel will have the same z' value in the new coordinate. Hence, the calculation of this 3-D model becomes a 2-D calculation only in x'y' plane.

$$S(x,y,z)=\sum_{m=1}^{M}\sum_{n=1}^{N} w_{m,n}(x,y,z)s_{m,n}(x,y,z)e^{j\varphi_{m,n}(x,y,z)} \quad (1)$$

In a practical environment, the through-wall effects have to be taken into account in order to generate accurate images of the targets. The propagation wave slows down, encounters refraction, and decays as it passes through the wall. If the wall effects are not estimated accordingly, smearness and blurriness may occur in the recovered images. The through-wall attenuation is approximately calculated based on the ABCD matrix for plane wave [9], while the through-wall phase delay is calculated using the near-field model in Fig. 9 to acquire more accurate phase information. The selected pixel has a range of R_0 and an angle of θ_0. The wall is assumed to be homogeneous and low-loss, with a thickness t and a relative permittivity of ε_r. The detection radar has a standoff distance of d from the wall. Then, the equivalent electrical length L from the selected pixel to the observation point can be calculated using Equations (2)-(4).

$$\sin\theta_1 = \sqrt{\varepsilon_r}\sin\theta_2 \quad (2)$$

$$(R_0\cos\theta_0 - t - d)\tan\theta_1 + t\tan\theta_2 + d\tan\theta_1 = R_0\sin\theta_0 \quad (3)$$

$$\begin{aligned} L &= L_1 + \sqrt{\varepsilon_r}L_2 + L_3 \\ &= \frac{R_0\cos\theta_0 - t - d}{\cos\theta_1} + \sqrt{\varepsilon_r}\frac{t}{\cos\theta_2} + \frac{d}{\cos\theta_1} \end{aligned} \quad (4)$$

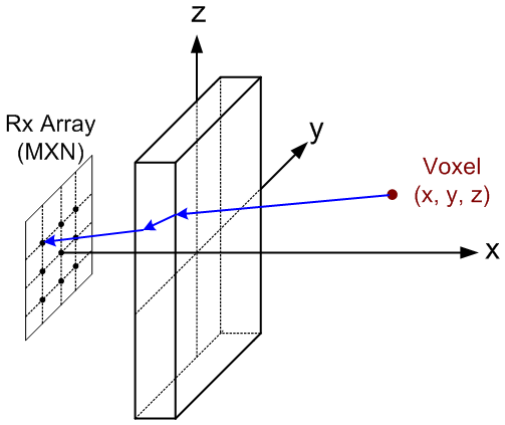

Fig. 8. 3-D microwave beamfomer model

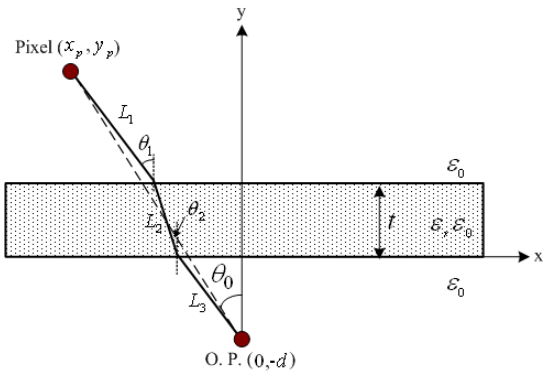

Fig. 9. Through wall effects

VI. 3-D Imaging Experiment

A 3-D imaging experiment was performed to detect an emulated human body using the designed UWB radar system. Both Tx and Rx antennas were moved mechanically in a vertical plane to transmit and receive the signals. Fig. 10 (a) indicates the locations of Tx antenna marked in red and Rx antenna marked in green. The grid has a spacing of λ_0 at its highest operating frequency (10 GHz) in order to achieve the maximum aperture size and avoid the grating lobes. A low-loss drywall was utilized in the experiment. Approximately 60% of the human body is comprised of water that has a very high dielectric constant of 81, therefore, a strong reflection is expected from the human body and it makes feasible to use a model covered by foil, as indicated in the right top corner of Fig. 10 (a), to emulate a real human body. The body model has a height of 1.4 m and a width of 0.6 m. It was located at a down range of 2.2 m.

Fig. 10 (b) presents the obtained 3-D image, as well as the real target position marked. It is clearly seen that the obtained image not only localizes the target precisely but also recognizes the shape of the human body accurately. The obtained 3-D image has a down range resolution of 5cm and a cross range resolution of approximately 15cm. Using a narrower pulse signal can further improve the down range resolution while increasing the number of detection points and the aperture size can further improve the cross range resolution. The 3-D imaging capability is indispensable for through-wall human beings detection, by distinguishing the human person from other objects successfully.

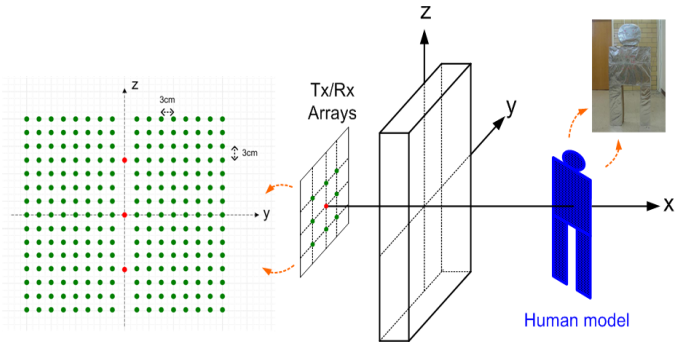

(a) 3-D experiment layout

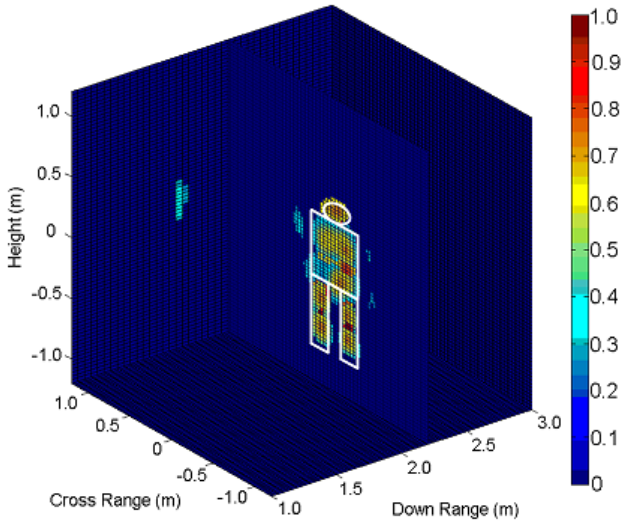

(b) Obtained 3-D image of the emulated human body

Fig. 10. 3-D detection imaging of an emulated human body

VII. Conclusion

A 3-D UWB radar system is designed to detect the positions of the targets behind the wall and identify them as well. The beam scanning is based on the mechanical movement of wideband Tx/Rx antennas that covers 2 to 10 GHz. The system components designs are introduced in details, including the system transceiver, data sampling using a low-cost equivalent-time scheme, wideband Vivaldi antenna, tunable Gaussian pulse generator, and 3-D microwave beamformer. An experiment was performed to recover the 3-D images of an emulated human body. The obtained 3-D images are very encouraging. These demonstrated results have indicated the capability of accurately locating, tracking and identifying human beings behind the wall.

References

[1] N. Hayashi, M. Sato, "A fundamental study of bistatic UWB radar for detection of buried objects," IEEE Int. Conference on UWB, Sep. 2008.

[2] I.J. Craddock et. Al, "Development and application of a UWB radar system for breast imaging," 2008 Loughborough Antenna & Propagation Conference, Mar. 2008.

[3] Y. Yang and A.E. Fathy, "Design and implementation of a low-cost real-time ultra-wide band see-through-wall imaging radar system," 2007 IEEE MTT-S Int. Microwave Symp., pp. 1467-1470, June 2007.

[4] Y. Yang and A.E. Fathy, "Development and implementation of a real-time see-through-wall radar system based on FPGA," IEEE Trans. on Geoscience and Remote Sensing, vol. 47, No. 5, May 2009.

[5] F. Ahmad, Y. Zhang, and M.G. Amin, "Three-dimensional wideband beamforming for imaging through a single wall," IEEE Geoscience and remote sensing letters, vol. 5, No. 2, Apr. 2008.

[6] Y. Wang, Y. Yang and A.E. Fathy, "Ultra-Wideband Vivaldi Arrays for See-Through-Wall Imaging Radar Applications," 2009 IEEE AP-S & URSI Int. Symp., June 2009.

[7] M.M. Zinieris et al., "A broadband microstrip-to-slot-line transition," Microwave and Optical Technology Letters, Vol. 18, No. 5, Aug. 1998.

[8] C. Zhang and A.E. Fathy, "Reconfigurable Pico-Pulse Generator for UWB Applications," 2006 IEEE MTT-S Int. Microwave Symp. Dig., pp. 407-410, June 2006.

[9] C. A. Balanis, Advance Engineering Electromagnetics, J. Wiley & Sons, pp. 229-236, 1989

Information-Theoretic Approaches to Data Selection and Model Inversion for UXO Classification Using Electromagnetic Induction Data

Stacy L. Tantum[1], Jeremiah J. Remus[2], Peter A. Torrione[1], and **Leslie M. Collins[1]**
[1]*Department of Electrical and Computer Engineering, Duke University, Durham, NC, USA, 27708-0291*
[2]*Department of Electrical and Computer Engineering, Clarkson University, Potsdam, NY, USA, 13699*
E-mail: lcollins@ee.duke.edu

Remediation of unexploded ordnance (UXO) is often a time-consuming and costly process, with the lack of adequate technologies for classifiying detected targets as either UXO or harmless non-UXO clutter driving much of the expense. UXO remediation efforts at several former military sites resulted in anywhere from 10 to 10,000 holes dug per UXO object recovered [1]. At an average cost of $150 per hole dug, the costs associated with excavating harmless clutter objects can be a significant proportion of the total expense of clearing a UXO-contaminated site. Accordingly, significant research effort has been directed toward classifiying detected subsurface anomolies as either UXO or non-UXO clutter.

The most advanced and effective approaches to UXO classification employ features derived from fitting measured electromagnetic induction (EMI) data to a phenomenological model (e.g., [2-7]). Model inversion routines typicaly utilize numerical optimization techniques to to search for the model parameters that provide the best match between the measured data and the phenomenological model. It is desirable for the model inversion process to be to be stable and robust so that the estimated model parameters, and therefore the features utililzed for target classification, are consistent for similar objects and insensitive to the inversion initialization. Two factors which may impact the model inversion process are the selection of data utilized for the model inversion and the objective function utilized to assess the quality of the estimated model parameters. In this work, information-theoretic approaches to data selection and model inversion to improve subsurface target classification using EMI data are investigated.

The model inversion process may be impacted by the data utilized for the inversion. Thus, selecting informative data is one of the challenges associated with developing robust, consistent inversion processes. Many modern geophysical data collections record multiple measurements over a detected target, either by recording single-axis (single-channel) sensor data at multiple spatial locations over the target or by employing a multi-axis (multi-channel) sensor to record multiple measurements while the sensor remains stationary over the target. Not all of the recorded data, however, are guaranteed to be informative for model inversion. There may be specific channels that have a deleterious effect on the inversion process due to a sensor or geological aberration. Alternatively, a subset of channels may be particularly informative, leading to more robust model inversion if only that subset of channels is utilized for model inversion. Information-theoretic metrics from optimal experiment design, such as Fisher information [8], are investigated for the selection from the full set of sensor measurements an optimal subset of informative measurements to use for the model inversion.

The model inversion may also be impacted by the objective function utilized to assess the quality of the estimated model parameters. Traditionally, the sum of squared error between the sensor measurement and the model prediction (L_2 norm) is utilized as the objective function for model inversion. However, information-theoretic approaches, such as Fisher information, in which a measure of the information conveyed by the estimated parameters is utilized as the objective function, may improve the stability of target parameters estimated through model inversion. Information-theoretic metrics are also investigated for assessing the quality of the model parameters estimated via model inversion.

Results are presented using measured sensor data collected in realistic field conditions.

References

1. Defense Science Board, "Report of the Defense Science Board Task Force on Unexploded Ordnance, Office of the Under Secretary of Defense for Acquisition, Technology, and Logistics," 2003.
2. T. H. Bell, B. Barrow, and J. T. Miller, "Subsurface discrimination using electromagnetic induction sensors," *IEEE Trans. Geosci. Remote Sensing*, vol. 39, pp. 1286-1293, 2001.
3. S. L. Tantum and L. M. Collins, "A comparison of algorithms for subsurface target detectionand identification using time-domain electromagnetic induction data," IEEE *Trans. Geosci. Remote Sensing*, vol. 39, pp. 1299-1306, 2001.
4. D. K. Butler, L. Pasion, S. D. Billings, D. Oldenburg, and D. E. Yule, "Enhanced discrimination capability for UXO geophysical surveys," *Proc. SPIE*, vol. 5089, pp. 958-969, Orlando, FL, USA, 2003.
5. Y. Zhang, L. M. Collins, H. Yu, C. E. Baum, and L. Carin, "Sensing of unexploded ordnance with magnetometer and induction data: Theory and signal processing," *IEEE Trans. Geosci. Remote Sensing*, vol. 41, pp. 1005-1015, 2003.
6. K. Sun, K. O'Neill, F. Shubitidze, I. Shamatava, and K. D. Paulsen, "UXO signature extraction from measurement data: Automatic weighting and regularization," *Proc. SPIE*, vol. 5794, pp. 275-286, Orlando, FL, USA, 2005.
7. L. R. Pasion, S. D. Billings, D. W. Oldenburg, and S. E. Walker, "Application of a library based method to time domain electromagnetic data for the identification of unexploded ordnance," *J. Applied Geophysics*, vol. 61, pp. 279-291, 2007.
8. T. M. Cover and J. A. Thomas, *Elements of Information Theory*. New York: Wiley-Interscience, 1991.

978-1-4244-5050-3/10/$26.00 ©2010 IEEE

An Ultra Wideband Antipodal Tapered Slot Antenna for Noise Radar Application

Y.M.M. Antar[1], A.P. Freundorfer[2], J.Y. Siddiqui[1], S.M. Mikki[1], T. Thayaparan[3]
[1] *ECE, Royal Military College of Canada, Kingston , ON K7K 7B4, Canada*
[2] *ECE, Queen's University, Kingston, ON, Canada K7L 3N6*
[3] *DRDC – Ottawa, 3701 Carling Avenue, Ottawa, ON K1A 0Z4, Canada*
antar-y@rmc.ca

In this paper we propose a design of an ultra wideband antipodal tapered slot antenna for noise radar application to detect covert weapons. Multioctave performances of antennas are increasingly being employed for radar applications [1]. Probing waveforms are transmitted to detect hidden objects and weapons. The detection depends on the resonant signatures of the size of weapons which are illuminated by the transmitted signal and corresponds to the wavelength of the tramsmitting waveform. An antenna with a wide bandwidth thus becomes imperative for such operations. The tapered slot antenna (TSA) [2] is a class of end fire, traveling wave antenna offering a wide bandwidth. The proposed antenna is planar in nature to facilitate easy integration with planar circuitry. Figure 1 shows the configuration of the proposed antenna printed on a dielectric substrate. A balun is used to excite the elliptic radiators printed on both side of the substrate. A smooth transition from microstrip to twin line facilitates the unbalanced to balanced transformation. The metallization on either side of the substrate is flared in opposite directions to form the tapered slot. Simple design equation is proposed to determine the lower cut off frequency of the antenna which depends on the dimension D which is given as

$$D = \frac{c}{f_L}\frac{1}{h.\sqrt{\varepsilon_r + 1}} \tag{1}$$

Where, c is the speed of light in free space, h and ε_r are the thickness and dielectric constant of the substrate, respectively and f_L is the lowest cutoff frequency of operation.

A prototype of the antipodal tapered slot antenna printed on a dielectric substrate with thickness 1.5748 mm having dielectric constant of 2.33 is fabricated and measured using an HP 8510 VNA. The flared radiators were formed with an ellipse having minor radius of 32.5 mm and an ellipticity ratio of 1.3. The dimension D, length L and width W were chosen as 132mm, 160 mm and 150 mm, respectively. The measured results were compared and verified with the simulation results obtained using HFSS [3]. Figure 2 shows the measured and simulated input return loss or the S_{11} of the fabricated prototype. The lower frequency is limited by the aperture width D which can be scaled for frequency tuning using the proposed formulation. Though not depicted, the far field radiation pattern of the antenna were measured and compared with simulation showing an average gain of 5.8 dBi and average half power beamwidth of 61.4 degrees. Although the geometry is planar, the proposed antenna is able to produce nearly symmetric radiation pattern in planes parallel to the surface. The necessary condition is that the parameters such as shape, length, substrate thickness and dielectric constant are chosen correctly. Due to their wideband wideband characteristics, they possess significant impact on the received waveforms, so a good time domain performance analysis becomes imperative which were simulated and obtained using CST [4].

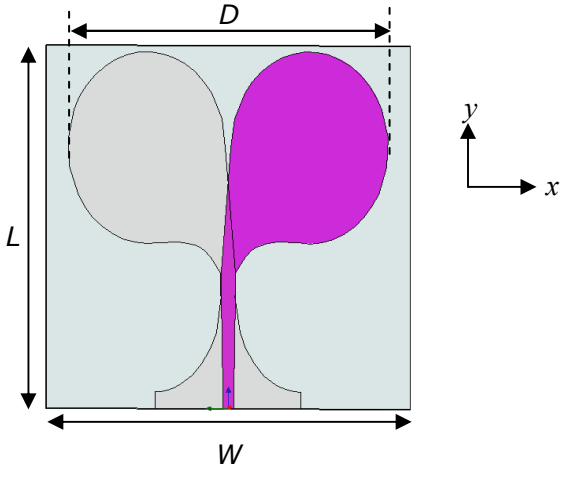

Fig. 1. Schematic of an antipodal tapered slot antenna

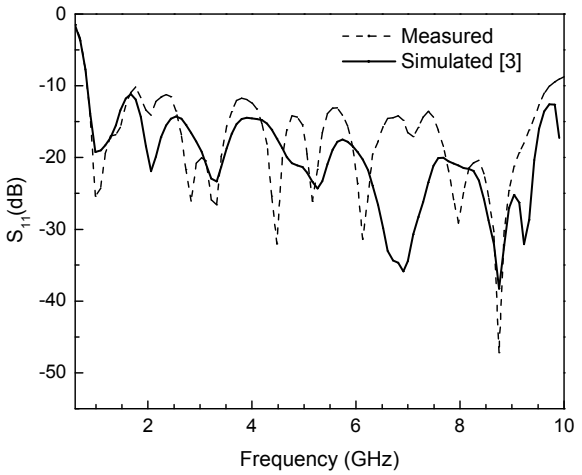

Fig. 2. Measured and simulated return loss characteristics of the proposed antipodal tapered slot antenna

References

1. J.D. Taylor, Introduction to ultra-wideband radar systems. CRC Press, 1995
2. K.S. Yngvesson, D.H. Schaubert, T.L. Korzeniowski, E.L. Kollberg, T.T Thungren, J. F. Johansson "Endfire tapered slot antennas on dielectric substrates," IEEE Transactions on Antennas Propagation, vol.33, pp. 1392-1400, Dec. 1985.
3. HFSS v.11, Ansoft corporation
4. CST Microwave Studio, CST Computer Simulation Technology AG

978-1-4244-5050-3/10/$26.00 ©2010 IEEE

Transfer function measurements of a computer network in a reverberation chamber compared with an open area test site

R. Hoad, A. Lambourne, S. P. Watkins, and **A. Wraight**
QinetiQ,Cody Technology Park, Farnborough, Hampshire, UK, GU14 0LX
E-mail: rhoad@qinetiq.com

An understanding of the coupling of High Power Electromagnetic (HPEM) environments to infrastructure assets is useful for the investigation of susceptibility and for the prediction of effects. Effects experiments on computer networks have previously been carried out in a reverberation chamber using mode stirring [1-2]. Coupling and effects experiments have recently been conducted through several studies permitting the gathering of data for statistical analysis over the VHF (30MHz to 300MHz) band. A computer network, comprising six standard Commercial Off the Shelf (COTS) computers and networking components was evaluated. The test system was configured in a manner to allow repeatable experiments to be conducted with an emphasis on minimising the number of random variables. The test setup will be described in the paper.

Coupling experiments were carried out on an Open Area Test Site (OATS) and within a large reverberation chamber. These experiments assisted in the identification of the mean coupling level to the system under test, the bounds of coupling (maximum and minimum) and have helped to identify the gain or directivity function of the test system. An example of the data obtained is given in Figure 1.

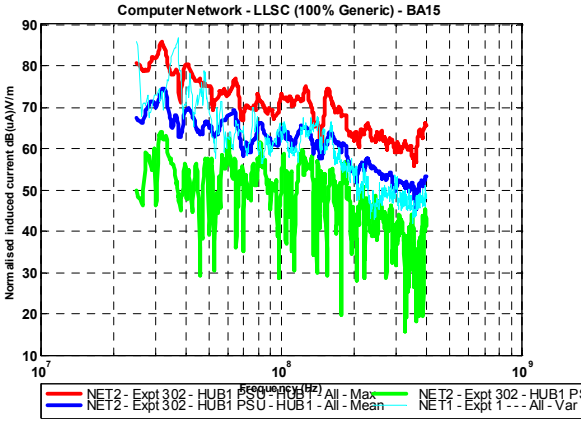

Figure 1: **Example Free-field and Modestirred coupling transfer functions**

The ultimate aim of these studies is to provide useful data to support High Power Microwave (HPM) and Intentional Electromagnetic Interference (IEMI) effects prediction analysis tools based on statistical rather than deterministic approaches.

Acknowledgments – The Authors would like to acknowledge the funding support of the United Kingdom Ministry of Defence (MoD) Defence Technology and Innovation Centre (DTIC) .

References

1. Hoad, R.; Carter, N.J.; Herke, D.; Watkins, S.P.; 'Trends in EM susceptibility of IT equipment', IEEE Transactions on Electromagnetic Compatibility, Volume 46, Issue 3, Aug. 2004 Page(s):390 – 395
2. Hoad, R.; Lambourne, A.; Wraight, A.; 'HPEM and HEMP susceptibility assessments of computer equipment', 17th International Zurich Symposium on Electromagnetic Compatibility, 2006. EMC-Zurich 2006. Feb. 27 2006-March 3 2006 Page(s):168 - 171.

978-1-4244-5050-3/10/$26.00 ©2010 IEEE

Modeling of the Surface Transfer Impedance by System Identifacation Approach

Lihua Shi Ying HuiZhou Qi Zhang
Laboratory of Electromagnetics, Nanjing Engineering Institute
Nanjing 210007, China
Shilih@tom.com

Surface transfer impedance(STI) of shielded cables is originally measured and described in frequency-domain. However, in evaluating the shielding effeciency of cabels under pulsed magnetic fields, it is sometimes required to have a time-domian model directly. A time-domain measurement and modeling method is proposed here to give an equivalent model of STI. The measurement system is based on a commonly used trixail STI test fixture except that pulse source and digital oscilloscope are employed instead of the network analyzer. Therfore, the measured signal in the inner conductor is the time-domian response of the shielded cable. This kind of test setup is suitable for testing EMP shielding effeciency directly. Furthermore, system indetification approach is used to establish a parametric model of the STI from the time-domian measurement waveform. This model is in the form of discrete transfer function(DTF) and can be conveniently used in time-domian numerical analysis of cable response under EMP. For an example, in analyzing the coupling of shielded inner conductors, STI is usually given as a frequency response curve which can not be used in time-domian calculations directly. By suing the new DTF model, the above problem can be solved.

978-1-4244-5050-3/10/$26.00 ©2010 IEEE

IMAGE-DOMAIN BASED TARGET DETECTION UNDER MODEL UNCERTAINTIES IN THROUGH-THE-WALL RADAR IMAGING

Christian Debes and Abdelhak M. Zoubir

Signal Processing Group
Technische Universität Darmstadt, Darmstadt, Germany

1. MOTIVATION

The problem of image-domain based detection of stationary targets in Through-the-Wall Radar Imaging (TWRI) is considered. Given is a three-dimensional (3D) TWRI image denoted as $Y(i,j,h)$ with $0 \leq i < N_i, 0 \leq j < N_j$ and $0 \leq h < N_h$ where N_i, N_j and N_h denote the number of voxels in crossrange, range and height, respectively. It is the aim to obtain a binary 3D image $B(i,j,h)$, $0 \leq i < N_i, 0 \leq j < N_j$, $0 \leq h < N_h$, which indicates the presence or absence of a target at each point in space, i.e.

$$B(i,j,h) = \begin{cases} 1, & \text{target present at } (i,j,h) \\ 0, & \text{target absent at } (i,j,h) \end{cases} \quad (1)$$

In order to obtain such a binary 3D image, a hypothesis testing framework has been considered in [1]. As the image statistics in practice are unknown and/or may change in time and space, an iterative detection approach has been developed in [2] which adapts itself to changing statistics.

One drawback of the iterative detection approach from [1, 2] is, however, the need for choosing target and noise models in the image domain. Although Gaussian and Rayleigh distributions have been suggested in the past [1] to model background-subtracted TWRI target and noise data, these models may not hold in all scenarios due to e.g. wall effects, limited resolution and generally the large variety of possible indoor targets to be considered in TWRI.

2. DETECTION UNDER MODEL UNCERTAINTIES

We present an extension of the detector from [1, 2] which adapts to changing and unknown noise and target models. The approach is depicted in Figure 1. Given a preset false-alarm

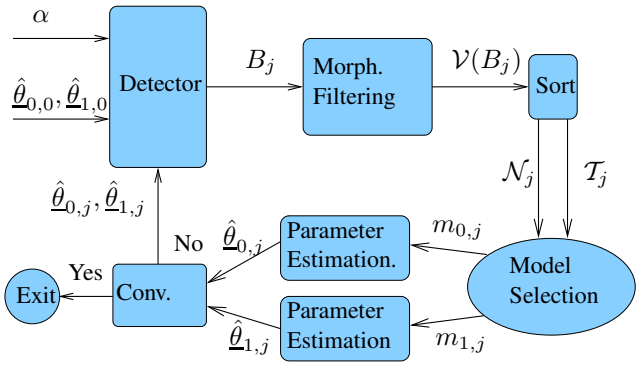

Fig. 1. Block diagram representation

rate α and initial parameter estimates $\hat{\underline{\theta}}_{0,0}, \hat{\underline{\theta}}_{1,0}$ describing the pdf's under the null and alternative hypothesis, a Neyman-Pearson test can be formulated, resulting in a binary image B_0, whereby the second subscript 0 stands for the $j = 0$-th iteration. Morphological filtering $\mathcal{V}(\cdot)$ is then applied to separate target and noise sets $\mathcal{T}_0$ and $\mathcal{N}_0$. These sets are used to select appropriate models $m_{0,0}$ and $m_{1,0}$. Based on the assigned models, revised parameter estimates $\hat{\underline{\theta}}_{0,1}, \hat{\underline{\theta}}_{1,1}$ can be obtained which are then forwarded to the detector to obtain a revised binary image B_1. The iteration stops when convergence is achieved.

Given target and noise sets in the j-th iteration, $\mathcal{T}_j$ and $\mathcal{N}_j$, it is the aim of the model selection step to decide for target and noise models $m_{0,j}$ and $m_{1,j}$. Models can be selected by considering classical goodness-of-fit tests, such as the Chi-Square test or the Kullback-Leibler divergence.

3. EXPERIMENTAL RESULTS

Detection results using TWRI images obtained from wideband sum-and-delay beamforming [3] are shown in Figure 2. Here, a metal dihedral (solid circle) and trihedral (dotted circle) have been imaged. Gaussian (target) and Rayleigh (noise) models have been chosen for the static approach, whereas for the new model-adaptive approach Gaussian, Rayleigh, Weibull and Gamma densities where adaptively chosen. The false-alarm rate was set to 0.01. As can be seen, the proposed method is able to choose appropriate density models, yielding improved detection results.

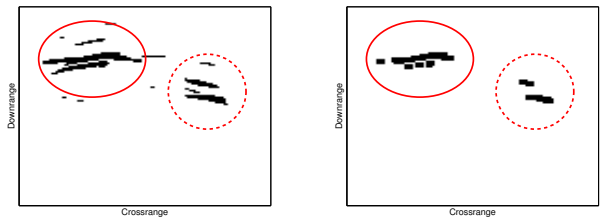

(a) Static model (b) Adaptive model

Fig. 2. Detection Results

4. REFERENCES

[1] C. Debes, M.G. Amin, and A.M. Zoubir, "Target detection in single- and multiple-view through-the-wall radar imaging," *IEEE Transactions on Geoscience and Remote Sensing*, vol. 47(5), pp. 1349 – 1361, May 2009.

[2] C. Debes, J. Riedler, M.G. Amin, and A.M. Zoubir, "Iterative target detection approach for through-the-wall radar imaging," in *IEEE ICASSP*, 2009, pp. 3061 – 3064.

[3] F. Ahmad and M.G. Amin, "Multi-location wideband synthetic aperture imaging for urban sensing applications," *Journal of the Franklin Institute*, vol. 345, no. 6, pp. 618–639, Sept. 2008.

978-1-4244-5050-3/10/$26.00 ©2010 IEEE

A Study in Antennae Characterization System Using Noise

A.P. Freundorfer[1], J. Siddiqui[2], Y.M.M. Antar[2] and T. Thayaparan[3]
[1]*Department of Electrical and Computer Engineering, Queen's University, Kingston, Canada*
[2]*Department of Electrical and Computer Engineering, Royal Military College, Kingston, Canada*
[3]*Defence Research and Development Canada, Ottawa, Canada*
E-mail: freund@queensu.ca

Abstract – The theory of antennae measurement using noise will be presented and a comparison with other methods such as ultra wideband (UWB) time domain and ultra wideband frequency domain using the vector network analyzer (VNA) will be given. It will be shown that the UWB time domain is most equivalent to the method of using noise measurement and that it does not suffer from noise degradation or synchronization issues as in the UWB time domain method. Another benefit of this measurement technique is that one gets to see the correlator output directly without Fourier transforming the data. This avoids potential data processing errors as in the frequency domain method.

Summary – UWB antennae measurements have been done both in frequency domain [1]-[3][8] and time domain [3][4]. Practical time and frequency domain techniques are not equivalent [3]. Transformation from one domain to the other is not a reversible process in the digital domain. Leakage errors are a redistribution of energy due to data windowing [2], which result from the Fourier or inverse Fourier transforms. Leakage error occurs when the values on each side of the time or frequency domain window are not continuous before performing the transformation operation. These discontinuities are normally caused by windowing [2] of obtained data or by the time duration limitation or bandwidth limitation of the measurement equipment. A more detailed discussion is given in [3].
The noise measurement technique has an advantage over the time domain technique since it is not susceptible to noise [6] [7] or jitter problems. The resulting waveform of the correlator output gives a direct physical insight into the characterization problem, as in the time domain technique. The noise domain technique does not suffer from the processing errors of the frequency domain technique. It can also be concluded, just as in the non-equivalence of the time and frequency domain techniques, that the noise domain is not equivalent to time domain or frequency domain. The correlator output of the noise domain system is the same as the output of the time domain under certain conditions. The time domain gives an instantaneous output, while the correlator output is averaged and depends on the integration length. This can be shown in the theoretical analysis. The ultra wideband (UWB) antennae measurements [4] shows that the pulse shape/dispersion of an UWB antenna changes as a function of orientation. Thus it is assumed that the output of the correlator will also change depending on antennae orientation. For noise applications, it would therefore be important to directly characterize the response in order to see the effect on the receiver output.
Noise domain techniques for antennae measurements will be discussed. As well, they will be compared with the current time [4] and frequency domain techniques[1]. The pros and cons of these methods will be summarized.

Acknowledgments – I would like to thank Defence Research and Development Canada for the funding of this project..

References

1. S. Licul, W.A. Davis, "Ultra-wideband (UWB) antenna measurements using vector network analyzer," IEEE Antennas and Propagation Society International Symposium 2004, Vol. 2, 20-25 June 2004, pp. 1319 – 1322.
2. A.V. Kalinin, "Wideband antenna measurements in anechoic chamber," Second International Workshop Ultrawideband and Ultrashort Impulse Signals, 19-22 Sept. 2004, pp. 151 – 153.
3. A.H. Muqaibel, "Characterization of Ultra Wideband Communication Channels," Ph.D. Thesis, The Bradley Department of Electrical and Computer Engineering, Virginia Polytechnic Institute and State University, March 5th 2003, pp. 67-73.
4. [S. Promwong, W. Hanitachi, J. Takada, P. Supanakoon, M. Chamchoy, P. Tangtisanon, and V. Vivek, "Free Space Transmission Measurements of Ultra Wideband Antenna for Wireless Personal Area Networks," Proceeding of EECON26, 2003, Petchaburi Thailand, pp. 1502-1505.
5. T. Thayaparan and C. Wernik, "Noise Radar Basics," Defence R&D Canada, Otawa, Technical Memorandum, DRDC Ottawa TM 2006-266, Dec. 2006.
6. E.K. Walton, I.P. Theron, S. Gunawan, L. Cai, "Moving vehicle range profiles measured using a noise radar," IEEE Antennas and Propagation Society International Symposium 1997, Vol. 4, 13-18 July 1997, pp. 2597 – 2600.
7. M. Dawood, R.M. Narayanan, "Ambiguity function of an ultrawideband random noise radar," IEEE Antennas and Propagation Society International Symposium 2000, Vol. 4, 16-21 July 2000, pp. 2142 – 2145.
8. C.J. Brouchu, G. Morin and J.W. Moffat, "Gain Measurement of Cavity-Backed spiral antennae from 4 to 18GHz using the three-antenna method," Defence R&D Canada, Ottawa, Technical Report, DREO, Ottawa Report No. 1337, Nov. 1998.

978-1-4244-5050-3/10/$26.00 ©2010 IEEE

Buried Object Detection Using Goodness-of-fit to Gumbel Distribution

Ahmet B. Yoldemir and **Mehmet Sezgin**
TÜBİTAK Marmara Research Center, Information Technologies Research Institute, PK: 21, 41470, Gebze, Kocaeli, Turkey
E-mail: burak.yoldemir@bte.mam.gov.tr

In this study, we propose a novel model-based buried object detection method using ground penetrating radar. The method is based on statistical hypothesis testing, where the null distribution is Gumbel distribution, which is also known as the extreme value type-1 distribution. An extensive analysis of this distribution is given in [1]. The motivation of such a test is the difference in the histograms of A-scans in the presence and absence of buried objects, as shown in Fig. 1. In this figure, each curve corresponds to the mean histogram of 100 A-scans, in the presence and absence of a buried object, respectively. It is clear that existence of an underground object causes the histogram to skew from normal distribution. This skewed histogram resembles a Gumbel distribution, which is governed by the following probability density function:

$$f(x) = \frac{1}{\sigma} exp(-z - exp(-z)) \tag{1}$$

where $z = (x - \mu)/\sigma$, μ and σ being the mean and standard deviation of the data set, respectively. A plot of this distribution is provided in Fig. 2. Due to the change in the histogram of the signals, one can decide on the existence of a buried object in the inspected region, if a Gumbel distribution can be successfully fitted to the histogram of the A-scan received at that point. To measure the goodness-of-fit to Gumbel distribution, we use the following test statistic, which is also used in many renowned hypothesis tests, such as Kolmogorov-Smirnov test and Lilliefors test:

$$\xi = \max_x |C\hat{D}F(x) - CDF(x)| \tag{2}$$

where $C\hat{D}F(x)$ is the empirical estimate of the cumulative distribution function(CDF) of the input vector, $CDF(x)$ is the CDF of an extreme value type-1 distribution with the same location and scale parameters as the input vector and ξ is the test statistic. A low value of this test statistic indicates a good fit to Gumbel distribution. A typical plot of the test statistic is given in Fig. 3, where the smallest value of the test statistic corresponds to the buried object location. This test statistic is normalized, which allows us to decide on the existence of an underground object using a single threshold value. In short, we reduce the detection problem into a binary hypothesis test, where the aforementioned test statistic is compared to a constant threshold. The proposed method is tested on a real terrain. The terrain includes a total of 346 metallic and nonmetallic disks (AP and AT mine equivalents and clutter), diameters of which range from 90 mm to 330 mm and heights of which range from 40 mm to 120 mm. The burial depth of the objects varies from 7 cm to 30 cm. In total, we reach a detection rate of 94.3% with a false alarm rate of only 0.9%. This algorithm works very fast, which makes it convenient for practical applications. As the tests were carried out on real terrain, given detection and false alarm rates are expected to hold in real-time applications.

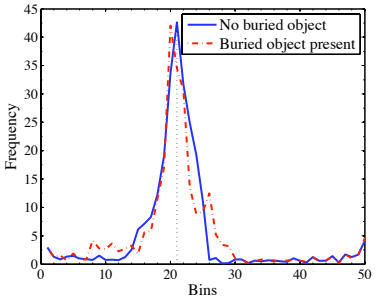

Figure 1: **Histograms of A-scans**

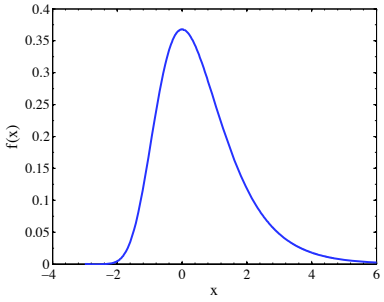

Figure 2: **Gumbel Distribution**

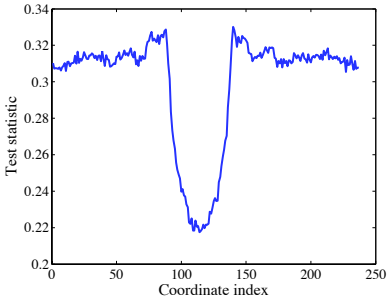

Figure 3: **Test statistic**

References

[1] Rolf-Dieter Reiss and Michael Thomas. *Statistical analysis of extreme values*. Birkhauser Verlag, Basel, Switzerland, 1997.

978-1-4244-5050-3/10/$26.00 ©2010 IEEE

THE ELLIPTICUS CW ILLUMINATOR OPERATED IN VERTICAL MODE

W.D. Prather
Air Force Research Laboratory
Directed Energy Directorate
Kirtland AFB NM 87117

M.R. Rooney
Defense Threat Reduction Agency
Ft. Belvoir, VA

G.J. Anderson
Oklahoma City ALC
Tinker AFB OK

J. Cafferky and M. Gruchalla
EG&G
Albuquerque, NM

The horizontally polarized Ellipticus Illuminator was designed and built to be a CW counterpart to the Horizontally Polarized Dipole (HPD) EMP Simulator for use in measuring the EMP response of shielded aircraft and for performing hardness maintenance/hardness surveillance (HM/HS) during the system's lifetime. It is a relatively inexpensive system to build and operate, and it has been shown to be comparable to the HPD simulator.

It is desirable to also have a vertically polarized CW illuminator, so the existing Ellipticus system was reconfigured to produce a vertically polarized field. Measurements of the fields in the working volume were made to investigate the possibility that the existing CW antenna could be used in both modes. If this were successful, it would save time and expense by avoiding having to erect a second antenna to get the vertical field.

In this paper, it is shown that with a minor reconfiguration, the Ellipticus antenna can be used in a vertical mode, and that the fields are comparable to those measured in the horizontally polarized mode. The experiment successfully demonstrated the desired performance, and a decision was made to implement this capability at the CW test pad in Oklahoma City.

This paper reviews the design and testing of an Ellipticus antenna reconfigured to radiate a vertically polarized field. The work was supported by the Defense Threat Reduction Agency.

978-1-4244-5050-3/10/$26.00 ©2010 IEEE

Achieving UWB Data Transmission under Non-Line-of-Sight Propagation Conditions

J. LeBel, D. Cule
Communications Research Centre Canada,
Satellite Communications and Radio Propagation Research
E-mail: j.lebel@crc.gc.ca

Abstract - The main purpose of the research project was to extend the range of applications of ultra-wideband (UWB) communications to non-line-of-sight (NLOS) propagation conditions. Such NLOS conditions exist in mine shafts, tunnels, storage areas, indoors, etc. UWB communications are usually designed for short-range line-of-sight (LOS) applications and low power. By using suitably selected microwave scatterers and multiple receive antennas one can greatly increase the range of applications of UWB communications, in the centimeter- and millimeter-wave frequency range, beyond normal LOS propagation. Under NLOS conditions there usually exist adverse propagation conditions as a result of multipath effects. The result of multipath propagation is to effectively reduce the useful bandwidth under the assumption of single-carrier modulation.

In order to solve the problem of limited bandwidth available for single-carrier transmission, one can use multi-carrier modulation such as orthogonal frequency-division multiplexing (OFDM). In this modulation process, many narrow-band sub-carriers, each of which is modulated by an individual data stream, carry information independently from other sub-carriers. Assuming that the same modulation technique and data rate are used for each sub-carrier, the total data transmission rate is then proportional to the number of sub-carriers used. Another property of OFDM is the fact that, for a stable (in time) propagation channel, each sub-carrier is orthogonal to the other sub-carriers in the frequency domain although it is affected by the transmission characteristics of the propagation channel. Using a suitable detection technique such as a digital Fourier transform (DFT), one can recover data from each of the modulated sub-carriers, although there is an overlap between neighboring modulated sub-carriers in the frequency domain.

An OFDM modulation standard has been proposed for UWB applications [1]. It consists in using 128 sub-carriers in a bandwidth of 528 MHz. According to this standard the center of one sub-carrier is separated from the center of its neighbor(s) by a frequency of 4.125 MHz, a rate that also corresponds to the symbol transmission rate. For reasons of spectral efficiency a 16-level quadrature amplitude-modulation (16QAM) scheme was selected for each of the sub-carriers. In order to simulate two mine shafts where one would use scatterers as means for propagating microwave radiation from one shaft to the other, two hallways intersecting at 90^o were selected, with circular aluminum cylinders at the intersection of the two hallways used as microwave scatterers. During the propagation experiments both transmit and receive antennas were located at 10 meters from the scattering cylinder(s) and pointed at the cylinder(s). Precise measurements of the frequency response of NLOS propagation channels were carried out in a 1 GHz band centered around 29.5 GHz, in the neighborhood of a former local multipoint communications systems (LMCS) frequency band, for various scatterer configurations and three laterally-displaced receive antenna positions. Small identical pyramidal horn antennas with a nominal gain of 23 dB were used at both ends. The dimensions of the antenna openings were 5.2 cm (V) and 6.8 cm (H). Based on these measurements, OFDM data transmission streams were simulated according to a method described earlier [2] but adapted to OFDM. For a single-input single-output (SISO) configuration, individual sub-channels of the OFDM data transmission stream suffered distortions to various degrees resulting in the unavailability of some sub-channels for data transmission. Using post-DFT multiple sub-carrier selection (MSCS) from multiple receive antennas (SIMO configuration), 3 in the present case, it was determined that data throughputs comparable to those achievable under perfect LOS conditions could be obtained in spite of adverse propagation conditions. Defined metrics were used as criteria to select individual sub-carriers. Signal-level and error-rate metrics were used for the selection of sub-carriers.

Results are presented for single cylinders with diameters of 10, 15 and 30 cm (each with a height of 233 cm) and combinations of the aforementioned circular cylinders. The physical disposition of the cylinders was selected to cause planned mutual differential delays of 0, 2, 4 and 8 ns in the propagation path between transmit and receive antennas in order to induce adverse propagation conditions. It was determined that in numerous cases, owing to the sub-carrier selection technique, a symbol error rate less than 1 in 10^6 could be achieved with an average signal-to-noise ratio (SNR) of 31 dB for all sub-carriers.

References

1. W. Pam Siriwongpairat, K. J. Ray Liu, "Ultra-Wideband Communications Systems, Multiband OFDM Approach", John Wiley & Sons, Inc, 2008.
2. J. LeBel, "Limitations of Non-Line-of-Sight Propagation for High-Speed High-Efficiency Local Multipoint Communication Systems," ITU Fachbericht, Proceedings of the '2nd European Personal and Mobile Communications Conference (EPMCC `97)' and of the '3rd Conference of the Information Technology Society (3. ITG Fachtagung), Bonn, Germany, Sept. 30 – Oct. 2nd, 1997, pp. 299-306.

978-1-4244-5050-3/10/$26.00 ©2010 IEEE

Degradation of Shielded Enclosure Made by Wire Mesh due to Weather Impact

Jostein Godø
Forsvarsbygg, Norwegian Defence Estates Agency, Oslo, Norway
E-mail: jostein.godo@forsvarsbygg.no

A shielded enclosure, 3x3x3 meter and made by wire mesh was built for test purposes. First we wanted to test a technique for mounting a metal mesh as an electromagnetic shield, and second we wanted to measure the effect of having two separated layers of the mesh.
The cube was made of wooden framework and had one layer of mesh on the outside of the framework, and one layer on the inside. The mesh was delivered in 1 meter wide rolls, so the mesh had to be joined to make a complete shield. The main technique for joining the mesh was having some overlap. A narrow metal plate was then placed over the overlap and the plate was screwed to the framework. A few places the mesh was joined between two metal plates. Parts of the floor and the entrance were made of steel plates.
Measurements were first carried out according to methods described in MIL-STD 285, i.e. antennas positioned 30 cm from the shield. Then we also tested the shield with antennas positioned 1 meter from the shield. Magnetic antennas were used in the frequency range 10 kHz up to 30 MHz, and electric antennas were used up to 1 GHz.
After finishing the tests, the cube was left outdoor. Since the walls and roof only consists of framework and mesh, the shield and framework got exposed to rain, snow and variations in temperature.
After 14 years, the measurements were repeated. The shielding was then considerably degraded. Some corrosion occurred on the screws holding the metal plates. The main problem however, was that the wood and the metal reacted different to weather changes; the metal expanding with temperature, and the wood expanding with humidity. As a result, the screws got slightly pulled out of the wood in which they were mounted. Tests by using near field probe showed that the degradation of shielding was considerably less on the parts where the mesh was joined between metal plates.

978-1-4244-5050-3/10/$26.00 ©2010 IEEE

A new method for strong broadband jammer rejection in noise radar systems

Slobodan Djukanović[1], Miloš Daković[1], Thayananthan Thayaparan[2], and **Ljubiša Stanković[1]**
[1]*Electrical Engineering Department, University of Montenegro, 81000 Podgorica, Montenegro*
[2]*Radar Applications and Space Technology, Defence Research and Development Canada, Ottawa, Ontario*
E-mail: slobdj@ac.me

In noise radar systems, a transmitted random noise signal is reflected from a target and received with a delay that is proportional to the distance from the target [1-3]. The received signal is correlated with delayed versions of the transmitted noise, and the correlation peak indicates the distance from the target. Noise radars outperform the conventional ones in many aspects, which is due to the truly random transmitting signal. In specific, noise radars are characterized by unambiguous range estimation, higher immunity to noise, jammer suppression, low probability of intercept. A low power jammer is significantly suppressed by the correlation, but a high power jammer can significantly deteriorate the receiver's performance [4-5].

In this paper, we propose a method for rejection of high power broadband jammers superimposed on the radar return. Jammers can cover both the frequency and time ranges of the radar. We developed an algorithm which adaptively divides the received signal into non-overlapping segments so that, for each segment separately, the phase of the jammer (and, in turn, the instantaneous frequency (IF)) can be approximated by a polynomial. The polynomial coefficients are estimated by using the product high-order ambiguity function (PHAF) [6]. Once we know the IF trajectory of the jammer, we can dechirp the received signal in order to move the jammer to the zero frequency (DC), and filter it by removing the DC component. The algorithm can be easily extended to the multiple jammers case. In addition, the PHAF allows the use of the algorithm in multipath environments.

The performance of the proposed method is evaluated by the peak-to-sidelobe ratio (PSR), and it outputs the PSR very close to the PSR of the jammer-free received signal. In simulations, we used various types of FM jammers, with both polynomial and nonpolynomial phase. For example, consider a highly nonstationary sinusoidal FM jammer, with jammer-to-signal ratio (JSR) of 30dB, that covers approximately 70% of the radar signal's bandwidth. The absolute value of the correlation without and with the jammer rejection is depicted in Fig. 1. Single point scatterer is considered.

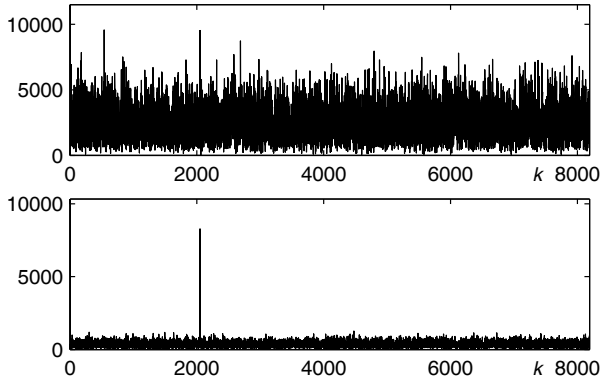

Figure 1: The absolute value of the correlation without and with the jammer suppression (upper and lower plot, respectively). *k* denotes the delay index.

References

1. I. P. Theron, E. K. Walton, S. Gunawan, and L. Cai, "Ultrawide-band noise radar in the VHF/UHF band", IEEE Trans. Antennas Propagat., vol. 47, 1999.
2. S. R. J. Axelsson, "Noise radar for range/Doppler processing and digital beamforming using low-bit ADC", IEEE Trans. Geosci. Remote Sens., vol. 41, 2003.
3. S. R. J. Axelsson, "Noise radar using random phase and frequency modulation", IEEE Trans. Geosci. Remote Sens., vol. 42, 2004.
4. M. Daković, T. Thayaparan, S. Djukanović, and Lj. Stanković, "Time-frequency-based non-stationary interference suppression for noise radar systems", IET Radar, Sonar & Navigation, vol. 2, 2008.
5. S. Djukanović, M. Daković, T. Thayaparan, and Lj. Stanković, "Method for nonstationary jammer suppression in noise radar systems", IET Radar, Sonar & Navigation, accepted for publication.
6. S. Barbarossa, A. Scaglione, and G. B. Giannakis, "Product high-order ambiguity function for multicomponent polynomial-phase signal modeling", IEEE Trans. Signal Process., vol. 46, 1998.

978-1-4244-5050-3/10/$26.00 ©2010 IEEE

Autofocusing of SAR Images Based on the LPFT and the PHAF

Vesna Popović[1], Igor Djurović[1], LJubiša Stanković[1], Thayananthan Thayaparan[2], and **Miloš Daković[1]**
[1]*University of Montenegro, Cetinjski put bb, 81000 Podgorica, Montenegro*
[2]*Radar Applications and Space Technologies, Defence R&D Canada - Ottawa, Ottawa, Ontario, Canada,*
E-mail: pvesna@ac.me

The Synthetic Aperture Radar (SAR) is a system for obtaining high resolution radar image. In the case when SAR targets are stationary, the radar signal is composed of a sum of complex sinusoids. The resulting SAR images, obtained by using the 2D Fourier Transform (2D FT) are well focused [1]. For moving targets, the corresponding signals are linear or higher-order phase frequency modulated [1-2]. Therefore, the SAR images of moving targets can be spread in the 2D Fourier domain [1-2]. One group of techniques for focusing SAR images is based on the motion compensation. The motion compensation can be performed by estimating parameters of received signal. One technique for focusing SAR images by using the product high-order ambiguity function (PHAF) for parameter estimation is proposed in [3]. The resulting SAR images are focused in the case when only one target exists in a range bin, or in the case when all targets in one range bin have similar motion parameters. As an alternative, the time-frequency analysis is used for focusing SAR images [1]. The adaptive S-method (SM) for SAR imaging has been proposed in [4]. It is computationally simple and produces highly concentrated SAR images. Recently, the local polynomial Fourier transform (LPFT) based technique is proposed in [5]. It outperforms the adaptive SM in case of close targets and in the presence of noise [6]. The drawback of the LPFT-based technique is its large amount of computations that are essential for selecting a chirp-rate that produces the best concentration, from a predefined set.
When one or more unfocused targets are detected in a range, instead of using a predefined set [5], the PHAF is evaluated in the algorithm proposed here, and its maximum is used for the coarse chirp-rate estimation. The obtained estimate is further improved by using a fine search in an interval of two frequency bins from each side of the frequency related to the coarse estimate. Number of chirp-rates in the fine search is rather small, usually not larger than several tens, which yields a significant decrease in computational complexity with respect to the technique proposed in [5], which requires hundreds or thousands. The fine search set is automatically adjusted to the motion parameters of each unfocused target. A procedure for the third-order phase compensation is applied in the proposed algorithm without significant increase of the calculation burden. In Figure 1, results obtained by the proposed algorithm are compared to those obtained by the 2D FT, the adaptive SM and the LPFT-based autofocusing algorithm with the predefined set of chirp-rates. The proposed algorithm produces high concentration of all moving targets, without defocusing the stationary ones or inducing cross-terms, Figure 1.

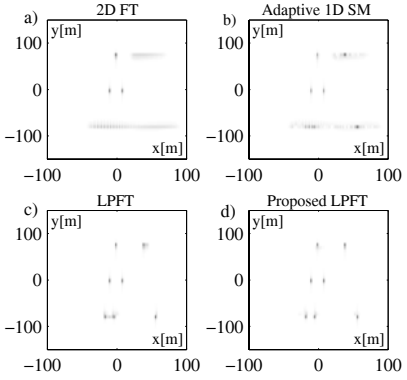

Figure 1: SAR image obtained by: a) 2D FT, b) Adaptive S-method, c) LPFT with predefined set of chirp rates d) Proposed LPFT.

References

1. V. C. Chen, H. Ling: Time-frequency transforms for radar imaging and signal analysis, Artech House, Boston, 2002.
2. J. J. Sharma, C. H. Gierull, and M. J. Collins: "Compensating the effects of target acceleration in dual-channel SAR-GMTI", IEE Proc. of Radar, Sonar and Navigation, vol. 153, 2006.
3. S. Barbarossa, A. Scaglione: "Autofocusing of SAR images based on the product high-order ambiguity function", IEE Proc. Radar, Sonar Navigation, vol. 145, 1998.
4. LJ. Stanković, T. Thayaparan, V. Popović, I. Djurović and M. Daković: "Adaptive S-method for SAR/ISAR imaging", EURASIP Journal on Advances in Signal Processing, vol. 2008, Article ID 593216, 10 pages, 2008.
5. I. Djurović, T. Thayaparan, LJ. Stanković: "SAR imaging of moving targets using polynomial Fourier transform", IET Signal Processing, vol. 2, 2008.
6. I. Djurović, LJ. Stanković, T. Thayaparan, V. Popović, M. Daković: "Time-frequency analysis for SAR and ISAR imaging", in GeoSpatial Visual Analytics, Springer Netherlands, 2009.

978-1-4244-5050-3/10/$26.00 ©2010 IEEE

Nonstationary Target Detection by Using the S-Method

Ljubiša Stanković*, Thayananthan Thayaparan, Miloš Daković***

**University of Montenegro, Podgorica, Montenegro*
***Defence Research and Development Canada, Ottawa, Ontario, Canada*
l.stankovic@ieee.org; Thayananthan.Thayaparan@drdc-rddc.gc.ca; milos@ac.me

It is known that nonstationary moving target produces nonstationary frequency modulated radar return. The detection of a nonstationary deterministic signal in a high noise environment is an important task in radar signal processing. In the case of stationary signal, for example, sinusoidal signal with constant frequency, the Fourier transform (FT) method concentrates all the signal energy in one frequency point while the noise is uniformly distributed over all frequencies. Thus, it is easy to conclude that the FT-based detection method provides the optimal detection in the case of stationary signal. However, for non-stationary signals, i.e., when the frequency content of a signal changes over time, the spectral content of such signals becomes time-varying, and thus the FT-based detector will not provide the optimal result.

Time-frequency formulation of the FT, the short time Fourier transform (STFT) is obtained by using a window in the time domain. The STFT has similar advantages and drawbacks as the FT [1], [2]. Therefore there is a need for more sophisticated time-frequency tools for analysis of highly non-stationary signals [3]-[6]. The S-method, originally proposed in [6] achieves high concentration of signal energy in time-frequency plane without unwanted interferences (cross-terms). Moreover the S-method is easy to implement due to the low calculation complexity. Here, we analyze performance of a S-method-based detection scheme proposed in [7] for the detection of maneuvering air targets in the presence of strong noise. The basic idea is to use a method that produces highly-concentrated energy of the desired signal around the instantaneous frequency (IF) and then apply the integration along the IF line. In the case of high noise, an algorithm for finding possible IF paths is proposed in [7]. In this way, the detection performance will be as high as in the case of constant frequency signal detection by using the FT method. The S-method-based detection method is compared with the FT-based detector. The proposed method is applied to the real nonstationary radar signals with varying artificial additive noise. Detection performances are presented in Fig.1. The S-method based detector outperforms Fourier based detector over the whole analyzed SNR range.

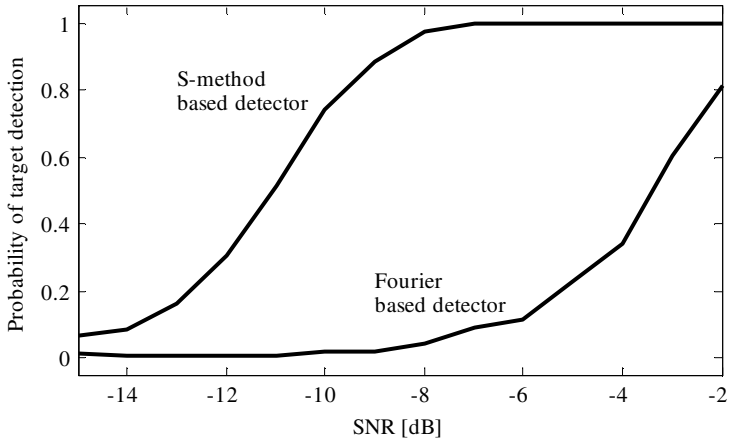

Figure 1. Probability of nonstationary target detection for Fourier-based and S-method based detector.

[1] L. Cohen, *Time-frequency analysis*, Prentice-Hall, 1995.
[2] V.C. Chen and H. Ling, *Time-Frequency transform for radar imaging and signal analysis*, Artech House, BOSTON.
[3] T. Thayaparan and S. Kennedy,"Detection of a manoeuvering air targets in sea-clutter using joint time-frequency analysis techniques," IEE Proc.-Radar Sonar Navig., Vol. 151, No. 1, pp 19-30, 2004.
[4] A. Yasotharan and T. Thayaparan, "A time-frequency method for detecting an accelerating target in sea or land clutter," IEEE Transactions on Aerospace and Electronic Systems, Vol. 42, Issue 4, pp. 1,289 -- 1,310, 2006.
[5] LJ. Stanković, T. Thayaparan and M. Daković, "Signal Decomposition by Using the S-Method with Application to the Analysis of HF Radar Signals in Sea-Clutter," IEEE Transactions on Signal Processing, Vol. 54, Issue 11, pp. 4,332 -- 4,342, 2006.
[6] LJ. Stanković, "A method for time-frequency signal analysis," IEEE Trans. Signal Processing, vol. 42, pp. 225-229, Jan. 1994.
[7] M. Daković, T. Thayaparan, Lj. Stanković, "Time-frequency based detection of fast maneuvering targets", *IET Signal Processing* Volume 4, 2010, in print

978-1-4244-5050-3/10/$26.00 ©2010 IEEE

Empirical Mode Decomposition in Radar Signal Processing

Miloš Daković*, Thayananthan Thayaparan **, Ljubiša Stanković*

**University of Montenegro, Podgorica, Montenegro*
***Defence Research and Development Canada, Ottawa, Ontario, Canada*
milos@ac.me; Thayananthan.Thayaparan@drdc-rddc.gc.ca; l.stankovic@ieee.org

The Empirical mode decomposition (EMD) is recently proposed signal processing technique able to separate signal into components in a simple and efficient manner. The EMD is originally proposed by Huang et al. [1]. In the past decade significant number of scientific papers is published where the EMD is analyzed and applied in a wide area of signal processing. Theoretical approach to EMD is presented in [2], application of EMD in the signal filtering is presented in [3] and [4], while the problem of close component separation is studied in [5]. However there is no significant research in application of EMD and similar algorithms to the radar signal processing, especially in the case of heavy clutter environment whose nature does not correspond to an FM signal. Here we will present basic EMD algorithm with application to the real radar data analysis. It is shown that EMD based approach can be used in separation of target and clutter signals.

We will demonstrate EMD capabilities in target detection within strong clutter. We will assume that we deal with fast maneuvering target in heavy clutter environment. As an example, we use experimental HFSWR data with fast maneuvering target within strong sea clutter. Results are presented in Fig.1 where left subplot presents radar return with sea clutter, middle subplot is extracted target signal and right subplot is residual signal after target extraction.

Result of the decomposition is set of Intrinsic mode functions (IMF). In ideal case IMFs contain individual signal components. Time-frequency analysis tools [6] can be used to extract parameters of each component (instantaneous frequency, amplitude) in order to perform component classification and target parameters detection.

The EMD is compared with other decomposition techniques, for example eigenvector based decomposition as described in [7].

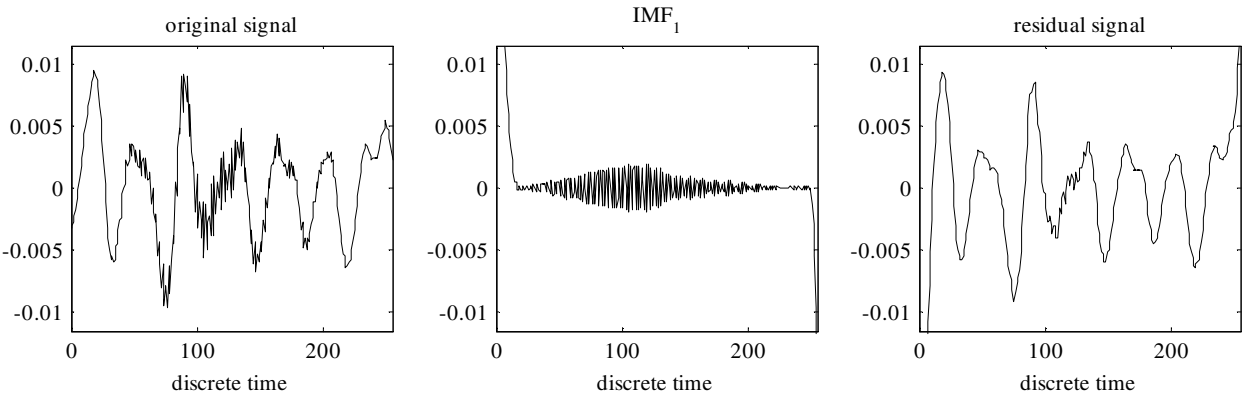

Figure 1. EMD of the real radar signal. Original signal (left subplot), target component (middle subplot) and residual signal (right subplot)

[1] N. E. Huang, Z. Shen, S. R. Long, M. L.Wu, H. H. Shih, Q. Zheng, N. C. Yen, C. C. Tung, and H. H. Liu, "The empirical mode decomposition and Hilbert spectrum for nonlinear and nonstationary time series analysis," *Proc. R. Soc. London A,* vol. 454, pp. 903--995, 1998.

[2] E. Deléchelle, J. Lemoine, and O. Niang,"Empirical Mode Decomposition: An Analytical Approach for Sifting Process," *IEEE Sig.Proc. Letters,* vol.12, no.11, Nov.2005, pp.764-767

[3] A. O. Boudraa, and J. C. Cexus, "EMD-Based Signal Filtering," *IEEE Trans. ON Instrumentation and Measurement,* vol.56, no.6, Dec.2007, pp.2196-2202

[4] P. Flandrin, G. Rilling, and P. Gonçalvés, "Empirical Mode Decomposition as a Filter Bank," *IEEE Sig.Proc. Letters,* vol.11, no.2, Feb.2004, pp.112-114

[5] G. Rilling and P. Flandrin, "One or Two Frequencies? The Empirical Mode Decomposition Answers," *IEEE Trans. on Signal Processing,* vol.56, no.1, Jan.2008, pp.85-95

[6] LJ. Stanković, "A method for time-frequency signal analysis," *IEEE Trans. on Signal Processing*, vol. 42, pp. 225-229, Jan. 1994.

[7] LJ. Stanković, T. Thayaparan and M. Daković, "Signal Decomposition by Using the S-Method with Application to the Analysis of HF Radar Signals in Sea-Clutter," *IEEE Transactions on Signal Processing*, Vol. 54, Issue 11, Nov.2006, pp. 4332-4342

978-1-4244-5050-3/10/$26.00 ©2010 IEEE

Lightning protection in stealth radomes

Björn Widenberg[1], Elisabeth Löfsved[2] and Mats Bäckström[3]

[1]*Applied Composites AB ACAB, P.O. Box 13070, S-58013 Linköping, Sweden*
[2]*Saab Systems, SE-581 88 Linköping, Sweden*
[3]*Combitech AB, SE-581 88 Linköping, Sweden*
E-mail: bjorn.widenberg@acab.se

Applied Composites AB ACAB has in collaboration with Combitech AB performed a study about lightning protection of stealth radomes. Stealth radomes have the task to reduce the radar cross section (RCS) of enclosed sensors. A stealth radome, also called frequency selective (FSS) radome, consists of a sandwich structure, where one or more layers are metallic (the other layers consists of dielectric materials; glass fiber, foam materials, etc.). The metallic layers consist of periodic patterns of metal and non-metal. In this way a filter can be constructed that transmit the radiation from the enclosed sensor, but blocks the incident field at other frequencies. External radar signals therefore apprehend the radome as a smooth metal surface, which greatly reduces the RCS [1].

The overall requirement is that a strike of lightning on the radome shall not to cause a crash (wreck), or risk pilot and crew. But a strike of lightning on the radome can be allowed to impair the stealth performance.

Without any special lightning protection devices radomes (and enclosed sensors) are in generally very vulnerable to damage caused by a direct strike of lightning. A traditional radome is protected by a lightning conductor (for example Pitot tube), and/or by providing the radome with some type of lightning diverters (for example diverter strips). Lightning diverters guide the lightning channel in a controlled way on the face of the radome [2].

On a frequency selective (FSS) radome you want to reduce such lightning diverters/conductors to a minimum, in order to maintain a low RCS. A potential opportunity to obtain an acceptable resistance to lightning could be to make the metallic layer in the FSS-radome sufficiently thick, so that it can take care of lightning current (all or partly) without melting.

Our study has consisted of two parts; on one hand studies and measurements of FSS-structures with thick metallic layers to determine the impact on and consequences for stealth performance, on the other hand simulations and verification of the lightning current through the metallic layers to determine its resistance against a lightning strike.

Simulations and measurements of the FSS parameters indicate that one can increase the thickness of the metallic layers from the traditional 18 µm up 180 µm without any essential changes in the stealth performance of the radome; both the sensor performance and the RCS-performance is retained. At thicknesses over 180 µm the stealth performance is affected, and this must be carefully taken into account in the design of the stealth radome. In addition, a thicker metallic layer has a significant impact on the manufacturing process and on the weight of the radome.

Lightning simulations on FSS structures with thick metallic layers showed that an increase of the layer thickness from today's typical value of 18 µm to approximately 500 µm significantly improved the resistance against typical lightning pulses of the order of 20 kA. However, extreme lightning pulses of 200 kA, which the radome is required to be able to withstand according to applicable standards [3], would require the metallic layer to be at least approximately 2 mm thick. This would not be possible to implement in a radome. These results and conclusions are valid for a direct strike of lightning, any form of spreading the lightning current would improve the lightning resistance significantly.

However, the situation would be improved if the requirement of resistance do not apply directly on whether the metallic structure melts or not, but rather whether the radome as a complete structure can withstand a lightning hit of 200 kA, without breaking down and risk the safety. This latter requirement would presumably soften the demands, because the metallic layers are surrounded by several thick layers of dielectric glass fiber and foam materials. These layers help the radome to keep mechanically together when the evaporation of metallic layers result in an internal pressure that tends to break down and divide the radome.

To validate and supplement the simulation results, lightning tests on samples of FSS-radom-structures were done at Culham Lightning's laboratory of Culham, Oxfordshire, England.

The overall result from the study is that it is difficult to construct a stealth radome with reasonable thick metallic layers, which can cope with the worst possible lightning pulse (200 kA) in accordance with applicable standards, without the help of other internal/external lightning-protection devices. However, if the FSS radome could be equipped with some form of lightning conductors/diverters that spread out the lightning current, then the FSS structure would be able to cope with the lightning pulse. A stealth radome on a ship can e.g. be constructed with a lightning conductor which spreads out the lightning current. On the other hand, a stealth radome on a fighter aircraft needs help of more sophisticated lightning protection devices to cope with a direct strike of lightning.

Acknowledgments – We thank Göran Eriksson, now at ABB, for his contributions and colleagues at the Swedish Defence Material Administration (FMV) for valuable discussions.

References

1. Björn Widenberg, "Thick Frequency Selective Structures", Doctoral Thesis, Department of Electroscience, Lund University, 2003.
2. Fisher, Perala, & Plumer, "Lightning Protection of Aircraft", Lightning Technologies inc., Pittsfield (MA), 1999.
3. SAE Aerospace, "Aircraft Lightning Environment and Related Test Waveforms", ARP5412, 2005.

978-1-4244-5050-3/10/$26.00 ©2010 IEEE

The Effect of Low Frequencies on Peak Amplitude in UWB Pulse Propagation

Natalie A. Cartwright
State University of New York at New Paltz, USA
E-mail: cartwrin@newpaltz.edu

Analytic and numeric studies of ultra-wideband electromagnetic pulses that propagate through causal, dispersive and attenuative dielectric material show that the evolved field contains the so-called Brillouin precursor. The significant feature of the Brillouin precursor is that, for finite propagation distances, it has a peak amplitude point that decays algebraically with propagation distance whereas the remainder of the field decays exponentially [1]. This slow decay rate of the Brillouin precursor is commonly attributed to the dc or low frequency content of the initial pulse, with no quantification given for the adjective low.

Here, the effect of low frequency components on the formation and peak amplitude of the Brillouin precursor is presented. We consider a linearly-polarized plane wave pulse that propagates in the positive z direction. On the plane $z = 0$, the electric field component is the field that results when a cascade of high-pass filters, each with transfer function

$$H(\omega) = \frac{i\omega/\omega_H}{1 + i\omega/\omega_H}$$

and cutoff angular frequency ω_H, is applied to a step-modulated sinusoid of fixed carrier frequency ω_c. The filtered spectrum

$$\tilde{E}(0,\omega) = \frac{i}{\omega - \omega_c}\left(\frac{i\omega/\omega_H}{1 + i\omega/\omega_H}\right)^n$$

is then propagated through a Debye-type material, such as distilled water. Uniform asymptotic methods are used to provide a closed-form asymptotic approximation to the field in which the accuracy of the approximation increases with increasing propagation distance z. The dependence of the propagated field on the cutoff frequency ω_H is given explicitly in these asymptotic expressions. Our results show that the decay rate of the peak amplitude point of the Brillouin precursor increases with increasing ω_H.

References

1. K. E. Oughstun, "Noninstantaneous, finite, rise-time effects on the precursor field formation in linear dispersive pulse propagation," Journal of the Optical Society of America A, vol. 12, 1995.

978-1-4244-5050-3/10/$26.00 ©2010 IEEE

Ultra Wideband Antennas with Efficient Band-Stop Functions

Abdelhalim Mohamed, Student Member, IEEE and Lotfollah Shafai, Life Fellow, IEEE
The University of Manitoba, Winnipeg, MB, R3T5V6, Canada
halim@ee.umanitoba.ca

In January and February 2001, The National Telecommunications and Information Administration of America (NTIA) conducted two important studies about the commercial use of UWB technology. One was about the compatibility between UWB devices and some Federal systems while the second was about the compatibility between UWB systems and Global Positioning System receivers (GPS) [1, 2]. In February 2002 and based on these studies, The Federal Communications Commission (FCC) issued its now well known report containing part 15, subpart F, about operating UWB systems on an unlicensed basis [3]. The rules set by FCC opened a new window for the commercial use of UWB systems. To reduce interference mitigation of UWB technology with other existing ones, UWB antennas are designed with band-stop functions. This way, the antenna works as a filter to reduce interference.

In this paper, novel UWB antennas with band-stop functions are studied. The study is done to enhance the functionality of the stop band characteristics. Different feature shapes and configurations are used to increase the mismatch level in the stop band and to keep other antenna characteristics unchanged over the pass band of operation. Single double and triple slots with different shapes are designed. New control parameters including slot position, shape and interaction between more than one slot are studied. Full wave analysis using Finite Element Method is used to design and analyze these antennas.

Band-stop feature parameters include length of the slot which determines the centre frequency of the stop-band, width of the slot which determines the bandwidth of the stop-band and position of the slot which contributes also in determining the stop-band bandwidth and centre frequency. The effectiveness of a stop-band feature is defined by how this feature will block the antenna radiation or receiving capability. For a square monopole antenna with a U-slot shape, it is found that the bandwidth of the stop-band is not affected by the change of the slot position. However the centre frequency decreases with the movement of the slot away from the feeding structure. It is worth noting that there should be a minimum distance between the slot and the feeding structure in order not to affect the pass band region of the antenna. By optimizing both slot position and length, a huge impedance mismatch increase in the stop-band is achieved. Such a design can give an impedance mismatch loss of 13dB. It is also found that a double U-slot configuration with optimum parameters can provide a series filtering effect that in turn increase the impedance mismatch to 16 dB. This paper also demonstrates how to control the bandwidth of the stop-band by implementing different slot shapes. Another new parameter introduced in this paper is the mutual coupling effect between two spiral-slots on creating and controlling the stop-band behaviour. Antenna designs with two slots coupled at different orientations and distances are studied. The antenna designed in this section is a circular monopole antenna with single feeding point structure. A spiral-slot at an optimum position can give an impedance mismatch of 15.5 dB. A circular monopole antenna with two spiral-slots on top of each other can give an impedance mismatch of 20 dB. Fig. 1 shows the relationship between the VSWR and impedance mismatch levels, a circular monopole antenna with two spiral-slots and the VSWR curves of the antenna at different spacing S1 between spirals. More results and discussions will be introduced in the conference presentation.

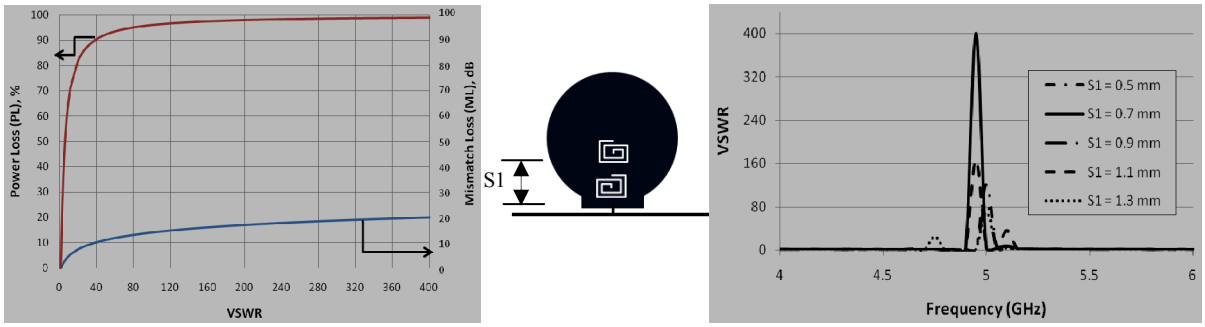

Fig. 1 shows the relationship between the VSWR and impedance mismatch levels, a circular monopole antenna with two spiral-slots and the VSWR curves of the antenna at different spacing S1 between spirals

References

[1] L. K. Brunson et al., "Assessment of compatibility between ultra wideband devices and selected federal systems", NTIA Special Publications 01-43, January, 2001

[2] D. S. Anderson et al., " Assessment of compatibility between ultra wideband (UWB) systems and global positioning system (GPS) receivers", NTIA Special Publications 01-45, February, 2001

[3] FCC 1st Report and Order on Ultra-Wideband Technology, Feb. 2002

978-1-4244-5050-3/10/$26.00 ©2010 IEEE

Potential Health Effects of Exposure to Radiofrequency Fields:
Epidemiological Studies and Risk Perceptions

Daniel Krewski, Michelle C. Turner, Louise Lemyre, and Riadh W. W. Habash
McLaughlin Center for Population Health Risk Assessment, University of Ottawa.

The expanded public use of wireless telecommunications devices over the last two decades has raised concerns about the potential for adverse health effects from exposure to radiofrequency fields from mobile phones, base station transmitters, and wireless computer networks. In this paper, the evidence from nearly 50 epidemiological studies of the association between handheld cellular telephone use and cancer risk is reviewed in detail. The strengths and limitations of the current epidemiological literature are examined, along with approaches to evaluating the overall weight of evidence linking mobile phone use and potential cancer risk. Ongoing epidemiological studies and future research needs in this area are also discussed as well as results from a series of studies conducted in Canada in order to assess risk perceptions of a variety of potential health hazards including cellular telephones. Understanding what shapes public perception is critical for effective risk communication and risk management decision-making.

Epidemiological study designs have included ecologic studies, examining at the population level, time trends in the incidence of (or mortality from) tumours of the head and neck with number of cellular telephone subscriptions, hospital-based case-control studies, population-based case-control studies, including the INTERPHONE study, a large, multinational study conducted in 13 countries, prospective record linkage studies, as well as several meta-analyses statistically combining the results from studies published to date. Overall, epidemiological studies provide little clear evidence of an association between cellular telephone use and brain cancer risk. Although some positive associations have been reported, there are several potential methodological limitations including exposure misclassification and potential biases in participant selection and recruitment, as well as limited numbers of long-term users of cellular telephones. Further epidemiological research is needed to clarify the possible association between cellular telephone use and brain cancer risk, including, laboratory, dosimetric, and methodological research, as well as further epidemiological studies in potentially sensitive subgroups including children, adolescents, and pregnant women.

In terms of public perceptions of the potential health risks associated with use of cellular telephones, results from a large national risk perception survey conducted in Canada revealed low levels of concern. When compared in relative terms to other health hazards, Canadians were less worried about the risks of cellular telephones, compared to other social or behavioral hazards including stress, poverty, cigarette smoking, or obesity. Canadians also reported low levels of worry about the potential health risks associated with cellular telephones. Results are compared to studies conducted elsewhere.

978-1-4244-5050-3/10/$26.00 ©2010 IEEE

PHYSICS OF ULTRAWIDEBAND ANTENNAS AND ITS EVOLUTION FROM HERTZ

Tapan K. Sarkar*, Magdalena Salazar-Palma**, Eric L. Mokole***

*Department of Electrical Engineering and Computer Science, Syracuse University, 323 Link Hall, Syracuse, New York 13244-1240, USA, E-mail: tksarkar@syr.edu,
Homepage: http://lcs.syr.edu/faculty/sarkar/

**Dept. of Signal Theory & Communications, Universidad Carlos III de Madrid, Avenida de la Universidad, 30, 28911 Leganés - Madrid, Spain, E-mail: salazar@tsc.uc3m.es

*** Radar Division, Naval Research Laboratory, 4555 Overlook Avenue; Washington, D.C. 20375;
Email: eric.mokole@nrl.navy.mil

Abstract - The objective of this presentation is to study the physics of ultrawideband antennas. As such, the phase responses of these antennas as a function of frequency are of great interest. In the ensuing analysis, the impulse responses of antennas in both the transmit and the receive mode are considered as they are not the same. Identification of this principle can lead to the design of very broadband dispersionless systems.
The second part of the talk will provide an overview of the evolution of ultrawideband antennas since Hertz and to the present time describing various antennas including one that can have a 100:1 bandwidth.

978-1-4244-5050-3/10/$26.00 ©2010 IEEE

Some Ultrawideband Definitions and Descriptions of Selected Ultrawideband Radar Systems

Eric L. Mokole[1] and Tapan K. Sarkar[2]
[1]*Radar Division, Naval Research Laboratory, Washington, DC, USA, 20375*
[2]*Department of Electrical Engineering and Computer Science, Syracuse University, Syracuse, NY, USA 13244*
E-mail: eric.mokole@nrl.navy.mil

The talk begins by discussing definitions of ultrawideband (UWB) components, waveforms, and systems, followed by descriptions of selected UWB radar systems and their associated applications. The last fifteen years have witnessed increased interest in UWB electromagnetic (EM) systems, particularly in the areas of radar, communications, and high-power directed energy [1]. Specifically, significant commercial developments in UWB communications systems and UWB radar for humanitarian demining have led to the creation of standards to define UWB systems, technologies, and permissible usage. Different groups within the engineering and scientific communities have preferred definitions of UWB and bandwidth that attempt to define a measure of the spectral widths of signals and systems and appropriate criteria to categorize them in a meaningful way [2]. Unfortunately, existing definitions are not mutually consistent, since they are also influenced by the special needs and the understandably limited viewpoints of the respective communities. Defining UWB signals and systems unambiguously requires: (1) a definition of bandwidth; and (2) a categorization scheme in terms of bandwidth. Currently, numerous definitions of bandwidth and at least four non-coincident definitions for UWB systems and signals exist. The differences in how categorization schemes define bandwidth and classification criteria are highlighted by analyzing some ideal UWB waveforms in terms of selected definitions of bandwidth (3-dB, 10-dB, and 20-dB power; root mean square; 90% and 99% energy). These waveforms include: the exponentially damped sinusoid; the Gaussian; half-cycle sinusoids; linear frequency modulated (LFM) sinusoid. Furthermore, since much recent research has addressed the design and optimization of waveforms, conditions on waveforms that ensure physical relevance to real systems are also postulated. Applications of UWB radar include detecting and imaging buried mines, detecting and mapping underground utilities, detecting and imaging objects obscured by foliage, through-wall detection in urban areas, short-range detection of suicide bombs, and the characterization of the impulse responses of various artificial and naturally occurring scattering objects. In particular, the Naval Research Laboratory's experimental, low-power, dual-polarized, short-pulse, ultra-high resolution radar is used to discuss applications, key supporting technologies, and issues of UWB radar. Some crucial issues that are problematic to UWB radar are spectral availability, electromagnetic interference and compatibility, difficulties with waveform control/shaping, hardware limitations in the transmission chain, and the unreliability of high-power sources for sustained use above 2 GHz.

[1] E. Mokole, "Survey of UWB radar," in *Ultra-Wideband, Short-Pulse Electromagnetics 7*, ed. by F. Sabath, E. L. Mokole, U. Schenk, and D. Nitsch, Springer Verlag, NY, 2007, pp. 571-585.
[2] F. Sabath, E. L. Mokole, and S. N. Samaddar, "Definition and classification of ultra-wideband signals and devices," *Radio Science Bulletin*, no. 313, pp. 12-26, June 2005.

978-1-4244-5050-3/10/$26.00 ©2010 IEEE

ANALYSIS OF ULTRAWIDEBAND SYSTEMS USING A STABLE TIME DOMAIN METHODOLOGY

Magdalena Salazar-Palma*, Tapan K. Sarkar**, Eric L. Mokole***

*Dept. of Signal Theory & Communications, Universidad Carlos III de Madrid, Avenida de la Universidad, 30, 28911 Leganés - Madrid, Spain, E-mail: salazar@tsc.uc3m.es

**Department of Electrical Engineering and Computer Science, Syracuse University, 323 Link Hall, Syracuse, New York 13244-1240, USA, E-mail: tksarkar@syr.edu,
Homepage: http://lcs.syr.edu/faculty/sarkar/

*** Radar Division, Naval Research Laboratory, 4555 Overlook Avenue; Washington, D.C. 20375;
Email: eric.mokole@nrl.navy.mil

Abstract - In this presentation, we propose a numerical method to obtain a solution for the time domain electric field integral equation (TD-EFIE) for arbitrary conducting shapes. This novel method does not utilize the customary marching-on in time solution method often used to solve a hyperbolic partial differential equation. Instead we solve the wave equation by expressing the transient behaviors in terms of Laguerre polynomials. By using these orthonormal basis functions for the temporal variation, the time derivatives can not only be handled analytically, but also they can be eliminated completely from the computations. Since these weighted Laguerre polynomials converge to zero as time progresses, the induced electric currents when expanded in a series of weighted Laguerre polynomials also converge to zero. In order to solve the wave equation, we introduce two separate testing procedures, a spatial and temporal testing. By introducing first the temporal testing procedure, the marching-on in time procedure is replaced by a recursive relation between the different orders of the weighted Laguerre polynomials. The other novelty of this approach is that through the use of the entire domain Laguerre polynomials for the expansion of the temporal variation of the current, the spatial and the temporal variables can be separated. For convenience, we use the Hertz vector as the unknown variable instead of the electric current density. To verify our method, we compare the results of a TD-EFIE and inverse Fourier transform of a frequency domain EFIE.
This methodology is then extended to the solution of FETD and FDTD methodologies. We present a numerical method to obtain a solution for the finite element method in time domain (FETD) for two-dimensional TEz case. Our method does not utilize the customary marching-on in time solution method often used to solve a hyperbolic partial differential equation. Instead we solve the time domain wave equation by expressing the transient behaviors in terms of weighted Laguerre polynomials. By using these causal orthonormal basis functions for the temporal variation, the time derivatives can be handled analytically. To verify our method, we apply it to two-dimensional parallel plate waveguide and compare the result to that of the conventional FETD using the Newmark-Beta method. Application of this technique may speed up the solution of FDTDS problem by as mush as a factor of 100.

978-1-4244-5050-3/10/$26.00 ©2010 IEEE

Lightning Risk in Research and Teaching of Power and Control Systems

Riadh W. Y. Habash
School of Information Technology and Engineering, University of Ottawa
rhabash@site.uottawa.ca

Interdisciplinary research projects and exercises are needed in engineering education to stimulate interest of undergraduate and postgraduate students in power and control systems, especially by providing links to other areas such as electromagnetic fields, computers, electromechanical systems, and risk assessment. This paper describes series of projects and case studies developed at the University of Ottawa involving investigation of lightning effects on a microhydro power plant, a substation and related facilities, and a wind turbine system. These educational activities provide a learning opportunity for engineering students to expand their research knowledge about power and control systems in general, and more specifically lightning effects and mitigation techniques. First, the paper defines the problem confronting protection systems engineers, reviews and investigates the protection systems conventionally used. Besides offering explanations of major concepts and models, the case studies utilize the dynamic environment of Internet to help create an opportunity for more detailed and often more visual representations for key design concepts, while the research projects use modeling and simulation tools to design lightning protection systems. The end goal for the students is to complete open-ended research exercises to see how they can immediately apply their newly acquired tools in lightning risk assessment to their knowledge of power and control systems.

Key Words: Lightning effects, mitigation techniques, risk assessment, power systems.

978-1-4244-5050-3/10/$26.00 ©2010 IEEE

The Control of Nonlinear Scattering of Waves on Microstrip Array with Nonlinear Loads

Diana V. Semenikhina
South Federal University, Taganrog, Russia, 347928
E-mail: anilsem@mail.ru

In the field of nonlinear radars the construction of correct mathematical models of nonlinear scatterers and electromagnetic methods of their analysis are required. The majority of researchers limit the consideration of models to only narrow class of the elementary antennas with nonlinear loads such as dipoles and circular loops, systems of such antennas connected between themselves or apertures with nonlinear loaded narrow slots. The developed models of nonlinear scatterers not always allow to carry out optimization of nonlinear radar's parameters from the point of view of a choice of power for achievement of demanded characteristics of detection range.

Besides, problems of development of new protection means based on nonlinear detection of the targets and nonlinear radars using not only the third harmonic are of present interest. For example, design of nonlinear scatterers working on a second harmonic frequency is actual.

In this paper a method based on construction of electromagnetic model of nonlinearly loaded object and a solution of a nonlinear boundary problem of scattering in the integral form are offered. Research of nonlinear effects using this method is reduced to definition of electromagnetic fields from Lorentz lemma and the formulated nonlinear boundary conditions (NBC) on sites of object with nonlinear surface properties. Nonlinear boundary conditions are given in both space-time and space-frequency domains.They connect instantaneous values or complex amplitudes of n is harmonics' number harmonics of surface electric and magnetic currents (i.e. field tangent (τ) components $E_{n,\tau}$ $H_{n,\tau}$ on loads) in consideration of given polynomial voltage-current (V-C) characteristic of nonlinear loads. In the elementary case for example if a wave exciting on nonlinear structure has a frequency ω, V-C characteristic parameters are constants and NBC for this load looks like

$$L_1 \cdot H_{n,\tau} = \sum_{\nu=0}^{\infty} Y_\nu F_n(\nu), \text{ where } Y_\nu = L_2 \cdot (a_\nu + in\omega b_\nu); F_n(\nu) = \sum_{n_1=-\infty}^{\infty} \sum_{n_2=-\infty}^{\infty} \sum_{n_{\nu-1}=-\infty}^{\infty} E_{n-n_1,\tau} E_{n_1-n_2,\tau} \ldots E_{n_\nu-1,\tau};$$

n is harmonics' number; L_1, L_2 are coefficients defined by geometric parameters of the loads, a_ν and b_ν are coefficients defined by load V-C characteristics [1].

Further, on the basis of Lorentz lemma the infinite system of the nonlinear integral equations. This system's dimension is limited to the maximum considered degree of V-C characteristic multinominal. The found solution of the system allows a definition of required spectral and polarization characteristics of the fields.

Base on the above method the problem solution of polyharmonic excitation of a microstrip reflective array with nonlinear loads is considered. Interaction of levels of the reradiated fields on harmonics and combinational frequencies with parameters of nonlinear loads and with fields in a microstrip array are investigated. It is clear in this connection that the level of the voltage rectified on nonlinear loads depends on intensity of external excitation. The parameters of the nonlinear loads allowing to achieve reflection coefficient from array at combinational frequencies comparable in value with reflection coefficient at the fundamental frequencies are found .

The developed method has allowed to solve one of the important problems arising at design of nonlinear reflectors with controlled dispersion namely to achieve effective adaptive control of nonlinear products of scattering. It results from of the executed research that convenient way of realization of an internal feedback in a design of a microstrip array with nonlinear loads-diodes is use of the information on the rectified voltage on diodes at irradiated array. In this case the rectified voltage on diodes shows its maximum (fig.1,a) and scattered field (reflection coefficient) on the second harmonic frequency (fig.1,b) is simultaneously also maximal.

Obtaining the information on the rectified voltage and arranging displacement voltage to be maximum of the rectified voltage provides the greatest energy swapping at frequency of the second harmonic and enrichment of the spectrum of the reradiated field, thereby raising performance efficiency of nonlinear scatterers.

The same control principle of intensity of nonlinear scattering products can be used as basis of construction of other types of nonlinear scatterers (not microstrip scatterers) with both lumped and distributed nonlinear loads, for example, nonlinear markers.

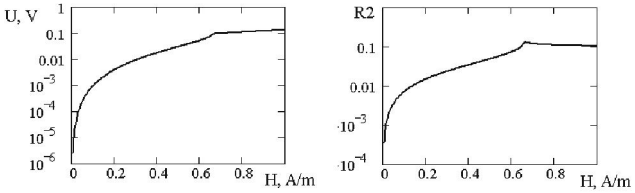

a b

Figure 1: Graphs of rectified voltage and reflection coefficient

References

1. B.M. Petrov, D.V. Semenikhina, A.I. Panichev A New Analysis Method of Nonlinear Scattering for Solution EMC Problem // 11th International Wroclaw Symposium on Electromagnetic Compatibility, 1992, Part 1, pp.45-49.

978-1-4244-5050-3/10/$26.00 ©2010 IEEE

Dosimetric Evaluation of Cylindrical Waveguide Exposure System for EMF- Health Effect Studies in Small Rodents

S. Wasoontarajaroen[1], A. Thansandote[2], G. Gajda[2], E. Lemay[2], J. McNamee[2] and P. Bellier[2]
[1]*University of Regina, Regina, Canada, S4S 0A2*
[2]*Consumer and Clinical Radiation Protection Bureau, Health Canada, Ottawa, Canada, K1A 1C1*
E-mail: wasoonts@uregina.ca

A cylindrical waveguide exposure system has recently been developed at the Consumer and Clinical Radiation Protection Bureau of Health Canada and used to conduct biological effect studies with unrestrained small rodents (mice) exposed to 1.9-GHz electromagnetic energy. The system consists of four individual column chambers made from circular waveguide (120-mm diameter and 430-mm long) sharing the same electromagnetic energy source via a network of power dividers. The fundamental TE11 mode with circular-polarization is employed in the waveguides. Each waveguide is cut in the middle into two sections in order to allow the insertion of a cylindrical Plexiglas cage (dimensions 100-mm diameter and 100-mm high). Prior to being used for the biological studies, the system was characterized for radiofrequency (RF) dosimetry, which is the evaluation of the absorbed electromagnetic energy in tissue resulting from the exposure. The RF dosimetry is quantified in terms of specific absorption rate (SAR) and has units of watts per kilogram (W/kg). In an unrestrained system, the SAR will vary due to the multiple possible postures and locations of the animal. Biological studies of specific organ tissue types require knowledge of the SAR pertaining to those specific tissues. However, whole-body-average SAR (WBA-SAR) is an important parameter for setting power levels in the experimental protocol. Follow-up research will look into tissue-specific SAR data but will not be included this presentation. The purpose of the work presented is to investigate bounds or limits on the WBA-SARs for each body mass of the animal. Data obtained for this investigation were from both experimental and numerical techniques. The experimental technique is based on measuring the difference in the power entering and exiting the waveguide exposure chamber before and after insertion of the animal. For the numerical technique, electromagnetic simulation was performed using a commercially available software tool (SEMCAD X). An investigation on a 10-g mouse cadaver, for example, was performed. Its WBA-SAR variation due to posture and location in the cage is given in Figure 1. According to the graph, the lowest value of the SAR with 1-W incident power was found to be 13.6 W/kg when the cadaver was made to stand upright in the center of the cage, whereas the highest value of 41.8 W/kg was observed when the cadaver was positioned lying prone and in touch with the curved cage wall. The results of electromagnetic simulation gave the same trend with the experimental measurements. The details with respect to the exposure system and the dosimetric evaluation will be discussed during our presentation.

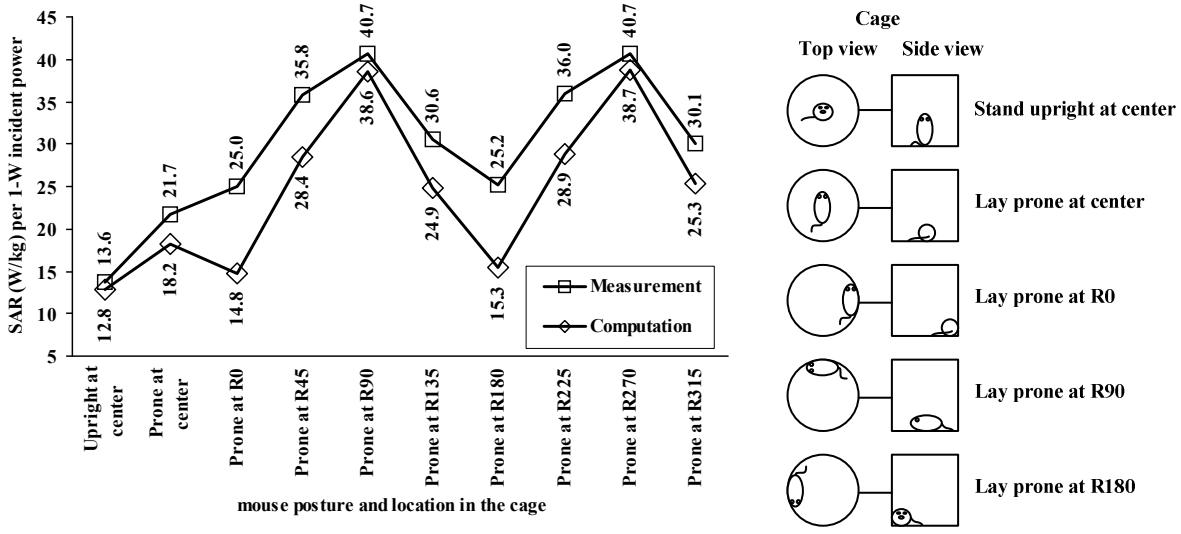

Figure 1: WBA-SARs of a 10-g mouse cadaver variation due to posture and location in the cage.

Acknowledgement ─ The authors would like to thank Schmid & Partner Engineering AG for their support with respect to the use of the electromagnetic computation tool SEMCAD X.

978-1-4244-5050-3/10/$26.00 ©2010 IEEE

Development of a Prediction Code for Close-Range Nuclear EMP Effects

J.M. Pottage
Plasma Physics Dept., AWE, Aldermaston, England
E-mail: John.Pottage@awe.co.uk

This presentation describes how AWE's existing general-purpose electromagnetic simulation code, which is an implementation of the well-established Transmission Line Matrix (TLM) method [1], was modified to allow the calculation of currents induced by nuclear Electro-Magnetic Pulses (EMP) on metallic objects placed at any distance from the detonation point, enabling the effects of EMP on electrical and electronic equipment to be evaluated even within the strongly-ionised source region. The validity of the additional source-region environment routines is verified by comparison with results generated by a more modern variant (called UKLEMP) of the EMP code developed by Longley [2].

Our code differs from previous work [3] because it includes both Gamma scattering and Compton electron deflection effects, and there is no requirement to assume any geometrical symmetries in the 3D structure when calculating the coupling to the object.

In a lot of published work on the effects of EMP on wires and other metallic structures, the detonation point is assumed to be sufficiently far away that three approximations can be made: that the air is not significantly ionised, the Compton electron current is negligible, and the wavefronts of the EMP radiation are parallel planes. If, however, the burst-point is not far away, then these approximations are no longer valid, and it is then necessary to perform coupled simulations of both the charged particle environment and the electromagnetic effects on the metallic structure. The volume inside which the air-ionisation and the Compton current cannot be neglected is known as the source region. The source-region code that was referred to above [2], can simulate source region environments but cannot take account of EMP coupling effects, whilst the existing TLM code can calculate EMP coupling but cannot accurately handle source-region environments. The code described in this presentation resolves this dilemma. From Figure 1, it can be seen that sufficiently good agreement has been obtained between UKLEMP and the SREMP environment part of the modified TLM code to have confidence in the new code.

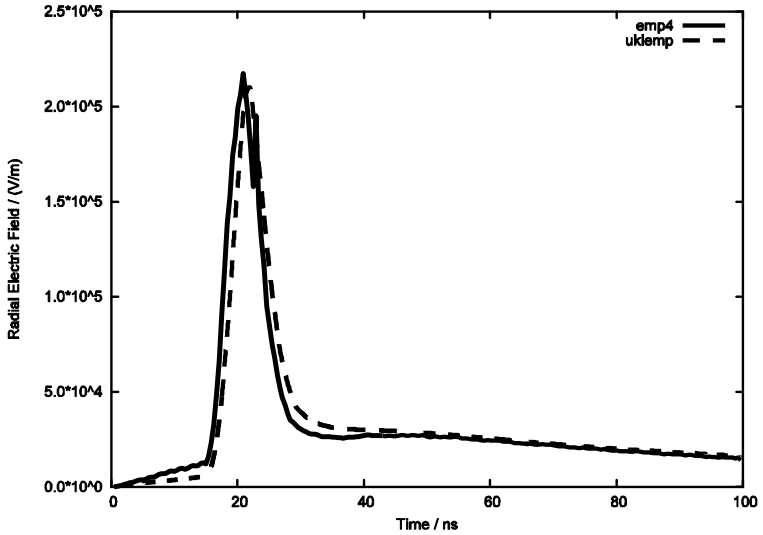

Figure 1: Calculated radial electric field strength, E_r, at a range of 250m.

1. A. Scaramuzza, "Simulation of Conductive Environments using Transmission Line Modelling", PhD Thesis, Univ. Nottingham, 1993.
2. H.J. Longley, "Compton Current in Presence of Fields for LEMP 1", Los Alamos National Laboratory, 1970.
3. D.F. Higgins, T.A. Tumolillo, W.A. Radasky, K.S. Smith, J.P. Wondra, "Source Region EMP Coupling to Long Lines," IEEE Trans. Nuclear Science. Vol. 28, No. 6, pp. 4440-4445, 1981.

978-1-4244-5050-3/10/$26.00 ©2010 IEEE

The coaxial vircator as an HPM source

Sten E Nyholm, Mattias Elfsberg, Tomas Hurtig, Cecilia Möller
Swedish Defence Research Agency (FOI)
Defence & Security, Systems and Technology
SE-147 25 Tumba, Sweden
e-mail: sten.e.nyholm@foi.se

Abstract— **The vircator is a simple, lightweight and compact radiation source for generating High Power Microwaves (HPM). It requires no external magnetic field and is tolerant for variations in feeding voltage pulses. The vircator may sometimes show unstable behavior, such as frequency jumps or amplitude variations. However, the simple geometry of the vircator is easily modified so that microwave pulses with different characteristics can be generated in a controlled way.**

The coaxial vircator, in which anode and cathode are concentric cylinders, has a potential for being developed into a compact and versatile source. In the traditional coaxial vircator the emitter is a circular ring on the inside of the cathode. Experiments and simulations of coaxial vircator configurations are presented, and examples of how radiation characteristics can be manipulated are discussed. One example is sectioning the emitter area in order to directly generate the TE11 mode and at the same time obtaining control over the polarization of the generated radiation. Another example is the use of a reflector in the output waveguide to improve the radiated power and energy, both in a traditional coaxial vircator and in a coaxial vircator with sectioned emitter.

Keywords- HPM, coaxial vircator, sectioned emitter, TE11 mode, reflector

978-1-4244-5050-3/10/$26.00 ©2010 IEEE

Representation of Fields in Reverberation Chambers Using a Superposition of Standing Waves

Mathias Magdowski and **Ralf Vick**
Otto-von-Guericke University, Magdeburg, Germany
E-mail: mathias.magdowski@ovgu.de

A plane wave integral representation for well-stirred fields in an ideal reverberation chamber is known from [1]. In [2] it has been shown that the original analytical integral method using an infinite number of waves can be replaced by a numerical sum with a finite number. Only a relatively small number of waves and boundary conditions are required to achieve valid results, which makes a simple, fast and reliably accurate simulation for practical applications. As the reverberation chamber is a cavity resonator whose eigenmodes can be described by standing waves, there is also a field representation by a superposition of standing waves conceivable. A standing wave representation is also deducible from the original plane wave approach, because two plane waves with same amplitude A_0

$$\mathbf{E}^{+}_{pw}(\mathbf{r}) = A_0(e_x\hat{\mathbf{x}} + e_y\hat{\mathbf{y}} + e_z\hat{\mathbf{z}})\,\mathrm{e}^{-j(\mathbf{k}\cdot\mathbf{r})}\,\mathrm{e}^{j\beta^+}\quad , \qquad \mathbf{E}^{-}_{pw}(\mathbf{r}) = A_0(e_x\hat{\mathbf{x}} + e_y\hat{\mathbf{y}} + e_z\hat{\mathbf{z}})\,\mathrm{e}^{j(\mathbf{k}\cdot\mathbf{r})}\,\mathrm{e}^{j\beta^-}\quad , \tag{1}$$

but different phases β^+ and β^- traveling in antiparallel directions $\mathbf{k}$ and $-\mathbf{k}$ form a standing wave. To simplify the resulting equation for $\mathbf{E}^{+}_{pw} + \mathbf{E}^{-}_{pw}$ it is helpful to split the phase angles $\beta^+ = \beta + \delta$ and $\beta^- = \beta - \delta$ into two parts. The associated H-field can be derived from the second Maxwell equation $\mathbf{H} = -\frac{1}{j\omega\mu}\nabla\times\mathbf{E}$. In the yielded standing wave β represents a temporal and δ a spatial phase angle. The direction of the H-field is $\mathbf{h} = \hat{\mathbf{k}}\times\mathbf{e}$.

$$\mathbf{E}_{sw}(\mathbf{r}) = 2A_0(e_x\hat{\mathbf{x}} + e_y\hat{\mathbf{y}} + e_z\hat{\mathbf{z}})\cos(\mathbf{k}\cdot\mathbf{r} - \delta)\,\mathrm{e}^{j\beta} \qquad \mathbf{H}_{sw}(\mathbf{r}) = -j2\frac{A_0}{\eta}(h_x\hat{\mathbf{x}} + h_y\hat{\mathbf{y}} + h_z\hat{\mathbf{z}})\sin(\mathbf{k}\cdot\mathbf{r} - \delta)\,\mathrm{e}^{j\beta} \tag{2}$$

The description in Cartesian coordinates is necessary for the superposition. A conversion from polar coordinates is useful to equally distribute the wave directions and polarizations over the full solid angle. The components of $\mathbf{k}$, $\mathbf{e}$ and $\mathbf{h}$ can be calculated from polarization α, azimuth φ and polar angle ϑ in the following way:

$$k_x = k\sin\vartheta\cos\varphi \qquad e_x = \cos\alpha\cos\vartheta\cos\varphi - \sin\alpha\sin\varphi \qquad h_x = -\sin\alpha\cos\vartheta\cos\varphi - \cos\alpha\sin\varphi \tag{3a}$$

$$k_y = k\sin\vartheta\sin\varphi \qquad e_y = \cos\alpha\cos\vartheta\sin\varphi + \sin\alpha\cos\varphi \qquad h_y = -\sin\alpha\cos\vartheta\sin\varphi + \cos\alpha\cos\varphi \tag{3b}$$

$$k_z = k\cos\vartheta \qquad e_z = -\cos\alpha\sin\vartheta \qquad h_z = \sin\alpha\sin\vartheta\ . \tag{3c}$$

The statistical distribution of angles is summarized in Tab. 1, where U denotes a uniform distribution. The analytical properties of the resulting field for statistic distribution and correlation are exactly the same as for the plane wave assumption in [1]. Also numerical simulations as in [2] are correct. An example with 100 boundary conditions each consisting of 100 waves is shown in Fig. 1. The only difference between the traveling and standing wave approach is that the Poynting vector in the numerical solution is always zero, which is true in a high-quality resonator.

Table 1: Statistic distribution of angles

name	variable	distribution
azimuth angle	φ	$U(0, 2\pi)$
polar angle	ϑ	$\arccos(U(-1, 1))$
phase angle (temporal)	β	$U(0, 2\pi)$
phase angle (spatial)	δ	$U(0, \pi)$
angle of polarization	α	$U(0, \pi)$

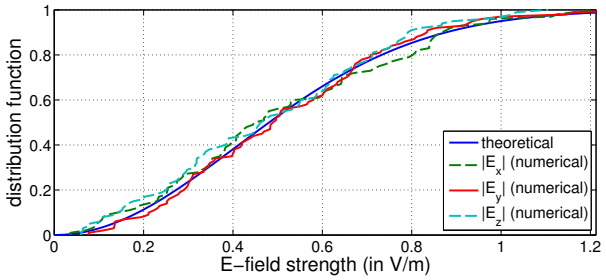

Figure 1: Comparison of numerically simulated and theoretical cdf of the magnitude of E-field components

References

[1] David A. Hill. Plane wave integral representation for fields in reverberation chambers. *IEEE Transactions on Electromagnetic Compatibility*, 40(3):209 – 217, August 1998.

[2] L. Musso, V. Berat, F. Canavero, and B. Demoulin. A plane wave Monte Carlo simulation method for reverberation chambers. In *International Symposium on Electromagnetic Compatibility*, 2002.

978-1-4244-5050-3/10/$26.00 ©2010 IEEE

A New High Gain Quad Ridged Horn Antenna

H. Amjadi[1*] and **Farzad Tavakkol Hamedani** [1]
Electrical and Computer Engineering Department of Semnan University, Semnan, Iran
[*]*E-mail: Hana_amjadi@yahoo.com*

A novel design of a broadband and high gain dual-polarized horn antenna is presented. The designed quad- ridged horn antenna operating over 2-18 GHZ with VSWR≤ 2.2. Ultra wide band and high gain antennas are among of the most important devices for EMC testing and microwave applications [1-2].
A novel technique for tapering the flared section of the horn and the additional flared part is introduced to improve impedance matching and increase the gain of antenna. In order to increase the impedance matching between the quad-ridged waveguide and the free space, all ridges are tapered both laterally and longitudinally, it means that height and width of ridges varies in flared part of horn. Tapering of ridges in longitudinal plate is based on exponential function and in lateral plate, ridges tapered linearly. The second flared part is added to quad ridged horn to achieve good radiation and high gain. The aperture size and overall length of the proposed horn antenna is 10×10 cm^2 and 18 cm, respectively (which the length of quad-ridged horn is 6cm and the length of additional flared part is 12cm). Two coaxial connectors are used: one for vertical polarization and the other for horizontal polarization [3]. The isolation between the two coaxial ports is less than 20 dB and the modified antenna has a stable radiation pattern over the entire frequency band. Ansoft HFSS and CST Microwave Studio, have been applied to simulate the structure and results have good agreement.
Fig.1(a) shows the configuration of the proposed antenna and Fig.1(b) shows the gain of the modified antenna in comparison with usual quad-ridged horn over the 2-18GHZ frequency range.

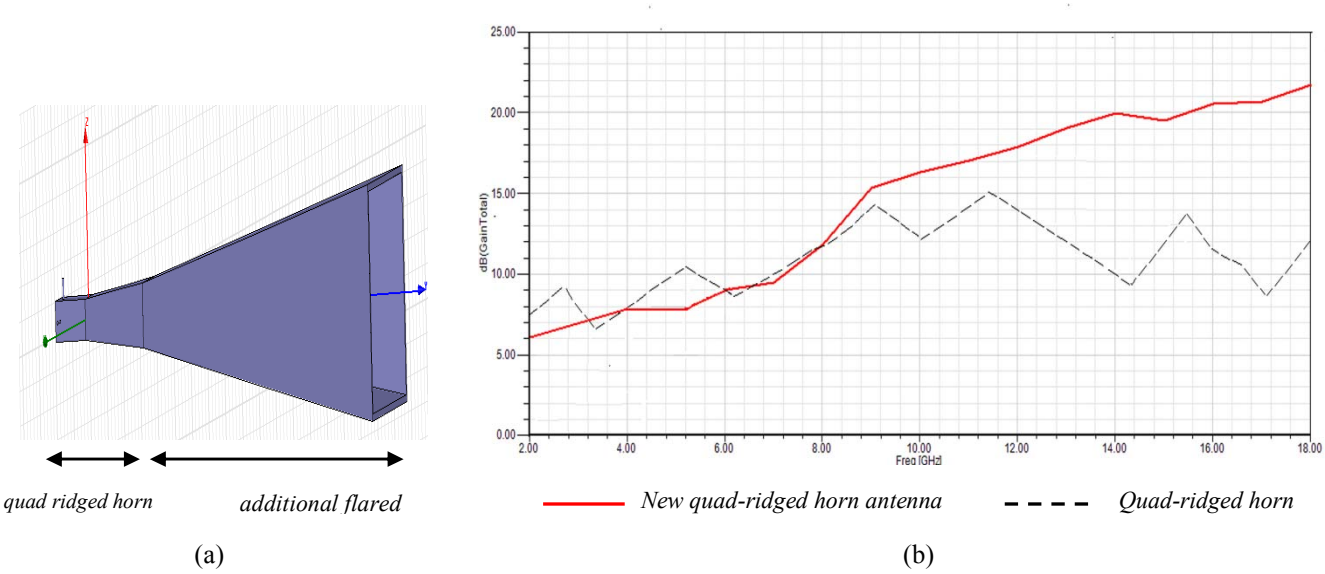

Figure1: **(a) Configuration of the antenna, (b) Broadside gain of quad-ridged horn antenna and new quad-ridged horn.**

As we seen in Fig.1(b), new technique for tapering of ridges and adding a flared part to quad-ridged horn antenna lead to about 10 dB increase in gain at higher frequency.

References

1. K. L. Walton and V. C. Sundberg, "Broadband ridged horn design," *Microw. J.*, pp. 96–101, Mar. 1964.
2. Sun, W. and C. A. Balanis, "Analysis and design of quadruple ridged waveguide," *IEEE Trans. Microwave Theory & Tech.*, Vol. 42, No. 12, 2201–2207, Dec. 1994.
3. Shen, Z. and C. Feng, "A new dual-polarized broadband horn antenna," *IEEE Antenna and Wireless Propag. Letters*, Vol. 4, 270–273, 2005.

978-1-4244-5050-3/10/$26.00 ©2010 IEEE

On the Mathematical Structure of Instabilities in Electronic Systems Caused by IEMI

I. Kohlberg[1]
[1]*Kohlberg Associates, Inc., Reston, USA, 20190*
E-mail: etoton@comcast.com

Over the past four decades many experiments have been performed in the international EMC community to assess the response and susceptibility of specific information and control systems to High Power Electronics (HPE) and High Power Microwaves (HPM). With the exception of the U.S.'s MURI program and perhaps a few other isolated studies the principle focus of the aforementioned tests was to evaluate operational consequences of permanent damage and temporary upset on systems. Experimental parameters included: microwave frequency, pulse duration, pulse repletion rate, peak power, average power, type of equipment, computer clock rate, the number of components used in the experiment, etc. These parameters by themselves are not always sufficient to allow much extrapolation of results between systems or in fact extrapolation between different waveforms for the same system to occur. Anomalous and unpredictable effects were often observed that to this date remain unresolved. It has recently been suggested (Kohlberg/APEMC 2010) that perhaps a complementary set of variables rooted in the theories of differential equations, stochastic control theory and chaos could explain heretofore unexplainable observations. Should this approach be fruitful EMC technology could make electronic and control systems more resilient against HPE/HPM attacks.

There has recently been a greater awareness that chaos—a bounded noise-like waveform, could be a factor in susceptibility assessments. Chaos has been known to occur in power electronics equipment such as ripple regulators, protection circuits, magnetic amplifiers, etc. A major conclusion from the MURI program was that wave-chaos, produced by the electromagnetic field, was responsible for chaotic voltages generated in the "Back Door" of some systems. Chaotic waveforms have also been observed in tests of SCADAs. The APEMC paper developed an approach that incorporated chaos waveforms in the theory of HPM susceptibility. Within certain limits connected with ergodic theory, it was proposed that chaos could be treated as a stochastic process and that unwanted energy absorbed by the system could be determined from the Wiener-Khintchine theory. Periodicity of the HPM waveform was also incorporated in the analysis. This paper takes the next step by extending the theory to nonlinear effects, simultaneous inclusion of Front-Door unwanted signals, and other instabilities associated with the Mathieu and Hill equations.

978-1-4244-5050-3/10/$26.00 ©2010 IEEE

High Power Electromagnetic Pulse Vulnerability Characterized as Low Probability – High Consequence Events

M. Frankel[1], I. Kohlberg[2], and **E. Toton[3]**
[1]*L3 Communications, Reston, USA, 20190*
[2]*Kohlberg Associates, Inc., Reston, USA, 20190*
[3]*TOTON LLC, Reston, USA 20194*
E-mail: etoton@comcast.net

It has long been recognized that high value systems such as reconnaissance aircraft and satellites that used high-gain sensors were susceptible to high power electromagnetic pulses: these pulses, if containing spectral components consistent with the operational characteristics of the sensors, could induce saturation and overload of the sensors and associated processing electronics that could lead to instantaneous and catastrophic failure of the sensor systems and loss of value of the support platform. In consequence, considerable design effort was invested in achieving hardening against these "front-door" intrusion paths of such electromagnetic pulses. The so-called back-door entry paths, however, continue to be problematic in that high power, short duration pulses can contain high frequency spectral components able to tunnel through narrow apertures that generally exist in the platform structures or, if physically sealed at construction, are difficult to ensure continued performance during planned operational lifetimes. Experimental programs continue to investigate the responses of systems to high power pulses but it is recognized that these represent a sparse mapping of response when small changes in the physical characteristics of the tested system and small geometrical orientations can in principle produce changes in the locations and magnitudes of regions of constructive interference within the tested system. We therefore recognize that there is a low probability of catastrophic failure from high power pulses in well-designed systems when described in qualitative terms. In this paper we discuss the challenges of quantification of the probability of catastrophic failure in terms of the general properties of system components, physical construction, and what can be known through component testing and the extensive, but nonetheless sparse, characterization of the system as a whole.

978-1-4244-5050-3/10/$26.00 ©2010 IEEE

Improvement in S-band relativistic magnetron

A. Sayapin, Y. Hadas, T. Kweller, and Ya. E. Krasik

Physics Department, Technion, Haifa 32000, Israel

The operation of a relativistic magnetron powered by a Linear Induction Accelerator with $\leq$ 400 kV, $\leq$ 4 kA, and ~150 ns output pulses is characterized by low efficiency as compared to non-relativistic magnetrons. Microwave pulse compression is a method which can be used to increase the output peak power with a decrease in the pulse duration of the microwave pulse. This method is based on relatively slow microwave energy storage in a resonator with optimized coupling coefficient and fast switching of the stored energy to the load. The latter results in high microwave power in expense of decreased compressed pulse energy with respect to the magnetron microwave output energy.

Different phenomena are revealed when the coupling between the magnetron and resonator allows part of the electromagnetic energy to be reflected towards the magnetron. It is shown that, under optimal coupling, the efficiency of the magnetron operation increases by ~40%. The latter means that the total microwave energy which could be extracted from the resonator exceeds the microwave energy when the magnetron operates with a matched load. In addition, in this operation mode the generated microwave power reaches the power of the electron beam. These results can be explained by a positive feedback mechanism established by the reflected microwaves.

978-1-4244-5050-3/10/$26.00 ©2010 IEEE

Correlation between the parameters of the cathode plasma and microwave in a relativistic magnetron

Y. Hadas, A. Sayapin, T. Kweller, and Ya. E. Krasik

Physics Department, Technion, Haifa 32000, Israel

V. Berrnshtam

Weizmann Institute of Science, Rehovot 76100, Israel

I. Vintezenko

Nuclear Physics Institute, Tomsk 634050, Russia

The operation of a relativistic S-band magnetron engaged intrinsically with plasma generation on its cathode surface. The magnetron is driven by a Linear Induction Accelerator whose high voltage output amplitude was changed in the range of 250-400kV with a time duration of ~150ns. In addition, the external magnetic field was changed between 0.28-0.4T in order to optimize the power of the microwave generation.

The parameters of the plasma, namely ions and electron temperature and plasma electron density, were measured using space- and time-resolved spectroscopy. It was found that the microwave generation is accompanied by a fast increase in the cathode plasma electron and ion temperature. The correlation between the dynamics of these plasma parameters and the microwave power is revealed. The model based on the plasma electron heating in a thin cathode plasma skin layer by electric field of microwaves and the energy transfer to the cathode bulk plasma is suggested

In addition, it was shown an absence of the anode plasma formation for microwave power < 150 MW and velocity of the cathode plasma expansion towards the anode $<10^6$ cm/s. Thus, microwave pulse "shorting" effect because of the plasma expansion should be excluded from the suggestions made in previous works.

978-1-4244-5050-3/10/$26.00 ©2010 IEEE

Transient versus Steady State Responses for Resonating Systems

Jürgen Nitsch[1], Sergey Tkachenko[1], and **Stefan Potthast[2]**
[1]*Otto-von-Guericke University, Magdeburg, Germany, D-39106*
[2]*Federal Armed Forces Institute, Munster, Germany, D-29633*
E-mail: sergey.tkachenko@ovgu.de

Modern computer and telecommunication systems use more and more densely packed electronic elements, which are more and more sensitive to natural and man-made electromagnetic interferences as, for example, UWB and HPEM sources. This leads to the necessity to investigate and test the sensitivity and vulnerability of systems and components to these electromagnetic interferences [1]. Test criteria are given by corresponding EMC standards.
A number of physical and technical objects (electromagnetic fields in resonator, electronic circuits, and sensitive parts of devices under test) can be described by the mathematical model of oscillators excited by external forces. Generally, the equations describing the set of oscillators contain some non-linearities, and these oscillators are coupled to each other (see, for example, [2]). The investigation of such systems is the subject of the general theory of ordinary differential equations with quite complicated mathematical equations. In the present research, however, we deal with some partial aspect of this general problem: We will investigate the excitation of linear oscillating systems in time domain with emphasis on their transient behavior.
Those considerations are of practical relevance: In most cases the tests are conducted with cw-excitation. But every signal is switched-on and/or switched-off. Thus, besides of the steady-state part of the signal there is always also a transient part which is generally disregarded. Depending of the choice of the excitation parameters it may happen that the amplitude of the transient part is many times larger than the steady-state amplitude. It will be shown that for digital systems the transient part of the switched-on sinus-excitation causes malfunction of the tested system.
In nature there are many different systems which mathematically can be modeled as resonating/oscillating systems: Simple oscillators, transmission lines, and 3-dim resonators (e.g. MSC) to name just a few. We will investigate these systems in time domain and will find analytical solutions which show a dominant transient effect. In addition an experiment is described which confirms our hypothesis. We start with a simple oscillator model as a basic element for further considerations. The oscillator is excited by different signals: a switch-on sinusoidal signal, a switch-off sinusoidal signal, a double-exponential signal, etc.. Different mathematical methods are used and adopted to the excitations. 1). The convolution integral method (integration with the response kern - Green's function in time domain), 2). Summation of the general solutions of the uniform differential equation and a partial solution of the non-uniform differential equation, 3). Fourier transformation of the exciting signal and oscillator response function to the time domain. It was shown that the expected phenomenon occurs in all these cases. Phase diagrams exhibit this effect quite clearly.
The calculation of the current induced by an external field in an unmatched transmission line was reduced to a time-domain integration of the excitation with the (one dimensional) space - time Greens function as a kern. This kern can be represented as a sum of oscillator response functions multiplied by one dimensional spatial eigenmodes. It was shown that the amplitude of transient oscillations can be larger than the steady-state amplitude, if the line is excited by a switch-on sinusoidal pulse with frequency larger than the resonant frequency of the chamber. Moreover, applying the SEM method [3] our results can be generalized to the high–frequency case, when the characteristic wavelength is less or comparable with the transverse dimension of the line and radiation has to be taken into account.
The same consideration was curried out for the excitation of the rectangular resonator by an electromagnetic wave penetrating through a small aperture. Again the solution in the time domain is represented as a time-domain integral of the excitation with the (three-dimensional) space-time Green's function as a kern. This kern can be represented as a sum of products of spatial resonator eigenmodes and oscillator–like time responses of each mode. It was shown that the considered effect appears also in this case.
The research of time-domain responses is important for investigations in a Mode-Stirring Chamber, which, of course, is a resonator which eigenfrequencies are different for different angles of the stirrer. However, in this case the pseudo - stochastic picture of the resonance excitation is observed. At the same time, the experiments in the MSC excited by pulse-modulated harmonic signals have shown that the considered effect can be observed for some frequencies of excitation and positions of the stirrer. Then sensitive elements can fail although the averaged level of the pulse does not reach the threshold value.

References

1. M. Magg, J.B.Nitsch, "HPM coupling to genetic targets: CW – vs pulse coupling". 11th International Zurich Symposium and Technical Exhibition on Electromagnetic Compatibility, March 7-9,1995, pp. 361-367.
2. H.G.Krauthäuser, S.Tkachenko, J.Nitsch, „Strong linear and non-linear coupling to system-cavity modes from repetitive high frequency illumination", ICEAA 01, September 10-14, 2001,Torino, Italy, pp. 103-106.
3. F. M. Tesche, M. Ianoz, and T. Karlsson, EMC Analysis methods and computational models. New York: Wiley Interscience, 1997.

978-1-4244-5050-3/10/$26.00 ©2010 IEEE

HF Electromagnetic Field Coupling to Small Scatterers in a Rectangular Resonator

Sergey Tkachenko[1], Jürgen Nitsch[1], Frank Sonnemann[2], Jürgen Urban[2], and **Ralf Vick[1]**
[1]*Otto-von-Guericke University, Magdeburg, Germany, D-39106*
[2]*Diehl BGT Defence, Röthenbachh, Germany, D - 90552*
E-mail: sergey.tkachenko@ovgu.de

Coupling of high-frequency electromagnetic fields caused by intentional electromagnetic interferences to linear structures is an actual topic. Usually experiments and corresponding simulation models deal with devices and apparatus in free space [1]. However, in reality, electronic equipment is enclosed in different kinds of resonator-like shells: cabinets of computers, airframes, frames of cars, etc. This enclosing changes the interaction of electromagnetic fields with the scatterers due to re-reflections of electromagnetic fields inside the resonator. This phenomenon changes the transfer (response) function (field->coupled current) compared to the case of free space, as well as the cavity's resonance frequencies (see, e.g. [2]).

It was shown in many experiments that the main mechanism of such interaction in free space is electromagnetic coupling to interconnections of different scales. Often these interconnections are electrically small (printed circuit board, chips, etc.) but can have own resonances. Currents and voltages induced in such objects in free space can be evaluated by a method which includes two simple models: a model of a small near–resonance linear antenna to describe the common mode, and a model of a small near-resonance loop to describe the differential mode [3].

In our papers [4-5] we proposed a method to analyze the coupling to an electrically small dipole antenna positioned in a resonator (Method of Small Antenna, MSA) using scattering theory. The MSA is based on the analysis of an integro-differential equation describing the induced current in the neighborhood of the antenna. The corresponding resonator Green's function is divided into a singular and a regular part. The singular part is connected with electrostatic and magnetic energy stored in the neighborhood of the antenna, and coincides with the singular part of the Green's function in free space. The regular part is connected with the far field and contains all information about the system's resonances. Of course, this part is different for the free space and the resonator case. However, for both cases the regular part is constant in the neighborhood of the antenna. This circumstance gives the possibility to derive analytically the solution for the coupled current into the small antenna from the free space solution, and also to investigate the input impedance of the small antenna, the current transfer ratio for two small antennas, the coupling of the penetrated radiation with a small antenna, etc.

In the present work we expand our method for the case of electromagnetic coupling with a small near – resonance loop in the resonator. Again, using an approximate solution for the induced current in free space and a regularized cavity Green's function (magnetic current->magnetic field) we derive an equation for the induced current in an electrically small loop in a resonator. The solution looks as the one for free space, but contains a so-called "resonator impedance", instead of the radiation resistance in free space. This "resonator impedance" depends on the parameters of the antenna, the parameters of the resonator and also on the coordinates of the loop.

The developed theory was applied to investigate an important problem in praxis: The calculation of the transfer function (external electromagnetic field->scattered current) for electrically small wiring objects (printed circuit, chip, etc.) inside a rectangular resonator. It is assumed that electromagnetic waves penetrate into the cavity through a small aperture, where they excite the scattering objects to a common as well as to a differential current mode. We show that both types of modes, in general, can have the same order of magnitude and that the analytical evaluations are in good agreement with results of numerical simulation.

It is known that the coupling with scatterers inside the housing of a computer, an aircraft fuselage, etc. is smaller in comparison with the coupling of the penetrating field with one scatterer in an almost empty resonator. This effect can be explained by the effective shielding of the penetrating electromagnetic field by the internal scatterers. In the present paper we numerically model this effect describing stochastically distributed small dipoles and loops inside the resonator. The obtained results are compared with results of a simple macro-electrodynamical model with effective relative electric permittivity and relative magnetic permeability.

References

1. M. Camp and H. Garbe, "Susceptibility of Personal Computer Systems to Fast Transient Electromagnetic Pulses", IEEE Transactions on Electromagnetic Compatibility, Vol. 48, No 4, November 2006.
2. M. Magg, J.B.Nitsch, "HPM coupling to genetic targets: CW – vs pulse coupling". 11th International Zurich Symposium and Technical Exhibition on Electromagnetic Compatibility, March 7-9,1995, pp. 361-367.
3. V.I. Kravchenko, E.A. Bolotov, and N.I.Letunova, Communication facilities and powerful electromagnetic interferences. Moscow: Radio i sviaz, 1987 (in Russian).
4. S.V.Tkachenko, G.V.Vodopianov, L.M. Martinov, "Electromagnetic field coupling to an electrically small antenna in a rectangular cavity", 13th International Zurich Symposium on EMC Electromagnetic Compatibility, February 16-18 1999, pp.379-384.
5. S.Tkachenko, F.Gronwald, H.-G.Krauthäuser, J. Nitsch, "High Frequency Electromagnetic Field Coupling to Small Antennas in Rectangular Resonator", V International Congress on Electromagnetism in Advanced Applications (ICEAA), 15-19 September, 2009, pp. 74-78.

978-1-4244-5050-3/10/$26.00 ©2010 IEEE

Electromagnetic Hyperthermia Modeling in Human Intra-Abdominal Region

Erdal Korkmaz[1], Omer Isik[1]
[1]*Fatih University, Department of Electrical and Electronics Engineering, Buyukcekmece, Istanbul,TURKEY*
E-mail: ekorkmaz@fatih.edu.tr

Hyperthermia is a well known method for cancer treatment for many centuries. In late seventies the scientists started to interest in electromagnetic hyperthermia. Research in last two decennia demonstrated that high temperatures obstruct the cancerous cells evolution and even kills them. Since the cancerous cells dispositions are weaker than the healthy ones the healthy cells near the cancerous cells are damaged lesser [1, 2]. For these reasons it is known as a therapeutic technique. Because the physical energy is applied externally it is a minimal invasive method and the expectations are high. In addition electromagnetic hyperthermia can be used in conjunction with other treatment methods like radio therapy and chemotherapy.

In electromagnetic hyperthermia the tissues are exposed to electromagnetic radiation to cause a temperature heat between 42-45 ˚C which induces a tumor necrosis in the tissues. The method is mostly applied by relatively low power multiple sources focused on tumor tissues. In this way the aim is to add the fields constructively in the tumor region while keeping the healthy tissues relatively much less affected. However the energy distribution in the tissues strongly depends on tissues characteristics and is thereby inhomogeneous. The temperature distribution is not simply a result of the energy distribution but also depends on thermal tissue characteristics and blood flow. Since the electromagnetic interaction in human tissues depends on different individuals it makes the method a patient specific method.

In this paper, in order to be able to apply the method patient specific a detailed human tissue model of a human intra-abdominal region is introduced. Subsequently the tradeoff frequency in consideration of penetration depth and focusing is determined. The phase delay calculations of multiple sources are performed which are essential to add the fields constructively at the tumor region. Then the electromagnetic distribution calculations have been performed. For these calculations the finite difference time domain method is mostly used due to be suited for simulating non-homogeneous models, scales well with the resolution increase, implicitly incorporates coupling between models and the antenna and can be implemented in hardware accelerator. Then from the calculated electromagnetic field values specific absorption rates are calculated within the tissues. Finally by using of these values in Pennes bio-heat equation the temperature distributions are calculated. The result show that the proper choice of frequency, the number of sources and their positions, and the phase corrections can elevate the temperature on some tissues at 42 ˚C and even above.

Acknowledgments – This work is supported by the Scientific Research Fund of Fatih University under the project number P50060902-2.

References

1. Hildebrandt, B., P. Wust, O. Ahlers, A. Diein, G. Sreenivasa, T. Kerner, R. Felix, H. Riess, “The cellular and molecular basis of hyperthermia”, Critical Reviews in Oncology/Hematology, Vol. 43, pp. 33-56, 2002.
2. Yang, X., J. Du, Y. Liu, ”Advances in Hyperthermia Technology”, *IEEE Engineering in Medicine and Biology 27th Annual Conference*, Shanghai, China, September 1-4, 2005, pp. 6766-6769.

978-1-4244-5050-3/10/$26.00 ©2010 IEEE

Behavior of Combined Lightning- HEMP- Protection Devices to HPEM Overvoltage Input Signals

M. Nyffeler[1], A.W. Kaelin[2], D. Rolle[3], P.-F. Bertholet[1], A. Jaquier[4]
[1]armasuisse, HPE Laboratory, Spiez and Thun, Switzerland
[2]Meteolabor AG, Hofstrasse 92, CH-8620 Wetzikon, Switzerland
[3]Maxwell Technologies SA, Rossens, Switzerland
[4]armasuisse, Science and Technology, Thun, Switzerland
E-mail: markus.nyffeler@armasuisse.ch

Abstract

The majority of the Swiss defense equipment is lightning and HEMP protected by using combined lightning- HEMP protection devices. The goal of this study was to investigate the behavior of existing protection devices to some HPEM overvoltage input signals, especially such having a much faster risetime than HEMP.

To match the output impedance of damageable high voltage sources to differing input impedances of protection devices it was tried to use two 50 Ω antennas, one as a transmitting and the other as a receiving antenna, to prevent the source from damage by reflections. But it turned out that the field coupling efficiency was too low to induce overvoltage signals which could activate protection devices. Therefore it was decided to couple the source directly to the target by using a tap-off and a small resistor in front of the input path of the DUT (device under test) as shown on Figure 1.

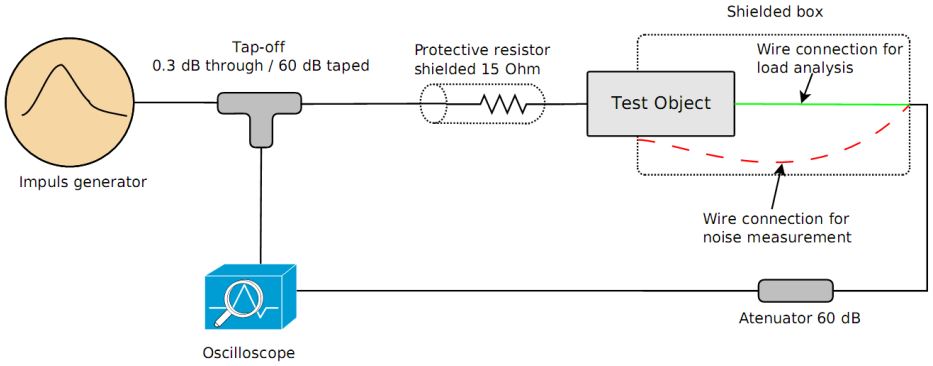

Figure 1: Test setup for applying and measuring the effect of HPEM signals on a protection device

A HVPS (high Voltage power Supply) pulse source of Grant Applied Physics Inc. providing 1.5 kV pulses with a pulse rise time of < 150 ps was used to determine the behavior of nonlinear combined lightning and HEMP protection devices from Meteolabor AG when fed with sub nanosecond overvoltage signals. The noise of the system was maesured to validate the measurement.

The experiment showed that selected protection devices (DUT here: USS1-24V) limit this kind of HPEM threats to acceptable low values for COTS (commercial off the shelf) systems used in common army goods (see figure 2). All parts of the test setup have been placed individually in shielded enclosures to prevent interferences. On the unprotected side of the DUT the high voltage signal was always fed to the inner conductor.

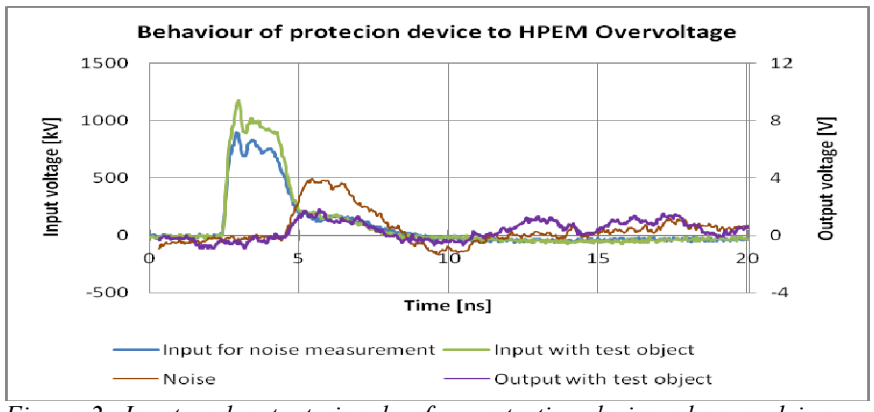

Figure 2: Input and output signals of a protection device when applying HPEM signals

On the protected side of the DUT the residual output voltage was always measured between the inner conductor and the system ground (green wire on figure 1). To measure the noise, the DUT was open and the measurement was taken on the shielded enclosure near to the DUT (red wire on figure 1).

The presentation will show the behavior of additional protection devices to known HPEM threats and how they entail the requested immunity levels when used for systems in C4I facilities.

978-1-4244-5050-3/10/$26.00 ©2010 IEEE

Estimating the Reliability of Complex Systems Against IEMI Threats by Topological Methods

S. Fisahn, **E. Genender**, and **H. Garbe**
Leibniz Universität Hannover, Institute of the Basics of Electrical Engineering and Measurement Science, Hannover, Germany

Modern electronic systems are of particular importance to many aspects of our daily live such as security, medicine, economy, traffic, communication or armed forces. Since civil and military systems include many electronic components and subsystems, they must be highly reliable against various electromagnetic influences. A malfunction of such a device could lead to unexpected consequences, especially if the system has got safety critical functionalities. Thus, the knowledge of the reliability of electronic systems is of great interest. Due to the complexity of the electronic systems with many individual components and interconnections, it is almost impossible to solve this problem analytically as a whole. An approach to deal with this problem is the electromagnetic (EM) topology [1]. In a first step, the space occupied by the system is divided into different volumes surrounded by surfaces and the interaction between these volumes is described by an interaction sequence diagram (graph). In a second step, the graph can be written as a general matrix equation, which is a form of the Baum-Liu-Tesche (BLT) equation. Since this methodology is very powerful and suited for the analysis and the design of complex electronic systems, it is sufficient in most cases to use only the qualitative description of this method for the estimation of the reliability of an electronic system against electromagnetic interferences (EMI). The qualitative description of a system consists of the volume/surface topology and the related interaction graph.

In this contribution, the estimation of the reliability of complex electronic systems against intentional electromagnetic interferences (IEMI) by applying the EM topology will be presented by means of a generic microcontroller board within an enclosure. Therefore, the principles of the EM topology like the volume/surface topology will be treated first. Then, the topological description for the system will be derived and discussed in detail. After this, the reliability will be estimated for different IEMI threats. Additionally, the measurements, which have been performed for that system with EMP and UWB pulses as well as HPM, will be described. The results, which show a good agreement with the previously made estimations, will be presented. The limitations of the estimation approach will be discussed. Furthermore, a possible usage of the results for other topics like the risk analysis of complex systems will be proposed.

References

1. C. E. Baum, "Electromagnetic topology: "A formal approach to the analysis and design of complex electronic systems", 4th International Zurich Symposium on Electromagnetic Compatibility, 1981.

978-1-4244-5050-3/10/$26.00 ©2010 IEEE

Susceptibility of Electrical Systems to UWB Disturbances due to Layout of Exit Cables

Dirk Zamow, David Hamann, and **Heyno Garbe**
Leibniz Universität Hannover, Institute of the Basics of Electrical Engineering and Measurement Science
Hannover, Germany
E-mail: zamow@ieee.org

The importance of susceptibility test standardization of electrical systems to UWB disturbances has grown during the past years. Most standards are valid as long as the equipment under test (EUT) is electrically small. That means that the dimensions of the EUT are smaller than the shortest wavelength of the disturbance signal. According to IEC 61000-4-20, an EUT will be electrically large if a cable is attached. Most systems need supply cables that connect the EUT to a terminal(exit cable). Therefore the influence of these cables cannot be neglected in susceptibility measurements. The authors of [1] show that the influence of the cable decreases with rising frequencies. Our study validates this effect and focuses on the radiation of exit cables depending on cable decoupling and cable layout in test scenarios in UWB frequency range.

Measurements in two different GTEM cells, a fully anechoic chamber (FAC) and a semi anechoic chamber (SAC) are performed. For these measurements an UWB source has been designed to impress a common mode current onto the exit cable. Additionally, the radiation patterns for different exit cable configurations are simulated for the UWB frequency range using the software tool CONCEPT II.

The measurements show, that radiated power from the cable decreases with higher frequencies. Laying the cable in a sine shape compared to a straight laid cable shows drastic differences up to 15 dB. Frequencies with decreased and increased radiated power alternate. The effect grows smaller with higher frequencies. Figure 1 shows the maximum deviation between a cable that has been laid in a straight line, and cable that has been laid in a bundle. The effect of the decoupling shows similar results.

The numerical simulation confirms the measurements. Moreover, the reason for the measured effects becomes evident. According to [2], the directivity of a cable grows for frequencies which have a shorter wavelength than the length of the cable. The simulation shows the same current distribution for a cable laid in a straight line or in a sine curve with moderate amplitude. Thus, the radiation effects do not result from changed current distribution but from interferences due to the form in which the cable is laid. These interferences amplify the directivity. The difference between the total maximum radiation due to different ways in which the cable is laid decreases with higher frequencies. Nevertheless, figure 2 shows, that the radiation pattern can be different for frequencies where the layout does not influence the maximum radiated field significantly.

Most systems are susceptible at discrete frequencies. For these systems, the susceptibility can be altered by varying the way the cable is laid. In this case increasing and decreasing the amplitude of the sine curve amplifies the effect. The length of the cable in the test volume and the cable decoupling shifts the frequencies for which the amplification occurs. The study shows that the way the cable is laid is also important for high frequencies due to the directivity and complex radiation pattern. From a statistical point of view the maximum radiation or susceptibility will not be detected by the established standards and will be underestimated therefore.

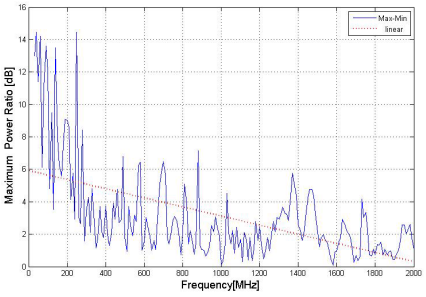

Figure 1: **Maximum Power Ratio of a Straight Cable to a Varied Layout at One Observation Coordinate**

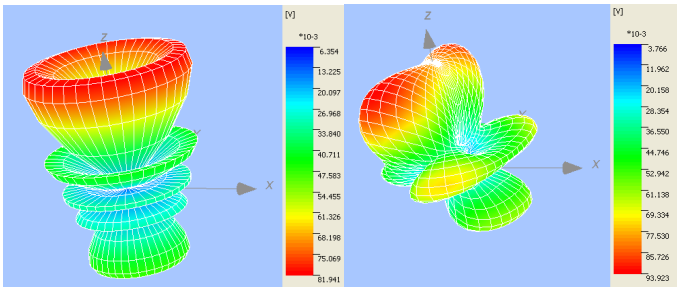

Figure 2: **Radiation Pattern of a Cable Laid in Straight Line(Left) and a Cable Laid in the Curve of a Sine (Right) with Constant Length of 50 cm at 1.5 GHz**

Acknowledgments – The authors would like to thank Uwe Karsten from TESEQ AG and Dr. Sven Battermann from WAGO Kontakttechnik GmbH & Co. KG for allocation of their test sites.

References

1. H. Garbe, S. Battermann, “Converting Total-Radiated-Power Measurements to Equivalent E-Field Data”,. EMC 2008. IEEE International Symposium on Electromagnetic Compatibility, Aug. 2008, Detroit, USA
2. P. Wilson, “Emission and immunity testing: test object electrical size and its implication”, 2004 IEEE International Symposium on EMC, 9-13 August, 2004, Silicon Valley, USA

978-1-4244-5050-3/10/$26.00 ©2010 IEEE

High-Voltage, Tunable Mesoband Sources Based on Blumlein Geometry

J. Scott Tyo[1], Michael C. Skipper[2], Michael D. Abdalla[2], Samuel P. Romero[2], Brett Cockreham[3], William D. Prather[4], and **Julie E. Lawrance[4]**

[1]*College of Optical Sciences, University of Arizona, Tucson, AZ 85721 USA*
[2]*ASR Corporation, 7817 Bursera NW, Albuquerque, NM 87120 USA*
[3]*Solid Design, Inc., 7113 Lantern NE, Albuquerque, NM 87109 USA*
[4]*AFRL/RDH 3550 Aberdeen SE, Kirtland AFB, NM 87117 USA*
E-mail: tyo@ieee.org

Recently there has been an increase in the research on the generation and radiation of mesoband (MB) waveforms [1]. Mesoband waveforms are attractive for IEMI applications because they fill the niche between narrow band (NB) and WB systems. NB systems have extremely high power spectral densities, but very narrow coupling band widths. WB systems, on the other hand, have very broad coupling bandwidths, but very little power spectral density. MB systems are advantageous because they are typically built with the much simpler WB technologies. Furthermore, MB technologies have the added advantage of lending themselves to tunable topologies. We recently presented a strategy for a tunable MB source based on a mechanically-adjustable, parallel-plate Blumlein topology [2]. We previously showed a low-voltage prototype system that could change the typical Blumlein waveform to a damped sinusoid by moving the center conductor closer to the switched electrode, thus breaking the impedance balance and increasing Q of the output waveform. Furthermore, the center frequency of the output pulse could be altered by changing the length of the charge storage line. These parameters could be tuned continuously, making the source dynamic and flexible. In our previous work [1] we demonstrated a low-voltage prototype of a parallel-plate Blumlein system, and we subsequently built a high-voltage system capable of being charged to approximately 20 kV [2]. The high power system was immersed in a SF6 bath, and the high-voltage hold off was accomplished in a monolithic, high-pressure hydrogen switch. The system worked well, but the monolithic switch caused significant problems with the tunability aspects.

In the current paper we present design issues associated with the development of a next-generation, fully integrated tunable Blumlein source. The source is designed to have voltage hold off in excess of 100 kV with center frequencies in the range of 100 MHz – 1 GHz. The Q of the system should be tunable so that we can generate anywhere from a single half-cycle at a chosen frequency f_0 up to approximately five cycles in a damped sinusoidal waveform. In order to accomplish these performance parameters, we have designed a system with an integrated switch and full Blumlein structure inside a high pressure hydrogen enclosure. This strategy adds significant mechanical complexity, but provides for the best electromagnetic waveform. We present results concerning the shaping of electrodes in order to manage the high fields in the system, as well as discussing the tradeoffs among charge voltage, center frequency, and Q of the system as the system is tuned. We have designed a retractable switch and tested a static prototype of the switch that will allow for full tuning, and no loss of rise time as the electrode positions are altered. The full high power system has been prototyped, including a feed through system to allow the output to be fed to a balanced antenna. An engineering drawing of the system is shown in Fig. 1.

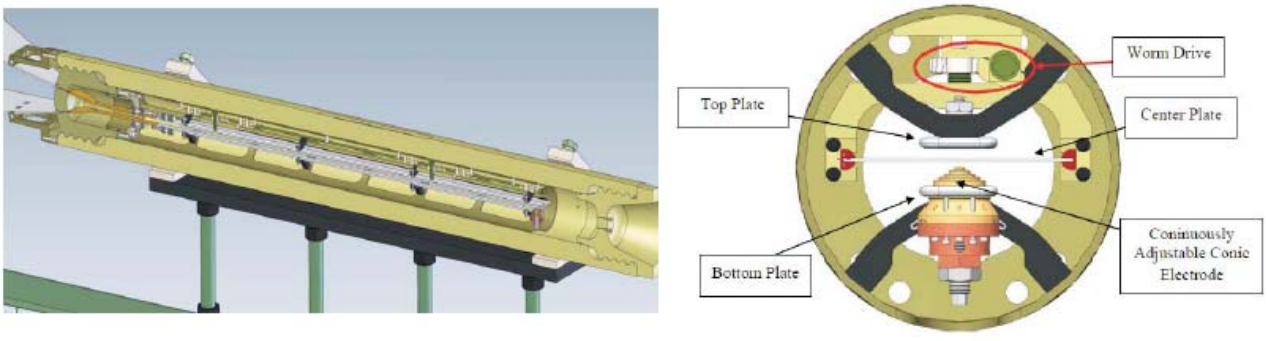

Figure 1: **High-power, Tunable, Blumlein Mesoband source.**

Acknowledgments – This work was supported by a Small Business Innovative Research Award administered by AFRL/RDH, Contract #FA9451-06-C-0029

References

1. E. G. Farr, L. H. Bowen, C. E. Baum, and W. D. Prather, "The folded horn antenna," *IEEE Trans. Antennas Propagat*., **55**, pp. 3341 – 3344, (2007).
2. J. S. Tyo, M. C. Skipper, M. D. Abdalla, S. P. Romero, and B. 'Cockreham, "Frequency and bandwidth agile pulser for use in wideband applications," *IEEE Trans. Plasma Sci*., **32**, pp. 1925 – 1931, (2004).
3. J. S. Tyo, M. C. Skipper, M. D. Abdalla, and S. P. Romero *AMEREM 2006*

978-1-4244-5050-3/10/$26.00 ©2010 IEEE

Discrimination of Canonical Scatterer Based on Singularity Expansion Method

Dhiraj K. Singh,D C Pande
Electronics & Radar Development Establishment
Bangalore, India
dhiraj_lrde@rediffmail.com

A. Bhattacharya
Indian institute of Technology, Kharagpur
West Bengal, India
amit_gappy@yahoo.com

***Abstract*— Radar target identification methods using the time domain response of a target to a transient incident waveform have generated considerable interest in the recent past. Radiation of narrow time domain pulse has its own limitation for long-range radars where energy on target is important for getting detection. Exciting targets with short pulses has got its own advantages for short-range radars for better resolution like see through wall radar, foliage penetration radars etc. This paper describes extraction of singularity from transient response using generalized pencil of function (GPOF) method and discrimination between scatterer using Extinction pulse (E-Pulse) technique.**

The transient response of the scatterer is collected using finite difference time domain solver wherein a scene as shown in Figure 1, consisting of transmitting impulse radiating antenna (IRA), receiving IRA and the scatterer is simulated.

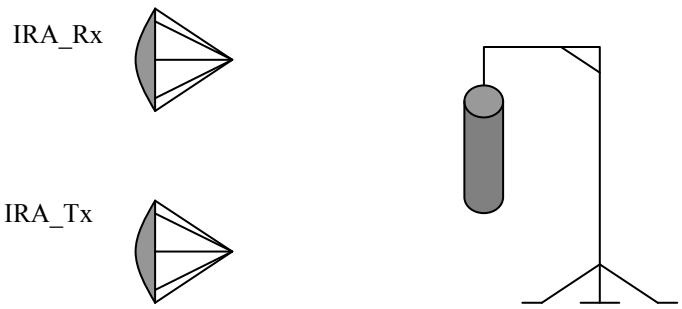

Figure 1. Simulation of Scattering Scene

The late-time impulse response as collected from IRA Rx of above simulation may be expressed in time-domain as the sum of a finite number of resonant modes as follows:

$$y(t) = \sum_{m=1}^{P} c_m .e^{smt} .u(t - T_{et})$$

Where, T_{et} is the early-time duration, s_m are the complex poles on the s-plane, and c_m the residues (or mode amplitudes). GPOF method has been used extract the optimum number of poles for near faithful replication of the transient response.

The extinction-pulse based techniques (E-pulse) used here is a specifically synthesized filter (one for each target class) to annihilate the scattered response of the detected target. The advantage of using them lies in their aspect independency. There will be a library of E-pulses stored for different class of targets, which will be convolved with the transient response of the requisite scatterer. The minimum values of the Extinction discrimination ratio (EDR) ascertain the class of the scatterer.

Keywords-IRA, GPOF, Singularity extraction,FDTD ,E-pulse

REFERENCES

[1] F.M.Tesche et. al, "Scattered EM field Response of Canonical Scatterers by an Impulse Radiating Antenna (IRA)", Circuit and Electromagnetic Design Notes 53, April 2006.

[2] Hoi-Shun Lui, and N.V.Z Shuley, "Radar Target Identification Using a Banded E pulse Technique", *IEEE Trans.*, AP, Vol. 54, No.12, December 2006

.

978-1-4244-5050-3/10/$26.00 ©2010 IEEE

Modeling of a commercial Ultra-wideband impulse Ground Penetrating Radar for landmine detection

María A. González-Huici, Udo Uschkerat
Fraunhofer Institute for High Frequency Physics and Radar Techniques FHR
53343 Wachtberg, Germany
Email: maria.gonzalez@fhr.fraunhofer.de

Ultra-wideband GPR systems constitute a promising technology for remote imaging of surface-laid or shallow-buried targets.
When dealing with the detection and classification of small low-contrast objects and in particular, concerning the landmine problem, high precision and spatial resolution is needed in order not only to find the mines but to identify them and decrease the false alarm coming from other scatterers. Thus, an accurate modeling of the complete GPR scattering scenario becomes essential to understand and predict the signature of such targets in realistic conditions.

This contribution focuses on the modeling of a commercial ultrawide-band impulse radar for landmine detection employing a finite element method based modeling software. With this modeling tool it is possible to apply an adaptative meshing which resolves properly narrow regions and reduces dramatically the solution time and the computational weight of the numerical problem. Electrical parameters of inhomogeneous and dispersive materials can be easily defined by an analytical function or via interpolation from measurements. The roughness of the surface can be directly incorporated applying the desired random function and correlation length to describe the topography.

In previous works [1] we showed some simulation results for such complex GPR scenarios but the antenna model assumed was still very simple. It consisted of a pair of transmitting and receiving bow-ties placed side-by-side and suspended in air with a Gaussian pulse input signal at the transmitter. The source impedance at the feed port was adjusted by comparison with the measured voltage at the receiver in laboratory and the geometry was just adapted to the real external dimensions of the GPR head box. The antenna crosstalk contained some ringing but the results were satisfactory to predict the scattering by small objects in air. For a half-space and near field case, the scattering may be very sensitive to the antenna characteristic and it can differ significantly from reality for such a simplified model. In order to distinguish the reflected signal by the target from clutter, like direct coupling and ground surface reflection, it is then crucial to simulate the antenna illumination accurately. The signal ringing should be also minimized.

In this paper, we describe the modeling process to obtain a reliable antenna representation which exhibits a similar time domain response as the actual system. The above mentioned model is modified adding a rectangular shielding box to maximize the radiation into the soil and reduce the direct coupling. This cavity is filled with absorber material which will decrease the antenna ringing. We analyze the radiated field pattern and the directivity for several box parameters and various antenna flare angles. We carry out a parametric study of its height, permittivity and conductivity influence on the antenna impedance through simulations and applying transmission line theory. In this way, we are able to choose proper parameters to get broadband impedance at the required frequency band while high radiation efficiency is ensured. Then, we match the cable impedance at the transmitter port with the derived antenna impedances for the corresponding configurations to avoid undesired ringing. And next, we simulate the time domain response for every case investigating the effects on the received voltages in order to select the best antenna model to fit the measured signals in laboratory.

Finally, we apply this model to simulate the scattered pulses by some testmines buried in an "unfriendly" test field getting a high correlation between synthetic and measured results.

REFERENCES

[1] Gonzalez-Huici, M.A., Uschkerat, U., "Modeling of a complex GPR scenario in landmine detection ", IWAGPR 2009, Granada.

978-1-4244-5050-3/10/$26.00 ©2010 IEEE

Nano-Trimetaspheres Enhanced Detection and Destruction of Breast Tumors Using Terahertz Pulsed Radiation: Balram Prasad[1] and Kenneth Grimm[2]

[1] *Physical Scientist, Retired Defense Threat Reduction Agency, Ft Belvoir, VA (Currently Consultant to ITT Advanced Science and Engineering to DTRA, KAFB, Albuq. NM)*

[2] *Electromagnetic Research Engineer*, *BAE Systems Inc. Technology Solutions and Services, Ft Belvoir, VA.*

An innovative 3-yr research and development effort to test-prove the task of the title has been proposed to the IMAT R21_ CA_009 Application of NIH by a team of six PhDs and MDs including bio-engineers, physicists, physicians, and electronics engineers for THz spectrometric detection, 3D tomography and eventual destruction of breast tumors induced in animal samples in-vivo and ex-vivo at the University of Pittsburgh Medical MRI Research Center.

The theoretical model underlying the terahertz pulse imaging and detection of breast tumors has been fully researched and developed by scientists and surgeons at Teraview Ltd. and the Cavendish laboratory, Cambridge University, Cambridge, UK. Their research results on breast tumor detection and surgery published in reputable journals for the last ten years have achieved 100% success in complete detection, imaging and surgical removal of malignant tumors - including ductal cancer in-situ (DCIT). The procedures are accompanied by chemo-therapy and drugs to prevent the recurrence of any residual legions.

We have improved their model for terahertz (THz) pulse spectrometric detection, imaging and tomography of breast tumors along the lines worked out by the Defense Department for remote detection of enemy missiles/rockets or WMD debris by application of appropriate THz coherent, broadband radiation pulses. The Teraview and Cavendish laboratory scientists have published in ref. [1], THz spectral data/curves on three main types of tissues located inside the matrix of human breast tumors viz. fat, fibers/collagen and cancerous tissues. They have measured the THz resonance quality factor (Q) of the electric field impulse response functions of the three tissue types. The Q's are different from each other and they distinguish between the malignant and non-malignant tumors. Note that the THz impulse response of the fat tissue is completely different, but the difference between the responses of fiber and cancer-invasive tissues cannot be resolved. However, our improved model of infusing nano-trimetaspheres in the animal breast tumor samples will greatly (~100 times) enhance the signal to noise ratio (S/N) of the responses in the latter two tissue types as shown in fig.3 of ref.[1]. It also increases the tissue penetration of the applied THz pulse radiation. If the trimetaspheres are first incubated with the cancer cell lines of the breast sample for two or three days and then injected into the test samples, the nano-trimetaspheres will stick to or penetrate the cancer cell membranes only. So if the low power, broadband THz pulses are illuminated on the treated tumor samples, only the electric impulse field's characteristic response of the cancerous cell tissue will be obtained and its characteristic THz resonance factor Q_c and electric field E_c shall be determined. The Einstein's quantum theory of radiation from matter in free space will allow us to estimate the actual number of cancer cells in the tumor matrix from the well known formula, $V_c E_c^2 / 4\pi f_c = h N_c f_c$, where V_c is the volume determined by 3D tomography, N_c the total number of cancer cells in the cancer invaded volume and h is the Heisenberg constant. If now, a Q_c modulated low-power narrowband THz signal is applied repeatedly to the trimetasphere tagged cancer cells, it will resonantly evoke antibodies inside each of the tagged cancer cells' immune responses and cause selective apoptosis of the THz signal illuminated cancer cells. In effect the proposed model procedure will provide a new and noninvasive treatment of breast cancer and will be cost effective and free from any side effects.

The THz electromagnetic response of a breast cell can be modeled by a lumped element RLC circuit composed of RNAi molecules of the resistance (R), DNA molecules of inductance (L), the double pairs of chromosomes of capacitance (C). The THz spectrum of the biological cell has a resonant response determined by RLC parameters . When excited by an impinging THz plane wave, the cells will scatter and absorb the RF plane wave energy, accompanied with a resonant absorption at the unique cell frequency f_c with a bandwidth Δf_c . These two quantities will yield the resonance quality factor $Q_c = f_c / \Delta f_c$ of the THz reflective resonances. It is assumed that the RLC circuit is linearly excited in resonance mode upon the application of the first low-power THz radiation pulse. By solving the linear circuit resonance equations, numerical values of the RLC circuit parameters can be determined to monitor the progression or degradation of the tumors toward their remission or transition to their total destruction to be confirmed by the normal MRI.

Reference [1] P. C. Ashworth, V. P. Wallace, E. Pickwell, Cavendish Laboratory, Cambridge University, UK , and D. A. Amone, Teraview Ltd, Cambridge, UK, " Terahertz Detection and Imaging of Breast Tumours", IEEE, Electromagnetic Propagation, 2008.

978-1-4244-5050-3/10/$26.00 ©2010 IEEE

Calculation of Transient Electromagnetic Fields Radiated from Underground Cables Buried in Lossy Ground

Pooya Taheri, Behzad Kordi, and **Ani M. Gole**
ECE Department, University of Manitoba, Winnipeg, MB, Canada
E-mail: ptaheri@ee.umanitoba.ca

Underground cables are one of the most critical components of power system transmission and distribution networks from an electromagnetic point of view. A considerable portion of electromagnetic fields around power system substations and telecommunication centers originate from underground cables. Increasing usage of underground cables for power delivery purposes demands investigation of the coupling between underground cables and nearby power system equipment.

Radiated electromagnetic fields, which are of strong amplitudes, are produced during normal and transient operation of current-carrying cables. Electromagnetic interference can cause major problems for electronic and digital devices installed in the vicinity of transmission networks for measurement, protection, and control purposes. To ensure normal functioning of the electronic equipment in this electromagnetic environment, the radiated transient electromagnetic fields in the air and in the ground must be accurately calculated. It is the main purpose of this paper to calculate the transient electromagnetic fields associated with an underground cable illuminated by a known transient current or voltage waveform.

In this work, the per-unit-length parameters of the underground cable are approximated using Wedepohl's formulation [1]. Then, the current distribution along the excited cable is found using the Modified Finite-Difference Time-Domain (MFDTD) technique [2]. To obtain the transient fields in the vicinity of an underground cable, the current-carrying cable is assumed to be made up of a large number of small dipoles [3].

The pioneering work of Sommerfeld [4] formulates the problem of radiation from a horizontal electric dipole into an integral form in terms of electric potential vector. One of the methods to approximate the Sommerfeld-type integrals is the complex image theory [5]. The essence of the complex image theory is based on approximating the reflection coefficient term by its first term of corresponding Taylor series. An alternative solution suggested by R. W. P. King et. al. [6] deals with the electric and magnetic field intensity vectors rather than potential vectors. In this method, using Fourier transform, the Maxwell's equations are directly solved and the associated electric and magnetic field components in the upper half-space, air, and the lower half-space, lossy ground, are determined.

The contribution of each dipole is calculated using the aforementioned frequency-domain solutions. Finally, the total radiated field is calculated by making use of superposition in conjunction with inverse Fourier transform.

The general formulation used in this research permits the observation point to be located in the air or soil for an arbitrary network of energized cables. The main restricting assumptions in each applied technique are discussed and the range of validity of the proposed approach is determined.

Using the proposed method, the effects of multi-conductor cable configuration, shielding, depth of burial, and ground loss are studied. Different excitation waveforms such as step-function, Gaussian waveform, and Heidler function [7] are applied and the corresponding transient fields are obtained. These results may be used for electromagnetic compatibility studies regarding underground cables, high voltage substation, and grounding networks.

References

1. L. M. Wedepohl and D. J. Wilcox, "Transient Analysis of Underground Power Transmission Systems", *Proceeding of IEE*, 1973, vol. 120, no. 2, pp. 253-260.
2. B. Kordi, J. Lo Vetri, and G. E. Bridges, "Finite-Difference Analysis of Dispersive Transmission Lines within a Circuit Simulator", *IEEE Transaction on Power Delivery*, vol. 21, no. 1, pp. 234-242, January 2006.
3. D. W. P. Thomas, C. Christopoulos, and E. T. Pereira, "Calculation of Radiated Electromagnetic Fields from Cables Using Time-Domain Simulation", *IEEE Transaction on Electromagnetic Compatibility*, vol. 36, no. 3, pp. 201-205, August 1994.
4. A. Sommerfeld, "Propagation of Waves in Wireless Telegraphy", *Annalen der Physik*, vol. 81, pp. 1135-1153, 1926.
5. P. R. Bannister, "Applications of Complex Image Theory", *Radio Science*, vol. 21, no. 4, pp. 605-616, August 1986.
6. R. W. P. King, M. Owens, and T. T. Wu, *Lateral Electromagnetic Waves*, Springer, New York, U.S.A., 1992.
7. F. Heidler, J. M. Cvetic, and B. V. Stanic, "Calculation of Lightning Current Parameters", *IEEE Transaction on Power Delivery*, vol. 14, no. 2, pp. 399-404, April 1999.

978-1-4244-5050-3/10/$26.00 ©2010 IEEE

The 2010 Status of IEC SC 77C Standardization

W. Radasky[1], R. Hoad[2]
[1]*Metatech Corporation, Goleta, California USA*
[2]*QinetiQ, Cody Technology Park, Farnborough, Hampshire, UK*
E-mail: wradasky@aol.com

The International Electrotechnical Commission (IEC) Subcommittee 77C has been preparing standards and reports covering high-power transient phenomena and the protection of civil equipment and systems from High-altitude Electromagnetic Pulse (HEMP) and Intentional Electromagnetic Interference (IEMI) for more than 20 years. During that period of time 20 publications were produced as summarized in Figure 1 below.

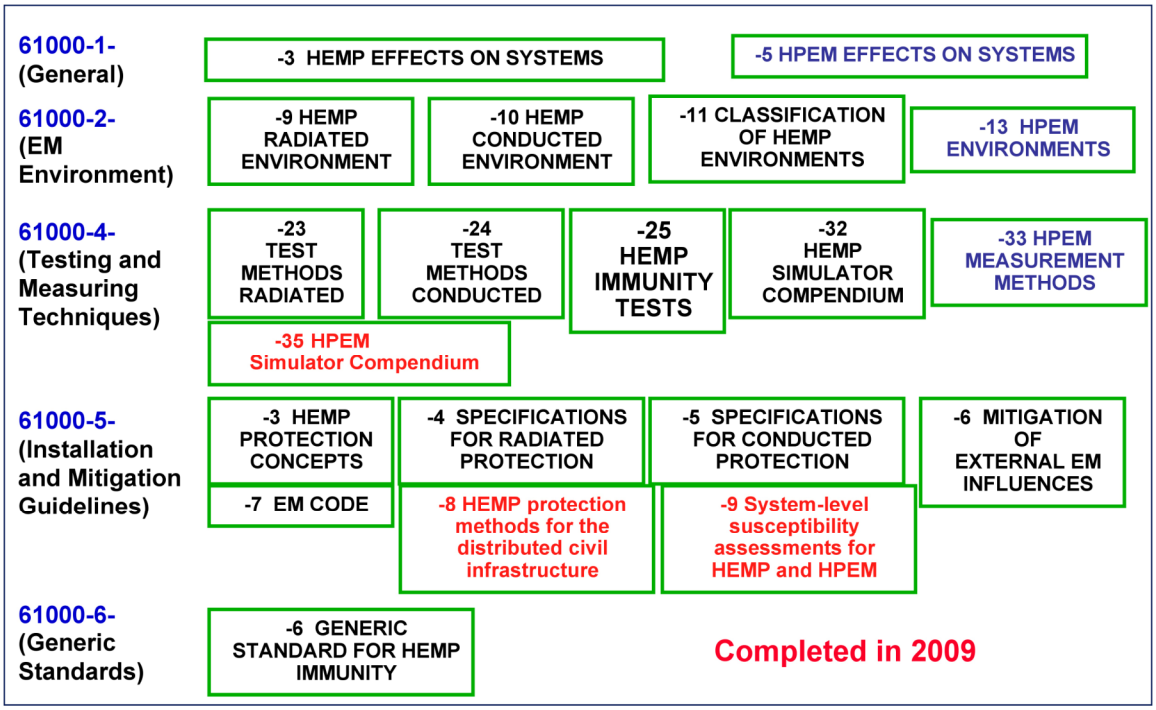

Figure 1. Publications produced by IEC SC 77C dealing with HEMP and IEMI.

It is noted that Figure 1 indicates that three documents (in blue) deal with high power electromagnetic (HPEM) aspects covering the field of IEMI, while those in black indicate documents that deal primarily with HEMP. The three documents in red represent publications completed in late 2009.

This paper will highlight the work completed in 2009 and will also discuss the current 2010 program to update and maintain these and other publications in the coming years.

978-1-4244-5050-3/10/$26.00 ©2010 IEEE

Penetration of High Frequency EM Signals on Building Wiring

E.B. Savage, W.A, Radasky, J.L. Gilbert, M.J. Madrid, and **K.S. Smith**
Metatech Corporation, Santa Barbara, California, USA
E-mail: savagee@cox.net

A major IEMI (Intentional Electromagnetic Interference) concern is harm caused by high-level high-frequency signals maliciously introduced onto building wiring, with the intent of causing harmful effects to the attached equipment [1]. Examples of such wiring are network cabling and AC power wires. With technology advance, cabling in buildings has increased significantly, along with the growth in the usage of attached electronic devices. Our modern life depends more and more on these complex electronic devices for all aspects of our infrastructure, which puts us at increased IEMI risk, especially as acquisition of IEMI sources becomes easier [2], and the knowledge of this vulnerability becomes more wide-spread.

One type of IEMI concern involves radiation of high-level EM signals at the building, with coupling to the external cabling, and then propagation of that coupled interference into the building, where it attacks the enclosed equipment[2,3]. This has an advantage of simultaneously attacking many systems within the building, however, in order to get high enough coupled signal levels, the attacking source equipment, including the antenna, must be very large. Restrictions on physical access, such as for parking of vehicles, could hamper such attacks. Compact sources, such as suitcase size, have been developed, and could be carried into the public-accessible parts of the building. However, such sources also have the inefficiency of using radiated EM energy for their attack. An alternative approach is a IEMI source that can be clandestinely directly attached to any accessible AC outlet, so that EM energy could be introduced into the building's wiring [2]. This might not even require interior building access, as often there are external AC outlets. Another access point could be network connection jacks. This work considers high-frequency signals introduced onto building wiring – experimentally looking at network cables (Ethernet) and AC power. Besides IEMI, this work could apply to other types of building EM vulnerability, such as HEMP.

For IEMI there are, in general, three issues:

1. The EM source – such as its characteristics, including waveform shape, repetition, and signal level.
2. Coupling and signal propagation of the signals along wiring, from the source to the vulnerable equipment.
3. The vulnerability of the attached equipment.

This work looks at the middle stage – characterizing signals on the wiring. Of special concern is loss of signal strength, such as from EM attenuation or reflection from impedance mismatches. Work in [2] showed, not unexpectedly, signal level falling at junctions (branch nodes) in the wiring tree of an AC circuit. In the work we look at common and differential modes, and also conversion of signal from common mode to differential mode. We do this for injection excitation by both pulses and CW (continuous wave).

Figure 1 shows a sample result. This uses a 20 meter network cable, situated away from any other objects, and 60 centimeters off the concrete building floor. A fast pulse is driven onto the cable, and the common mode current at three locations is shown. The current near the end (green line) shows a little decrease in level, but this is mostly due to interference from the reflected pulse (the cable is open on the end). The pulse reflection at the cable start (red line, negative pulse) shows a little attenuation of high frequencies (the peak is not as sharp), and some dispersion (the pulse is wider).

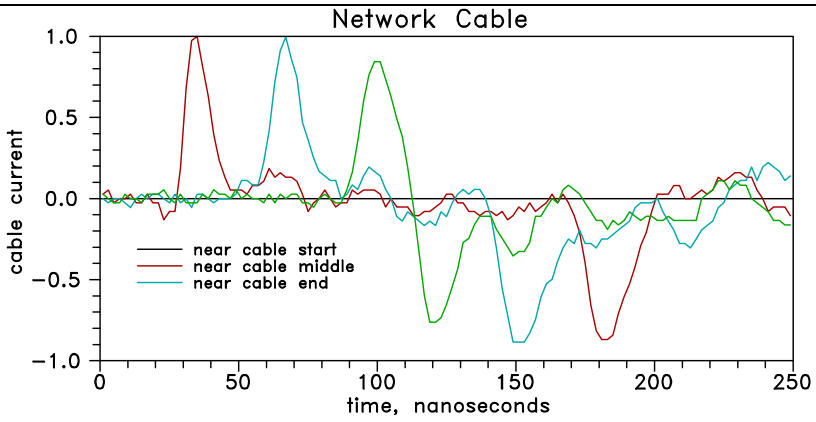

Figure 1. Sample of EFT pulse common mode propagation on a 20 meter Ethernet cable.

References

1. W. A. Radasky, C. E. Baum, and M. W. Wik, "Introduction to the Special Issue on High-Power Electromagnetics (HPEM) and Intentional Electromagnetic Interference (IEMI)", IEEE Transactions on Electromagnetic Compatibility, Vol. 46, No. 3, pp. 312-321, August 2004.
2. Daniel Månsson, Rajeev Thottappillil and Mats Bäckström, "Propagation of UWB Transients in Low-Voltage Power Installation Networks", IEEE Transactions on Electromagnetic Compatibility, Vol. 50, No. 3, pp. 619-629, August 2008.
3. Y. V. Parfenov, L. N. Zdoukhov, W. A. Radasky, and M. Ianoz, "Conducted IEMI Threats for Commercial Buildings:, IEEE Transactions on Electromagnetic Compatibility, Vol. 46, No. 3, pp. 404-411, August 2004.

978-1-4244-5050-3/10/$26.00 ©2010 IEEE

Computation of Radar Cross Section (RCS) of a Finite Planar Sheet Using Surface Equivalence Principle and Multiple Network Theory (SEMN)

F. Tavakkol-Hamedani[1], A. Tavakoli[2], and M. Tivai[2]
[1]*The University of Semnan, Semnan, Iran*
[2]*Amirkabir University of Technology, Tehran, Iran*
E-mail: farzadtavakkol@gmail.com

RCS measurements have been considered in a wire antenna metal detector system [1]. Applying SEMN method, radar cross sections of a flat rectangular leaf and a flat rectangular metal plate are calculated by two approaches: electric field integral equation (EFIE) and magnetic field integral equation (MFIE). The numerical results are compared with each other and those of other theoretical methods. They exhibit excellent agreement with measurements.

Modeling of planar sheets is of significant importance in numerous electromagnetic problems including remote sensing of vegetation canopy [2]. A widely used model for thin dielectric layers is the resistive sheet model by which the sheet is modeled as an electric current sheet whose strength is proportional to the local tangential electric field via a single measurable quantity R (resistivity). On the basis of this model, physical optics and moment method approaches have been developed to analyze resistive strips and plates of arbitrary shapes [2]. Previously, SEMN method was introduced for the analysis of finite size microstrip structures [3, 4]. It is capable of precisely modeling all faces of a finite planar sheet including its edges.

Conclusions: Radar cross sections of a flat rectangular leaf and a flat rectangular metal plate are calculated by EFIE and MFIE approaches of SEMN method and are compared with each other, results of other theoretical methods and measurements as follows:

For E polarization, all theoretical methods have excellent agreement with measurements at lower incidence angles. Edges have larger effects on RCS values at higher incident angles. SEMN method is capable of giving more accurate results for the whole range of incident angles by utilizing sufficiently small segments for edges.

Using SEMN method for E polarization, EFIE gives better results compared to MFIE at grazing incidence ($\theta i = \pm 90°$). This is due to the existence of electric field excitation not only on edges but also on broad faces of the sheet (magnetic field excitation just exists on edges) at grazing incidence. This reduces the sensitivity of computed RCS values to the edge segments' sizes. For H polarization, except the physical optics method all other theoretical methods have excellent agreement to measurements over most of the angular range. This good agreement may be attributed to weak fields of edges for H polarization.

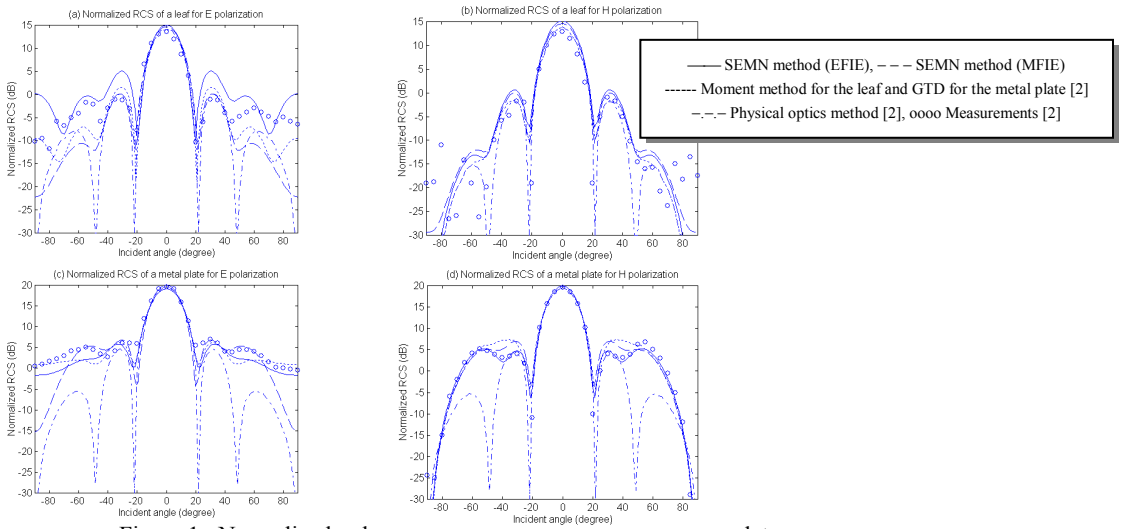

Figure 1: Normalized radar cross sections of a leaf and a metal plate

References

1. A. Ghaffari and F. Tavakkol-Hamedani, "Design of a Wire Antenna Metal Detector System," In *URSI 2007 North American Radio science Conference*, Ottawa, July 2007, No. 231.
2. K. Sarabandi, "Remote sensing of vegetation canopy, " Ph.D. Dissertation, The university of Michigan, Ann Arbor, 1989.
3. F. Tavakkol-Hamedani and A. Tavakoli, "Analysis of a thick finite microstrip antenna using surface equivalence principle and multiple network theory (SEMN)," In *Dig. IEEE AP-S Int. Symp.,* Atlanta, June 1998, pp. 1606-1609.
4. F. Tavakkol-Hamedani and A. Tavakoli "Analysis of a slot-coupled microstrip line coupler with finite size substrates using surface equivalence principle and multiple network theory (SEMN)," In *Proc. Symp. on Antenna Technology and Applied Electromagnetics*, Ottawa, pp. 169-172, Aug. 1998.

978-1-4244-5050-3/10/$26.00 ©2010 IEEE

Infrared Techniques for EM Field Imaging and Measurement

J-P. Parmantier*(1), F.Issac(2), F. Lemaître(1), J-L. Lasserre(2), A. Paupert(2)
M. Wilbanks (3), M. Harrison(1), H. Pohle(3)
(1) ONERA, 2 avenue Edouard Belin, 31055 Toulouse, France
(2) CEG (CEA-Gramat), 46500 Gramat, France
(3) AFRL/RDHE, 3550 Aberdeen Ave, KAFB, Albuquerque, NM 87117, USA
E-mail: jean-philippe.parmantier@onera.fr

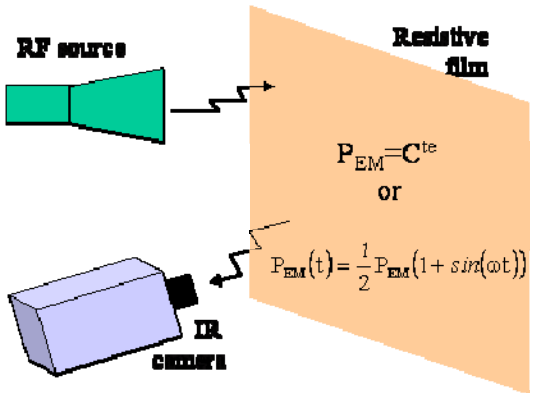

Figure 1 : Principle of measurement

ONERA and CEG plus AFRL have independently developed diagnostic techniques based upon the use of IR cameras to view the heating of thin, resistive films, such as carbon impregnated film (Kapton), that are illuminated with high power RF sources (Figure 1). The techniques employed by both groups acquire IR images of the film heating and data processing yields the incident tangent electric field at the film surface. The potential applications, in a 500 MHz to 300 GHz frequency range, are 1) measurement of the radiated field of high-power microve sources, 2) measurement of near-field antenna radiation patterns and 3) identification of EM leaks in shielded structures. In its multidisciplinary program CIRCE, ONERA is investigating improvements to the EMIR technique (D. Balageas and P. Levesque, Revue Générale Technique, 37, 1998, pp. 725-739) by proposing several candidate methods for post-processing the temperature increase of the film recorded by an IR camera. To obtain a simple relation between temperature variation and the tangent electric field depositing energy on the film, the technique must minimize the effects of convection. For short observation times, techniques based on integration or derivative analysis must face the problem of signal-to-noise ratio, whereas, for long observation times, techniques based on averaging cold and equilibrium levels generally face convection-induced errors. For CW sources, low-frequency modulation-demodulation based techniques (typically 1-2 Hertz) provide efficient ways to get rid of convection. For transient signals, short-time analysis techniques for times before convection effects appear are required. This is an important requirement for CEG and AFRL who are diagnosing the radiated fields of high-power RF sources. The three organizations performed a joint experiment in Jan 2010 to compare their complementary techniques based on the use of different IR cameras and different RF absorbing films. Results of cross comparison measurements carried out with a CW source and a transient, repetitive magnetron source will be presented. These will show the capabilities of the various post-processing techniques depending upon the type of application considered.

978-1-4244-5050-3/10/$26.00 ©2010 IEEE

A Compact Repetitive High Power Microwave (HPM) Source

V.G.Baryshevsky*†, A.E.Borisevich*†, A.A.Gurinovich*†, G.Yu.Drobyshev*, P.V. Molchanov*†, A.V.Senko*

*Research Institute for Nuclear Problems, 11 Bobruiskaya str., Minsk 220050, Belarus, e-mail:gur@inp.minsk.by

† Private Research and Production Company «Electrophysical Laboratory», 15 Smolenskaya Str., Minsk 220088,Belarus

HPM has emerged as a new technology allowing new applications and offering innovative approaches to existing applications.

An HPM source generates short high-power electromagnetic pulses able to disrupt or destroy electrical and electronic systems, which our society is rapidly becoming more and more depending on. The vulnerability of infrastructure (computers, communication systems, electronics of a car, etc.) is suspected, but not definitely known. Simulators and test facilities for evaluating the HPM affect on electronics could provide missing data and enable to study protection measures. A range of HPM sources from small, autonomous systems to large high power devices have been developed.

A compact repetitive HPM source is reported. Single or repetitive microwave pulses of 2 ns durations are generated by direct excitation of an antenna with a high-voltage generator. A compact 10-stage Marx generator produces 300 kV voltage pulses with the rise-time as short as 50 ns. The disk-cone antenna is oil-insulated and operates in the self-breakdown regime. Radiation frequency is within 800 MHz to 2 GHz range. The HPM source is used for studying vulnerability of computers and different electronic components.

978-1-4244-5050-3/10/$26.00 ©2010 IEEE

High Frequency Electromagnetic Field Coupling to Multi-Conductor Transmission Lines of Arbitrary Geometry

Jürgen Nitsch[1] and **Sergey Tkachenko**[1]
[1]*Otto-von-Guericke-University, Magdeburg, Germany, D-39106*
E-mail: sergey.tkachenko@ovgu.de

The necessity to consider electromagnetic field coupling with complex multi-conductor structures arises from the analysis of electromagnetic compatibility for a number of different objects: cars, ships, aircraft, and space apparatuses. For parallel conductors and relative low frequencies classical transmission-line theory (TL) can be applied [1]. However, for high frequencies, when this condition is no longer valid, and (or) in the case of the multi-conductor transmission lines consisting of non-parallel wires, the classical TL approximation is not applicable.

Different attempts were undertaken for the generalization of the TL approximation for high frequencies on the basis of the exact system of Mixed Potential Integral (-differential) Equations (MPIE) which are deduced from Maxwell's equations in the thin-wire approximation [2, 3]. These MPIE in turn can be reduced to a system of first order differential equations.

The focus of the present work ([4]) lays on the full-wave description of the electromagnetic interaction of multi-conductor transmission lines with arbitrary geometry. These lines are fed by lumped sources and terminated by lumped loads. Also the excitation by distributed sources (electromagnetic field excitation) is discussed. In order to cast the MPIE into a system of first-order differential equations for the unknown currents and potentials one has to solve integral equations for the per-unit-length parameter matrix which occurs as coefficient matrix in the first-order differential equations. The resulting equations are the extended telegrapher equations. Because there are no known general analytical solutions for these equations iterative or perturbation procedures are suggested which give very good results even after one iteration.

The position-dependent per-unit-length parameters become complex and frequency-dependent. The extended telegrapher equations with these parameters correctly model the propagation of electromagnetic waves along non-uniform multi-conductor transmission lines, the radiation of electromagnetic energy, and also the coupling of external fields for all frequencies. There is no restriction to the quasi TEM mode like in the classical transmission- line theory.

Acknowledgments – This work was sponsored by the German Research Foundation (DFG), Contract Number: NI633/5-1.

References

1. F. M. Tesche, M. Ianoz, and T. Karlsson, EMC Analysis methods and computational models. New York: Wiley Interscience, 1997.
2. F. Rachidi and S. Tkachenko (ed.), Electromagnetic Field Interaction with Transmission Lines: from Classical Theory to HF Radiation Effects. Southampton (UK), WIT Press, 2008.
3. J. Nitsch, F. Gronwald, G. Wollenberg, Radiating Nonuniform Transmission-Line Systems and the Partial Element Equivalent Circuit Method. New York: Wiley Interscience, 2009.
4. J. Nitsch and S. Tkachenko, "High-Frequency Multiconductor Transmission-Line Theory", Interaction Notes, Note 611.

978-1-4244-5050-3/10/$26.00 ©2010 IEEE

Radiation from an Axial Electric Dipole Located on an Oblate Spheroid Made of Non-isoimpedance DNG Metamaterial

Piergiorgio L. E. Uslenghi
Department of ECE, University of Illinois at Chicago, USA
uslenghi@uic.edu

An oblate spheroid made of DNG metamaterial is considered. The material is linear, homogeneous and isotropic, with a real negative refractive index that is opposite in sign to the refractive index of the surrounding space. The intrinsic impedances of the spheroid and of the surrounding space are both real positive, but not necessarily equal to each other. The primary source is an electric dipole located outside the spheroid, on the axis of symmetry of the spheroid, and axially oriented. The analysis of radiation from such a structure is conducted in phasor domain with time-dependence factor $\exp(-i\omega t)$.

The primary and secondary fields outside the spheroid and the total field inside it are expanded in infinite series of oblate spheroidal wave functions whose modal coefficients are determined analytically by imposing the boundary conditions across the surface of the spheroid. The explicit determination of the coefficients is possible because the angular oblate spheroidal wave functions are independent of the sign of the refractive index. The notation for the spheroidal functions is that of Flammer (*Spheroidal Wave Functions*, Stanford University Press, 1957).

The far field outside the spheroid is analyzed in detail in order to determine the influence of both geometry (size and eccentricity of the spheroid, location of the primary source) and material (ratio of the intrinsic impedance of the spheroid to that of the surrounding space) on the field pattern. The particular cases of a sphere and of a very flat spheroid (almost a disk) are studied in detail.

978-1-4244-5050-3/10/$26.00 ©2010 IEEE

Evaluation of Imaging Algorithms for Prototype UWB Microwave Tomography Systems

J. LoVetri, **P. Mojabi**, **A. Zakaria**, and **C. Gilmore**
Dept. of Electrical and Computer Engineering, University of Manitoba
Winnipeg, Manitoba, Canada R3T 5V6
E-mail: Joe_LoVetri@UManitoba.Ca

In recent years, several state-of-the-art microwave tomography (MWT) inversion algorithms applicable to biomedical imaging have been developed and well described in the literature [1, 2]. Most have been evaluated and compared on synthetically generated scattered field data where various amounts of noise are added so as to avoid an 'inverse crime'. Comparatively few have been evaluated using data obtained from experimental MWT systems [5]. When uniformly distributed noise is added to synthetically generated data, the imaging results obtained using different algorithms do not necessarily reflect the performance that will be achieved when those same algorithms are used on experimentally generated data. This is because the modelling error, which is the error in the electromagnetic system model being used in the algorithm to approximate the actual physical system, is not well modelled by adding uniformly distributed noise to the synthetically generated data. As such, the performance of the various algorithms is best evaluated on experimentally generated data.

Recently, we've developed several MWT prototypes to study their application to biomedical imaging. One is an ultra-wideband MWT system using a plexiglas enclosure with 24 co-resident vivaldi antennas being used to acquire scattered field data in the microwave frequency range of 1 to 6 GHz [3]. The second type of MWT prototype uses a conductive enclosure with co-resident monopole antennas to collect the scattered field data [4, 6].

We present imaging results using scattered field data obtained from these MWT prototypes and evaluate various state-of-the-art inversion algorithms and regularization schemes. The algorithms are based on either the Gauss-Newton Inversion or the Contrast Source Inversion. We test different multiplicative and additive regularization techniques as well as different calibration methods. The regularization techniques are used to deal with the ill-posedness of the inverse problem while the calibration methods are used to diminish the modelling error. The MWT system model can be based either on integral equation formulations or partial differential equation formulations. Both are examined and it is shown how the latter can be discretized using the finite-element method leading to more accurate system models which take into account the details of the geometry of the actual MWT system, including the antennas. The goal is to evaluate these techniques as applied to the microwave tomography prototypes being developed. The evaluation is based on image reconstruction accuracy, resolution, and the computational resources required for the inversion.

References

[1] A. Abubakar, P. M. van den Berg, and S. Y. Semenov. Two– and three– dimensional algorithms for microwave imaging and inverse scattering. *Journal of Electromagnetic Waves and Applications*, 17(2):209–231, 2003.

[2] A. E. Bulyshev, A. E. Souvorov, S. Y. Semenov, V. G. Posukh, and Y. E. Sizov. Three dimensional vector microwave tomography: Theory and computational experiments. *Inverse Problems*, 20:1239–1259, 2004.

[3] C. Gilmore, P. Mojabi, A. Zakaria, M. Ostadrahimi, C. Kaye, S. Noghanian, L. Shafai, S. Pistorius, and J. LoVetri. A wideband microwave tomography system with a novel frequency selection procedure. *To appear IEEE Trans. Biom. Eng.*, 2010.

[4] P. Mojabi, C. Gilmore, A. Zakaria, and J. LoVetri. Biomedical microwave inversion in conducting cylinders of arbitrary shapes. In *Antenna Technology and Applied Electromagnetics and the Canadian Radio Science Meeting, 2009. ANTEM/URSI 2009. 13th International Symposium on*, pages 1–4, Feb. 2009.

[5] T. Rubaek, P. M. Meaney, P. Meincke, and K. D. Paulsen. Nonlinear microwave imaging for breast-cancer screening using Gauss-Newton's method and the CGLS inversion algorithm. *IEEE Trans. Antennas Propag.*, 55(8):2320–2331, Aug 2007.

[6] A. Zakaria, C. Kaye, I. Jeffrey, and J. LoVetri. Experimental validation of thin-wire FVTD models. In *Antenna Technology and Applied Electromagnetics and the Canadian Radio Science Meeting, 2009. ANTEM/URSI 2009. 13th International Symposium on*, pages 1–4, Feb. 2009.

978-1-4244-5050-3/10/$26.00 ©2010 IEEE

Dual Vibrating Intrinsic Reverberation Chambers for High-Dynamic Range Shielding Effectiveness Measurements

J. Schipper[1], R. Serra[1], and **F.B.J. Leferink[1,2]**
[1]*THALES Netherlands, Hengelo, The Netherlands*
[2]*University of Twente, Enschede, The Netherlands*
E-mail: leferink@ieee.org

A test setup is described using two small Vibrating Intrinsic Reverberation Chambers (VIRCs) with a common wall. A Device Under Test (DUT) can be mounted in this common wall, by means of standard hatches. The electromagnetic fields are stirred by moving the walls of both VIRCs. The walls can be moved by means of a simple motor with a crankshaft and rubber strings.
A previous setup with one conventional reverberation chamber and a VIRC was described in [1]. The VIRC has a major advantage over conventional mode stirred chambers, because the modes are changed much better at lower frequencies, and they are changed faster. Therefore the combination of two movable small VIRCs is developed. A picture of the test setup is shown in Figure 1.
The two small VIRCs are made of copper cladded cloth that is sewn together, creating two boxes. These two boxes are mounted in two metal frames by means of spiral springs. On one end, both boxes are ending on a metal plate. One of the metal plates contains a standard hatch that normally is used in the wall between the control room and anechoic room of the EMC measurement facility. The other plate contains a knife-edge that fits the hatch of the first VIRC. The hatch is used to mount the DUT.
The Q-factor of both VIRCs is this high that only a moderate input power level is needed to create high level field strengths inside VIRC 1, using a broadband microwave horn antenna. The shielding of both VIRCs is high and therefore small signal levels can be detected in VIRC2. This means that High Dynamic Range Shielding Effectiveness Measurements can be carried out by means of this setup. As an example, only the output power of a (scalar) network analyzer is sufficient for achieving over 100dB dynamic range.

Figure 1: Dual VIRC test setup

The shielding effectiveness of many samples has been measured , e.g. :

- Composite boxes with metallic loading
- Several metalized fabrics

The test setup will be presented and several test results will be shown.

References

1. J. Schipper, M. Melenhorst, F.B.J. Leferink, Dual Reverberation Chambers for High-Dynamic Range Shielding Effectiveness Measurements, EUROEM 2008, Lausanne.
2. F.B.J. Leferink, W.C. van Etten, Optimal Utilization of a Reverberation Chamber, 4th European Symposium on Electromagnetic Compatibility, Brugge, 2000, pp. 201-206

978-1-4244-5050-3/10/$26.00 ©2010 IEEE

An Efficient Macromodel for Calculating Induced Overvoltages on Transmission Lines Caused by Lightning Radiated Electromagnetic Fields

Sina Mashayekhi, **Behzad Kordi**, and **Greg E. Bridges**
Department of Electrical and Computer Engineering, University of Manitoba, Winnipeg, MB, Canada
E-mail: sina@ee.umanitoba.ca, bkordi@ee.umanitoba.ca, bridges@ee.umanitoba.ca

Calculation of induced overvoltages on transmission lines is critical for the purpose of design, protection and maintenance of equipment connected to power transmission networks. A typical cause of overvoltages is due to external sources of energy such as lightning radiated electromagnetic fields which are capable of inducing overvoltages in the range of kilo-volts. In circuit model, the effect of external electromagnetic fields appear as distributed current and voltage sources along the transmission line which are determined by field-to-line coupling models [1]. By integration of these sources along the line, the distributed sources, can be replaced by two controlled sources at the terminals of the line and the problem can be analyzed as an unexcited line. This has already been done for uniform plane wave excitation of line, where the only effect of propagation of the radiated field is delay [2]. However, this is not true for the case of non-uniform wave excitation and knowledge of the electromagnetic fields at every point on the line is required. This is time consuming and impractical for fast and efficient calculation of lightning induced overvoltages. In this paper, a fast and efficient time-domain macromodel for calculating the effect of non-uniform radiated electromagnetic fields of lightning return stroke channel (RSC) is presented. The transfer function of the macromodel is extracted first where the channel-base current and electric field along the transmission line are the input and output, respectively. This transfer function is then approximated by poles and residues using the Vector Fitting algorithm [3]. The variation of poles and residues is interpolated as the observation point moves along the line, enabling us to calculate the electromagnetic fields at any arbitrary point. Finally, the distributed sources, whose variation with position along the line has been determined, are integrated and lumped at the terminals of the transmission line. This gives us the ability to use already-developed transmission line models available in commercial circuit simulators. The proposed procedure is capable of incorporating the results of frequency-domain approaches, such as those obtained by NEC, with those working in the time-domain such as PSCAD/EMTDC.
An example of a frequency-dependent overhead transmission line over a lossy ground is shown in Fig. 1.a. In this figure, the RSC is represented by a monopole antenna and the line is excited by a non-uniform electromagnetic field radiated by this channel. Fig. 1.b represents the equivalent circuit model that includes controlled current and voltage sources placed at the terminals of transmission line representing the integration of distributed sources. In this case the line is considered as an unexcited line. In each time step, these dependant sources are updated using the algorithm developed in this work. The effect of different parameters such as finite conductivity of the ground, channel length and propagation velocity along the RSC are considered in this macromodel.

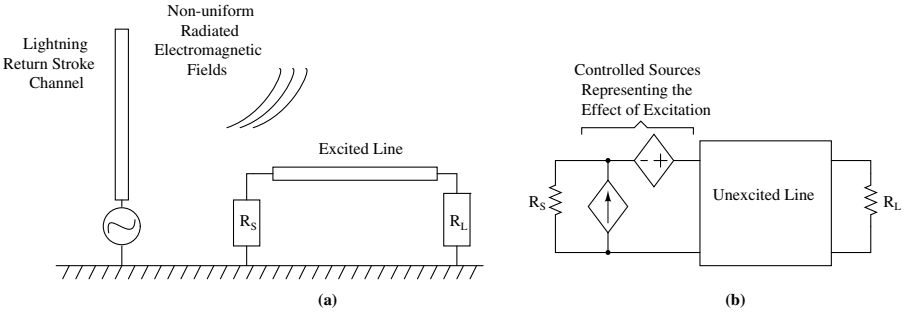

Figure 1: **a) Excited transmission line, b) Equivalent circuit representation**

Acknowledgements – Support from Manitoba Hydro and MITACS is acknowledged.

References

1. M. Paolone, F. Rachidi, A. Borghetti, C. A. Nucci, M. Rubinstein, V. A. Rakov, and M. A. Uman, "Lightning Electromagnetic Field Coupling to OverheadLines:Theory, Numerical Simulations, and Experimental Validation," IEEE Transactions on Electromagnetic Compatibility, Vol. 51, No. 3, August 2009, pp. 532-537.
2. G. S. Shinh, N. M. Nakhla, R. Achar, M. S. Nakhla, A. Dounavis, and I. Erdin, "Fast transient analysis of incident field coupling to multiconductor transmission lines," IEEE Transactions on Electromagnetic Compatibility, Vol. 48, No. 1, February 2006, pp. 57-73.
3. B. Gustavsen and A. Semlyen, "Rational approximation of frequency domain responses by vector fitting," IEEE Transactions on Power Delivery, Vol. 14, No. 3, July 1999, pp. 1052-1061.

978-1-4244-5050-3/10/$26.00 ©2010 IEEE

MR Coil Array Engineering for Clinical Applications

M. Fallah-Rad, H. Zhu, W. Schellekens, L. Petropoulos
IMRIS Inc., Winnipeg, MB, Canada

Abstract: Advance developments in Magnetic Resonance (MR) phased array coils as well as parallel image processing techniques have led to more complex MR coils with higher number of channels. MR coils (Fig. 1) are used to image local areas on the body such as the head/neck, cardiac, torso, etc. Typical available commercial coils at field strengths of 1.5T or 3T have anywhere between 4 to 128 channels available for imaging. The higher number of channels provide better signal to noise ratio (SNR) with higher acceleration factors which, leads to reduce scan times for the patients. As a result of an increase in the number of channels, the circuits have become more complex with far more electronic components and cables. This in turn has made the design and optimization process more challenging due to different factors such as space limitations, the coupling between components and coil elements, as well as possible instabilities caused by the pre-amps within the coil array. The coupling and instabilities can significantly deteriorate the SNR (lower image quality) and in extreme cases the scanned images are not readable. In addition to image quality, heating produced by the induced currents as a results of high RF transmit power during scanning are a cause for patient safety concerns. The temperature of coils can not exceed the specified standard limits.

Fig. 1 Split Array Head Coil

In this paper the basic design principles for MR coils are presented. Coil design techniques including coil tuning, and active/passive decoupling circuits are discussed. The active/passive decoupling circuits are a safety measure to protect the electronics in the MR receive coils from large amounts of induced currents caused during the RF transmit cycle of a sequence. This also prevents localized heating of the coils and coupling of the RF power to the examined subject. Other topics covered include the pre-amplifier decoupling circuits [1,2] along with their benefits in MR phased array coils. Methods of increasing coil Q factor are shown along with measured SNR values at 1.5T and 3T field strengths. Different element decoupling techniques are discussed with the pros and cons. Cable traps and other shielding techniques that are used to reduce the shield currents and prevent localized heating are presented. Finally, different types of MR coils for a variety of clinical applications such as Cardiovascular, Neurosurgical, and MR Guided radiation therapy are shown along with images obtained at different magnetic field strengths.

[1] P.B. Roemer, W. A. Edelstein, C. E. Hayes, S. P. Souza, O. M. Mueller; “The NMR Phased Array”, Magnetic Resonance in Medicine, 16, 192-225 (1990)

[2] A. Reykowski, S. M. Wright, J. R. Porter; “Design of Matching Networks for Low Noise Preamplifiers”, Magnetic Resonance in Medicine, 33, 848-852 (1995)

978-1-4244-5050-3/10/$26.00 ©2010 IEEE

Influence of the Observation Point Elevation upon the Vertical Component of the Electric Field at 2 km away due to Inclined Lightning to a Tall Structure

Ivan Boev[1], Wasyl Janischewskyj[1], Farhad Rachidi[2], and **Volodymyr Shostak[3]**
[1]*University of Toronto, Dept. of Electrical and Computer Engineering, Toronto, Canada*
[2]*Swiss Federal Institute of Technology, EPFL, EMC Group, Lausanne, Switzerland*
[3]*National Technical University of Ukraine, Kyiv, Ukraine*
E-mail: ivan.boev@utoronto.ca

In the presented theoretical study, the influence of the measuring equipment elevation above ground level upon the observed vertical component of the electric field due to lightning to a tall structure is analyzed. The developed model includes an approximation of the current waveform at any time and at any height along the lightning current path, including the lightning channel and the bottom part represented by the CN Tower. It is based on the Modified Transmission Line Model with exponential decay (MTLE) [1-2], and takes into account the presence of the tall structure. In particular the five section model described in [3] is used and the injected current is represented by a Heidler function [4]. The expression used to describe the vertical component of the electric field was derived in Cartesian coordinates [3]. Taking advantage of the flexibility to work in 3-D plane, the lightning channel (straight lightning channel is used in this study) is allowed to assume any inclined position in the range from 0 to 90º with respect to the base case involving straight vertical lightning channel attached to the top of the CN Tower. The projection of the inclined lightning channel onto the horizontal x-y plane is allowed to assume any angle in the whole range from 0 to 360º. Under these conditions the vertical component of the electric field due to lightning to the CN Tower is calculated at 2 km away, on ground level and also at 50 m above ground level. The calculated peak values for various channel inclinations and rotations are summarized in respective graphs and compared for the ground level observation point cases and for the 50 m above ground level observation cases. Conclusions are drawn based on the produced calculation results. General comparison to actual records is also elaborated upon.

References

1. Nucci, C. A., C. Mazzetti, F. Rachidi, and M. Ianoz, “On lightning return stroke models for LEMP calculations”, paper presented at 19th international conference on lightning protection, Graz, May 1988.
2. Rachidi, F., and C. A. Nucci, “On the Master, Uman, Lin, Standler and the Modified Transmission Line lightning return stroke current models”, Journal of Geophysical Research, 95, 20389-20394, 1990.
3. I. Boev, W. Janischewskyj, “Calculation of electric and magnetic fields at the CN Tower in cartesian coordinates,” Presentation, MOCA-09, the IAMAS-IAPSO-IACS 2009 Joint Assembly, Montréal, Québec, Canada, July 27, 2009.
4. F. Heidler, J. M. Cvetic, B. V. Stanic, “Calculation of lightning current parameters,” IEEE Trans. On Power Delivery, vol. 14, no. 2, pp. 399–404, Apr. 1999.

978-1-4244-5050-3/10/$26.00 ©2010 IEEE

Compressive Sensing for Ultra-wideband Through-the-Wall Imaging Radar

Wenji Zhang, Moeness G. Amin, Fauzia Ahmad, Ahmad Hoorfar, and Graeme E. Smith

Radar Imaging Lab, Center for Advanced Communications, Villanova University,
800 Lancaster Ave, Villanova, PA 19085, USA
E-mail:wenji.zhang@villanova.edu

An ultra-wideband through-the-wall imaging radar (TWIR) system images the targets behind the wall by transmitting short pulses and processing the reflected signals by applying appropriate time delays at the different antennas followed by coherent summation. In order for a TWIR to achieve high resolution in both down-range and cross-range, an ultra-wideband signal needs to be transmitted and a long array aperture should be synthesized. This results in a large number of space-time/space-frequency data samples, leading to long data collection and processing times as well as a large storage memory requirement. The emerging theory of compressive sensing (CS) allows a signal/image which is sparse or has a sparse representation in some basis to be captured from a small number of random non-adaptive linear projections onto the measurement basis. The capability of CS to reconstruct a sparse signal from far fewer measurements than required by Nyquist provides a new perspective for data reduction in radar imaging without compromising the imaging quality.

There have been several approaches that apply CS for radar imaging. Most of these compressive radar imaging algorithms are discussed in the framework of stepped-frequency continuous-wave (SFCW) radar [1-2]. As a viable alternative to SFCW radar, the impulse radar is commonly used for subsurface and through-the-wall imaging applications due to its ability to provide high resolution imaging for improved target detection and classification. In order to improve the imaging quality while significantly reducing the number of measurements, the impulse radar based through-the-wall imaging problem is cast into the framework of compressive sensing and solved by the sparse constraint optimization. By employing the point target model, a linear relation between the received signal and the target space is obtained and represented in vector-matrix form. The matrix in the linear equation is the dictionary for the impulse radar based through-the-wall imaging problem. For the compressive TWIR system, instead of measuring the time domain returned signal at the Nyquist rate, linear projections of the returned signals with random ±1 sequences, called random modulation pre-integration (RMPI) architecture in [3], are used to reduce the number of CS measurements below the conventional Nyquist sampling, without any noticeable degradation of the image quality.

In order to show the effectiveness of the proposed approach for ultra-wideband or impulse radar in through-the-wall applications with compressive sensing, we present the following simulation example. Three point targets are located at (-0.05m, 0.5m), (-0.05m, 0.45m), and (0, 0.5m. Fig.1 shows the imaging result obtained using the standard time domain backprojection algorithm, which corresponds to the minimum energy solution (L_2 norm). is The imaging result using the non-adaptive projection measurement and L_1 constraint optimization is depicted in Fig. 2. From these two figures, it is evident that by using the proposed compressive impulse TWIR, we not only improve the imaging resolution in the cross-range and down-range, but also obtain much less cluttered imaging result. It is important to note that for the CS imaging result in Fig. 2, only 20 samples at each antenna location was used, while for the conventional beamforming result in Fig. 1, 600 samples per antenna location are needed, which is a very welcome reduction in data acquisition and processing time.

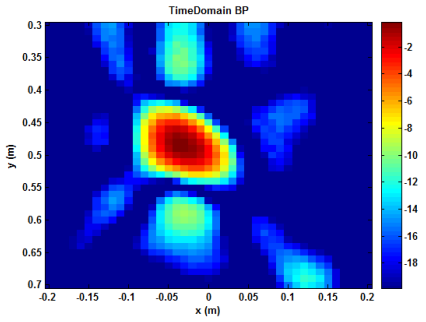

Fig.1 Time Domain BP imaging result

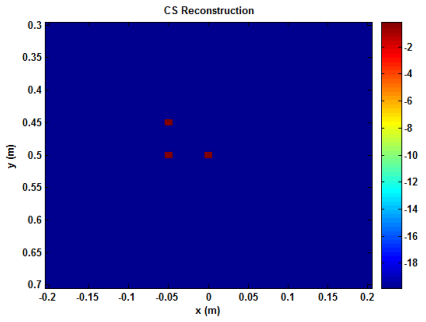

Fig.2 CS Reconstruction Result

References

[1] Y. Yoon, M. G. Amin, "Compressed sensing technique for high-resolution radar imaging," in Proc. SPIE Signal Processing,Sensor Fusion, and Target Recognition XVII Conference, vol. 6968, pp. 69681A-69681A-10, 2008.
[2] A. C. Gurbuz, J. H. McClellan, W. R. Scott, "A compressive sensing data acquisition and imaging method for stepped frequency GPRs," IEEE Trans. on Signal Processing, vol. 57, pp. 2640-2650, 2009.
[3] A. C. Gurbuz, J. H. McClellan, W. R. Scott, "Compressive sensing for subsurface imaging using ground penetrating radar," Signal Processing, vol.89, pp. 1959–1972, 2009.

978-1-4244-5050-3/10/$26.00 ©2010 IEEE

Millimetre-Wave Extra Low Radiation Measuring System for Environment and Biomedical Applications

Yaroslav Savenko [1], Volodymyr Vodotovka [2] and Fedir Repa [1]
1 – National Technical University of Ukraine "Kiev Polytechnic Institute"
2 – Kyiv National University of Technology and Design

E-mail: yaroslav_savenko@ieee.org

This paper reports results of the research work on development of techniques and devices for measuring of extra low radiation in mm-range. There are considered basic engineering aspects of measuring extra low mm-range radiation in the paper. It is also described an original measurer that helps researchers to get more clear understanding about environment physics and biomedical physiology, how low energy mm-range radiation interacts with human organism. Certain applications have been proposed for the measurer as for testing calibrating and diagnostic devices.

Analytic review of using a millimeter-wave radiation in medical practice has shown that are positive effects for clinical application of millimeter-wave medical systems. But such systems have no unique methodological principals of its development and application. Solution of such problem has been obtained as result of: experimental investigation of information interaction mechanisms on biological and physical levels; analytic review and systematization of techniques for diagnostics and therapy in millimeter range exactly according to confirmed mechanisms of information interaction on physical and biological levels; analytic review and systematization of engineering solution, which are used in medical therapeutic-diagnostic practice; realization of all side metrological inspection of used systems.

It has been proposed a cell model for investigation of millimeter-wave microinteraction and propagation mechanisms on cell level. It represents parallel-serial nets of complex wave impedance. Cell membrane has been represented by capacitive component, which is determined as a property of membrane itself and membrane potential as well. Intracellular liquid is represented by inductive component. Intracellular bodies have been represented similar to cell as membrane and intracellular bodies of more low levels.

It has been proposed an original model for physical model remote sensing measurement system as result of analytic review of MMW instrumentation techniques for diagnostic application. Proposed measuring system consists of subsystem of reflected or/and self radiation scanning and subsystem of hardware-software processing scanned data from the object. Subsystem of hardware-software scanned data processing consists of multichannel correlation receiver, receiver to PC junction and program of analyzing and indication of scanning results

There was the main problem, that it was required to measure radiation at the noise level and even lower him. That is why the main task had been decided how these measurements must be provided. An original measurer was developed for investigations above mentioned. Self-radiation of human organism amounts $10^{-21}...10^{-22}$ W/Hz. Measuring of this level of radiation requires the development of special techniques and devices. It has been proposed original device.

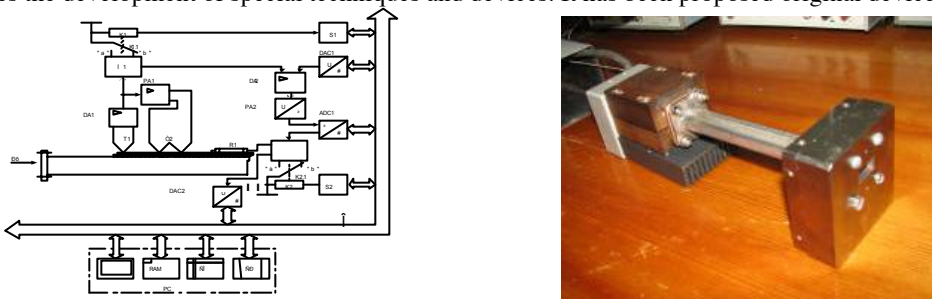

Fig. 1. Measurer of extra low mm-range radiation.

Main part of hardware system is multichannel correlation receiver, where it is operated correlation comparison of test signals and signals obtained during scanning process. Test signals are obtained previously for certain conditions of certain object and they are saved as special test data. Results of computer modelling of biological cell for investigation of biophysical properties in millimetre-wave monitoring system have been used as test data.

The measurer helps researchers to get more clear understanding about environment and biomedical physics, in particular, how low energy mm-range radiation interacts with human organism. In medical practice it could be used as diagnostic device and calibrating unit of therapeutic low energy mm-range device as well. In conclusion we must determine that getting of regulate statistic data of medical engineering investigations at different levels of complexity from a cell to a whole organism will be the next step in the way to make clear understanding about the role of low energy mm-range EMW in human life.

978-1-4244-5050-3/10/$26.00 ©2010 IEEE

Space-Time Focusing Transmission For UWB Networks

Yafei Tian and Chenyang Yang
School of Electronics and Information Engineering, Beihang University,
Beijing, China, 100191
E-mail: ytian@buaa.edu.cn, cyyang@buaa.edu.cn

Impulse-radio ultra-wideband (IR-UWB) signals have large bandwidth, which can resolve a large number of multipath components in densely scattered channels. For communication links connecting different pairs of users, the correlation between their multipath channel coefficient vectors are weak even when the users locate very close. Exploiting these characteristics, space-time focusing transmission using time-reversal (TR) prefiltering was proposed in IR-UWB communications [1-3], which can focus the signal energy to a specific time instant and geometrical position. This can dramatically simplify the receiver design.

TR prefiltering is the simplest way to implement space-time focusing transmission, whose performance depends on the auto-correlation and cross-correlation of the channel responses. When channel information of other users are known, advanced preprocessing algorithms based on the zero-forcing (ZF) and minimum-mean-square-error (MMSE) criteria can be employed to further reduce the multiuser interference. Exploiting the low duty-cycle feature of UWB signals, only the interference at the sampling time instant should be suppressed, this significantly reduces the receiver complexity.

In *ad hoc* networks with randomly distributed nodes, each user only knows its own channel information, therefore TR prefiltering is a natural way to implement space-time focusing transmission. In *ad hoc* networks, TR-UWB systems essentially use a combined random time-division and random code-division multiple access scheme. The random propagation delay of the low duty-cycle signal leads to a random accessing time, and the random multipath response of the communication link induces a random "spreading code". The cochannel interference has a random power and occupies fraction of the frame length. The performance of the desired user degrades only when its focusing peak collides with interference signals meanwhile the aggregate interference power exceeds its desired tolerance. Large number of multipath components bring high "spreading gain", but may also lead to large collision probability.

To understand the potential of using TR transmission in UWB *ad hoc* networks, we study the achievable spatial user density considering these two conflicting factors. We first derive the power distribution of the aggregate interference in AWGN and multipath channels, and then investigate the collision probability between the desired focusing peak signal and interference signals. The outage probability is finally obtained considering both the impact of interference power and the impact of collision probability. After introducing some approximations, we can obtain the upper and lower bound of the achievable spatial user density. Analysis results reveal the connections between the achievable spatial user density and various system and channel parameters such as antenna gain, frame length, path loss factor, and multipath delay spread, which provide design guidelines for IR-UWB *ad hoc* networks.

To extend the coverage of UWB communications, we consider to use parallel relay networks where a source node tries to transmit information to a destination node through multiple relays. To reduce the multiuser interference and simplify the receiver design, space-time focusing preprocessing is employed in each node both at the broadcast (BC) and multiple-access (MA) phase. Since joint synchronization among the relay nodes is hard to be implemented, we propose to transmit independent streams from different relays to the destination. With each stream has a lower transmission rate, the coverage can be extended just as with the joint energy focusing scheme.

In BC mode, the source transmits multiple streams to different relays using pre-MUD schemes, where ZF and MMSE preprocessors can be employed. In MA mode, each relay forwards its stream to the destination employing pre-EQU algorithms. With the growing of the number of relays, both the interference among BC links and the collision among MA links will increase. Theoretical analysis and numerical results on network throughput indicate that there exists an optimal relay number to maximize the network throughput, and the simple TR scheme only performs well in few relay nodes and low-rate scenarios.

References

1. H. T. Nguyen, I. Z. Kovcs, and P. C. F. Eggers, "A time reversal transmission approach for multiuser UWB communications," *IEEE Trans. Antennas Propagat.*, vol. 54, pp. 3216–3224, Nov. 2006.
2. N. Guo, B. M. Sadler, and R. C. Qiu, "Reduced-complexity UWB time-reversal techniques and experimental results," *IEEE Trans. Wireless Commun.*, vol. 6, pp. 4221–4226, Dec. 2007.
3. C. Zhou, N. Guo, and R. C. Qiu, "Time-reversed ultra-wideband (UWB) multiple input multiple output (MIMO) based on measured spatial channels," *IEEE Trans. Veh. Technol.*, vol. 58, pp. 2884–2898, July 2009.

978-1-4244-5050-3/10/$26.00 ©2010 IEEE

An Overview of Multiuser Interference-Sensing Concepts and Receiver Designs

David J. Young and **Norman C. Beaulieu**
iCORE Wireless Communications Laboratory,
Department of Electrical and Computer Engineering
University of Alberta, Edmonton, Canada, T6G 2V4
E-mail: {djyoung,beaulieu}@ece.ualberta.ca

Ultra-wideband (UWB) wireless communication systems have seen much research interest and industrial activity. One class of UWB systems uses time-hopped (TH) impulse-radio signaling [1, 2], in which ultra-short pulses are transmitted at baseband. Such systems typically use a repetition code, by which a number of pulses are used to transmit one source symbol. They are also characterized by low duty-cycle transmission, with transmitted signal energy occupying only a small fraction of the available transmission time. In applications where several UWB devices are located at close range, multiple-user interference (MUI) can impair uncoordinated TH-UWB transmissions, and mitigation of MUI becomes an important element in TH-UWB receiver design.

It has been established that the MUI in TH-UWB systems is impulse-like and poorly approximated by a Gaussian distribution [3]. Therefore, conventional matched filter (CMF) receiver designs, which are optimal for Gaussian noise, are not fully efficient for UWB applications. Alternative models for MUI-plus-Gaussian noise, with associated receiver designs, are reviewed and compared. These receivers apply a transformation to the partial decision statistics (PDSs) formed by correlating each received pulse with a template at the receiver [3]. The most effective receivers adapt the transformation to the additive Gaussian noise and MUI environment. Multipath propagation is abundant in UWB channels [4], and is exploited by a Rake receiver. Since the CMF-based Rake receiver is likewise inefficient for TH-UWB applications, Rake structures utilizing these receiver designs apply nonlinear transformations to the PDSs formed by correlating each pulse in each finger with a template pulse.

Recently, novel TH-UWB Rake receiver structures have been designed that instead aim to sense the presence of MUI in each PDS. An overview of this MUI-sensing concept, and accompanying receiver structures, is given. The concept is motivated by considering the probability density function of a PDS after conditioning on an interference-sensing (IS) statistic, for a simplified scenario. Connections to diversity combining problems in other radio systems are also considered. The proposed IS techniques do not rely on assumptions about the distribution of the aggregate interference process, or knowledge of interferer timing or hopping codes, but utilize the low duty-cycle property of the TH-UWB system and the impulse-like nature of the transmitted pulses.

Two methods have been developed to perform the sensing. The first method responds to the presence of mistimed pulses due to interfering users, and provides MUI-sensing for each repeated pulse (frame) of the transmitted symbol, in each Rake finger. Alternative implementations are provided, one that uses a novel correlator design, and another that repurposes receiver synchronization components. The second IS method utilizes the presence of distinctive multipath channels for each transmitting user and provides MUI-sensing at the frame level using alternate Rake finger combining weights. Both methods yield an output signal that is correlated with signals from interfering users but uncorrelated with the desired-user signal.

Due to the repetition code and multipath propagation, a Rake receiver has many PDSs available for use in forming a symbol decision, and effectively is a diversity system. Therefore, receivers have been developed that use IS in selection of the best PDSs for combining, that is, PDSs less likely to be catastrophically corrupted by a pulse due to an interfering user. Receivers have also been developed that employ interference estimates based on IS to alter the weights used to combine PDSs in forming a decision statistic, in order to de-emphasize PDSs that may have experienced corruption. These techniques improve performance when MUI is significant. Also considered are non-linear receiver structures following from the receivers presented in [3]. In these structures, MUI-sensing is used to tailor the nonlinear function applied to each PDS, or select a subset of PDSs to undergo nonlinear processing. By this approach, PDSs which are potentially MUI-corrupted benefit from an appropriate nonlinear transformation, while Gaussian noise performance is improved due to linear or near-linear treatment of the remaining PDSs. Performance is thus superior to that of the underlying receiver structure. Bit-error rate and complexity comparisons for the proposed structures are provided.

References

[1] M. Z. Win and R. A. Scholtz, "Impulse radio: how it works," *IEEE Commun. Lett.*, vol. 2, no. 2, pp. 36–38, Feb. 1998.

[2] ——, "Ultra-wide bandwidth time-hopping spread-spectrum impulse radio for wireless multiple-access communications," *IEEE Trans. Commun.*, vol. 48, no. 4, pp. 679–689, Apr. 2000.

[3] N. C. Beaulieu and D. J. Young, "Designing time-hopping ultrawide bandwidth receivers for multiuser interference environments," *Proc. IEEE*, vol. 97, no. 2, pp. 255–284, Feb. 2009.

[4] A. F. Molisch, J. R. Foerster, and M. Pendergrass, "Channel models for ultrawideband personal area networks," *IEEE Wireless Commun. Mag.*, vol. 10, no. 6, pp. 14–21, Dec. 2003.

978-1-4244-5050-3/10/$26.00 ©2010 IEEE

2010 14th International Symposium on Antenna Technology and Applied Electromagnetics [ANTEM] and the American Electromagnetics Conference [AMEREM]

Transceiver Design for Multiuser Broadcast in Pre-Rake UWB Communication

– Invited Paper –

Zahra Ahmadian, **Michael B. Shenouda**, and **Lutz Lampe**
University of British Columbia, Vancouver, Canada
E-mail: zahraa, shenouda, Lampe@ece.ubc.ca

Introduction: Ultra-wideband (UWB) technology is suited to be used as physical layer in low-cost, low-power, short-range, and high-capacity wireless communications links. However, the widespread adoption of UWB is hampered by the relatively high receiver complexity. Therefore, it is desirable to move computational complexity to a few dedicated devices, deployed at network base stations, data fusion centers, etc., and keep the receivers, integrated into peripherals, sensor devices, etc., simple. This can be accomplished by pre-rake UWB systems, in which rake combining is performed at the transmitter rather than at the receiver. The major drawback with pre-rake combining scheme is the remaining inter-symbol interference (ISI) experienced at the receiver, which can result in high error floors. One approach to reduce these error floors is the combination of pre-rake combining and pre-equalization at DS-UWB base stations equipped with multiple antennas [1].

Approach: We consider the design of *multiuser* UWB systems that enable high data rate communications for short-range wireless applications. In particular, we consider the downlink of a direct sequence UWB (DS-UWB) system in which the base station is equipped with multiple antennas and employs pre-rake combining, while each user employs a simple single antenna receiver. We propose the use of *multiuser* filters for the purpose of pre-equalization at the transmitter in order to mitigate the combined effects of ISI *and* multiuser interference (MUI) that are generated at the receivers as a result of the wideband nature of the users' channels. For this system, we have studied the joint design of the transmitter's pre-equalization filters (PEF) and each receiver's scalar gain that minimizes the total transmitted power from the base station subject to achieving physical layer quality of service requirements of the users [2]. We have shown that the calculation of the pre-equalization filters and the receiver gains can be formulated as an efficiently solvable convex optimization problem. In this work, we present the complementary approach of minimizing a weighted sum of user mean-square-errors subject to a given total power constraint. In order to obtain a computationally tractable solution for this design criterion, we exploit the dual DS-UWB uplink that employs rake combining and post-equalization filters at a central receiver. We study the performance of the optimized multiuser pre-rake UWB system under realistic models of UWB channel propagation and demonstrate the effectiveness of the proposed multiuser pre-equalization filter designs in mitigating ISI and MUI, and thus their ability to enable reliable pre-rake DS-UWB downlink transmission.

Results: The bit-error rate versus normalized transmission power for an all-pre-rake DS-UWB system with BPSK transmission and in an indoor office non-line-of-sight environment is shown in the figure below. The base station has 4 transmit antennas and user-specific spreading codes are selected as mutually orthogonal sequences of length 8. The results are shown for $U = 2, 3, 4$ users and pre-rake transmission without and with multiuser PEFs of length $L_q = 10$ is considered. It is observed that the high error floor experienced by pre-rake UWB without pre-filtering is overcome using the optimized PEFs. Thus, the developed optimization framework is shown to be highly effective in enhancing the performance of multiuser pre-rake UWB broadcast systems.

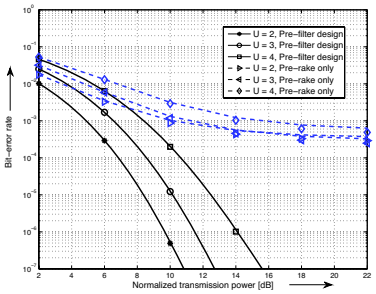

References

[1] E. Torabi, J. Mietzner, and R. Schober, "Pre-Equalization for MISO DS-UWB Systems with Pre-Rake Combining," *IEEE Trans. Wireless Commun.*, vol. 8, no. 3, pp. 1295–1307, Mar. 2009.

[2] Z. Ahmadian, M. Shenouda, and L. Lampe, "Design of Multiuser Pre-Rake Systems for Reliable Ultra-wideband Communications," in *Proc. International Conf. on Communications (ICC)*, Cape Town, South Africa, May 2010.

978-1-4244-5050-3/10/$26.00 ©2010 IEEE

The γ-ray Interference Threshold of E-field Sensor In The Source Region EMP Measurement

MENG Cui[1,2] LIU Yinong[1,2] GUO Xiao_Qiang[3] CHEN Xiang_Yue[3] NIE Xin[3]

1.Department of Engineering Physics, Tsinghua University ,Beijing 100084, China;

2.Key Laboratory of Particle & Radiation Imaging, Ministry of Education

3. Northwest Institute of Nuclear Technology, Xi′an 710024, China

γ-ray irradiated from nuclear explosion interacting with surrounding substances can generate high electromagnetic Pulse (EMP). The field intensity is up to several tens of thousands v/m. Wide spectrum can generate high electromagnetic pulse coupling effect on electronic system. At the same time, nuclear electromagnetic pulse is one of parameters distinguishing nuclear explosion. Therefore, it is very important to measure electromagnetic pulse field in the source region. When nuclear radiation simulator radiates γ-ray, X-ray and neutron, it also generates EMP. We have independently developed an optical fiber based dipole antenna electric field sensor. Signal transmission is based on optical fiber, featured by strong electromagnetic pulse immunity. However, Electro-Optical conversion module at the front end is in the nuclear radiation environment and rays can penetrate shielding box and direct act on the integrated circuit and the laser. γ-ray will generate instantaneous radiation effect on electronic components and electronic system. However, Electro-Optical conversion module at the front end is in the nuclear radiation environment and rays can penetrate shielding box and direct act on the integrated circuit and the laser. γ-ray will generate instantaneous radiation effect on electronic components and electronic system. The γ-ray irradiation effect includes interference, latch up and burn out, these will make the measurement result unbelievable. In this paper, the experimental method researching the γ-ray irradiation effect of high electromagnetic pulse sensor on Qiangguang- I accelerator is introduced. Figure2 indicates the diagram of the experiment diagram.

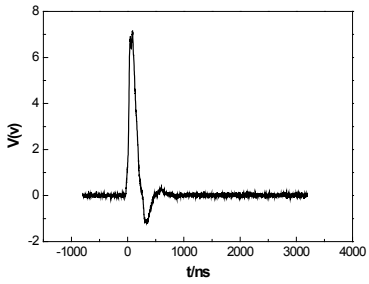

Figure.1 time-domain waveform of γ-ray

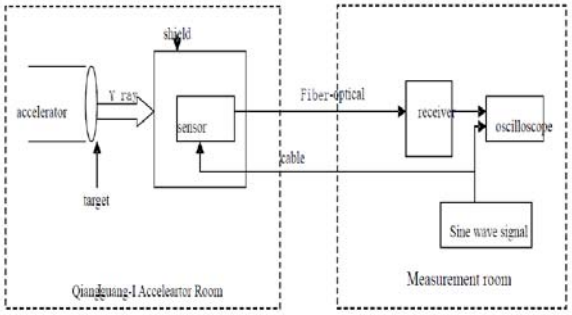

Figure 2 diagram of experiment

Total 4 shots have been taken in the experiment.The radiation experiment of γ-ray with different doses shows that the γ dose rate interference threshold of integrated circuit of sensors is about $2\times10^{6}Gy(Si)/s$. Under radiation with dose higher than $2\times10^{6}Gy(Si)/s$, capacity of the sensor would be damaged temporarily, while this short period is just the time for the sensor to induce the electromagnetic pulse electric filed energy. Thus, the sensor fails to work normally under the radiation of γ does higher than the threshold. Limited by the experiment conditions, we do no experiment under radiation of γ with higher dose, so the dose rate threshold for complete lapse of the sensor is not obtained yet and is to be further studied. In the practical application, the circuit part of the sensor should be reasonably shielded with lead so as for the circuit to radiated by γ ray with dose less than $2\times10^{6}Gy(Si)/s$.

Project 10927506 supported by Special Fund for Basic Research on Scientific Instruments of NSFC

978-1-4244-5050-3/10/$26.00 ©2010 IEEE

Generation and Measurement of Electromagnetic Pulses with Rise Time to 30 ps

L. Siniy, Yu. Dmitriev, V. Molochkov and V. Neustruev
All Russia Research Institute of Automatic, Sushovskaya St. 22, Moscow, 127055 Russia
E-mail: cemc@niit.ru

Testing of the technical means for the study of Intentional EMI (IEMI) is the important problem for nanosecond and subnanosecond EMP with rise times less than 100 ps. To obtain reliable test results, accuracy of monitoring of test pulse parameters is important; therefore, along with the development of UWB EMP sensors, methods and tools for their calibration must be improved.

In practice, to measure the rise time of the transient response of a sensor, it is sufficient that the ratio of rise times of the incident pulse and the response at the sensor output would be no larger than 1:3, and the duration of the flat pulse top should be sufficient to measure the response steady-state level and fall off time (1/e).

The EMP can be produced in field-forming systems such as TEM and GTEM cells, being constructively modified sections of conventional transmission lines. Both types of field-forming systems have specific advantages and disadvantages when calibrating sensors. TEM cells are characterized by good uniformity of test field in rather large volumes; however, they feature not enough upper frequency, due to the excitation of the highest wave modes in the regular section. GTEM cells allow obtaining EMP with shorter rise times in similar volumes; however, due to their configuration, they have low field uniformity. A greater value of the upper frequency relatively to the above cells can be achieved by a symmetric (three plates) strip line, which is close to the TEM cell, but does not have a closed outer shield.

Two calibration cells with field-generation systems shaped as a symmetric strip line with an interplate gap of 80 mm (CC577 cell) and 200 mm (CC578 cell) in the regular part were developed. The impedances of the lines and their matched loads are 50 Ω. The field in the 80-mm line is excited by a TMG015010V ultrashort rise time voltage step generator ("Trim" Company, St.-Petersburg). The 200-mm line is excited by a GINP-20-1 high-voltage generator ("FID-Technology" Company, St.-Petersburg).

For an electric field sensor, a sectioned capacitive antenna was used. To measure the EMP magnetic component, a Moebius loop antenna was used. The operating frequency band of the latter was extended to low frequencies using a ferrite core.

978-1-4244-5050-3/10/$26.00 ©2010 IEEE